JAAVSO

Volume 42
Number 2
2014

The Journal of the American Association of Variable Star Observers

CT Lacertae
Another Long-period Carbon Star with Long-Timescale Variations?

AAVSO light curve for CT Lac, 1968 to mid-2014: The star has been well-observed visually for the past 15 years. This period has been characterized by a fading of the star's mean brightness by about two magnitudes.

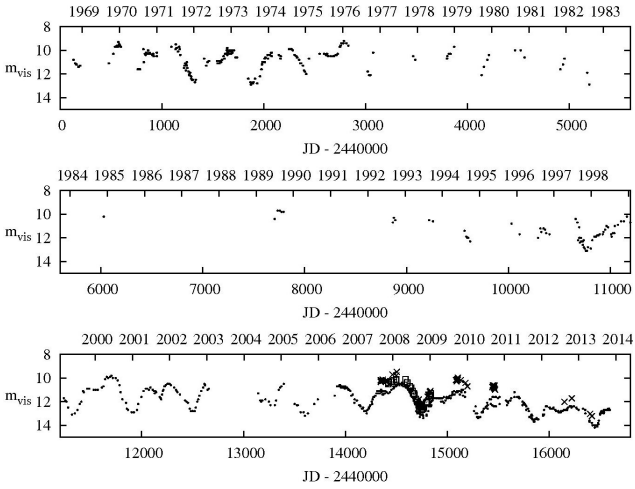

Also in this issue...

Complete table of contents inside...

THE AMERICAN ASSOCIATION OF VARIABLE STAR OBSERVERS
A A V S
FOUNDED 1911

49 Bay State Road
Cambridge, MA 02138
U. S. A.

ISSN 0271-9053

JAAVSO

The Journal of
The American Association
of Variable Star Observers

Volume 42
Number 2
2014

ISSN 0271-9053

49 Bay State Road
Cambridge, MA 02138
U. S. A.

The *Journal of the American Association of Variable Star Observers* is a refereed scientific journal published by the American Association of Variable Star Observers, 49 Bay State Road, Cambridge, Massachusetts 02138, USA. The *Journal* is made available to all AAVSO members and subscribers.

In order to speed the dissemination of scientific results, selected papers that have been refereed and accepted for publication in the *Journal* will be posted on the internet at the *eJAAVSO* website as soon as they have been typeset and edited. These electronic representations of the *JAAVSO* articles are automatically indexed and included in the NASA Astrophysics Data System (ADS). *eJAAVSO* papers may be referenced as *J. Amer. Assoc. Var. Star Obs., in press,* until they appear in the concatonated electronic issue of *JAAVSO*. The *Journal* cannot supply reprints of papers.

Page Charges

Unsolicited papers by non-Members will be assessed a charge of $15 per published page. Page charges may be waived if at least one significant author is an AAVSO member, and the paper is submitted by an AAVSO member.

Instructions for Submissions

The *Journal* welcomes papers from all persons concerned with the study of variable stars and topics specifically related to variability. All manuscripts should be written in a style designed to provide clear expositions of the topic. Contributors may submit digitized text in MS WORD, plain-text format, or LATEX+POSTSCRIPT. Manuscripts may be mailed electronically to journal@aavso.org or submitted by postal mail to *JAAVSO*, 49 Bay State Road, Cambridge, MA 02138, USA.

Manuscripts must be submitted according to the following guidelines, or they will be returned to the author for correction:

Manuscripts must be:
1) original, unpublished material;
2) written in English;
3) accompanied by an abstract of no more than 100 words.
4) not more than 2,500–3,000 words in length (10–12 pages double-spaced).

Figures for publication must:
1) be camera-ready or in a high-contrast, high-resolution, standard digitized image format;
2) have all coordinates labeled with division marks on all four sides;
3) be accompanied by a caption that clearly explains all symbols and significance, so that the reader can understand the figure without reference to the text.

When submitting original figures, be sure to allow for reduction in size by making all symbols, letters, and division marks sufficiently large. Symbols used in figures must not be color-dependent, as figures in the printed version of the journal are reproduced in black and white. Maximum published figure space is 4.5" by 7".

Photographs and halftone images will be considered for publication if they directly illustrate the text.

Tables should be:
1) provided separate from the main body of the text;
2) numbered sequentially and referred to by Arabic number in the text, e.g., Table 1.

References:
1) References should relate directly to the text.
2) References should be keyed into the text with the author's last name and the year of publication, e.g., (Smith 1974; Jones 1974) or Smith (1974) and Jones (1974).
3) In the case of three or more joint authors, the text reference should be written as follows: (Smith *et al.* 1976).
4) All references must be listed at the end of the text in alphabetical order by the author's last name and the year of publication, according to the following format:
   Brown, J., and Green, E. B. 1974, *Astrophys. J.*, **200**, 765.
   Thomas, K. 1982, *Phys. Rep.*, **33**, 96.
5) Abbreviations used in references should be based on recent issues of the Journal or the listing provided at the beginning of *Astronomy and Astrophysics Abstracts* (Springer-Verlag).

Miscellaneous:
1) Equations should be written on a separate line and given a sequential Arabic number in parentheses near the right-hand margin. Equations should be referred to in the text as, e.g., equation (1).
2) Magnitude will be assumed to be visual unless otherwise specified.
3) Manuscripts may be submitted to referees for review without obligation of publication.

Journal of the American Association of Variable Star Observers
Volume 42, Number 2, 2014

Table of Contents continued on following pages

Table of Contents continued on next page

Does the Period of a Pulsating Star Depend on its Amplitude?

John R. Percy
Jeong Yeon Yook
Department of Astronomy and Astrophysics, University of Toronto, Toronto, ON M5S 3H4, Canada; john.percy@utoronto.ca

Received July 8, 2014; revised October 10, 2014; accepted October 10, 2014

Abstract Several classes of pulsating stars are now known to undergo slow changes in amplitude; these include pulsating red giants and supergiants, and yellow supergiants. We have used visual observations from the AAVSO International Database and wavelet analysis of 39 red giants, 7 red supergiants, and 3 yellow supergiants to test the hypothesis that an increase in amplitude would result in an increase in period because of non-linear effects in the pulsation. For most of the stars, the results are complex and/or indeterminate, due to the limitations of the data, the small amplitude or amplitude variation, and/or other processes such as random cycle-to-cycle period fluctuations. For the carbon giants, however, of those which have substantial amplitude variation, and reasonably simple behavior, over 90 % show a positive correlation between amplitude and period. For the non-carbon giants, and the red and yellow supergiants, the numbers showing positive and negative correlation between amplitude and period are comparable.

1. Introduction

Galileo Galilei is noted for (among other things) observing that the period of the swing of a pendulum does not depend on the amplitude of the swing. For most vibrating objects, however, there are non-linear effects which cause the period to increase slightly if the amplitude becomes sufficiently large.

We have recently noted that there are systematic, long-term variations in amplitude in pulsating red giants (Percy and Abachi 2013), pulsating red supergiants (Percy and Khatu 2014), and pulsating yellow supergiants (Percy and Kim 2014). The purpose of this exploratory project was to investigate whether there might be systematic increases in period which accompany the increase in amplitude. This possibility has already been suggested as occuring in R Aql, BH Cru, and S Ori (Bedding *et al.* 2000; Zijlstra *et al.* 2004). BH Cru is a carbon star; the other two are normal M-type giants.

Our study is complicated by several factors. Stars undergo small, slow evolutionary changes in period. They also undergo random cycle-to-cycle fluctuations in period (Eddington and Plakidis 1929; Percy and Colivas 1999). We have shown that, for some reason, the amplitudes themselves are variable. The stars are complicated: red giants and supergiants have large, convective

hot and cool regions on their surfaces. Furthermore, the stars rotate with periods which are comparable with the time scales for amplitude change. For these reasons, it may be difficult to isolate any non-linear effect of changing amplitude on period.

2. Data and analysis

We used visual observations, from the AAVSO International Database, of the stars listed in Tables 1–3. See section 3.5 for remarks on some of these. Percy and Abachi (2013) discussed some of the limitations of visual data which must be kept in mind when analyzing the observations and interpreting the results, but only visual observations are sufficiently dense, sustained, and systematic for use in this project. The data, extending from JD(1) to JD(1) + ΔJD (JD = Julian Date, in days) as given in the tables, were analyzed using the VSTAR package (Benn 2013), especially the wavelet (WWZ) analysis routine. The periods of the stars had previously been determined with the DCDFT routine. For the wavelet analysis, as in our previous papers, the default values were used for the decay time c (0.001) and time division Δt (50 days). The results are sensitive to the former, but not to the latter.

We generated light curves and graphs of period and amplitude versus JD, but our main tool for analysis was graphs of amplitude versus period, as shown in Figures 1–12, which are for stars which are representative and/or interesting. For each of these, the method of least squares was used to determine the straight line of best fit (which is the simplest assumption), the slope k of this fit, the standard error σ of the fit, and the coefficient of correlation R. The spectral types in the figure captions are from SIMBAD.

Tables 1–3 give the star, period in days, initial JD and range of JD, amplitude and amplitude range in magnitudes, k, σ, k/σ, R, and any notes. In Table 1, carbon stars are marked with an asterisk (*) next to the star name. In the last column of Tables 1–3, a symbol "a" indicates additional notes in section 3.4; a symbol "b" indicates that k/σ is greater than 3, and a symbol "c" indicates that $R \geq 0.5$, that is, the results are, in some sense, significant. The notation e–x means 10 to the power –x. The Notes column also includes a qualitative description of the shape and trajectory of the semi-amplitude versus period plots: 1 indicates positive slope, 2 negative slope, 3 non-linear, 4 vertical lines, 5 counterclockwise, 6 clockwise, 7 irregular trajectory, and 8 a sinusoidal trajectory.

3. Results

3.1. Red giants

Table 1 shows the results for the single-mode variables from Kiss *et al.* (2006), Percy and Abachi (2013), Bedding *et al.* (2000), and Zijlstra *et al.* (2004).

Table 1. Variability and WWZ results of pulsating red giants.

Star	*P(d)*	*P Range*	*JD(1)*	*ΔJD*	*A*	*A Range*	*k*	σ	k/σ	R	*Notes*
RV And	165	38	2428000	28300	0.30	0.20–0.60	–2.54e–3	2.9e–3	–0.88	1.2e–1	3, 7
RY And	392	11	2427500	30000	1.69	0.68–2.20	1.89e–2	1.9e–2	1.00	1.3e–1	a, 4, 7
R Aql	294	54	2415000	40000	2.25	1.79–2.59	1.46e–2	7.6e–4	19.32	9.1e–1	a, c, 1, 7
S Aql	143	8	2420000	36300	0.98	0.65–1.20	–1.45e–2	1.7e–2	–0.88	1.0e–1	a, 4, 7
GY Aql	464	8	2447000	9300	2.35	1.90–2.20	–2.23e–2	3.2e–3	–7.05	6.0e–1	a, b, 8
RS Aqr	280	8	2430000	27500	2.73	2.58–2.97	–2.00e–2	7.2e–3	–2.80	3.6e–1	4, 7
T Ari	320	13	2428000	28300	0.91	0.70–1.35	1.59e–2	6.2e–3	2.55	3.2e–1	3, 5
S Aur*	596	33	2416000	40300	0.61	0.45–0.85	8.46e–3	1.4e–3	6.15	5.7e–1	c, 3, 7
U Boo	204	10	2420000	49300	0.62	0.35–0.80	1.62e–2	7.0e–3	2.32	2.6e–1	3, 7
V Boo	887	50	2415000	40000	0.31	0.06–0.50	–3.43e–3	9.7e–4	–3.53	3.7e–1	b, 3, 5
RV Boo	144	29	2434000	22300	0.09	0.05–0.15	1.16e–3	5.7e–4	2.04	1.9e–1	a, 3, 7
S Cam*	327	10	2417000	39300	0.34	0.23–1.00	1.77e–2	2.9e–3	6.18	5.7e–1	c, 3, 7
RY Cam	134	6	2435000	21300	0.16	0.10–0.40	1.99e–2	5.9e–3	3.38	3.1e–1	a, b, 4, 7
T Cnc*	488	19	2417000	39300	0.34	0.23–0.47	2.89e–3	1.6e–3	1.78	2.0e–1	3, 7
RT Cap*	400	75	2417000	39300	0.31	0.25–0.45	4.52e–4	3.4e–4	1.35	4.5e–4	a, 3, 7
T Cen	91	19	2413000	43300	0.62	0.50–1.20	–4.51e–2	1.8e–2	–2.47	2.6e–1	a, 4, 7
DM Cep	367	40	2435000	21300	0.12	0.05–0.10	–7.26e–4	1.0e–4	–6.94	5.6e–1	a, c, 4, 7
T CMi	321	23	2415000	40000	1.86	1.24–2.27	1.25e–2	5.0e–3	2.50	2.7e–1	4, 5
RS CrB	331	7	2435000	21300	0.19	0.13–0.38	7.79e–3	3.5e–3	2.21	2.1e–1	5, 7
BH Cru*	518	38	2440000	10000	1.21	0.91–1.38	1.20e–2	3.0e–4	40.24	9.8e–1	b, 1
T CVn	291	15	2415000	40000	0.83	0.57–1.27	–1.59e–2	6.5e–3	–2.44	6.5e–3	3, 7
RU Cyg	234	14	2415000	40000	0.38	0.11–0.77	1.33e–2	7.1e–3	1.87	2.1e–1	3, 7

Table continued on next page

Table 1. Variability and WWZ results of pulsating red giants, cont.

Star	*P(d)*	*P Range*	*JD(1)*	*ΔJD*	*A*	*A Range*	*k*	σ	k/σ	R	*Notes*
V460 Cyg*	160	15	2435000	21300	0.08	0.04–0.14	2.51e–3	1.2e–3	2.12	2.0e–1	a, 3, 7
V930 Cyg	247	43	2442000	14300	0.72	0.30–0.70	–5.83e–3	2.3e–3	–2.52	2.9e–1	a, 3, 7
EU Del	62	25	2435000	21300	0.08	0.05–0.17	–1.20e–3	1.3e–3	–0.93	9.0e–2	a, 3, 7
SW Gem	700	117	2427500	28800	0.10	0.05–0.35	1.55e–3	8.0e–4	1.94	2.5e–1	a, 3, 7
RR Her*	250	12	2435000	21300	0.54	0.10–0.70	1.33e–2	3.8e–3	3.48	3.2e–1	a, b, 3, 5
RT Hya	255	29	2415000	41300	0.06	0.04–0.16	9.30e–3	5.1e–3	1.83	2.0e–1	a, 3, 7
U Hya*	791	98	2420000	36300	0.06	0.04–0.16	–2.22e–4	1.2e–4	–1.90	2.2e–1	a, 3, 7
U LMi	272	31	2427500	30000	0.50	0.23–0.85	3.98e–3	3.7e–3	1.07	1.4e–1	a, 3, 7
X Mon	148	9	2415000	41300	0.59	0.25–0.85	–3.04e–2	7.8e–3	–3.90	4.0e–1	a, b, 4, 7
S Ori	422	36	2415000	40000	1.93	0.30–2.39	1.52e–2	3.1e–3	4.85	4.9e–1	a, b, 3, 5
S Pav	387	11	2415000	40000	0.70	0.30–1.29	2.38e–2	8.6e–3	2.77	2.9e–1	a, 3, 7
Y Per*	251	11	2415000	40000	0.72	0.34–0.99	2.49e–2	6.3e–3	3.95	4.1e–1	b, 3, 7
SY Per*	477	23	2446000	10300	0.89	0.67–0.92	1.83e–2	1.5e–3	12.26	8.7e–1	a, b, 1
UZ Per	850	11	2448000	8300	0.25	0.23–0.29	–4.95e–3	3.9e–4	–12.55	8.1e–1	b, 2
W Tau	243	39	2415000	41300	0.27	0.10–1.50	3.15e–2	3.4e–3	9.31	7.2e–1	a, b, 1
V UMa	198	42	2420000	36300	0.19	0.15–0.50	5.71e–4	1.1e–3	0.50	6.0e–2	3, 7
SS Vir*	361	17	2420000	36300	0.82	0.60–1.15	4.56e–3	2.8e–3	1.64	1.9e–1	3, 5

**Carbon star. (a) See note in section 3.5. (b) k/σ > 3. (c) R ≥ 0.5. Plot descriptions: (1) positive slope; (2) negative slope; (3) non-linear; (4) vertical; (5) counterclockwise; (6) clockwise; (7) irregular trajectory; (8) sinusoidal trajectory.*

Table 2. Variability and WWZ results of pulsating red supergiants.

Star	*P(d)*	*P Range*	*JD(1)*	*ΔJD*	*A*	*A Range*	*k*	σ	k/σ	R	*Notes*
BO Car	337	20	2443000	14000	0.13	0.07–0.21	–5.6e–3	1.3e–3	–4.45	4.5e–1	a, b, 2, 7
PZ Cas	846	24	2440000	15000	0.24	0.13–0.50	6.5e–3	1.4e–3	4.66	4.6e–1	b, 3, 5
BC Cyg	703	25	2440000	15000	0.30	0.14–0.51	7.6e–3	2.1e–3	3.71	3.8e–1	b, 3, 5
W Ind	194	45	2443000	14000	0.40	0.95–1.09	–9.0e–4	1.4e–3	–0.63	7.0e–2	a, 3, 7
S Per	809	44	2420000	35000	0.57	0.33–0.85	–9.1e–5	1.4e–3	–0.06	7.5e–3	a, 3, 7
W Per	489	87	2415000	40000	0.35	0.19–0.48	–1.0e–4	3.3e–4	–0.31	3.4e–2	a, 3, 7
VX Sgr	760	87	2427500	30000	0.73	0.57–1.30	–7.1e–3	1.3e–3	–5.36	5.8e–1	a, c, 3, 7

(a) See note in section 3.5. (b) k/σ > 3. (c) R ≥ 0.5. Plot descriptions: (1) positive slope; (2) negative slope; (3) non-linear; (4) vertical; (5) counterclockwise; (6) clockwise; (7) irregular trajectory; (8) sinusoidal trajectory.

Table 3. Variability and WWZ results of pulsating yellow supergiants.

Star	*P(d)*	*P Range*	*JD(1)*	*ΔJD*	*A*	*A Range*	*k*	σ	k/σ	R	*Notes*
AV Cyg	88	5	2430000	27500	0.37	0.12-0.56	–1.0e–2	1.4e–2	–0.73	9.9e–2	3, 7
DE Her	173	10	2442500	12500	0.42	0.14-0.64	–4.4e–2	4.1e–3	–10.77	7.9e–1	c, 3, 7
RS Lac	238	2	2427500	30000	0.72	0.35-1.03	7.4e–2	5.3e–2	1.40	1.8e–1	4, 7

(a) See note in section 3.5. (b) k/σ > 3. (c) R ≥ 0.5. Plot descriptions: (1) positive slope; (2) negative slope; (3) non-linear; (4) vertical; (5) counterclockwise; (6) clockwise; (7) irregular trajectory; (8) sinusoidal trajectory.

Carbon stars are marked with an asterisk. In total, 39 pulsating red giants are listed in the table and 26 of them have a positive k and 13 of them have a negative k.

Figure 1 shows the semi-amplitude versus period relationship for BH Cru. It displays a strong, positive correlation between semi-amplitude and period; and there is almost no non-linearity. It is our "best case" for a relation between changing amplitude and changing period. The relation is also clear from the plots of period versus JD and amplitude versus JD (Bedding *et al.* 2000). Note that we are using about 14 more years of data than Bedding *et al.* (2000).

Figure 2 shows the semi-amplitude versus period plot for R Aql. There is a strong, positive correlation between them as listed in Table 1. This agrees with the discussion of Bedding *et al.* (2000) that R Aql shows some correlation between period and amplitude. However, there is local non-linearity in addition to the linear correlation, which suggests that there is also some other process which affects the period. The individual period and amplitude plots show that, whereas the period is decreasing monotonically from 310 to 270 days, the amplitude is decreasing but also undergoing fluctuations, perhaps due to stochastic excitation and decay.

Figure 3 is the semi-amplitude versus period plot for S Ori, which is again from Bedding *et al.* (2000). This one also has a positive correlation; however, there is a global non-linearity and the linear fit does not represent the relationship between amplitude and period very well. In this case, the individual period and amplitude plots show that the period is undergoing fluctuations between 405 and 440 days.

Figure 4 is for GY Aql, a pulsating red giant from Percy and Abachi (2013). The semi-amplitude and the period of GY Aql have a sinusoidal relationship and the linear fit is not a good representation of the data. This plot is non-linear; however, this sinusoidal pattern shows more regularity than other non-linear plots. Note, however, that the change in amplitude is small, both absolutely and as a fraction of the average amplitude.

Figure 5 is for S Aur from Percy and Abachi (2013). There is a positive correlation between the semi-amplitude and period, but this obviously not the dominant process affecting the period.

Figure 6 shows the semi-amplitude versus period for S Cam. There is a positive correlation with some non-linearity. The change in amplitude is relatively small.

Figure 7 is for DM Cep and it has a negative slope with some non-linearity. The data has a gap in the mid-region of the data, and the amplitude is very small.

Figure 8 is for SY Per and there is a positive correlation. There is a local non-linearity in the plot; however, the line of the best fit is a good representation of the data globally.

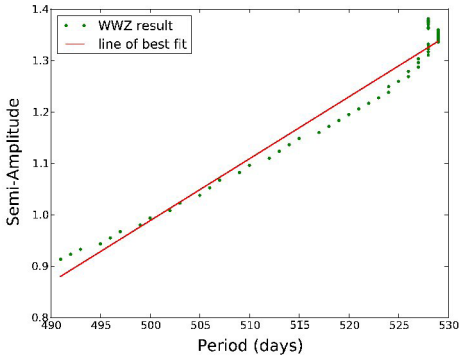

Figure 1. Semi-amplitude versus period for BH Cru (SC4.5-7/8e). The correlation is excellent, as was apparent from the graphs of period and amplitude versus JD (Bedding *et al.* 2000).

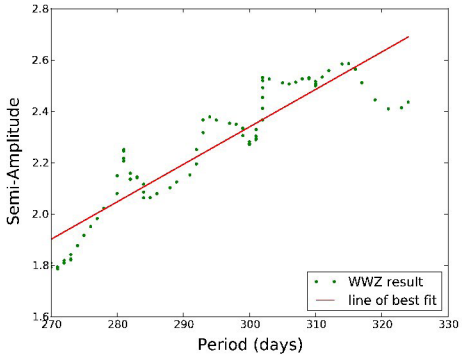

Figure 2. Semi-amplitude versus period for R Aql (M6.5-9e). The positive correlation was suggested by Bedding *et al.* (2000) on the basis of the graphs of period and amplitude versus JD. The deviations from the straight-line fit suggest that there is one or more additional factors which affect the period and/or amplitude.

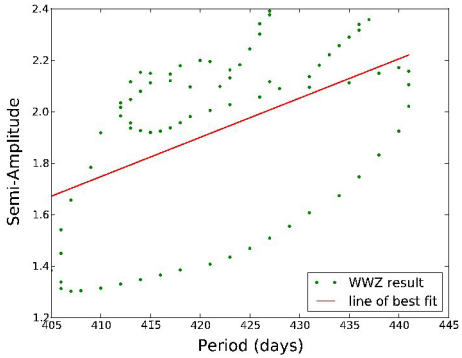

Figure 3. Semi-amplitude versus period for S Ori (M6.5-7.5e). A positive correlation was suggested by Bedding *et al.* (2000) but it is clear that, although this graph shows such a correlation, the correlation is weak, presumably because of other processes which affect the period and/or amplitude.

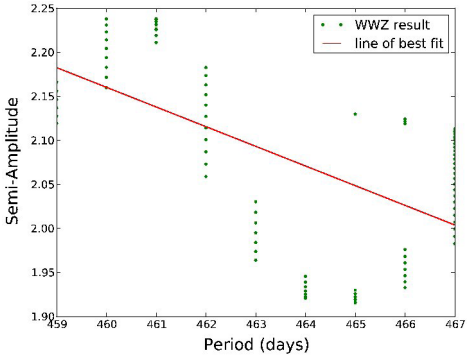

Figure 4. Semi-amplitude versus period for GY Aql (M6e). The correlation is negative but the change in amplitude and period is very small, relative to their mean values.

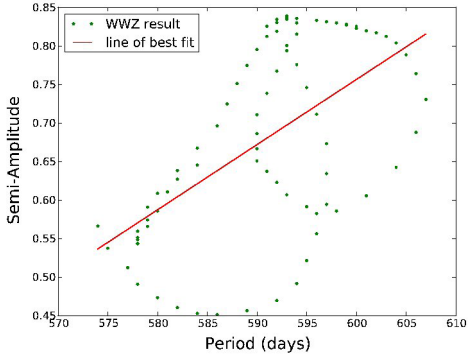

Figure 5. Semi-amplitude versus period for S Aur (N0). The correlation is positive but weak and non-linear, indicating that other factors are important in determining the changes in period and/or amplitude.

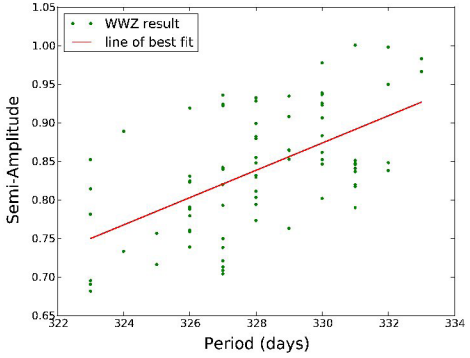

Figure 6. Semi-amplitude versus period for S Cam (R8e). The correlation is positive but scattered and weak. The change in period is small.

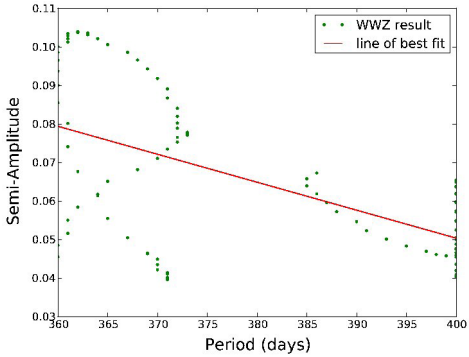

Figure 7. Semi-amplitude versus period for DM Cep (M3D). The small amplitude and amplitude change make any correlation meaningless.

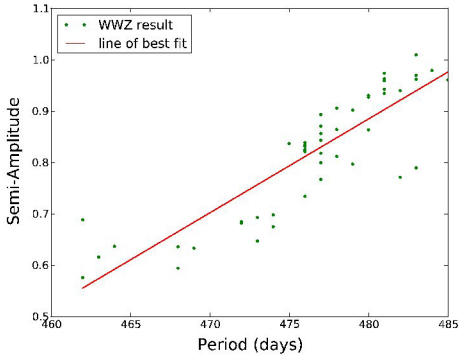

Figure 8. Semi-amplitude versus period for SY Per (C6,4e). There is a significant positive correlation, with some deviations from this.

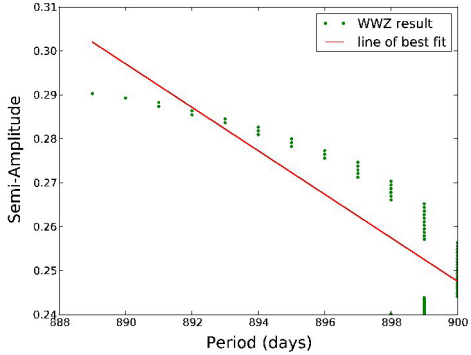

Figure 9. Semi-amplitude versus period for UZ Per (M5II-III). The correlation is negative, but the amplitude and its change are very small.

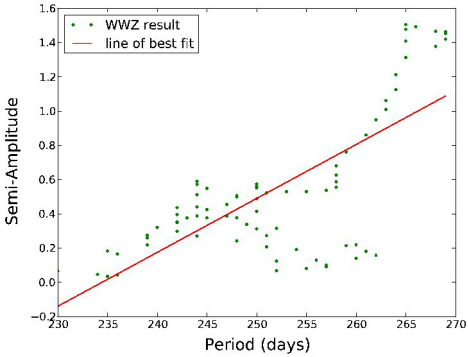

Figure 10. Semi-amplitude versus period for W Tau (M6D). There is a positive correlation, with some deviations. The change in period is exceptionally large—15 per cent.

Figure 9 is for UZ Per. UZ Per has a long period and a small change in amplitude, so the negative slope is not really meaningful.

Figure 10 is for W Tau. There is a positive correlation between semi-amplitude and period, with some non-linearity in the plot in addition to the global linear trend.

3.2. Red supergiants

Table 2 presents the results of WWZ analysis for some red supergiants. The notations used are the same as in Table 1. Seven red supergiants were studied. One had a negative correlation and six had a positive correlation between the semi-amplitude and the period.

Figure 11 is the semi-amplitude versus period plot for VX Sgr. VX Sgr has a long period which is a characteristic of supergiants. There is some negative correlation. However, the plot is non-linear and the line of best fit does not represent the plot well. This is not surprising, in view of the complexity of this class of stars.

3.3. Yellow supergiants

Table 3 displays the result of WWZ analysis for some yellow supergiants. The notations used are the same as in Table 1. Three yellow supergiants were studied and they all have a non-linear relationship between the semi-amplitude and the period, but only one is significant.

Figure 12 is the semi-amplitude versus period plot for DE Her. There is a weak negative correlation. The plot is non-linear and the line of best fit does not describe the plot in a meaningful way.

3.4. Summary statistics

Figure 13 is a plot for k versus amplitude range. There is a positive correlation, and almost all of the slopes are positive, especially for the carbon stars (crosses).

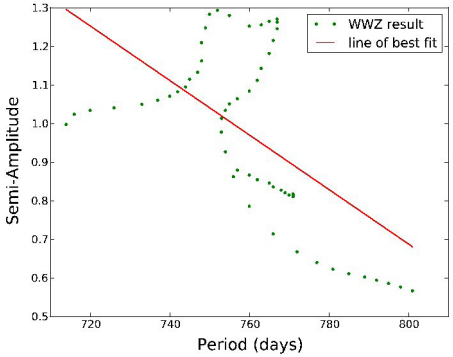

Figure 11. Semi-amplitude versus period for VX Sgr (M5/6III or M4Iae). There is a negative correlation, but the relation is certainly not linear. This is not surprising in a star as complex as a red supergiant. The change in period is large -- 10 per cent.

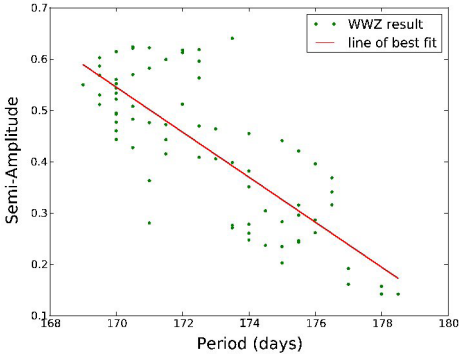

Figure 12. Semi-amplitude versus period for DE Her (K0D), a *yellow* semiregular variable star. There is a strong negative correlation, with significant deviations from this.

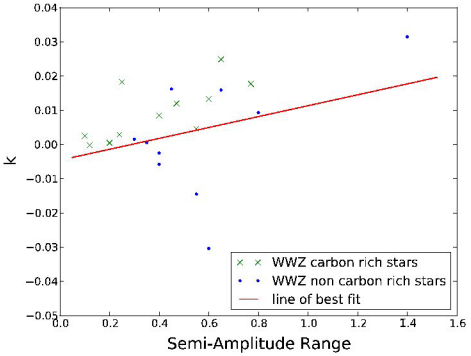

Figure 13. The relationship between the slope k and the range in semi-amplitude. There is a small positive correlation. Most of the values of k are positive, especially for the carbon stars, which are indicated by crosses.

3.5. Notes on individual stars

RY And There are some sparse regions of data in between dense regions.

R Aql The data are sparse before JD = 2420000. There is an outlier in period in the beginning.

S Aql There is an abrupt change in period at the end of the data.

GY Aql The data are sparse.

RV Boo The period is not smooth.

RY Cam The period is not smooth.

RT Cap The data are sparse near JD = 2430000. There is an abrupt change in period in the middle.

BO Car The data are sparse before JD = 2443000.

T Cen The period is not smooth. The data are sparse near JD = 2430000. There is an abrupt change in period in the middle.

DM Cep The data are sparse between JD = 2440000 and JD = 2442500. There is an abrupt change in period in the middle.

V460 Cyg The period is not smooth.

V930 Cyg The data are sparse before JD = 2445000. There is an outlier in period in the beginning.

EU Del The period and the semi-amplitude are not smooth. There are two outliers in the light curve.

SW Gem There is an abrupt change in the middle.

RR Her The period and the semi-amplitude are not smooth.

U Hya The data are sparse near JD = 2430000 There is an abrupt change in period in the middle. The luminosity class is uncertain.

RT Hya There is an abrupt change in period. The semi-amplitude is not smooth.

W Ind The data are sparse near JD = 2452500. There is an abrupt change in period and amplitude at the end. The luminosity class is uncertain.

U LMi There is an abrupt change of period at the end.

X Mon The period and the semi-amplitude are not smooth.

S Ori The data are sparse before JD = 2420000.

S Pav The data are sparse from JD = 2420000 to JD = 2427000.

S Per The data are sparse before JD = 2420000.

W Per There is an abrupt change in period in the beginning.

SY Per The data are sparse before JD = 2448000.

VX Sgr There is an abrupt change in period in the beginning.

W Tau There is an abrupt change in period in the middle.

4. Discussion

There are a variety of mechanisms which could cause period (or amplitude) changes in pulsating red giants and supergiants and other cool, luminous stars: evolution, random cycle-to-cycle fluctuations, helium shell flashes, or simply

the complexity of a star with large convective cells which is rotating and losing mass. Nevertheless, if we restrict our attention to stars whose amplitude and amplitude changes are sufficiently large, and whose amplitude versus period relation has a significant linear slope, then 9 of 11 pulsating red giants show a period which increases with increasing amplitude. Choosing slightly differently, among stars with amplitudes greater than 1.0 magnitude, and significant *ranges* in amplitude, 10 of 12 have a positive correlation between amplitude and period. Closer examination shows, however, that this result is entirely due to the carbon giants, over 90 % of which show a positive correlation.

Note that we have fitted a linear relation to the amplitude-period diagrams to test for a positive correlation. There is no *a priori* reason to believe that the relation would be linear, but a linear fit is the simplest. Intuitively, we might expect the non-linear effects to be minimal at small amplitudes, and much greater at large ones. This was the case in Stobie's (1969) hydrodynamic pulsation models of Cepheids; the period was independent of velocity amplitude up to 50 km/sec, but then increased quickly by several percent at higher amplitudes. For BH Cru (Figure 1) and R Aql (Figure 2)—two of our best cases—a linear relation between period and amplitude is a reasonable fit.

For this and other reasons, R and k/σ are not true measures of significance. The individual points in the figures are not independent (see below), given the decay constant and timestep that we have chosen. But the figures would not be too much affected if only every tenth point was used. Bedding *et al.* (2000) and Zijlstra *et al.* (2004) identified the behavior of RR Aql, BH Cru, and S Ori by inspection of the period versus JD and amplitude versus JD diagrams. The amplitude versus period diagrams provide another way of visualizing the behavior. Figure 3, for instance, shows the same behavior for S Ori as Figure 3 of Bedding *et al.* (2000). Generally, the visual appearance of these diagrams is consistent with the values of R and k/σ, in terms of scatter. Nevertheless (and we thank the referee for emphasizing this), the validity of these diagrams may be limited by the time resolution of the data.

One advantage of plotting every timestep in the figures (such as Figures 1–12) is that the figures then show *patterns* or *trajectories* which may eventually help to understand what causes the variations in period and amplitude. The notes in the last columns of the Tables reflect these patterns.

Wavelets are sensitive to edge effects and gaps. In principle, we could have dealt with this by using the significance values given by "WWZ statistic" to identify and remove low-confidence points. We have, however, tried to avoid the problem by (1) choosing program stars which had sufficient data; and (2) beginning the JD range where the data were not too sparse. We also ensured that the period versus JD plots were smooth, rather than jagged and discontinuous as they are when there are significant gaps in the data.

We must also remember that the visual light curve is not necessarily a measure of the amplitude of the *pulsation*, nor is it a bolometric light curve.

Furthermore, magnitude itself is logarithmic, and therefore intrinsically non-linear at higher amplitudes. For red stars, the visual band is especially sensitive to temperature, because of the presence of molecular bands. Carbon stars, and especially SC stars, are much less affected by this than oxygen-rich stars. Among the 39 pulsating red giants in Table 1, 11 are carbon stars; they are marked with an asterisk. Of these, 10 out of 11 have positive k/σ, though only 6 have k/σ greater than 3. The 11th star, U Hya, has a slope close to zero; its slope is not significant. The carbon stars are: S Aur (C4–5 (N3)), S Cam (C7,3e(R8e)), T Cnc (C3,8–C5,5(R6–N6)), RT Cap (C6,4(N3)), BH Cru (SC4.5/8e–SC7/8e), V460 Cyg (C6,4(N1)), RR Her (C5,7e–C8,1e(N0e)), U Hya (C6.5,3(N2)(Tc)), Y Per (C4,3e(R4e)), SY Per (C6,4e(N3e)), and SS Vir (C6,3e(Ne)). There is no spectral classification at SIMBAD for V930 Cyg.

Why do we find a positive correlation for the carbon red giants, but not for the non-carbon stars? We must first realize that the period changes may not be *caused* by the amplitude change; they may simply be correlated through some other process. We also note that, as noted above, for the M-type red giants, the visual flux is determined by both the size of the star (its pulsation), and by its temperature because of the temperature-sensitive TiO bands. Modelling of the pulsating atmosphere is probably necessary to answer this question definitively.

5. Conclusions

In stars with a variable pulsation amplitude, does an increase in pulsation amplitude result in an increase in period? The majority of the almost-50 pulsating stars in our sample do *not* show a *significant* positive or negative relation between the instantaneous period and amplitude. Clearly, there are other processes which affect either the period and amplitude. But, of the *carbon* giants which show sufficiently large amplitude and amplitude change, over 90% show a noticeable positive correlation between the instantaneous amplitude and period. For non-carbon giants, and other stars, the numbers of positive and negative correlations are comparable.

This project was an exploratory project, but it was successful in raising questions about the complex behavior of these stars—questions which could perhaps be answered through in-depth studies of a few stars from Tables 1–3, analyzed with more sophisticated techniques, and with even better data.

6. Acknowledgements

This project would not have been possible without the efforts of the hundreds of AAVSO observers who made the observations which were used in this project, and the AAVSO staff who processed and archived the measurements. We also thank the team which developed the VSTAR package, and made it user-friendly and publicly available. We are especially grateful to Professor Tim Bedding

for suggesting this project in the first place, and to the anonymous referee for some very insightful and helpful suggestions. Author JRP thanks author JYY, an undergraduate major in Physics who, with no background in Astronomy, organized and carried out this project so professionally. We thank the University of Toronto Work-Study Program for financial support. This project made use of the SIMBAD database, which is operated by CDS, Strasbourg, France.

References

Bedding, T. R., Conn, B. C., and Zijlstra, A. A. 2000, in *The Impact of Large-Scale Surveys on Pulsating Star Research*, eds. L. Szabados and D. W. Kurtz, ASP Conf. Ser. 203, Astronomical Society of the Pacific, San Francisco, 96.

Benn, D. 2013, VSTAR data analysis software (http://www.aavso.org/vstar-overview).

Eddington, A. S., and Plakidis, S. 1929, *Mon. Not. Roy. Astron. Soc.*, **90**, 65.

Kiss, L. L., Szabó, Gy. M., and Bedding, T. R. 2006, *Mon. Not. Roy. Astron. Soc.*, **72**, 1721.

Percy, J. R., and Colivas, T. 1999, *Publ. Astron. Soc. Pacific*, **111**, 94.

Percy, J. R., and Abachi, R. 2013, *J. Amer. Assoc. Var. Star Obs.*, **41**, 193.

Percy, J. R., and Khatu, V. 2014, *J. Amer. Assoc. Var. Star Obs.*, **42**, 1.

Percy, J. R., and Kim, R. Y. H. 2014, *J. Amer. Assoc. Var. Star Obs.*, **42**, 267.

Stobie, R. S. 1969, *Mon. Not. Roy. Astron. Soc.*, **144**, 461.

Zijlstra, A. A., *et al.* 2004, *Mon. Not. Roy. Astron. Soc.*, **352**, 325.

CT Lacertae: Another Long-period Carbon Star with Long-Timescale Variations?

Matthew R. Templeton
Peter Maurer
Wolfgang Kriebel
Wayne M. Lowder (1932–2003)
Etienne Morelle
Steve O'Connor
Andrzej Arminski
Laurent Bichon
John E. Bortle
AAVSO, 49 Bay State Road, Cambridge, MA 02138; address email correspondence to matthewt@aavso.org

Received August 11, 2014; revised September 9, 2014; accepted September 9, 2014

Abstract The poorly-studied semiregular-type variable CT Lacertae is a long-period variable of the carbon spectral type, and is also a member of the LPV subclass that exhibits double maxima. More importantly, CT Lac is also undergoing a long-timescale dimming episode spanning the last few thousand days. Analysis of the AAVSO's 45-year visual light curve shows no clear changes in period during the course of its observational history, but current and past changes in mean light and amplitude suggest long-term, observable changes occur in the star itself or in its circumstellar environment. Long-term data are currently too short and sparse to say whether dimming episodes are cyclical as they are in some other long-period carbon Miras and semiregulars, but the ongoing dimming episode could be related to similar events which do recur in other long-period carbon stars like RU Vir and V Hya. CT Lac is an interesting variable and is recommended as a long-term target for both visual and instrumental observation. Increased visual observation is strongly encouraged, as are multicolor photometry and high resolution spectroscopy.

1. Introduction

Asymptotic giant branch (AGB) stars with very long periods (> 550 days) are uncommon; the period distribution of observed Mira variables peaks around 300 days, with a very sharp drop off above 450 days. The reason for this drop off could be a selection effect but is also partly due to their true scarcity. Theoretical studies of AGB stars by Willson and collaborators (Willson 2000) showed that mass loss rates of AGB stars should be maximal when they reach maximum luminosity, after which their mass loss rates become so high that they become optically obscured and undetectable. As an example, S Cas has a period

of 612 days and a mass loss rate of 10^{-5} $M_{\odot}$ per year, close to the upper limit for an optically-visible Mira star. Maximum evolutionary luminosity for a Mira star also correlates with the maximum period, and this suggests there is a point beyond which long-period Miras become scarce because obscuration by lost mass overwhelms the optical luminosity, perhaps leaving them as pulsating IR sources (e.g. QX Pup). We selected CT Lac for further study because of its long period as part of a larger study of AGB evolution and behavior focusing on Mira and semiregular variables with long periods, double maxima, and/or period changes.

CT Lac (R.A. 22^{h} 06^{m} 39.93^{s}, Dec. +48° 27' 06.9" (J2000)) was discovered by Morgenroth (1936) and noted as an "irregular" variable. Subsequent spectral surveys showed the star to be a carbon star of late spectral type (Stephenson 1973) while variability surveys found it to be a pulsator with a long period of 562 days. Alksnis (1981) noted the presence of double maxima along with a highly variable light curve from cycle to cycle. The star was observed by Hipparcos and the optical variability is very clear. Price *et al.* (2010) analyzed the COBE/DIRBE near-IR photometry and found no significant variability, but the photometry for this star had low signal-to-noise; the variability is weakly present in period-folded 4.9-μm data, but is very noisy. There has been little work on variability in CT Lac beyond these papers. CT Lac is instead much better known and studied as a bright carbon star, having late R- or N- spectral type with substantial carbon dust absorption and mass loss (Knapp *et al.* 2001).

CT Lacertae has not been historically well-observed by AAVSO observers, but what data exist are very interesting (AAVSO 2014). Notably, the star was followed for several thousand days by the late observer Wayne Lowder (AAVSO observer initials LX), from the late 1960s to the early 1980s, and the star was listed in the *AAVSO Circular* in the 1970s for a time; CT Lac was originally considered to be a potential R CrB variable. Coverage subsequently declined, but the star was picked up again in the late 1990s by Peter Maurer (MPR) and later by Wolfgang Kriebel (KWO). In addition to visual observations, CT Lac is now also a target for a few CCD imagers as well. The full light curve including both visual data and V-band and tri-color green (TG) instrumental data is shown in Figure 1; identification of AAVSO observers and information about the observations is shown in Table 1. All data are freely available from the AAVSO website at http://www.aavso.org/data-download.

2. Time-series analysis

Though sparse, the AAVSO data clearly show the cycle-to-cycle variability, and its overall behavior places CT Lac in the semiregular category. To quantify the variability, we analyzed the unaveraged visual data from 1968 to late 2008, omitting subsequent data that show the significant drop in mean magnitude. Early data also show some decline in maximum magnitude—from $m_{vis} = 9.5$ to 10.5—but less substantially than the decline from 2008 to 2014. We used an

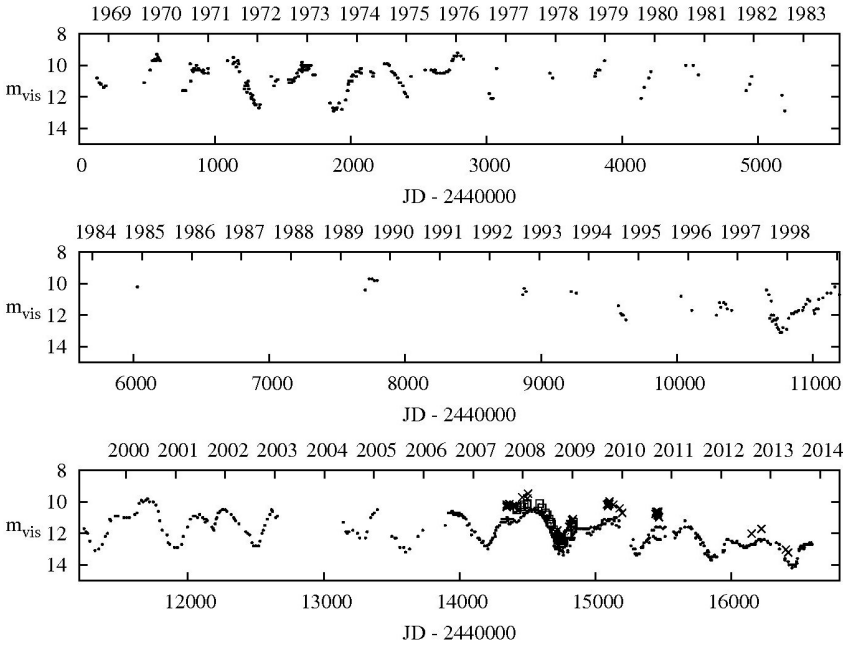

Figure 1. AAVSO light curve for CT Lac, 1968 to mid-2014: filled circles, visual data; open squares, tri-color green data; crosses, V-band data. The star has been well-observed visually for the past 15 years. This period has been characterized by a fading of the star's mean brightness by about two magnitudes.

Table 1. Observers of CT Lac through 2014 August 1.

Observer (AAVSO Obs. code)	*Obs. band*	*Min(MJD)*	*Max(MJD)*	*No. of Obs.*
Maurer (MPR)	Visual	50685	56871	281
Kriebel (KWO)	Visual	53939	56870	194
Lowder (LX)	Visual	40134	46029	164
Morelle (MEV)	Tricolor G	54420	54841	47
O'Connor (OCN)	Visual	43467	51044	41
Arminski (AAM)	Johnson V	54348	55470	38
Bichon (BIC)	Visual	53145	54089	28
Bortle (BRJ)	Visual	41643	42167	14
Sharpe (SHS)	Visual	54413	54765	5
Holmberg (HGUA)	Johnson V	56151	56420	4
Ford (FD)	Visual	40820	40951	2
Bueno (BUO)	Visual	42149	—	1

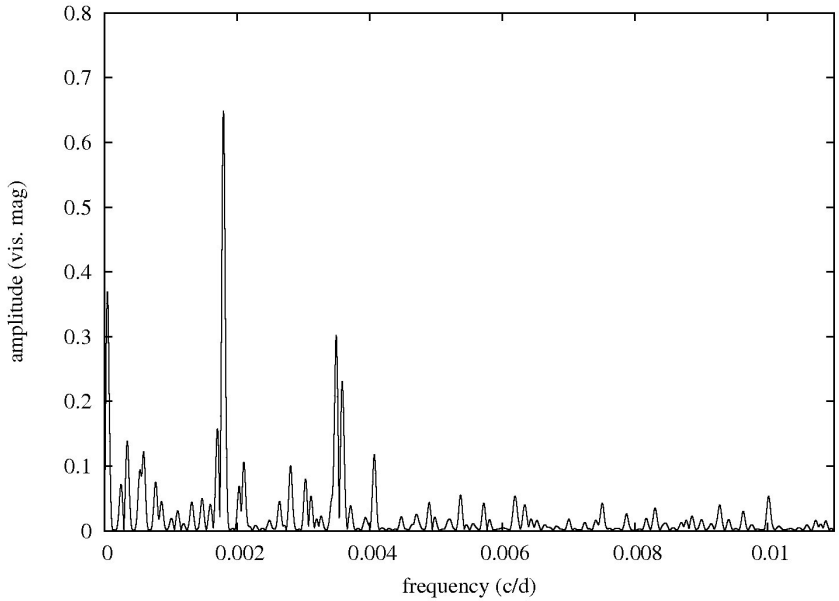

Figure 2. Fourier transform of CT Lac visual data 1968 to 2008 for the low frequency portion of the tested frequency range; frequencies above 0.005 c/d do not show any statistically significant signals and so we only show frequencies up to 0.01 c/d (P = 100 days). A list of signficant peaks is given in Table 2. The peak with amplitude > 0.35 magnitude near zero frequency is an artifact of the change in mean light early in the light curve, which typically causes low-frequency power. The frequency of that peak yields a period longer than the span of the data, and is not periodic.

Table 2. Significant peaks in the Fourier amplitude spectrum of CT Lac, 1968–2008.

Frequency $\times 10^{-3}$ *c/d*	*Amplitude* *Visual mag.*	*Phase* *rad.*	*ID*
1.7915(7)	0.65(13)	–0.16(3)	f_0
3.492(1)	0.30(13)	–2.61(7)	f_1
3.583(2)	0.23(13)	+0.86(9)	$2f_0$
1.701(3)	0.16(13)	+2.95(13)	f_2
4.067(4)	0.12(13)	+2.55(17)	f_3

Note: *Uncertainties were calculated using the formulae of Lenz and Breger (2005) for the ideal case, and assuming mean photometric uncertainties of 0.2 magnitude. Phases are relative to the temporal center of the data, JD 2447466.5.*

iterative, discrete Fourier transform code that uses the method of Roberts *et al.* (1987) to compute the Fourier spectrum for frequencies between 0 and 0.05 c/d. We show the Fourier spectrum in Figure 2, and provide a table of significant frequencies in Table 2.

We find the dominant frequency during the 40 year span to be $f_0 = 0.0017915$ c/d, corresponding to a period of 558.2 days, slightly different from the current VSX (Watson *et al.* 2014) value of 562 days. We also clearly detect the first Fourier harmonic of the dominant signal (twice the main frequency) at $2f_0 = 0.003583$ c/d (P=279.1 days). Along with this, we also detect a second peak at slightly lower frequency than the second harmonic, $f_1 = 0.003492$ c/d (P=286.3 days). This peak is clearly resolved and separate from the $2f_0$ component, and so it is almost certainly a real feature. There is a weak peak adjacent to f_0, having frequency $f_2 = 0.001701$ c/d, and the sum of this frequency and the f_0 yields f_1 exactly. Finally, we note another peak with frequency $f_3 = 0.0040670$ c/d, with very marginal statistical signifigance. We do not see statistically significant peaks at higher Fourier harmonics of the dominant frequency f_0 beyond $2f_0$.

The two frequencies f_0 and $2f_0$ are responsible for the main pulsation at 558.2 days, and appear to be stable to within the uncertainties of the data. What is interesting is the presence of f_1 and f_2. The f_1 peak has substantial amplitude, exceeding that of $2f_0$, and is capable of perturbing the light curve. It should create a beat pattern with the $2f_0$ peak, and may be responsible for (or be a manifestation of) the cycle-to-cycle variability. Its origin isn't clear, but the fact that its frequency is the sum of f_0 and f_2 suggests one of two things: that it may be a distinct pulsation mode (e.g. a radial overtone) at a frequency very close to twice that of f_0, or that the variability mechanism responsible for producing f_0 is being modulated in some way that is producing sidelobes. As an example, there are a number of stars (including RV Tauri stars and Type II Cepheids) that show some evidence of "period-doubling" and that could be happening here. Further discussion is beyond the scope of this paper especially given the relatively short span of data, but future analysis of a longer light curve may provide some interesting insight into the cause of such variations.

3. Recent and past behavior: cyclical or not?

As Figure 1 shows, CT Lac is currently undergoing a long-term dimming event that started in the late 2000s. It isn't clear whether the star is in the middle of a cyclical change and will return to its previous mean magnitude within the next decade, or whether some longer-term and more exceptional event is happening. The current change in mean magnitude appears to coincide also with a strong reduction in amplitude; the most recent pulsation cycle (from early 2012 to mid-2013) has a flat-topped shape that only weakly recovered from the preceeding minimum light. The cause of this fading isn't known, but dimming by dust is a likely explanation.

Beyond its being a long-period pulsator, what made CT Lac notable enough for deeper study was this fading behavior. There are other cases of long-period, semiregular and Mira stars of the carbon sub-type that show fading events, with RU Vir and V Hya being two prominent examples. Lloyd-Evans (1997) noted that at least two prominent carbon stars—V Hya (SRa, P=530d) and R Lep (M, P=445d)—show modulations in optical emission from C_2 molecules (carbon dust) that are anticorrelated to the optical brightness; the Swan C_2 bands are bright when the star is optically faint. Like those stars, CT Lac is also a carbon star, with some ambiguity as to whether it is of the R- or N-subtype (Eglitis *et al.* 2003 (EEB); Zamora *et al.* 2009). In either case, it is of late type, and C_2 was strongly present in the optical spectrum at the time of the EEB study. What is not known is the variability of the Swan bands, either during individual pulsation cycles or over long periods of time. A contemporary spectroscopic observation and re-measurement of the Swan bands observed by EEB may provide a useful comparison of the C_2 brightness circa 2003 versus now. Such a measurement might make clear whether the current dimming episode is quantitatively similar to those seen in other pulsating carbon stars with long-period supercycles.

Barring further spectroscopy, the most important observational study should be the continued (and increased) observation of CT Lac during the next several years to two decades. The dimming apparent in the light curve from the late 1960s to early 1980s gives a hint that there may be something cyclical in CT Lac's behavior, but current data archives are simply too sparse to make a definitive statement. Past data may be available from plate archives, and we plan to check Harvard plate data once the DASCH (Grindlay *et al.* 2009) public archive includes the Lacerta region. Future observations by both visual observers and instrumental observers will also be required. Visual observers have provided the majority of the existing time-series to date, and these data are fully capable of tracking these long-term variations simply, efficiently, and accurately. Instrumental data would provide additional useful information, especially if Johnson B and V data were taken and properly transformed so that both the overall V-band brightness and the (B−V) color could be accurately tracked with time.

4. Acknowledgements

MT thanks all of the AAVSO observers for providing the observational data that made this study possible. He would also like to point out important contributions to this field by two individuals who have passed on: Wayne Lowder and, very recently, Tom Lloyd-Evans. First, this work would not have been possible at all if Wayne Lowder had not begun observations in the 1960s, and this star is just one among many whose observational histories in the AAVSO archives began with his work. Second, the 1997 paper on carbon

star spectra that was cited here is one example among many where Tom Lloyd-Evans helped expand our understanding of variable stars. He respectfully dedicates this paper to both of their memories.

This research has made use of the International Variable Star Index (VSX) database, operated at AAVSO, Cambridge, Massachusetts, USA, and the SIMBAD database and VizieR catalogue access tool, both operated at CDS, Strasbourg, France.

References

AAVSO. 2014, observations from the AAVSO International Database (http://www.aavso.org).

Alksnis, A. 1981, *Mitt. Veränderliche Sterne*, **9**, 25.

Eglitis, I., Eglite, M., and Balklavs, A. 2003, *Baltic Astron.*, **12**, 353.

Grindlay, J., Tang, S., Simcoe, R., Laycock, S., Los, E., Mink, D., Doane, A., and Champine, G. 2009, in *Preserving Astronomy's Photographic Legacy: Current State and the Future of North American Astronomical Plates*, ASP Conf. Ser. 410, eds. W. Osborn and L. Robbins, Astronomical Society of the Pacific, San Francisco, 101.

Knapp, G., Pourbaix, D., and Jorissen, A. 2001, *Astron. Astrophys.*, **371**, 222.

Lenz, P., and Breger, M. 2005, *Commun. Asteroseismology*, **146**, 53.

Lloyd-Evans, T. 1997, *Mon. Not. Roy. Astron. Soc.*, **286**, 839.

Morgenroth, O. 1936, *Astron. Nach.*, **261**, 261.

Price, S. D., Smith, B. J., Kuchar, T. A., Mizuno, D. R., and Kraemer, K. E. 2010, *Astrophys. J., Suppl. Ser.*, **190**, 203.

Roberts, D. H., Lehar, J., and Dreher, J. W. 1987, *Astron. J.*, **93**, 968.

Stephenson, C. B. 1973, *Publ. Warner Swasey Obs.*, **1**, 1.

Watson, C., Henden, A. A., and Price, C. A. 2014, AAVSO International Variable Star Index (VSX; http://www.aavso.org/vsx).

Willson, L. A. 2000, *Ann. Rev. Astron. Astrophys.*, **38**, 573 .

Zamora, O., Abia, C., Plez, B., Domínguez, I., and Cristallo, S. 2009, *Astron. Astrophys.*, **508**, 909.

Amplitude Variations in Pulsating Yellow Supergiants

John R. Percy
Rufina Y. H. Kim
Department of Astronomy and Astrophysics, University of Toronto, Toronto, ON M5S 3H4, Canada

Received June 12, 2014; revised July 24, 2014; accepted July 24, 2014

Abstract It was recently discovered that the amplitudes of pulsating red giants and supergiants vary significantly on time scales of 20–30 pulsation periods. Here, we analyze the amplitude variability in 29 pulsating *yellow* supergiants (5 RVa, 4 RVb, 9 SRd, 7 long-period Cepheid, and 4 yellow hypergiant stars), using visual observations from the AAVSO International Database, and Fourier and wavelet analysis using the AAVSO's VSTAR package. We find that these stars vary in amplitude by factors of up to 10 or more (but more typically 3–5), on a mean time scale (L) of 33 ± 4 pulsation periods (P). Each of the five subtypes shows this same behavior, which is very similar to that of the pulsating red giants, for which the median L/P was 31. For the RVb stars, the lengths of the cycles of amplitude variability are the same as the long secondary periods, to within the uncertainty of each.

1. Introduction

The amplitudes of pulsating stars are generally assumed to be constant. Those of multi-periodic pulsators may appear to vary because of interference between two or more modes, though the amplitudes of the individual modes are generally assumed to stay constant. Polaris (Arellano Ferro 1983) and RU Cam (Demers and Fernie 1966) are examples of "unusual" Cepheids which have varied in amplitude. The long-term, cyclic changes in the amplitudes of RR Lyrae stars—the Blazhko effect—are an ongoing mystery (Kolenberg 2012), period-doubling being a viable explanation. There are many reports in the literature of Mira stars which have varied systematically in amplitude.

Percy and Abachi (2013) recently reported on a study of the amplitudes of almost a hundred pulsating red giants. They found that, in 59 single-mode and double-mode SR variables, the amplitudes of the modes varied by factors of 2–10 on time scales of 30–45 pulsation periods, on average. Percy and Khatu (2014) reported on a study of 44 pulsating red *supergiants*, and found similar behavior: amplitude variations of a factor of up to 8 on time scales of 18 pulsation periods, on average.

In the present paper, we study the amplitudes of 29 pulsating *yellow* supergiants, including 9 RV Tauri (RV) stars, 9 SRd stars, 7 long-period

Cepheids, and 4 yellow hypergiants. RV Tau stars show alternating deep and shallow minima (to a greater or lesser extent). RVa stars have constant mean magnitude. RVb stars vary slowly in mean magnitude; they have a "long secondary period." SRd stars are semiregular yellow supergiants. Actually, there seems to be a smooth spectrum of behavior from RV to SRd and possibly to long-period Population II Cepheids (Percy *et al.* 2003).

Population I (Classical) Cepheids and yellow hypergiants differ from RV and SRd stars in that they are massive, young stars, whereas the latter two classes are old, lower-mass stars. Classical Cepheids tend to have shorter periods in part because the period is inversely proportional to the square root of the mass. We did not analyze short-period Cepheids because, with visual observations, it is necessary to have much denser coverage (a large number of observations per period) in order to beat down the observational error, which is typically 0.2–0.3 magnitude per observation. Bright short-period Cepheids such as δ Cep should have enough photoelectric photometry, over time, to detect amplitude variations if they exist. We recommend that such a study be carried out. Indeed, Derekas *et al.* (2012) analyzed 600 days of ultra-precise Kepler photometry of the 4.9-day Cepheid V1154 Cyg, and found small, cyclic variations in amplitude on a time scale of tens of pulsation periods. In the present project, we analyzed the prototype Population II Cepheid, W Vir, but the period is short (17.27 days), and the data are sparse, so the results are not very meaningful.

The periods of the yellow hypergiants are poorly defined, partly because the pulsation is semiregular at best, and partly because the light curves are affected by the heavy mass loss and occasional "eruptions" in these stars (e.g. Lobel *et al.* 2004). Furthermore, the periods are so long that the number of cycles of amplitude variation is very poorly determined.

2. Data and analysis

We used visual observations from the AAVSO International Database of the yellow supergiant variables listed in Table 1. See "Notes on Individual Stars," and the last two columns in Table 1 for remarks on some of these. Our data extend for typically 10,000–30,000 days; not all the stars have the same length of dataset. Percy and Abachi (2013) discussed some of the limitations of visual data which must be kept in mind when analyzing the observations and interpreting the results. In particular: some of the stars have pronounced seasonal gaps in the data, which can produce "alias" periods and cause some difficulty in the wavelet analysis.

The data, extending over the range of Julian Date given in Table 1 were analyzed with the AAVSO's VSTAR time-series analysis package (Benn 2013), especially the Fourier (DCDFT) analysis and wavelet (WWZ) analysis routines. The JD range began where the data were sufficiently dense for analysis. The DCDFT routine was used to determine the best period for the JD range used.

It was invariably in good agreement with the literature period; in any case, the results are not sensitive to the exact value of period used. For the RV stars, we used the dominant period: either the "half" period—the interval between adjacent minima—or the "full" period, the interval between deep minima. We found that, whichever of these two periods we used, the value of L/P was the same to within the uncertainty.

Note that, in this paper, we use the term "amplitude" in a general way, to denote the strength of the variation. We actually measure the *semi-amplitude*—the coefficient of a sine curve which would fit the data in the DCDFT analysis; this is what is given in the figures and tables. The full amplitude or range would be the difference between maximum and minimum magnitude.

For the wavelet analysis, the default values were used for the decay constant c (0.001) and time division Δt (50 days). The results are sensitive to the former, but not to the latter. For the WWZ analysis: around each of the adopted periods, we generated the amplitude versus JD graph, and determined the range in amplitude, and the number (N) of cycles of amplitude increase and decrease, as shown in Figures 1 through 10. N can be small and ambiguous (see below), so it is not a precise number.

For a few stars with slow amplitude variations, we checked and confirmed the amplitude variability by using the DCDFT routine to determine the amplitude over sub-intervals of the range of JD chosen. For a few stars, we also repeated the analysis using c = 0.003 and 0.005 as well as 0.001. The results did not change though, for one or two of the stars, the amplitude-JD curves were slightly more scattered when c = 0.005.

3. Results

Table 1 lists the results. It gives the name of the star, the type of variability, the adopted period P in days, the range of JD of the observations, the maximum and minimum amplitude, the number N of cycles of amplitude increase and decrease, the average length L in days of the cycles as determined from the JD range and N, the ratio L/P, a rough measure D of the average density of the light curve relative to the period (1 = densest, 3 = least dense), and a rough measure R of the robustness or reliability of the amplitude versus JD curve (1 = most reliable, 3 = least reliable). The least reliable curves have gaps, much scatter, and are generally the ones that are least dense. The Cepheids tended to be less reliable because of their shorter periods, lower density, and smaller amplitudes. They also tend to be less well-observed visually because observers assume that they are best observed photoelectrically. The yellow hypergiants are moderately reliable in the sense that the data are dense and the amplitude-time graphs are well-defined, but the number of cycles is small, the amplitude is small, and the variability is inherently semi-regular at best. Note that the stars in Table 1 have a wide range of amplitudes and amplitude ranges.

Table 1. Amplitude variability of pulsating yellow supergiants.

Star	*Type*	*P(d)*	*JD Range*	*A Range*	*N*	*L/P*	*D*	*R*
V1302 Aql	YHG	359	2442542–2455368	0.02–0.09	1.5	23.8	2	2
Z Aur	SR/SRd	110.40	2423000–2456651	0.20–0.76	15	20.3	1	1
AG Aur	SRd	96.13	2441000–2456600	0.15–0.78	11	14.8	2	2
U Car	DCEP	38.83	2443617–2456627	0.33–0.63	9	37.2	1	2
IW Car	RVb	71.96	2446037–2456646	0.05–0.24	8	18.4	1	2
l Car	DCEP	35.54	2426096–2456609	0.22–0.42	12	71.5	1	3
V509 Cas	YHG	878	2446923–2456719	0.03–0.06	0.25	44.6	2	2
ρ Cas	YHG	659	2433000–2456723	0.02–0.07	1.35	26.7	1	2
V766 Cen	YHG	871	2446933–2456709	0.09–0.15	0.40	28.1	1	2
TZ Cep	SRd	82.44	2451426–2456635	0.33–0.76	2.2	28.7	2	1
AV Cyg	SRd	87.97	2429012–2456630	0.11–0.57	9	34.9	1	1
DF Cyg	RVb	24.91	2441000–2456600	0.20–0.86	20	31.3	2	1
SU Gem	RVb	24.98	2446000–2456250	0.00–1.35	15	27.4	3	3
UU Her	SRd	44.93	2432000–2456622	0.02–0.18	15	36.5	2	2
AC Her	RVa	37.69	2435500–2456600	0.28–0.49	12.5	44.8	1	2
DE Her	SRd	173.10	2442000–2456622	0.13–0.64	1.5	56.3	1	1
SX Her	SRd	103.50	2425000–2456631	0.08–0.44	6.5	47.0	1	1
RS Lac	SRd	237.57	2427592–2456635	0.35–1.02	3.5	34.9	1	1
SX Lac	SRd	195.48	2446000–2456282	0.10–0.17	3.75	14.0	2	1
T Mon	DCEP	27.03	2441500–2456400	0.28–0.53	15	36.7	1	2
TT Oph	RVa	30.51	2427946–2456615	0.25–0.76	39	24.1	1	2
UZ Oph	RVa	43.71	2445500–2456626	0.20–0.70	9.5	26.8	1	1

Table continued on next page

Table 1. Amplitude variability of pulsating yellow supergiants, cont.

Star	*Type*	*P(d)*	*JD Range*	*A Range*	*N*	*L/P*	*D*	*R*
TX Per	RVa	76.38	2427964–2456654	0.12–0.75	7.5	50.1	2	1
X Pup	DCEP	25.96	2434287–2456416	0.15–1.04	15	56.8	3	3
AI Sco	RVb	35.76	2445000–2455750	0.15–1.10	11	27.3	2	2
W Vir	CWA	17.27	2425000–2456458	0.16–1.29	41	16.3	2	3
S Vul	DCEP	68.30	2439626–2456558	0.10–1.20	11	22.5	3	2
V Vul	RVa	76.31	2446000–2456649	0.20–0.35	6.5	21.5	1	1
SV Vul	DCEP	44.98	2439622–2456637	0.33–0.54	13.5	28.0	1	1

The maximum and minimum amplitudes were determined with due regard to the scatter in the amplitude versus JD curves and the number of points defining each maximum or minimum. The process of counting the number of cycles was somewhat subjective, but was consistent, having been done by co-author Kim using Percy and Abachi (2013) and Percy and Khatu (2014) as a model. Figures 1 and 2 show examples of the process for the RVa star AC Her and the SRd star SX Her and its uncertainty. They also show the difference between the amplitude versus JD curves for a shorter-period star and a longer-period one. One could argue for adding or removing one or two cycles in each case, but the number should be reliable to ±10–20 percent. Figures 3–10 show examples of the amplitude versus JD curves for other representative stars.

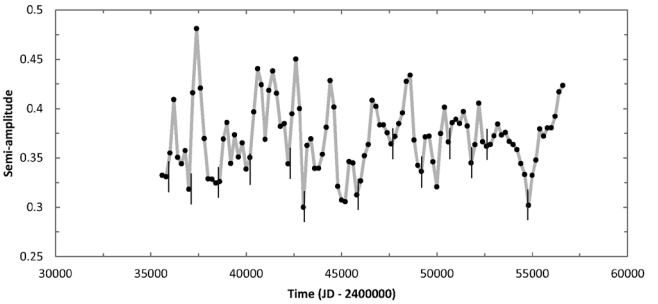

Figure 1. Amplitude versus Julian Date for the RVa star AC Her, showing where we assume the minima to be. We count 12.5 cycles in a JD range of 21100 days, giving a cycle length L of 1688 days, but the uncertainty in doing this is apparent from the graph; one could argue for the addition or removal of one or two maxima or minima. The dominant pulsation period is the "half" period, 37.69 days. Compare this diagram with that for SX Her, which has a longer period.

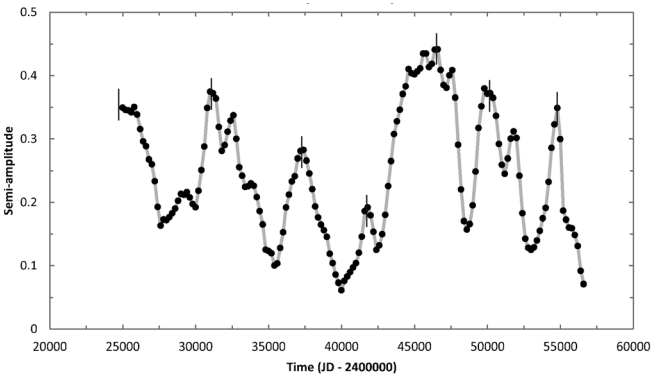

Figure 2. Amplitude versus Julian Date for the SRd star SX Her, showing where we assume the maxima to be. We count 6.5 cycles in a JD range of 31631 days, giving a cycle length L of 4866 days. The uncertainty in doing this is apparent from the graph, but it is less than for AC Her (Figure 1). The pulsation period is 103.50 days.

Table 2. Summary statistics: amplitude variability of pulsating yellow supergiants.

Type	*Mean P (SD)*	*Mean L/P (SEM)*	*Mean D*	*Mean R*
Cepheids	41.09 (14.45)	38.46 (7.38)	1.71	2.29
RVa	52.92 (21.89)	33.45 (5.83)	1.20	1.40
RVb	39.40 (22.30)	26.11 (2.72)	2.00	2.00
SRd	125.72 (2.30)	31.94 (4.75)	1.44	1.22
Hypergiants	700:	31:	1.5	2:
Robust	104.73 (65.12)	32.82 (3.67)	1.33	1.00

Table 2 presents summary statistics for the sub-groups of stars: Cepheids, RVa, RVb, SRd, and hypergiant. Note that the mean L/P is the same, within the standard error of the mean (SEM), for all groups, and is the same as the median L/P (31) for pulsating red giants (Percy and Abachi 2013). The values for the hypergiants are very uncertain, so we have listed only approximate numbers. The last line ("Robust") refers to the stars whose amplitude versus JD curves appear to be the most dependable. Given the uncertainty in the value of L for each star, the uniformity of the *average* values of L/P is most significant.

3.1. Notes on individual stars

These notes are given in the same order as the stars are listed in Table 1. See also the last two columns in Table 1 for information about the denseness of the light curves, and the robustness of the amplitude versus JD curves.

SU Gem: The seasonal gaps are very conspicuous.

AC Her: Figure 1. The increase in amplitude since JD 2455000 is confirmed by the AAVSO photoelectric photometry.

Z Aur: Figure 5. This star shows periods of 112 and 135 days, and switches between them (Lacy 1973). There is some evidence that the amplitude of pulsation decreases before a switch takes place. Period switches occur at the following Julian Dates: 2428000 (112 to 135 days), 2439000 (135 to 112 days), 2443000 (112 to 135 days), and 2448500 (135 to 112 days), with the middle two switches being less distinct.

TZ Cep: Figure 6. The data are sparse since JD 2454200.

DE Her: This star shows 1.5 cycles of a long secondary period, but is classified as SRd rather than RVb.

UU Her: This star switches between periods of 45–46 and 72 days (Zsoldos and Sasselov 1992).

RS Lac: Figure 7. The amplitude variation is apparent from the light curve.

SX Lac: Figure 4. The data are initially sparse.

S Vul: The middle of the dataset is sparse.

V509 Cas: Later in the visual dataset, the dominant period is 259 days. The photoelectric V data, however, show periods between 350 and 500 days.

V1302 Aql: The period is suspiciously close to one year. Furthermore: the data are sparse and the amplitude is small.

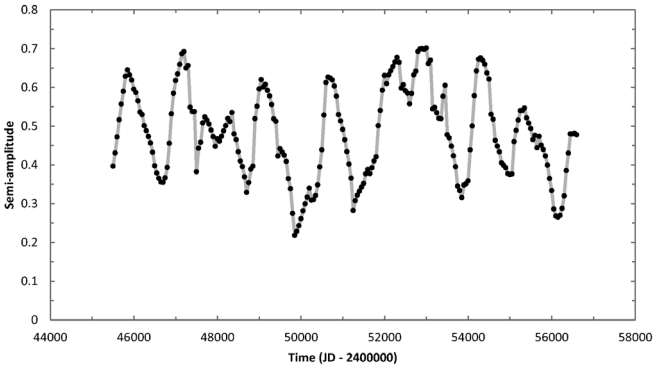

Figure 3. Amplitude versus Julian Date for the RVa star UZ Oph. We count 9.5 cycles. The curve is well-defined. The dominant pulsation period is the "half" period, 43.71 days.

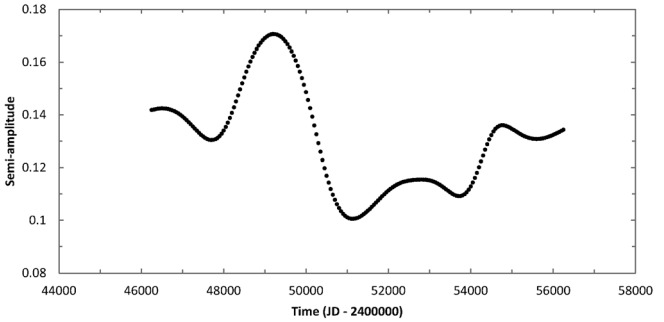

Figure 4. Amplitude versus Julian Date for the SRd star SX Lac. We count 3.75 cycles. The pulsation period is 195.48 days. Compare this graph with e.g. Figure 3 for UZ Oph, a shorter-period star, but note that the amplitude of SX Lac is small, and that presumably adds to the uncertainty in determining N.

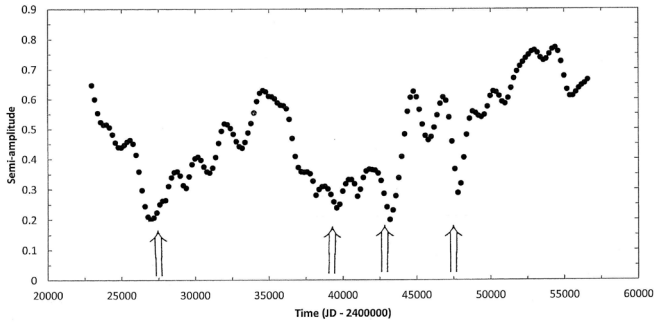

Figure 5. Amplitude versus Julian Date for the SRd star Z Aur. We count 15 cycles. This star is unusual in that its dominant period switches between about 112 and 135 days. The amplitude tends to decrease before period switches, which occured around JD 2428000 (112 to 135 days), 2439000 (135 to 112 days), 2443000 (112 to 135 days), and 2448500 (135 to 112 days), with the middle two switches being less distinct.

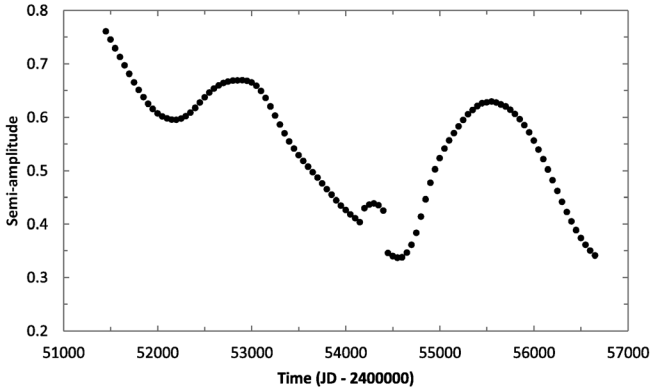

Figure 6. Amplitude versus Julian Date for the SRd star TZ Cep. We count 2.2 cycles. The pulsation period is 82.44 days.

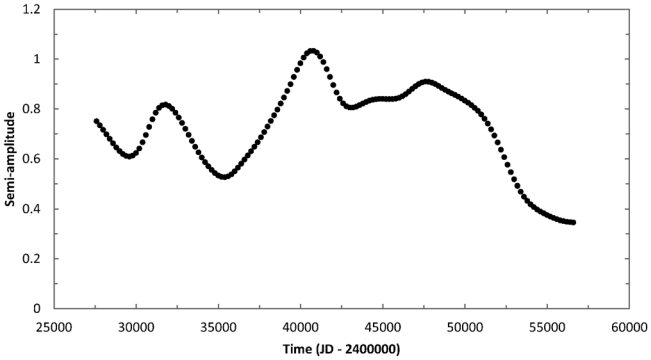

Figure 7. Amplitude versus Julian Date for the SRd star RS Lac. We count 3.5 cycles. The pulsation period is 237.57 days.

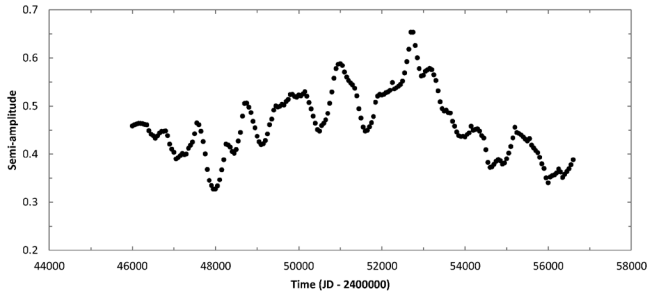

Figure 8. Amplitude versus Julian Date for the Cepheid U Car. We count 9 cycles. There is a slow change in amplitude, as well as the rapid ones. The pulsation period is 38.83 days. The rapid changes in amplitude are relatively small, suggesting that the mechanism which causes them is not dominant in this star.

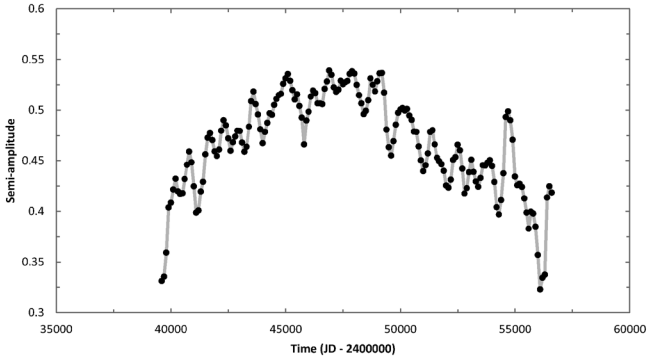

Figure 9. Amplitude versus Julian Date for the Cepheid SV Vul. We count 13.5 cycles. These are small and rapid, and therefore not well defined by our limited visual observations. There is also a slow change in amplitude, with the amplitude being smaller at the beginning of the observing period, larger in the middle, and smaller again at the end. The pulsation period is 44.98 days. The rapid changes in amplitude are relatively small, suggesting that the mechanism which causes them is not dominant in this star.

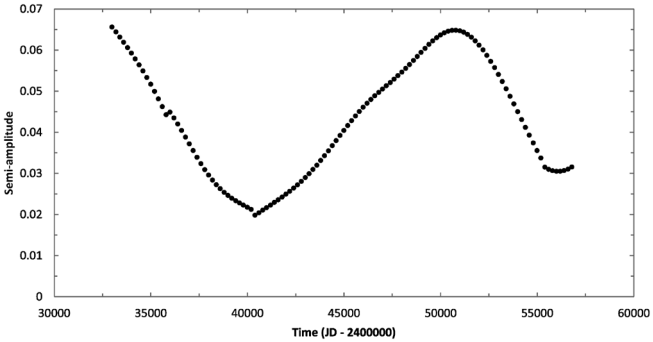

Figure 10. Amplitude versus Julian Date for the yellow hypergiant ρ Cas. We count 1.35 cycles, though this is obviously very uncertain—even more so for the other yellow hypergiants. The adopted pulsation period is 659 days.

4. Discussion

We have found that almost all of the pulsating yellow supergiants that we have studied vary in pulsation amplitude by a factor of up to 10 on a time scale of about 33 ± 4 pulsation periods. The behavior is similar in each of the subtypes of variables, and that behavior is similar to that of pulsating red giants (Percy and Abachi 2013). In particular: the RV Tauri variables showed similar L/P to the other types, whether the half-period or the full period was dominant. These results were pleasantly surprising to us, as we had no *a priori* reason to think that these stars would show amplitude variations or, if so, that these would

be similar to those in red giants and supergiants. In some cases, however, the amplitude variation in these stars is visible in the light curve.

We note that, for the RVb stars, the lengths of the cycles of amplitude variability are the same as the lengths of the long secondary periods, within the uncertainties of each. For SU Gem, L = 683, LSP = 682; for IW Car: L = 1326, LSP = 1430; for DF Cyg: L = 780, LSP = 784; for AI Sco: L = 977, LSP = 975, the units being days in each case. Percy (1993) noted that, during the long secondary minima in the RVb star U Mon, the pulsation amplitude was low. This coincidence between L and LSP may help to elucidate the cause of both the RVb phenomenon and the amplitude variation.

Percy and Abachi (2013) proposed two possible explanations for the amplitude variation in pulsating red giants: (i) the rotation of a star with large inhomogeneities in its photosphere; and (ii) stochastic excitation and decay of pulsations, driven by convection (this possibility was suggested to us by Professor Tim Bedding). Red giants and supergiants are highly convective, and there is evidence (e.g. Kiss *et al.* 2006, Xiong and Deng 2007) that the convection interacts with the pulsation. Cepheid pulsations are excited by the kappa (opacity) mechanism; hydrodynamic models (e.g. Stobie 1969) show that the pulsation amplitude grows until the pulsational energy generation is balanced by dissipation. As for the amplitude *variations*, since yellow supergiants are not expected to show large inhomogeneities in their photospheres, stochastic excitation and decay is the more likely explanation. All of the stars in our sample are cooler than the sun (their (B–V) colors range from +0.9 to +1.8) so they all have significant external convection zones (though some of the stars, especially the yellow hypergiants, may be reddened by dust). We note that, in the long-period Cepheids U Car and SV Vul (Figures 8 and 9), the amplitude fluctuations are relatively small, but there are also slow changes in amplitude as well as the small, rapid ones. Derekas *et al.* (2012) also raised the possibility that convective processes might cause the period and light-curve fluctuations which they observed in V1154 Cyg. In addition to the possibility of stochastic excitation, these stars are subject to possible non-linear effects such as period doubling and chaos (Buchler and Kovacs 1987; Fokin 1994; Buchler *et al.* 1996; Buchler *et al.* 2004).

Amplitude variations complicate the study of these stars in the sense that, to compare photometric behavior with other types of behavior—spectroscopic, for instance—the observations must be made within a few pulsation periods of each other. The AAVSO provides an important service by monitoring many of these stars.

5. Conclusions

We have studied the amplitude variation in 29 pulsating yellow supergiants of several types: RV Tauri stars (RVa and RVb), SRd stars, long-period Cepheids,

and hypergiants. In each case, we find amplitude variations of a factor of up to 10 (but more typically 3–5) on a time scale of 33 pulsation periods. The behavior is similar for each type of star, and is similar to that found by Percy and Abachi (2013) in pulsating red giants.

6. Acknowledgements

This project would not have been possible without the efforts of the hundreds of AAVSO observers who made the observations which were used in this project, and the AAVSO staff who processed and archived the measurements and made them publicly available, and the team which developed the VSTAR package and made it user-friendly and publicly available. We thank the University of Toronto Work-Study Program for financial support, and Professors Tim Bedding and Laszlo Kiss for reading and commenting on a draft of this paper. Author JRP thanks author RYHK, an undergraduate major in Ecology and Evolutionary Biology who, with no previous background in Astronomy, organized and carried out this project so professionally. This project made use of the SIMBAD database, which is operated by CDS, Strasbourg, France.

References

Arellano Ferro, A. 1983, *Astrophys. J.*, **274**, 755.

Benn, D. 2013, VSTAR data analysis software (http://www.aavso.org/node/803 and www.aavso.org/vstar-overview).

Buchler, J. R., Kolláth, Z., and Cadmus, R. R., Jr. 2004, *Astrophys. J.*, **613**, 532.

Buchler, J. R., Kolláth, Z., Serre, T., and Mattei, J. A. 1996, *Astrophys. J.*, **462**, 489.

Buchler, J. R., and Kovács, G. 1987, *Astrophys. J., Lett. Ed.*, **320**, 57.

Demers, S., and Fernie, J. D. 1966, *Astrophys. J.*, **144**, 440.

Derekas, A., *et al.* 2012, *Mon. Not. Roy. Astron. Soc.*, **425**, 1312.

Fokin, A. B. 1994, *Astron. Astrophys.*, **292**, 133.

Kiss, L. L., Szabó, G. M., and Bedding, T. R. 2006, *Mon. Not. Roy. Astron. Soc.*, **372**, 1721.

Kolenberg, K. 2012, *J. Amer. Assoc. Var. Star Obs.*, **40**, 481.

Lacy, C. H. 1973, *Astron. J.*, **78**, 90.

Lobel, A., Stefanik, R. P., Torres, G., Davis, R. J., Ilyin, I., and Rosenbush, A. E. 2004, in *Stars as Suns: Activity, Evolution, and Planets*, eds. A. K. Dupree and A. O. Benz, IAU Symp. 219, Astronomical Society of the Pacific, San Francisco, 903.

Percy, J. R. 1993, in *Non-Linear Phenomena in Stellar Variability* (*Astrophys. Space Sci.*, **210**), eds. M. Takeuti and J.-R. Buchler, IAU Collq. 134, Kluwer Academic Publishers, Dordrecht, The Netherlands, 123.

Percy, J. R., and Abachi, R. 2013, *J. Amer. Assoc. Var. Star Obs.*, **41**, 193.

Percy, J. R., Hosick, J., and Leigh, N. W. C. 2003, *Publ. Astron. Soc. Pacific*, **115**, 59.

Percy, J. R., and Khatu, V. 2014, *J. Amer. Assoc. Var. Star Obs.*, **42**, 1.
Stobie, R. S. 1969, *Mon. Not. Roy. Astron. Soc.*, **144**, 461.
Xiong, D. R., and Deng, L. 2007, *Mon. Not. Roy. Astron. Soc.*, **378**, 1270.
Zsoldos, E., and Sasselov, D. D. 1992, *Astron. Astrophys.*, **256**, 107.

Long-term Secular Changes in the Period of Mira Stars

Thomas Karlsson
Almers väg 19, 432 51 Varberg, Sweden; tkn@seaside.se

Received June 3, 2014; revised October 8, 2014; accepted October 24, 2014

Abstract A possible secular change of the period is investigated for 362 Mira stars. Mean periods and the proportion of stars with increasing and decreasing period were calculated using all available maxima found. The state as it was known in 1938 is compared year by year up until 2013. Analysis of O–C diagrams for the stars shows a rate of change of $+6.8 \times 10^{-6}$ days/day, standard error 3.8×10^{-6}. The mean period over 75 years shows an increase by 0.15 day for the investigated stars, and by 2013 58% of them had an increasing period.

1. Introduction

Mira stars are pulsating red giants with large amplitudes in visual light and periods typically in the range from 100 to over 600 days. In the H-R diagram they are located at the Asymptotic Giant Branch (AGB). There has been a debate about the predominant mode in which Miras pulsate. Recent research now suggests that Miras are fundamental mode pulsators (Willson and Marengo 2012).

Although the pulsation period (P) for a typical Mira is quite regular it features short and long term variations of several kinds. All Miras have small random cycle-to-cycle variations in amplitude, cycle length, and in the shape of their light curves. About 15% also have a meandering behavior where P alters by up to 10% within 50 years (Zijlstra and Bedding 2002), a process not fully understood. Eight stars (R Aql, R Cen, BH Cru, LX Cyg, W Dra, R Hya, Z Tau, and T UMi) are identified as having large period changes (Templeton *et al.* 2005). Those stars either have a continuously increasing or decreasing P over their observed history or have a large sudden change in P after a long time of stability.

The random and meandering behavior has made it difficult to identify long term evolutionary changes in P for individual stars besides the eight stars mentioned above. Sterken *et al.* (1999) found evidence for a linear increase of P for χ Cygni at a rate of $+36 \times 10^{-6}$ days/day over its more than 300-year history. On the other hand, no significant long term change of P for o Ceti seems to have occurred during its over 400 years of recorded history.

The aim of this study is to investigate if a secular change in P can be detected in the available data by averaging a large number of stars with the longest history of observation, and also to see if a longer baseline gives a stronger signal for period changes or if the periods are dominated by random fluctuations at all time scales. The present paper is a follow-up to a similar study made by Percy and Au (1999).

2. Models

Evolutionary models for AGB-stars from Wood and Zarro (1981) and Vassiliadis and Wood (1993) show some interesting features in the supposed evolution of P for AGB-stars.

1) With intervals of ~10^5 years the star goes through a thermal pulse (TP) when accreted helium from hydrogen fusion ignites and for a period of ~10^3 years is the main energy source. The TP causes P to decrease and increase in rapid succession, but after the pulse is over P is reset to a shorter value than before the TP started.

2) Between the TPs hydrogen fusion again takes over as the main energy source. During this phase P slowly increases.

Since the TPs only last for 1–2% of the total time spent in the AGB-phase we would expect a small percentage of the Miras to have a rapidly changing period and the majority to have a period that increases very slowly.

From the models of Vassiliadis and Wood, Percy and Au (1999) estimated the rate of change of P in the intra-TP phase. The average change for a 1 solar mass-star was estimated to be $+29 \times 10^{-6}$ days/day for a star pulsating in the fundamental mode and $+11 \times 10^{-6}$ days/day for a star pulsating in the first overtone.

3. Analysis

In their study Percy and Au analyzed O–C diagrams from Kowalsky *et al.* (1986), data that span 75 years (1900–1975) of observations in the AAVSO International Database, and include 391 long period variables (Mira and SR). They calculated the rate of change from parabolic fits to O–C diagrams and found an average change from all stars of $+17 \times 10^{-6}$ days/day, standard error 10×10^{-6}, and that 55% of the stars had an increasing period.

This analysis is based on a collection of maxima for 489 Mira stars compiled by the author (Karlsson 2013). The collection contains maxima of two types, those computed and fitted by the author to individual observations and those collected from various published sources. For the fitted maxima, data from the organizations AAVSO, AFOEV, VSOLJ, and BAAVSS were used. The published maxima were used to complement these and to extend the baseline backward and fill in gaps among the fitted maxima.

From the original 489 stars those with the longest record were selected. The criterion was that at least twenty maxima before 1938 must exist. Some stars have one or a few very early maxima, sometimes of uncertain or dubious quality, followed by a long gap with no observations. To prevent such outliers

from affecting the results, another criterion was that at least five maxima within twenty cycles must be available at the beginning of the series for each star. If not, the earliest maximum was removed until this criterion was fulfilled. The eight stars with known large period changes, mentioned above, were also removed, as they may be in a TP while the aim of this study is to investigate intra-TP behavior.

For each of the thus-selected 362 stars three different tests were made.

- The mean P was calculated from a linear fit to all maxima for the star.

- An O–C diagram was constructed by using the determined P, and a parabola was fitted to the diagram and the rate of change (β) in days/day was calculated as the coefficient of $E^2 \times 2 / P$, where E is the cycle number.

- The maxima were divided in two halves of equal time and P was calculated for the first and second half by linear fits on both groups.

These calculations were first done with all maxima up to 2013-01-01. Then all maxima for one year, first 2012, then 2011, and so on, were removed and the calculations were repeated until only maxima older than 1938-01-01 remained. This process makes it possible to analyze how P and β develops over time as more data becomes available.

The average time span between the first and last maxima for the 362 stars was 52 years for 1938, and 127 years for 2013.

4. Results

Figure 1 shows, up to each year, the mean and standard error of β from the O–C diagrams. After fluctuating at a much higher level, after 1975 β stabilizes between $+7 \times 10^{-6}$ and $+9 \times 10^{-6}$ days/day. With all maxima, the result for 2013 is the average rate of change $+6.8 \times 10^{-6}$ days/day, standard error 3.8×10^{-6}, a significance level of 1.8σ. The standard deviation for the individual stars is 73×10^{-6}.

Figure 2 shows the frequency distribution of β for 2013 and a comparison with the distribution from Percy and Au (1999). The distribution is more compressed towards the center compared to Percy and Au, probably an effect of the longer timeline used in this study.

Figure 3 shows the relation between β and P. The three stars with the largest rate of change are V Del -520×10^{-6}, Z Sco -390×10^{-6}, and R Nor $+330 \times 10^{-6}$ days/day.

The mean period year by year for the 362 stars is shown in Figure 4. During the 75 years the mean period increases by 0.15 day. For 1938 it was 306.17 days and for 2013 it was 306.32 days.

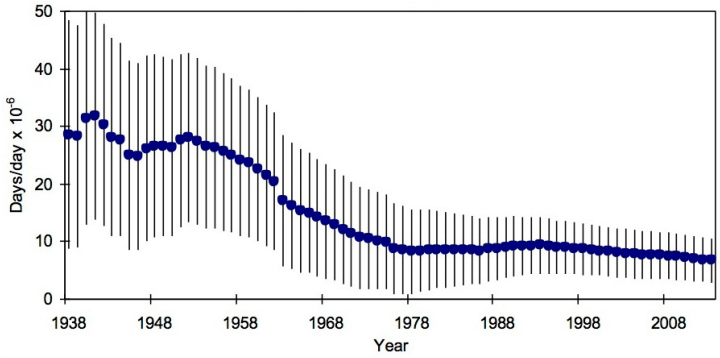

Figure 1. Average rate of change (β) when including maxima up up to specified year. The error bars show the standard error.

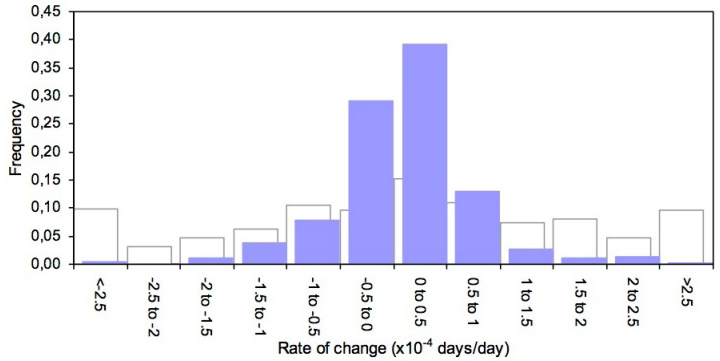

Figure 2. The distribution of β in this study (blue) and the distribution from Percy and Au (1999) (white).

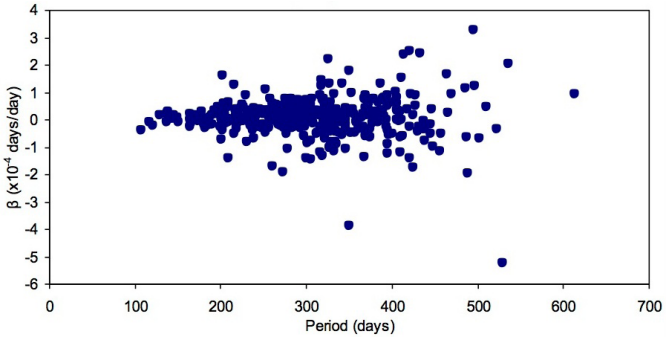

Figure 3. The relation between β and period for the 362 stars.

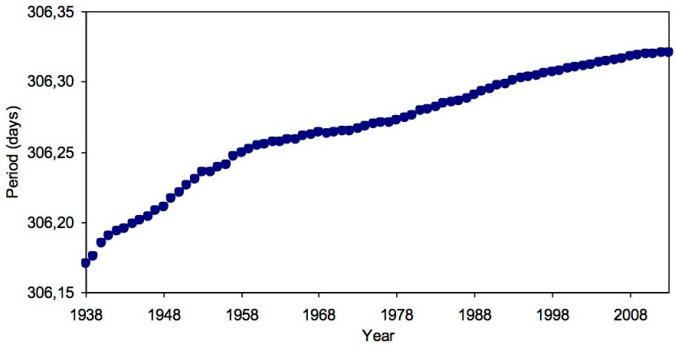

Figure 4. The mean period for the 362 stars when including maxima up to the specified year.

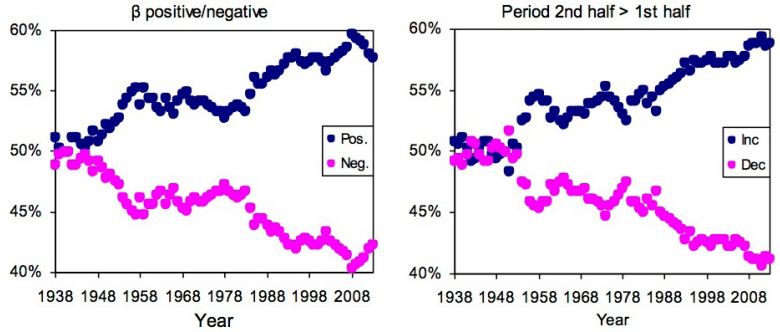

Figure 5. Percentage of stars with increasing/decreasing P up to the specified year. To the left, positive or negative sign of β from the O–C diagrams; to the right, mean P for the second half compared to the first half of each star's series of maxima.

The results from two countings of the number of stars that had an increasing or decreasing P at each year are shown in Figure 5. Figure 5, left panel, shows the proportion with a positive or negative value of β when including all maxima up to the specified year. Figure 5, right panel, shows the proportion with longer or shorter P for the second half compared to the first when dividing the maxima of the stars in two parts of equal length. Both tests shows about the same result. For the early years the proportions are about 50% each. As more maxima are added the proportion of stars with increasing P goes up. For 2013 58% of the stars from the first and 59% from the second test have an increasing P.

5. Discussion

The means and totals from all four tests support the theoretical models that Mira stars in their intra-TP phase can have a slowly increasing period, as well as that the P on shorter time scales, as the 127 years in this study, is dominated by random and meandering features.

The two tests that count the number of stars with increasing or decreasing P show that as more data are added the tendency for increasing P gets stronger. The two tests show for the 1938 case a near-equal distribution of stars having a increasing or decreasing period. 75 years later, 209 of 362 stars have a positive value for β and 213 of 362 have a longer mean period for the second half compared to the first half over their observed history. If the probability would be 0.5 each for the cases of increasing and decreasing period, a pure random distribution of 209 (or more) of 362 would have a probability of 0.13%, which corresponds to a significance level of 3.0σ.

The investigation of β from the O–C diagrams has a lower significance level of 1.8σ (for 2013) for the case of an increasing P, but the rate of change is quite stable, $+7 \times 10^{-6}$ to $+9 \times 10^{-6}$ days/day, over the last 37 of the 75 investigated years. The mean P computed with data up to each year is increasing throughout the whole 75-year interval, although with different paces. The alternate method to compute the rate of change, from a linear fit to the mean periods, gives a change of about $+10 \times 10^{-6}$ days/day.

The spread of the rate of change for the individual stars varies from -520×10^{-6} days/day to $+330 \times 10^{-6}$ days/day, with a standard deviation of 73×10^{-6}. The spread seems to have a normally distributed shape around the mean. There is a weak, but not significant, correlation for stars with longer P to have a larger rate of change, from $+4 \times 10^{-6}$ days/day for a star with a P of 100 days to $+11 \times 10^{-6}$ days/day for a star with a P of 600 days.

Percy and Au determined the mean value for β to be twice as large as the value in this analysis. The significance levels are about the same in both studies. For the percentage of stars with a positive value of β Percy and Au got 55%. This is lower than the 58% in this analysis, but it is from only 75 years of data compared to 127 years. At 75 years of data in this analysis (at 1962) the percentage of stars with positive β was 54%. The difference in value of β between the two studies may to some extent depend on the fact that Percy and Au in their study also included SR stars and did not exclude the stars with known large period changes.

The rate of change of P in this analysis is on the order of the value estimated by Percy and Au (1999) from the models of Vassiliadis and Wood (1993) for a one solar mass AGB-star pulsating in the first overtone, but it is four times lower than the estimated value for a star pulsating in the fundamental mode from the same models. It is, however, unknown how the 362 analyzed stars' masses and evolutionary phases compare to the star used in the models or how accurate the models themselves are. Consequently it is hard to say to what degree the results contradict the information, reviewed by Willson and Marengo (2012), that Mira stars are predominantly fundamental mode pulsators.

6. Acknowledgements

Many thanks to Gustav Holmberg and Hans Bengtsson for their help in reviewing this text.

References

Karlsson, T. 2013, *J. Amer. Assoc. Var. Star Obs.*, **41**, 348.
Kowalsky, P. A., Percy, J. R., Mattei, J. A., and Waagen, E. O. 1986, *J. Amer. Assoc. Var. Star Obs.*, **15**, 236.
Percy, J. R., and Au, W. W.-Y. 1999, *Publ. Astron. Soc. Pacific*, **111**, 98,
Sterken, C., Broens, E., and Koen, C. 1999, *Astron. Astrophys.*, **342**, 167.
Templeton, M. R., Mattei, J. A., and Willson, L. A. 2005, *Astron. J.*, **130**, 776.
Vassiliadis, E., and Wood, P. R. 1993, *Astrophys. J.*, **413**, 641.
Willson, L. A., and Marengo, M. 2012, *J. Amer. Assoc. Var. Star Obs.*, **40**, 516.
Wood, P. R., and Zarro, D. M. 1981, *Astrophys. J.*, **247**, 247.
Zijlstra, A. A., and Bedding, T. R. 2002, *J. Amer. Assoc. Var. Star Obs.*, **31**, 2.

EQ Eridani, a Multiperiodic δ Scuti Star

Roy Andrew Axelsen
P.O. Box 706, Kenmore, Queensland 4069, Australia; reaxelsen@gmail.com

Received May 24, 2014; revised August 8, 2014; accepted August 11, 2014

Abstract DSLR photometry of the δ Scuti star EQ Eridani (HD 28665) was undertaken on six nights between 2 November and 8 December 2013. Comparison and check stars were HD 28508 and HD 28901, respectively. Inspection of the light curves revealed an irregular pattern and variation in amplitude that signified the presence of two or more periods. Fourier analysis using the software PERIOD04 yielded at least three pulsation frequencies of 14.3663, 11.6862, and 7.2128 cycles per day, corresponding to periods of 0.0696, 0.0856, and 0.1386 day, respectively. The first of these frequencies is very close to the period of 0.0700 day listed in a catalogue of δ Scuti stars published in 2000. This is the first report of multiperiodicity in EQ Eri. None of the period ratios fall within the range of 0.74–0.78 expected for the ratio of the first overtone to the fundamental mode of δ Scuti stars pulsating in the radial mode.

1. Introduction

Koen and Roberts (1993) reported the star HD 28665 to be a δ Scuti pulsator with a frequency of 15.136 cycles per day (period 1.58 hours) and a semi-amplitude of 0.049 magnitude. Koen *et al.* (1995) later reported a frequency of 14.2 cycles per day and an amplitude in V of approximately 0.1 magnitude. The catalogue of stars published by Rodríguez *et al.* (2000) lists EQ Eri as having a period of 0.0700 d, with no mention of other periods, and an amplitude in V of 0.1 magnitude. Because of the paucity of published studies of EQ Eri, it was decided to investigate its light curve utilizing DSLR photometry and Fourier analysis.

2. Observations

DSLR photometry reduction was performed on RAW images taken with a Canon EOS 500D DSLR camera imaging through a refracting telescope with an aperture of 80mm at f/7.5, mounted on a Losmandy GM8 German equatorial mount. A total of 680 magnitude determinations, transformed to the Johnson V system, were obtained during a cumulative observing time of 35.07 hours. The shortest observing run for one night was 3.38 hours, and the longest 7.54 hours, including short gaps in the data due to meridian flips and intermittent cloud. Photometric data reduction from instrumental magnitudes

utilized the software package AIP4WIN. The comparison and check stars were HD 28508 and HD 28901, respectively. Transformed magnitudes in V were calculated using transformation coefficients for the blue and green channels of the DSLR sensor, obtained from images of standard stars in the E regions (Menzies *et al.* 1989).

3. Analysis

Inspection of the light curves revealed an irregular shape and varying amplitude, indicating that the star has two or more periods. Fourier analysis using the software PERIOD04 revealed several frequencies of pulsation, which are shown in Figure 1. The first three frequencies (with standard errors in brackets), 14.3663 (±0.0002), 11.6862 (±0.0004), and 7.2128 (±0.0006) cycles per day, are each associated with a single peak in the Fourier spectra, but other adjacent peaks are seen, among which are peaks representing one cycle per day aliasing, as would be expected from data obtained at one geographic site. A fourth frequency of low amplitude, 11.0935 (±0.0009) cycles per day (Figure 1d), differed in amplitude (and power) by very little from adjacent close frequencies, and because of this it is not considered to be a proven real frequency of pulsation.

The standard errors of the above frequencies are assigned by the software PERIOD04. They represent uncertainties in the frequencies uncorrelated with amplitudes and phases, and apply to "an ideal case." It is therefore considered that they may be optimistic.

The periods corresponding to the above frequencies are 0.0696, 0.0856, and 0.1386 day, respectively.

Figure 2 shows the light curves from the six nights of observation, the fitted functions using the three frequencies noted above, and their corresponding amplitudes and phases from PERIOD04.The fit is considered sufficiently close to explain most of the irregularity of the light curves.

EQ Eri has been recognized as a δ Scuti variable star since the publication of Koen and Roberts (1993), who reported a frequency of 15.136 cycles per day, which corresponds to a period of 0.0661d. This frequency was derived from observations made over 1.9 hours, with the light curve in their Figure 1 showing only thirteen data points. The light curve showed two peaks, with the earliest of the measurement apparently being just after the first peak.

Koen *et al.* (1995) obtained data on EQ Eri over 4.5 hours, with the light curve in their Figure 10 exhibiting a variation in amplitude that implies more than one frequency of pulsation, although the authors do not mention this possibility. They reported a frequency of 14.2 cycles per day, which corresponds to a period of 0.0704d.

The catalogue of δ Scuti stars published by Rodriguez (2000) quotes the period as 0.0700d, as seen in the Vizier Catalogue (CDS 2014).

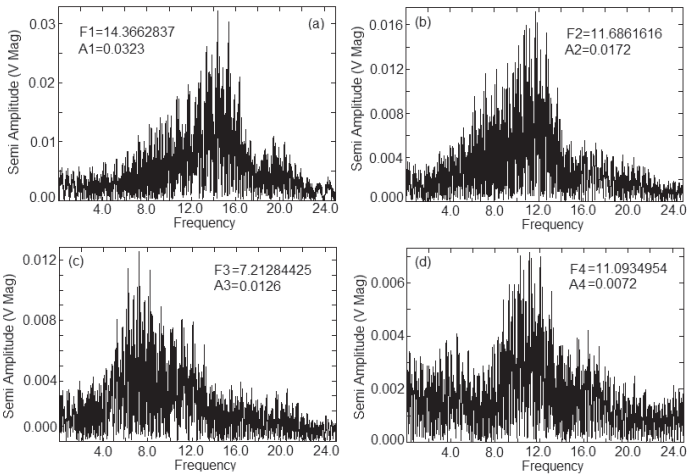

Figure 1. Periodograms of EQ Eri, showing the first four frequencies (F1 to F4) and corresponding amplitudes (actually, semi-amplitudes) (A1 to A4) revealed by the software PERIOD04. The first three frequencies (F1 to F3) appear to represent relatively isolated peaks, although other nearby peaks are seen, including those representing 1 cycle/day aliasing. The fourth frequency (F4) is so closely associated with nearby peaks that it is not considered to be a proven frequency of pulsation.

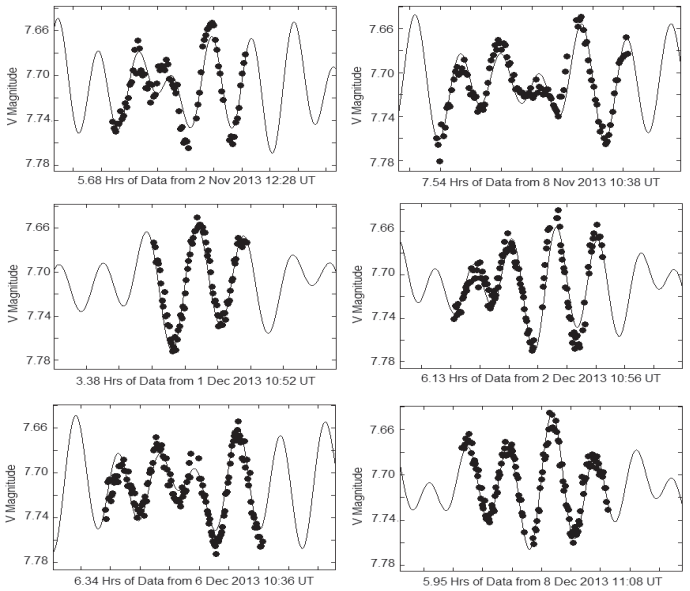

Figure 2. Light curves of EQ Eri obtained on each of the six nights on which measurements were made. The continuous lines associated with the data points represent the function fitted by PERIOD04 from the the first three frequencies shown in Figure 1, calculated from the frequencies themselves and their respective amplitudes and phases.

The present study revealed a principal frequency of 14.366 cycles per day, which corresponds to a period of 0.0696 day, very close to the period of 0.0700 day of Rodriguez (2000). Minor differences between previously published frequencies could perhaps be accounted for by the small datasets of the previous publications not providing a long enough baseline to accurately establish the primary frequency.

Although only one period is reported in the literature, the data presented in this paper suggest that EQ Eri is multiperiodic, with at least three frequencies being identified by Fourier analysis. Although the amplitude of pulsation is only 0.1 magnitude, and although there are limitations to the precision of photometry achievable in low amplitudes with the sensor of a DSLR camera in time series photometry, we believe that the fitted function from Fourier analysis is sufficiently close to the actual measured magnitudes to consider that the assumption of multiperiodicity is valid. It would, however, be more optimal to repeat the present study using a longer baseline and equipment capable of achieving higher precision in the determination of magnitudes.

For δ Scuti stars pulsating in the radial mode, the ratio of the first overtone to the fundamental mode should lie in the range 0.74 to 0.78 (Breger 1979). None of the period ratios which can be calculated from the present results fall within that range, implying that the star is not a purely radial pulsator oscillating in the fundamental and first overtone modes. The relationships between astrophysical parameters which determine the periods of δ Scuti stars are complex, and their detailed analysis is beyond the resources of the present author. In view of this, no definitive interpretation of the nature of the oscillations in EQ Eri can be provided in this paper. It is noted, however, that the period ratio of 0.8134 for the first and second periods from our data is close to the value of 0.810 listed by Breger (1979) in his Table II for the ratio of the second overtone to the first overtone, in a typical δ Scuti star with radial pulsation.

4. Conclusions

It is proposed that the present paper provides evidence for at least three frequencies of pulsation in EQ Eri, and if this conclusion is correct, it is a new discovery. However, the conclusion is based on analysis of data from only six nights of observation, and it would appear likely that a more extensive dataset collected from a larger number of observing runs might improve the quality of the results. Furthermore, the amplitude of each of the discovered frequencies is less than 0.1 magnitude in V, for which the precision of DSLR time series photometry is not entirely optimal. Ideally, CCD images (rather than images from a DSLR camera) should be used, in order to improve the precision of the photometry, provided that a sufficiently large field of view could be achieved, and that exposures could be long enough to avoid scintillation errors, as EQ Eri is a seventh magnitude star.

Another issue is that one cycle per day aliasing in the Fourier analysis is clearly evident, as would be expected for data collected at one geographic site. Since aliasing is recognized as a complicating factor in the analysis of data from δ Scuti stars with two or more frequencies, it would be appropriate to try to design a program of data collection at two or more geographic sites to reduce the number of alias peaks, and thereby enhance the ability of Fourier analysis to recognized true frequencies of oscillation.

References

Breger, M. 1979, *Publ. Astron. Soc. Pacific*, **91**, 5.

Centre de Données astronomiques de Strasbourg (CDS). 2014, Vizier Catalogue J/A+AS/144/469/ (http://vizier.u-strasbg.fr/viz-bin/VizieR).

Koen, C., and Roberts, G. 1993, *Inf. Bull. Var. Stars*, No. 3830, 1.

Koen, C., Kilkenny, D., van Wyk, F., Roberts, G., and Marang, F. 1995, *Mon. Not. Roy. Astron. Soc.*, **277**, 217.

Menzies, J. W., Cousins, A. W. J., Banfield, R. M., and Laing, J. D. 1989, *S. Afr. Astron. Obs. Circ.*, **13**, 1.

Rodríguez, E., López-González, M. J., and López de Coca, P. 2000, *Astron. Astrophys., Suppl. Ser.*, **144**, 469.

Current Light Elements of the δ Scuti Star V393 Carinae

Roy Andrew Axelsen
P. O. Box 706, Kenmore, Queensland 4069, Australia; reaxelsen@gmail.com

Received May 1, 2014; revised July 1, 2014; accepted July 1, 2014

Abstract V393 Carinae is a 7th magnitude δ Scuti star which has a principal period of 0.1413 d and an amplitude of 0.2 magnitude in V. Previous publications have suggested the existence of a second period, but its duration has so far evaded discovery. In view of the uncertainty, and since the only two papers on this star were published in 1984 and 2001, DSLR photometry was performed to obtain time series data. Images were taken during 6 nights from December 2013 to March 2014. The data were analyzed using a discrete Fourier transform, which yielded a principal frequency of 7.07727 (±0.00005) cycles/day, corresponding to a period of 0.141297 (±0.000001) day. Prewhitening for this frequency revealed a harmonic frequency precisely twice that of the principal, but no further dominant frequencies could be found. O–C diagrams suggested that it would appropriate to derive a new linear ephemeris from three times of maximum obtained by another author from 1977 to 1979, combined with the 6 new times of maximum reported in this paper. The light elements are: T_{max} = HJD 2456732.0484 (6) + 0.14129328 (1). It is concluded that the current principal period of this star is almost identical to the period determined approximately 37 years ago. The issue of a second period is unresolved. None was detected, but it cannot be excluded that a second pulsation frequency of low amplitude could be hidden due to a low signal to noise ratio.

1. Introduction

V393 Car is a δ Scuti star with an average magnitude in V of 7.45, an amplitude of 0.2 magnitude, and a period of 0.1413 d, or 3 hours, 23 minutes approximately. The first detailed study of this star was published by Helt in 1984 (hereafter referred to as Helt). She performed uvby photoelectric photometry from 1977 to 1979, determined its principal period, and considered that there was strong evidence of a second period of lower amplitude. The second frequency could not be isolated, but its most likely value was stated to be either 12.58 or 13.58 cycles per day. Helt determined the light elements to be:

$$\text{HJD } 2443597.001\ (1) + 0.1412937\ (2)\ E \qquad (1)$$

The only other detailed study of this star was published by Garcia *et al.* in 2001 (hereafter referred to as Garcia), who performed CCD photometry and used a discrete Fourier transform to calculate a period of 0.1462828 (2) d,

which is 7.18 minutes longer than the period calculated by Helt about 23 years earlier. Garcia suggested that a phase shift had occurred, and that the phase shift supported the existence of a second period, although it could not be identified directly.

2. Observations

DSLR photometry was performed on RAW images taken with a Canon EOS 500D DSLR camera through a refracting telescope with an aperture of 80 mm at f/7.5, mounted on a Losmandy GM8 German equatorial mount. Exposures were of two minutes duration, with a gap of fifteen seconds between successive exposures. The comparison and check stars were HD 65578 and HD 66656, respectively. Photometric reduction of images of the star field, dark frames, and flat fields utilized the software package AIP4WIN (Berry and Burnell 2011). Raw instrumental magnitudes were calculated, and differential photometry allowed the calculation of transformed magnitudes in V of the variable and check stars, using transformation coefficients previously determined from images of standard stars from the E Region (Menzies *et al.* 1989). 778 measurements of the magnitude of the variable star were made over six nights from 21 December 2013 to 22 March 2014.

3. Analysis

Figure 1 is an example of a light curve from one night's observations. The heliocentric correction was calculated for the mid point in time of the observations for any one night, and applied to the times of all measurements for that night.

Six times of maximum in heliocentric Julian days were identified from regions around the peaks in the light curves, calculated from sixth-order polynomial functions fitted to the light curve segments by the software program PERANSO (Vanmunster 2013).

A discrete Fourier transform in the software program PERIOD04 (Lenz and Breger 2005) was used to examine the frequency of pulsation of the star (Figure 2). A principal frequency of 7.07727 (± 0.00005) cycles/day was found (Figure 2a), and after pre-whitening for that frequency a second frequency, 14.155 cycles/day, was identified (Figure 2b), but since it is almost exactly twice the principal frequency it represents a Fourier harmonic of that frequency. After pre-whitening again, no further dominant frequency could be identified (Figure 2c). The principal frequency, 7.07727 cycles/day, represents a period of 0.141297 (± 0.000001) day. This period is only 0.33 second longer than the period of 0.1412937 (± 0.0000002) d determined by Helt from observations made from 1977 to 1979.

In view of these results, a series of O–C (observed minus computed) diagrams were constructed to investigate the relationships among the data of

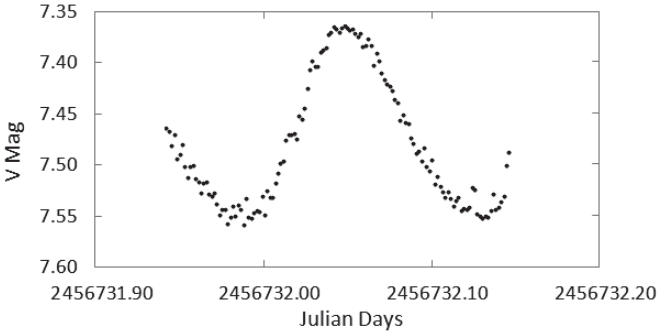

Figure 1. Example of a light curve of V393 Car derived from a single night's observations.

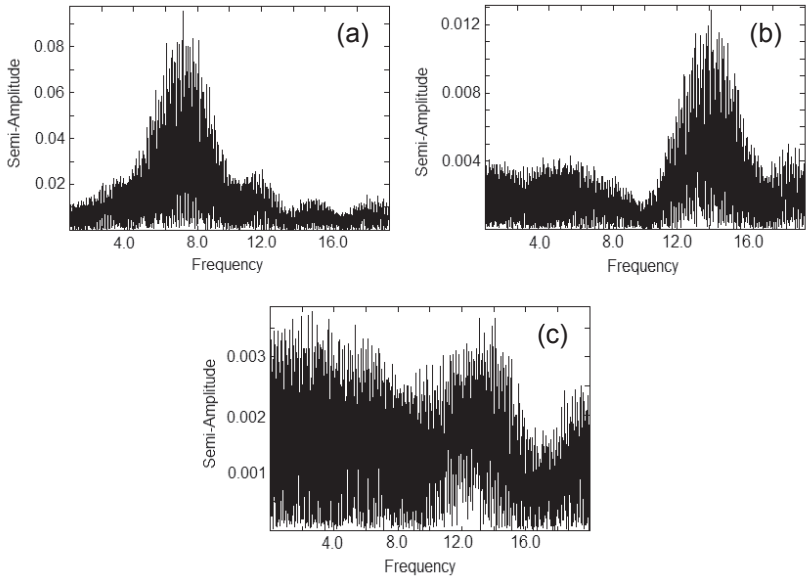

Figure 2 (a–c). Periodograms of V393 Car from a discrete Fourier transform in the software package PERIOD04 (Lenz and Breger 2005). (a) The principle frequency is 7.07727 c/d. (b) After prewhitening for the principle frequency, a second frequency 14.155 c/d is found, but as this is almost exactly twice the principle frequency, it represents a Fourier harmonic. (c) After further prewhitening, no additional dominant fequency could be found.

Helt, Garcia, and the author of this paper. For the calculation of the epochs and the O–C values, the initial period and the initial time of maximum chosen were those of Helt, with zero epoch being the first time of maximum determined by her.

The values for the O–C diagrams and the published sources of the data are listed in Table 1, and the O–C diagrams themselves are shown in Figure 3. The diagram in Figure 3a at the top left represents an attempt to apply a linear

Table 1. Data for O–C diagrams.

Max	T_{max} *(HJD)*	*Epoch*[1]	*O–C*	*Source*[2]
1	2443403.85220	0	0.00000	1
2	2443778.84730	2654	0.00162	1
3	2443939.63770	3792	–0.00021	1
4	2451953.73100	60511	0.05572	2
5	2456647.97863	93735	–0.03854	3
6	2456669.17052	93885	–0.04070	3
7	2456675.10847	93927	–0.03709	3
8	2456700.96365	94110	–0.03866	3
9	2456705.06099	94139	–0.03884	3
10	2456732.05019	94330	–0.03673	3

1. The initial epoch at HJD 2443403.8522 and the initial period 0.1412937 d for the calculation of the epochs and the O–C values were those of Helt. 2. The sources of the values of the times of maximum—T_{max} (HJD) in the 2nd column—are listed in the 5th column: 1. Helt (1984); 2. Garcia (2001); 3. Present paper.

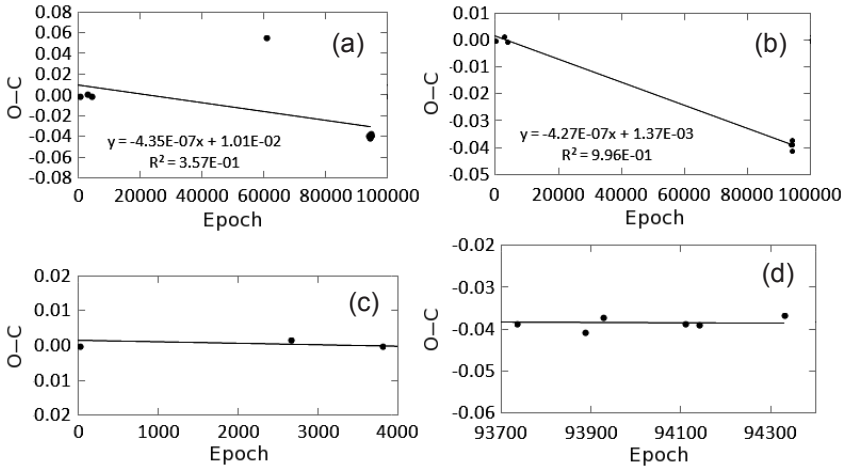

Figure 3 (a–d). O–C diagrams for V393 Carinae. All of the diagrams use the period and the time of maximum of Helt (1984) for the calculations of the epochs and the O–C values. (a) Based on the data of Helt (1984), Garcia (2001), and this paper, and using data from all eight rows of Table 1. The linear fit is not ideal. (b) Based on the data of Helt and the author of this paper, and using data from rows 1 to 3 and rows 5 to 10 of Table 1. The linear fit, as would be expected, passes through both sets of data. (c) Same as Figure 3b, but showing only part of the diagram, with only the data of the Helt being visible; i.e., it is a "zoomed in" view of the earlier part of the O–C diagram in Figure 3b. (d) Same as Figure 3b, but showing only part of the diagram, with only the data from the present paper being visible; i.e., it is a "zoomed in" view of the later part of the O–C diagram in Figure 3b.

function to the times of maximum of Helt, Garcia, and our own data, but the linear function is not an ideal fit. Figure 3b at the top right shows a linear function fitted to the data of Helt and our own data, which (as would be expected) passes through both sets of data. Figure 3c at the bottom left represents a small part of the diagram in Figure 3b, after "zooming in" to the data of Helt. Figure 3d at the bottom right also shows only a small part of the diagram in Figure 3b, after "zooming in" to the data of the present author. It is clear from Figures 3c and 3d that the linear function passing through the two sets of data is a good fit to both. It is our opinion that this result is evidence that the period of V393 Car now is almost identical to the period investigated by Helt 37 years ago.

In view of the results of the O–C analysis, it was concluded that it would be reasonable to calculate a new linear ephemeris for V393 Car by combining our own data with those of Helt. When that is done, with the most recent of our own observations (row 10 in Table 1) nominated as zero epoch, the light elements are:

$$T_{max} = \text{HJD } 2456734.0484\ (6) + 0.14129328\ (1)\,E \qquad (2)$$

Finally, the various determinations of the period of V393 Car from the literature and our own calculations are summarized in Table 2.

Table 2. The period of V393 Car, from the literature and from calculations performed during the present study.

Source	*Period (d)*	*SE**
Helt 1984	0.1412937	0.0000002
Discrete Fourier transform, Garcia 2001	0.1462828	0.0000002
Discrete Fourier transform, this paper	0.141297	0.000001
Linear ephemeris, Helt 1984 and this paper	0.14129328	0.00000001

** The value for the period from the linear ephemeris of Helt 1984 and this paper (last row of table) employed a least squares linear function to the times of maximum 1–3 and 5–10 from table 1, plotted against epoch.*

4. Conclusions

The only publications dealing with the period of V393 Car have been those of Helt in 1984 and Garcia in 2001. Helt's data were obtained during 1977–1979, 36–38 years ago, and Garcia's data were obtained in the year of publication. The period calculated from our own observations using a discrete Fourier transform is 0.141297 d, only 0.33 second longer than Helt's period of 0.1412937 d. In contrast, the period of 0.1462828 d determined by Garcia is 7.18 minutes shorter than Helt's, a dramatic change for a δ Scuti star over

approximately 23 years. In the presence of such differences, O–C diagrams were used to analyze the times of maximum of this star.

When all of the data in the literature are combined in an O–C diagram, a linear function does not provide an ideal fit, as is seen in Figure 3a. When our own data are combined with those of Helt (with Garcia's 2001 data omitted for the purposes of this particular analysis), a linear function is found to provide a good fit (Figures 3c and 3d). In view of the latter result, it was considered reasonable to derive a new linear ephemeris for V393 Car based on Helt's data combined with our own. The validity of that decision would be supported if observations in future observing seasons, using methods similar to those of the present paper, showed no significant change in the period of this star.

If the maximum of Helt at HJD 2443403.8522 is taken as zero epoch (in September 1977), the phase shift for Garcia's best time of maximum at HJD 2451953.731 (in February 2001) is 0.05572 day. The average phase shift between our own data between HJD 2456647.97863 and HJD 2456732.05019 (between January and March 2014) and that of Helt is –0.0384 day. The average phase shift between our own data and the best maximum of Garcia is –0.0941. The other issue is the question of a second period. Helt stated with conviction that a second period existed, but its frequency could not be determined precisely. Garcia reported finding a phase change in 2001, and cited this as evidence of a second period, but again it could not be isolated. New observations reported in the present paper again failed to find a second period, but if it does exist, it would appear to be of low amplitude. This conclusion is supported by the periodogram in Figure 3c, in which the semi-amplitude of remaining (non-dominant) frequencies after prewhitening is 0.0035–0.0040 magnitude, too small to be resolved by the sensor of the DSLR camera used in the present study.

References

Berry, R., and Burnell, J. 2011, "Astronomical Image Processing for Windows," version 2.4.0, provided with *The Handbook of Astronomical Image Processing*, Willmann-Bell, Richmond, VA.

Garcia, J. R., Busso, V. A., and Sosa, G. F. 2001, *J. Amer. Assoc. Var. Star Obs.*, **30**, 44.

Helt, B. E. 1984, *Astron. Astrophys., Suppl. Ser.*, **56**, 457.

Lenz, P., and Breger, M. 2005. *Commun. Asteroseismology*, **146**, 53 (http://www.univie.ac.at/tops/Period04/).

Menzies, J. W., Cousins, A. W. J., Banfield, R. M., and Laing, J. D. 1989, *S. Afr. Astron. Obs. Circ.*, **13**, 1.

Vanmunster, T. 2013, Light Curve and Period Analysis Software, PERANSO v.2.50 (http://www.peranso.com/).

AL Pictoris and FR Piscium: Two Regular Blazhko RR Lyrae Stars

Pierre de Ponthière
15 Rue Pré Mathy, Lesve, Profondeville 5170, Belgium; address email correspondence to pierredeponthiere@gmail.com

Franz-Josef (Josch) Hambsch
12 Oude Bleken, Mol, 2400, Belgium

Kenneth Menzies
318A Potter Road, Framingham, MA 01701

Richard Sabo
2336 Trailcrest Drive, Bozeman, MT 59718

Received June 25, 2014; revised July 16, 2014; accepted July 17, 2014

Abstract The results presented are a continuation of observing campaigns conducted by a small group of amateur astronomers interested in the Blazhko effect of RR Lyrae stars. The goal of these observations is to confirm the RR Lyrae Blazhko effect and to detect any additional Blazhko modulation which cannot be identified from all sky survey data-mining. The Blazhko effect of the two observed stars is confirmed, but no additional Blazhko modulations have been detected.

The observation of the RR Lyrae star AL Pictoris during 169 nights was conducted from San Pedro de Atacama (Chile). From the observed light curve, 49 pulsation maxima have been measured. Fourier analyses of (O–C), magnitude at maximum light (M_{max}), and the complete light curve have provided a confirmation of published pulsation and Blazhko periods, 0.548622 and 34.07 days, respectively. The second multi-longitude observation campaign focused on the RR Lyrae star FR Piscium and was performed from Europe, the United States, and Chile. Fourier analyses of the light curve and of 59 measured brightness maxima have improved the accuracy of pulsation and Blazhko periods to 0.45568 and 51.31 days, respectively. For both stars, no additional Blazhko modulations have been detected.

1. Introduction

The data-mining of automated sky surveys like the All Sky Automated Survey—ASAS (Wils and Sódor 2005) and the Northern Sky Variability Survey—NSVS (Wils *et al.* 2006) is frequently used to discover new RR Lyrae stars, to measure their pulsation periods, and for some of them to detect and measure Blazhko modulation. Automated sky surveys with their low

sampling frequencies (at best one sample per night) generate sparse datasets. As a result, spectral analysis of the datasets is not always fully reliable. Some Blazhko modulation periods are published as uncertain and multiple Blazhko modulations are not always detected. To overcome those shortcomings, more observations of identified RR Lyrae stars are required. Detailed study of long time-series observations allows the identification of individual brightness maxima of the light curve and other light curve details. Spectral analysis of the rich time-series is able to characterize the Blazhko modulation(s) in detail.

The results of observing campaigns presented herein are related to two RR Lyrae stars exhibiting the Blazhko effect, AL Pic and FR Psc, discovered from ASAS and NSVS surveys, respectively (Wils and Sódor 2005 and Wils *et al.* 2006).

The designation of AL Pic appeared in the *General Catalogue of Variable Stars* with the 79th Name List of Variable Stars (Kazarovets *et al.* 2008); previously this star was identified as GSC 8082-0469, NSV 1700, and ASAS J044131-5216.6. From the All Sky Automated Survey database, Wils and Sódor (2005) measured a pulsation period of 0.54861 day and also a Blazhko period of 34.0 days. The results presented herein are derived from data gathered during 169 nights between July 17, 2012, and February 1, 2013. A total of 17,416 magnitude measurements covering 5.8 Blazhko cycles were collected. All the observations were made by Franz-Josef Hambsch, remotely using a 40-cm f/6.8 telescope located in San Pedro de Atacama (Chile).

The designation of FR Psc appeared in the *General Catalogue of Variable Stars* with the first part of 80th Name List of Variable Stars (Kazarovets *et al.* 2011). This star was previously identified as GSC 0607-0591 and NSVS 9149730. From the Northern Sky Variability Survey data (Wozniak *et al.* 2004), Wils *et al.* (2006) have measured a pulsation period of 0.45570 day and an uncertain Blazhko period of 55 days. Our observations were made between August 18, 2012, and December 30, 2013. During the 126 observation nights, a total of 12,653 observations were made by Franz-Josef Hambsch remotely from Cloudcroft (New Mexico) and San Pedro de Atacama (Chile), by Richard Sabo from Bozeman (Montana), Kenneth Menzies from Framingham (Massachusetts) and Pierre de Ponthière from Lesve (Belgium). The numbers of observations for the different locations are 3597, 7272, 1106, 146, and 532, respectively.

For images of both stars, dark and flat field corrections were performed with MAXIMDL software (Diffraction Limited 2004), and aperture photometry was performed using LESVEPHOTOMETRY (de Ponthière 2010), a custom software which also evaluates the SNR and estimates magnitude errors. The photometric observations of both stars are available in the AAVSO International Database (AAVSO 2014).

AL Pic observations were performed with only a V filter and are not transformed to the standard system. The comparison stars are given in Table 1;

their coordinates and magnitudes in B and V bands were obtained from the AAVSO's Variable Star Database (VSD). The observations have been reduced with C1 as a magnitude reference and C2 as a check star.

The observations of FR Psc were also performed with a V filter and are not transformed to the standard system.

The FR Psc comparison star coordinates and magnitudes in B and V bands were extracted from the AAVSO APASS survey and are given in Table 8. All observations, except from Cloudcroft, were reduced with C1 as magnitude reference and C2 as check star. Cloudcroft observations were reduced with C2 and C3 as reference and comparison stars. A correction of 0.021 magnitude has been applied to the Cloudcroft observations. This correction has been calculated from the magnitude difference of C3 when measured with C1 and C2 as magnitude references.

2. Light curve maxima analyses

The times of maxima of the light curves have been evaluated with custom software (de Ponthiere 2010), fitting the light curve with a smoothing spline function (Reinsch 1967).

2.1. AL Pic

A total of 49 maxima have been observed for AL Pic. Table 2 provides the list of the observed maxima and Figure 1 shows the (O–C) and M_{max} (magnitude at maximum) values. A linear regression of all available (O–C) values has provided a pulsation period of 0.548549 d (1.822858 d^{-1}). The (O–C) values have been re-evaluated with this new pulsation period and the pulsation ephemeris origin has been set to the highest recorded brightness maximum: HJD 2456154.7560. The new derived pulsation elements are:

$$HJD_{Pulsation} = (2456154.7560 \pm 0.0080) + (0.548549 \pm 0.000044)\, E_{Pulsation} \quad (1)$$

The derived pulsation period is in good agreement with the value of 0.54861 published by Wils and Sódor (2005). The folded light curve on the newly determined pulsation period is shown in Figure 2.

To determine the Blazhko period, Fourier analyses and sine-wave fittings of the (O–C) values and M_{max} (magnitude at maximum) values were performed with PERIOD04 (Lenz and Breger 2005). These analyses were limited to the three first harmonic components and are given in Table 3. The frequency uncertainties have been evaluated from the Monte Carlo simulation module of PERIOD04. The Blazhko periods obtained from (O–C) and M_{max} are 34.23 ± 0.12 and 34.03 ± 0.07 days, respectively, which are in reasonable agreement. On this basis the best Blazhko ephemeris is

$$HJD_{Blazhko} = 2456154.75 + (34.03 \pm 0.07)\, E_{Blazhko} \quad (2)$$

The origin has been selected as the epoch of the highest recorded maximum. The (O–C) and M_{max} curves folded with this Blazhko period are given in Figure 3. The variations of (O–C) and M_{max} over the Blazhko cycles are 0.097 day and 0.639 magnitude, respectively.

Table 1. AL Pic comparison stars.

Identification	*R.A. (2000)* *h m s*	*Dec. (2000)* *° ′ ″*	*B*	*V*	*B–V*	*Reference Star*
GSC 8082-440	04 40 50.7	–52 22 27.4	12.608	12.006	0.602	C1
GSC 8082-564	04 42 14.3	–52 23 12.9	13.252	12.590	0.662	C2

Table 2. AL Pic measured maxima.

Maximum HJD	*Error*	*O–C (day)*	*E*	*Magnitude (V)*	*Error*
2456144.8755	0.0060	–0.0059	–18	13.2840	0.015
2456149.8190	0.0027	0.0003	–9	12.9820	0.012
2456150.9137	0.0020	–0.0022	–7	12.9020	0.010
2456154.7560	0.0030	0.0000	0	12.8060	0.011
2456155.8556	0.0026	0.0024	2	12.8710	0.011
2456160.7891	0.0040	–0.0014	11	13.1290	0.012
2456161.8840	0.0048	–0.0037	13	13.1720	0.013
2456167.8557	0.0049	–0.0664	24	13.3320	0.014
2456172.7790	0.0085	–0.0804	33	13.3760	0.019
2456177.7657	0.0059	–0.0310	42	13.3250	0.015
2456182.7317	0.0030	–0.0023	51	13.0730	0.012
2456183.8278	0.0043	–0.0034	53	13.0180	0.026
2456188.7707	0.0035	0.0022	62	12.8800	0.014
2456189.8658	0.0020	0.0001	64	12.8810	0.013
2456221.6849	0.0028	0.0010	122	12.8660	0.015
2456222.7875	0.0022	0.0065	124	12.8970	0.013
2456226.6283	0.0038	0.0071	131	13.0180	0.015
2456233.7125	0.0038	–0.0403	144	13.2920	0.016
2456234.8038	0.0068	–0.0462	146	13.3650	0.021
2456239.7063	0.0053	–0.0810	155	13.3470	0.017
2456240.8087	0.0079	–0.0758	157	13.4140	0.018
2456244.7041	0.0071	–0.0205	164	13.4160	0.017
2456245.8124	0.0048	–0.0094	166	13.3930	0.014
2456249.6738	0.0057	0.0119	173	13.1860	0.025
2456250.7666	0.0029	0.0075	175	13.1350	0.015
2456254.6044	0.0028	0.0052	182	12.8370	0.014
2456255.7034	0.0029	0.0070	184	12.8530	0.017

Table continued on next page

Table 2. AL Pic measured maxima, cont.

Maximum HJD	*Error*	*O–C (day)*	*E*	*Magnitude (V)*	*Error*
2456256.8042	0.0023	0.0106	186	12.8680	0.02
2456259.5492	0.0034	0.0127	191	12.9610	0.018
2456261.7435	0.0029	0.0126	195	13.0910	0.018
2456265.5621	0.0043	–0.0089	202	13.2590	0.014
2456266.6495	0.0055	–0.0187	204	13.2920	0.02
2456272.6187	0.0052	–0.0839	215	13.3530	0.015
2456273.7370	0.0085	–0.0628	217	13.4330	0.021
2456277.6083	0.0064	–0.0316	224	13.4250	0.013
2456278.7047	0.0043	–0.0324	226	13.4300	0.009
2456283.6765	0.0031	0.0021	235	13.1350	0.016
2456288.6169	0.0024	0.0052	244	12.8560	0.007
2456289.7104	0.0019	0.0015	246	12.8240	0.015
2456293.5592	0.0018	0.0102	253	12.9820	0.006
2456294.6572	0.0026	0.0110	255	13.0200	0.007
2456295.7542	0.0068	0.0108	257	13.1420	0.033
2456299.5782	0.0050	–0.0053	264	13.2820	0.016
2456300.6648	0.0034	–0.0159	266	13.2850	0.008
2456301.7665	0.0112	–0.0114	268	13.3850	0.021
2456305.5711	0.0153	–0.0469	275	13.4250	0.025
2456307.7435	0.0092	–0.0688	279	13.4450	0.015
2456317.6883	0.0043	0.0014	297	13.1820	0.013
2456321.5373	0.0040	0.0102	304	12.9370	0.021

Table 3. AL Pic Blazhko spectral components from light curve maxima.

From	*Frequency (cycle/days)*	*σ(d^{-1})*	*Period (days)*	*σ(d)*	*Amplitude*	*Φ (cycle)*	*SNR*
(O–C) values	0.02922	10×10^{-5}	34.23	0.12	0.037 day	0.758	21.1
M_{max} values	0.02939	6×10^{-5}	34.025	0.07	0.270 mag.	0.207	36.9

Table 4. AL Pic triplet component frequencies and periods.

Component	*Derived from*	*Frequency (d^{-1})*	*σ (d^{-1})*	*Period (d)*	*σ (d)*
f_0		1.822749	4.5×10^{-6}	0.548622	1.4×10^{-6}
f_B	f_0+f_B	0.029353	13×10^{-6}	34.07	0.02

Table 5. AL Pic multi-frequency fit results.

Component	*f*(d^{-1})	*σ(f)*	A_i *(mag.)*	$\sigma(A_i)$	Φ_i *(cycle)*	$\sigma(\Phi_i)$	*SNR*
f_0	1.822749	4.5×10^{-6}	0.2790	0.0007	0.5947	0.0005	99.8
$2f_0$	3.645498		0.0972	0.0008	0.5489	0.0013	38.5
$3f_0$	5.468248		0.0512	0.0007	0.4973	0.0022	22.3
$4f_0$	7.290997		0.0321	0.0008	0.4488	0.0033	14.5
$5f_0$	9.113746		0.0197	0.0007	0.4206	0.0065	11.2
$6f_0$	10.936495		0.0117	0.0008	0.3931	0.0102	7.4
$7f_0$	12.759244		0.0075	0.0007	0.3313	0.0167	5.3
$8f_0$	14.581993		0.0051	0.0007	0.2765	0.0215	4.3
f_0+f_b	1.852103	13×10^{-6}	0.1090	0.0007	0.9100	0.0012	39.1
f_0-f_b	1.793396		0.1006	0.0007	0.9945	0.0012	35.9
$2f_0+f_b$	3.674852		0.0797	0.0007	0.9162	0.0015	31.5
$2f_0-f_b$	3.616145		0.0703	0.0007	0.9495	0.0017	27.9
$3f_0+f_b$	5.497601		0.0504	0.0007	0.9529	0.0023	22.0
$3f_0-f_b$	5.438894		0.0460	0.0008	0.9602	0.0027	20.0
$4f_0+f_b$	7.320350		0.0271	0.0007	0.9422	0.0044	12.3
$4f_0-f_b$	7.261643		0.0233	0.0007	0.9605	0.0053	10.5
$5f_0+f_b$	9.143099		0.0129	0.0007	0.8866	0.0100	7.3
$5f_0-f_b$	9.084393		0.0142	0.0008	0.8988	0.0083	8.0
$6f_0+f_b$	10.965848		0.0102	0.0008	0.8041	0.0125	6.5
$6f_0-f_b$	10.907142		0.0107	0.0008	0.8459	0.0125	6.8
$7f_0+f_b$	12.788598		0.0073	0.0007	0.7938	0.0157	5.1

Table 6. AL Pic harmonic, triplet amplitudes, ratios, and asymmetry parameters.

i	A_i/A_1	A_i^+/A_1	A_i^-/A_1	R_i	Q_i
1	1.00	0.39	0.36	1.08	0.04
2	0.35	0.29	0.25	1.13	0.06
3	0.18	0.18	0.16	1.10	0.05
4	0.12	0.10	0.08	1.16	0.08
5	0.07	0.05	0.05	0.91	–0.05
6	0.04	0.04	0.04	0.95	–0.03
7	0.03	0.03	—	—	—
8	0.02	—	—	—	—

Table 7. AL Pic Fourier coefficients over Blazhko cycle.

Ψ (cycle)	A_1 (mag.)	A_2 (mag.)	A_3 (mag.)	A_4 (mag.)	Φ_1 (rad.)	Φ_{21} (rad.)	Φ_{31} (rad.)	Φ_{41} (rad.)
0.0–0.1	0.444	0.212	0.134	0.071	3.297	2.501	5.225	1.596
0.1–0.2	0.376	0.167	0.086	0.049	3.593	2.543	5.340	1.978
0.2–0.3	0.286	0.120	0.063	0.036	3.504	2.522	5.232	1.625
0.3–0.4	0.235	0.095	0.034	0.021	4.462	2.798	5.394	2.124
0.4–0.5	0.209	0.096	0.041	0.021	4.446	2.433	5.305	1.913
0.5–0.6	0.235	0.078	0.032	0.023	4.554	2.482	5.319	1.765
0.6–0.7	0.205	0.083	0.035	0.015	3.459	2.204	4.660	1.182
0.7–0.8	0.285	0.125	0.072	0.028	3.877	2.177	4.841	1.023
0.8–0.9	0.362	0.192	0.116	0.080	3.422	2.508	5.310	1.685
0.9–1.0	0.421	0.223	0.156	0.099	3.350	2.461	5.217	1.623

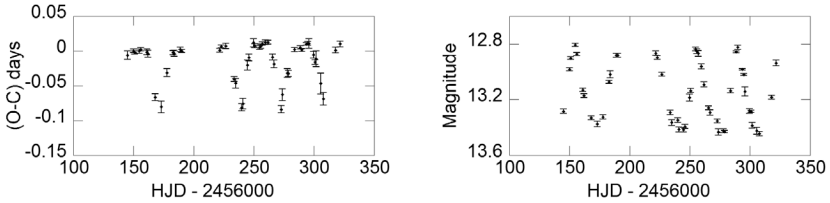

Figure 1. AL Pic O–C (days, left plot) and magnitude at maximum (right plot).

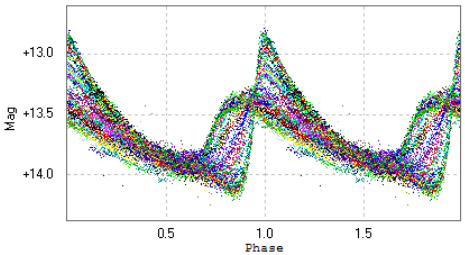

Figure 2. AL Pic light curve folded with pulsation period.

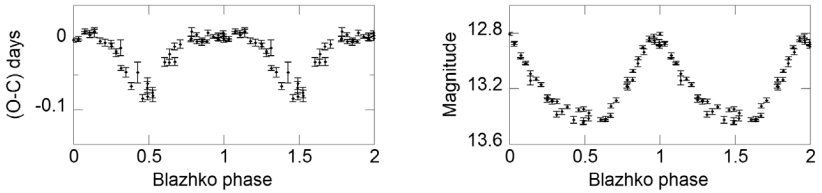

Figure 3. AL Pic O–C (left plot) and Magnitude at maximum (right plot) folded with Blazhko period.

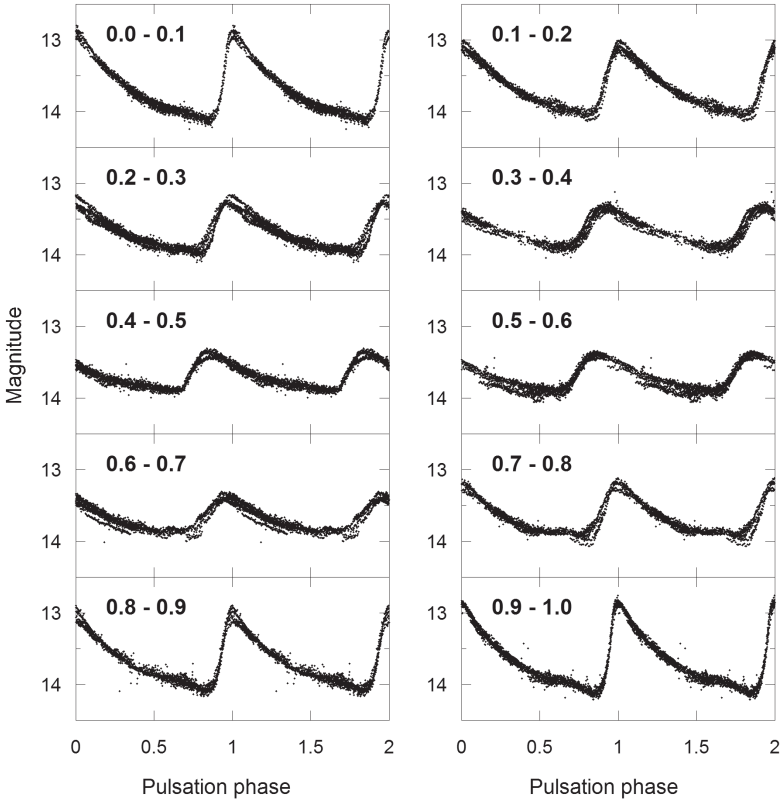

Figure 4. AL Pic light curves (magnitude vs. pulsation phase) for the ten temporal subsets based on Blazhko period.

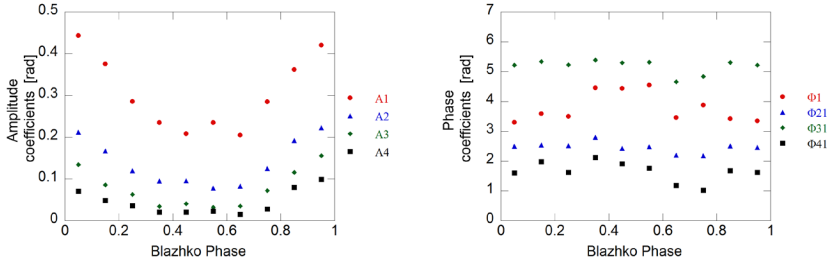

Figure 5. Al Pic Fourier amplitude (left plot) and phase coefficients (mag., right plot) for the ten temporal subsets based on a Blazhko period.

2.2. FR Psc

For FR Psc, the 59 observed maxima are listed in Table 9 and the graphs of (O–C) and M_{max} values versus time (HJD) are given in Figure 6. A pulsation period of 0.4555800 d (2.1945223 d^{-1}) was derived from a linear regression of the (O–C) values. The (O–C) values have been re-evaluated with this new pulsation period and the pulsation ephemeris origin has been set to the highest recorded brightness maximum: HJD 2456631.5796. The new derived pulsation elements are:

$$HJD_{Pulsation} = (2456631.5796 \pm 0.0021) + (0.4556800 \pm 0.0000042)\, E_{Pulsation} \quad (3)$$

The calculated pulsation period is very close to the value of 0.45570 day published by Wils *et al.* (2006). The Blazhko amplitude and phase modulations are clearly visible in Figure 7, which presents the graph of the light curve folded with the pulsation period.

The Blazhko period has been measured with PERIOD04 in the same way as for AL Pic. The results are given in Table 10. The Blazhko periods, from (O–C) and M_{max} are 51.32 ± 0.05and 51.35 ± 0.09 days, respectively, and agree within the errors. The Blazhko period of 55 days reported as uncertain by Wils *et al.* (2006) is slightly longer and not compatible with our improved results. The best Blazhko ephemeris is:

$$HJD_{Blazhko} = 2456631.58 + (51.32 \pm 0.05)\, E_{Blazhko} \quad (4)$$

The (O–C) and M_{max} curves folded with the Blazhko period are given in Figure 8. The (O–C) and M_{max} curves are anti-correlated and their shapes are very similar to the corresponding curves of AL Pic. The variations of (O–C) and M_{max} over the Blazhko cycles are 0.042 day and 0.396 magnitude, respectively.

Table 8. FR Psc comparison stars (AAVSO chart 8256CED).

Identification	*R.A. (2000)* *h m s*	*Dec. (2000)* *° ′ ″*	*B*	*V*	*B–V*	*Reference Star*
GSC 607-409	00 47 35.6	11 47 09.1	12.347	11.657	0.690	C1
GSC 607-679	00 47 54.0	11 42 16.4	14.017	13.310	0.707	C2
GSC 607-799	00 47 57.4	11 41 45.2	14.837	14.237	0.600	C3

Table 9. FR Psc measured maxima.

Maximum HJD	*Error*	*O–C (day)*	*E*	*Magnitude (V)*	*Error*	*Location**
2456158.5795	0.0020	–0.0042	–1038	11.639	0.010	1
2456159.4882	0.0045	–0.0069	–1036	11.629	0.013	1
2456192.7269	0.0051	–0.0328	–963	11.691	0.009	4
2456195.9113	0.0048	–0.0382	–956	11.682	0.045	4
2456202.7678	0.0055	–0.0169	–941	11.738	0.017	4
2456203.6806	0.0026	–0.0154	–939	11.708	0.016	4
2456205.9714	0.0049	–0.0030	–934	11.703	0.017	4
2456213.7200	0.0024	–0.0010	–917	11.477	0.014	4
2456214.6314	0.0014	–0.0010	–915	11.414	0.011	4
2456218.7341	0.0028	0.0006	–906	11.360	0.036	4
2456219.6433	0.0019	–0.0015	–904	11.343	0.010	4
2456259.7407	0.0031	–0.0040	–816	11.635	0.026	4
2456261.5653	0.0023	–0.0021	–812	11.564	0.014	4
2456264.7575	0.0024	0.00034	–805	11.493	0.017	4
2456265.6685	0.0019	–0.00002	–803	11.456	0.013	4
2456270.6801	0.0018	–0.00090	–792	11.357	0.011	4
2456540.4398	0.0014	–0.00379	–200	11.503	0.008	1
2456546.8092	0.0013	–0.01391	–186	11.659	0.005	2
2456546.8095	0.0016	–0.01361	–186	11.685	0.009	5
2456547.7192	0.0023	–0.01527	–184	11.678	0.006	2
2456551.8039	0.0040	–0.03169	–175	11.721	0.014	2
2456556.8141	0.0040	–0.03397	–164	11.724	0.017	5
2456560.4719	0.0037	–0.02161	–156	11.713	0.009	1
2456566.8696	0.0021	–0.00343	–142	11.668	0.010	5
2456567.7806	0.0035	–0.00379	–140	11.636	0.005	2
2456568.6969	0.0025	0.00115	–138	11.607	0.006	2
2456571.8873	0.0003	0.00179	–131	11.538	0.004	5
2456572.8007	0.0013	0.00383	–129	11.484	0.004	2
2456573.7104	0.0014	0.00217	–127	11.471	0.005	2
2456574.6216	0.0018	0.00201	–125	11.418	0.005	2
2456578.7206	0.0010	–0.00011	–116	11.374	0.005	2
2456588.7447	0.0011	–0.00098	–94	11.441	0.005	2
2456589.6550	0.0013	–0.00204	–92	11.480	0.005	2
2456589.6557	0.0007	–0.00134	–92	11.507	0.005	5
2456592.8414	0.0012	–0.00540	–85	11.584	0.005	5
2456593.7524	0.0015	–0.00576	–83	11.574	0.006	2
2456594.6623	0.0013	–0.00722	–81	11.623	0.006	3
2456594.6635	0.0022	–0.00602	–81	11.587	0.008	2
2456595.5729	0.0021	–0.00798	–79	11.636	0.003	2
2456599.6659	0.0016	–0.01610	–70	11.685	0.004	2

Table continued on next page

Table 9. FR Psc measured maxima, cont.

Maximum HJD	*Error*	*O–C (day)*	*E*	*Magnitude (V)*	*Error*	*Location**
2456600.5695	0.0019	–0.02386	–68	11.694	0.004	2
2456604.6661	0.0038	–0.02838	–59	11.703	0.005	2
2456605.5741	0.0025	–0.03174	–57	11.704	0.005	2
2456607.3937	0.0035	–0.03486	–53	11.711	0.007	1
2456609.6729	0.0030	–0.03406	–48	11.713	0.008	2
2456614.7092	0.0021	–0.01024	–37	11.708	0.010	2
2456615.6255	0.0030	–0.00530	–35	11.709	0.010	2
2456616.5376	0.0024	–0.00456	–33	11.681	0.010	2
2456619.7317	0.0008	–0.00022	–26	11.614	0.005	5
2456620.6441	0.0019	0.00082	–24	11.575	0.009	2
2456621.5584	0.0029	0.00376	–22	11.556	0.013	2
2456625.6577	0.0012	0.00194	–13	11.414	0.006	2
2456626.5695	0.0017	0.00238	–11	11.420	0.009	2
2456631.5796	0.0012	0.00000	0	11.342	0.015	2
2456636.5929	0.0016	0.00082	11	11.373	0.011	2
2456641.6030	0.0014	–0.00156	22	11.491	0.008	2
2456647.5211	0.0014	–0.00730	35	11.628	0.006	2
2456657.5222	0.0027	–0.03116	57	11.738	0.008	3

** Locations: 1—Lesve (Belgium); 2—Bozeman (Montana); 3—Framingham (Massachusetts); 4—Cloudcroft (New Mexico); 5—San Pedro de Atacama (Chile).*

Table 10. FR Psc Blazhko spectral components from light curve maxima.

From	*Frequency (cycle/days)*	*σ(d^{-1})*	*Period (days)*	*σ(d)*	*Amplitude*	*Φ (cycle)*	*SNR*
(O–C) values	0.01948	2×10^{-5}	51.324	0.053	0.015 day	0.948	33.1
M_{max} values	0.01947	3×10^{-5}	51.353	0.087	0.193 mag.	0.428	21.0

Table 11. FR Psc Triplet component frequencies and periods.

Component	*Derived from*	*Frequency (d^{-1})*	*σ (d^{-1})*	*Period (d)*	*σ (d)*
f_0		2.1945066	1.3×10^{-6}	0.4556833	2.7×10^{-7}
f_B	f_0+f_B	0.019490	6.1×10^{-6}	51.31	0.016

Table 12. FR Psc multi-frequency fit results.

Component	*f(d^{-1})*	*σ(f)*	*A_i (mag.)*	*σ(A_i)*	*Φ_i (cycle)*	*σ(Φ_i)*	*SNR*
f_0	2.194507	6.7×10^{-7}	0.4261	0.0011	0.1956	0.0004	252.2
$2f_0$	4.389014		0.1768	0.0011	0.7527	0.0011	139.5
$3f_0$	6.583521		0.0901	0.0010	0.3300	0.0019	77.9
$4f_0$	8.778028		0.0379	0.0010	0.9201	0.0039	34.8
$5f_0$	10.972536		0.0121	0.0009	0.3977	0.0138	11.9
$6f_0$	13.167043		0.0111	0.0008	0.8574	0.0147	13.1
$7f_0$	15.361550		0.0115	0.0010	0.3822	0.0175	16.3
$8f_0$	17.556057		0.0103	0.0010	0.9469	0.0177	17.0
$9f_0$	19.750564		0.0087	0.0010	0.5409	0.0182	13.2
f_0+f_b	2.213999	30×10^{-7}	0.0731	0.0011	0.7259	0.0019	43.7
f_0-f_b	2.175015		0.0664	0.0010	0.3003	0.0026	39.2
$2f_0+f_b$	4.408506		0.0627	0.0009	0.2775	0.0025	49.4
$2f_0-f_b$	4.369522		0.0591	0.0011	0.8392	0.0026	46.5
$3f_0+f_b$	6.603013		0.0608	0.0010	0.8647	0.0024	52.6
$3f_0-f_b$	6.564030		0.0543	0.0011	0.4355	0.0034	46.9
$4f_0+f_b$	8.797520		0.0391	0.0009	0.4688	0.0048	35.8
$4f_0-f_b$	8.758537		0.0357	0.0011	0.0446	0.0045	32.7
$5f_0+f_b$	10.992027		0.0264	0.0011	0.0512	0.0061	26.1
$5f_0-f_b$	10.953044		0.0216	0.0010	0.6616	0.0069	21.3
$6f_0+f_b$	13.186535		0.0161	0.0010	0.6491	0.0090	19.0
$6f_0-f_b$	13.147551		0.0122	0.0010	0.2430	0.0158	14.4
$7f_0+f_b$	15.381042		0.0087	0.0011	0.2217	0.0168	12.4
$7f_0-f_b$	15.342058		0.0065	0.0010	0.8239	0.0263	9.2
$8f_0+f_b$	17.575549		0.0040	0.0011	0.7335	0.0424	6.6
$8f_0-f_b$	17.536565		0.0022	0.0011	0.3048	0.0793	3.7

Table 13. FR Psc harmonic, triplet amplitudes, ratios, and asymmetry parameters.

i	*A_i/A_1*	*A_i^+/A_1*	*A_i^-/A_1*	*R_i*	*Q_i*
1	1.00	0.17	0.16	1.10	0.05
2	0.41	0.15	0.14	1.06	0.03
3	0.21	0.14	0.13	1.12	0.06
4	0.09	0.09	0.08	1.09	0.05
5	0.03	0.06	0.05	1.23	0.10
6	0.03	0.04	0.03	1.32	0.14
7	0.03	0.02	0.02	1.34	0.14
8	0.02	0.01	0.01	1.80	0.29
9	0.02	—	—	—	—

Table 14. FR Psc Fourier coefficients over Blazhko cycle.

Ψ (cycle)	A_1 (mag.)	A_2 (mag.)	A_3 (mag.)	A_4 (mag.)	Φ_1 (rad.)	Φ_{21} (rad.)	Φ_{31} (rad.)	Φ_{41} (rad.)
0.0–0.1	0.496	0.234	0.159	0.084	3.977	2.276	4.728	1.092
0.1–0.2	0.462	0.211	0.134	0.068	4.149	2.311	4.792	1.151
0.2–0.3	0.441	0.179	0.106	0.054	3.766	2.357	4.850	1.197
0.3–0.4	0.409	0.173	0.093	0.044	4.379	2.322	4.822	1.201
0.4–0.5	0.394	0.170	0.098	0.050	4.540	2.324	4.897	1.207
0.5–0.6	0.390	0.161	0.094	0.047	4.646	2.309	4.934	1.222
0.6–0.7	0.402	0.163	0.082	0.038	4.437	2.282	4.929	1.409
0.7–0.8	0.418	0.180	0.087	0.035	4.200	2.304	4.767	1.021
0.8–0.9	0.456	0.212	0.132	0.068	4.082	2.238	4.629	0.921
0.9–1.0	0.491	0.240	0.170	0.108	3.979	2.273	4.712	1.046

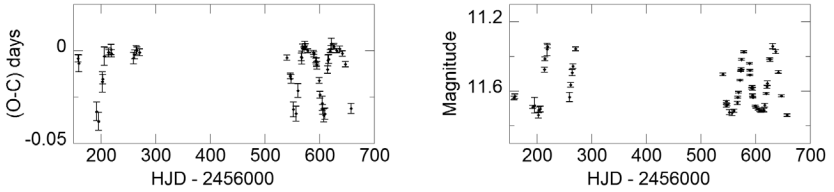

Figure 6. FR Psc O–C (days, left plot) and magnitude at maximum (right plot).

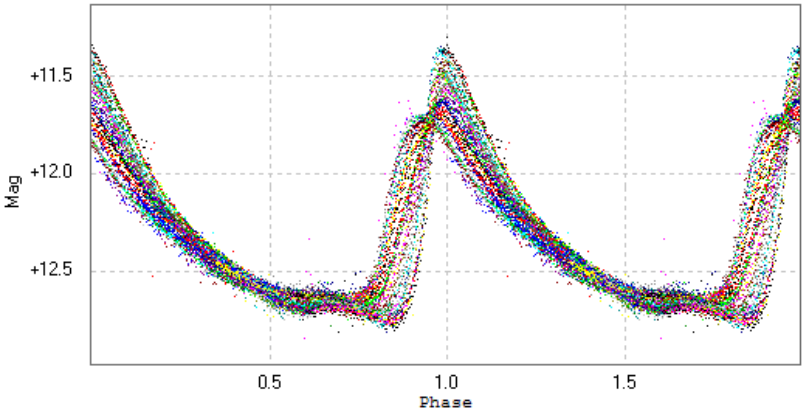

Figure 7. FR Psc light curve folded with pulsation period.

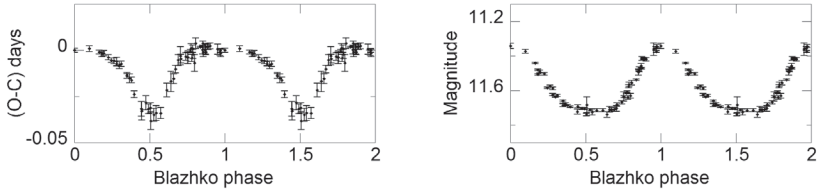

Figure 8. FR Psc O–C (left plot) and magnitude at maximum (right plot) folded with Blazhko period.

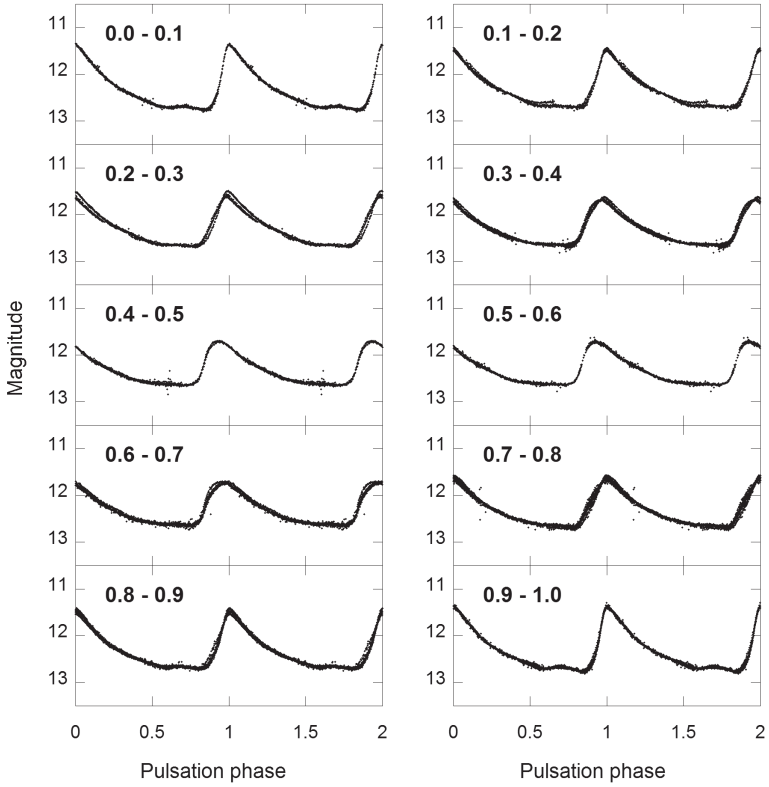

Figure 9. FR Psc light curves (magnitude vs. pulsation phase) for the ten temporal subsets based on Blazhko period.

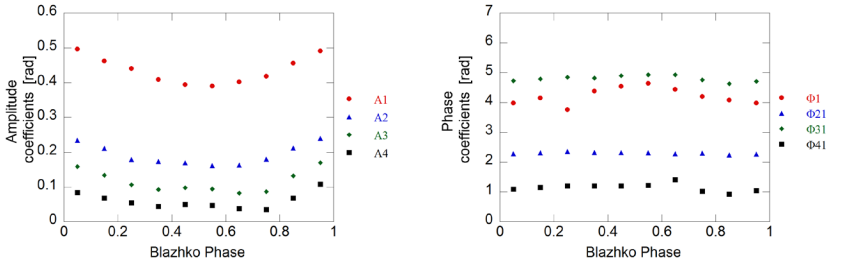

Figure 10. FR Psc Fourier amplitude (left plot) and phase coefficients (mag., right plot) for the ten temporal subsets based on a Blazhko period.

3. Frequency spectrum analyses of the light curve

For both AL Pic and FR Psc, the primary pulsations and Blazhko frequency have been derived from M_{max} and (O–C) analyses. The Blazhko modulation frequencies appear clearly in the spectrum of the complete light curves. The method used for spectrum analysis has already been detailed in other observation reports (de Ponthiere *et al.* 2014), but the method is nevertheless briefly recalled here.

The spectrum of a signal modulated in amplitude and phase is characterized by a pattern of peaks called multiplets at the positions $kf_0 \pm nf_B$, with k and n being integer numbers corresponding, respectively, to the harmonic and multiplet orders. The frequencies, amplitudes, and phases of the multiplets have been obtained with PERIOD04 by performing a succession of Fourier analyses, pre-whitenings, and sine-wave fittings. Only the harmonic and multiplet components having a signal to noise ratio (SNR) greater than 4 have been retained as significant signals. Tables 5 and 12, for AL Pic and FR Psc, respectively, provide the complete lists of Fourier components with their amplitudes, phases, and uncertainties. For both stars, besides the pulsation frequency f_0 and harmonics nf_0, one series of triplets $nf_0 \pm f_B$ based on the Blazhko frequency f_B has been found. The Blazhko frequencies and corresponding periods are tabulated in Tables 4 and 11 with their uncertainties. These Blazhko periods are close to the values obtained with the M_{max} analysis given in Tables 3 and 10.

During the sine-wave fitting, the fundamental frequencies f_0 and triplet $f_0 + f_B$ have been left unconstrained and the other frequencies have been entered as combinations of these two frequencies. The uncertainties of frequencies, amplitudes, and phases have been estimated by Monte Carlo simulations. The amplitude and phase uncertainties have been multiplied by a factor of two as it is known that the Monte Carlo simulations underestimate these uncertainties (Kolenberg *et al.* 2009). Tables 6 and 13 list for each harmonic the amplitude ratios A_i/A_1 and the ratios usually used to characterize the Blazhko effect, that is, A_i^+/A_1 ; A_i^-/A_1 ; $R_i = A_i^+/A_i^-$; and asymmetries $Q_i = (A_i^+ - A_i^-) / (A_i^+ + A_i^-)$.

In the present cases the side lobe amplitudes A_i^- and A_i^+ are similar, which leads to small values for the Q_i asymmetry ratios. Except for some higher order triplets of AL Pic, the asymmetry ratios are positive ($A_i^+ > A_i^-$). For the majority of Blazhko stars, the Q_i asymmetry ratios are larger and generally lie between 0.1 and 0.5, but smaller and negative values are not unusual (Alcock *et al.* 2003). The fact that first triplet values (A_i^+, A_i^-) are larger for AL Pic (0.39 and 0.36) than for FR Psc values (0.17 and 0.16) is due to the relative strength of Blazhko modulations and is consistent with the corresponding variations of the magnitudes at maximum light provided in the preceding section (0.639 and 0.396 magnitude).

4. Light curve variations over Blazhko cycle

Subdividing the data set into temporal subsets is a classical method to visualize and analyze the light curve variations over the Blazhko cycle. For both stars, ten temporal subsets corresponding to the different Blazhko phase intervals Ψ_i ($i = 0 , 9$) have been created using the epochs of the highest recorded maxima as the origins of the first subset. The folded light curves for the ten subsets are presented in Figures 4 and 9. For AL Pic, the data cover around six successive Blazhko cycles and are relatively well distributed over the different temporal subsets and Blazhko cycles. The population percentage of data points varies between 7.7% and 12% for the ten temporal subsets and between 8.4% and 30% for the six Blazhko cycles. The first and second observation seasons of FR Psc cover around 2.6 and 2.3 Blazhko cycles, respectively. The observation data are also well distributed over the temporal subsets, the population varying between 6.4% and 16%.

From a visual inspection of Figures 4 and 9, it is clear that the light curves are only affected by a small scatter during the successive Blazhko cycles. This fact is not surprising, indeed for both stars only one Blazhko modulation frequency has been detected in the spectrum analysis. Fourier analyses and Least-Square fittings have been performed on the different temporal subsets. For the fundamental frequency and the first four harmonics the amplitudes A_i and the epoch-independent phase differences ($\Phi_{kl} = \Phi_k - k\Phi_l$) are given in Tables 7 and 14 and plotted in Figures 5 and 10. The differences between maximal and minimal values of A_1 over the Blazhko cycle for AL Pic and FR Psc are 0.235 and 0.106 magnitude, respectively. The larger A_i value for AL Pic is a confirmation that the Blazhko modulation is stronger for AL Pic than for FR Psc.

5. Conclusions

The two analysis methods, maximum brightness and light curve Fourier analyses, have provided similar results for both stars. No multiple or irregular

Blazhko modulations have been detected and for the two stars the light curves repeat from one cycle to another. The FR Psc Blazhko period was previously published as uncertain. The new measured period value of 51.31 ± 0.02 days removes the uncertainty. The new period of 34.07 ± 0.02 days for AL Pic is in agreement with the previously published value. The objective of this small group of amateur astronomers is to observe and to analyze Blazhko RR Lyrae stars with the hope of finding stars affected by irregular or multiple Blazhko modulations. These two coordinated multi-longitude campaigns have not revealed such multiple modulations. However, observers should continue their regular and coordinated multi-longitude observations to precisely characterize Blazhko modulations in other RR Lyrae stars.

6. Acknowledgements

Dr. Arne Henden, Director of AAVSO and the AAVSO are acknowledged for the use of AAVSOnet telescopes at Cloudcroft (New Mexico). The AAVSO Charts and Sequence Team is thanked for preparing the comparison star sequences. The authors thank the referee for the comments and encouragements. This work has made use of The International Variable Star Index (VSX) maintained by the AAVSO and the SIMBAD astronomical database (http://simbad.u-strasbg.fr).

References

AAVSO. 2014, observations from the AAVSO International Database (http://www.aavso.org).

Alcock, C., *et al.* 2003, *Astrophys. J.*, **598**, 597.

de Ponthière, P. 2010, LESVEPHOTOMETRY, automatic photometry software (http://www.dppobservatory.net).

de Ponthière, P., *et al.* 2014, *J. Amer. Assoc. Var. Star Obs.*, **42**, 53.

Diffraction Limited. 2004, MAXIMDL image processing software (http://www.cyanogen.com).

Kazarovets, E. V., Samus, N. N., Durlevich, O. V., Kireeva, N. N., and Pastukhova, E. N. 2008, *Inf. Bull. Var. Stars*, No. 5863, 1.

Kazarovets, E. V., Samus, N. N., Durlevich, O. V., Kireeva, N. N., and Pastukhova, E. N. 2011, *Inf. Bull. Var. Stars*, No. 5969, 1.

Kolenberg, K., *et al.* 2009, *Mon. Not. Roy. Astron. Soc.*, **396**, 263.

Lenz, P., and Breger, M. 2005, *Commun. Asteroseismology*, **146**, 53.

Reinsch, C. H. 1967, *Numer. Math.*, **10**, 177.

Wils, P., Lloyd, C., and Bernhard, K. 2006, *Mon. Not. Roy. Astron. Soc.*, **368**, 1757.

Wils, P., and Sódor, A. 2005, *Inf. Bull. Var. Stars* No. 5655, 1.

Wozniak, P., *et al.* 2004, *Astron. J.*, **127**, 2436.

Report on the Photometric Observations of the Variable Stars DH Pegasi, DY Pegasi, and RZ Cephei

Ibrahim Abu-Sharkh
Shuxing Fang
Sahil Mehta
Dang Pham
Harvard Summer School, Harvard University, Cambridge, MA; address correspondence to Dang Pham (dang.c.pham@hotmail.com)

Received September 4, 2014; revised September 16, 2014; accepted September 16, 2014

Abstract We report 872 observations on two RR Lyrae variable stars, DH Pegasi and RZ Cephei, and on one SX Phoenicis variable, DY Pegasi. This paper discusses the methodology of our measurements, the light curves, magnitudes, epochs, and epoch prediction of the above stars. We also derived the period of DY Pegasi. All measurements and analyses are compared with prior publications and known values from multiple databases.

1. Introduction

The Harvard Summer School is a program of Harvard University for secondary and college students to experience a Harvard education through two undergraduate courses at Harvard. The authors were enrolled in "Fundamentals of Contemporary Astronomy" taught by Prof. Rosanne Di Stefano. Part of this paper was meant to be a class project, but we found this topic interesting and decided to do more—thus, we observed the stars instead of just researching facts about them.

Throughout this study, we have focused on pulsating variable stars with exceptionally short periods. We have inspected the length of their periods, their change in apparent magnitude, time of epoch, and general shape of their light curves. Measurements of the following stars are presented, DH Pegasi, DY Pegasi, and RZ Cephei, all taken at the Clay Telescope (Harvard University, 0.4 m) with the Apogee Alta U47 Imaging CCD coupled with the Johnson V filter. DH Peg and RZ Cep are both RR Lyrae (RRC) type variable stars while DY Peg is a SX Phoenicis (SXPHE) type variable star. We compared our data to Hopp (1981) and Tifft (1964) while data for DY Peg are compared to Oja (2011) and Hardie and Geilker (1958).

2. The stars

The stars observed are presented in Table 1. The stars are identified by their variable star name as well as by their Hipparcos Catalogue numbers (HIP;

Perryman *et al.* 1997). The coordinates are from The International Variable Star Index (VSX; Watson *et al.* 2014) provided by the AAVSO.

Table 1. The stars used in this study.

Name	*Type*	*Identifier*	*R.A. (J2000)* h m s	*Dec. (J2000)* ° ′ ″
DH Peg	RRC	HIP 109890	22 15 25.64 (333.85683)	+06 49 21.4 (+6.82261)
DY Peg	SXPHE	HIP 114290	23 08 51.19 (347.21329)	+17 12 56.0 (+17.21556)
RZ Cep	RRC	HIP 111839	22 39 13.18 (339.80492)	+64 51 30.6 (+64.85850)

3. Observations

3.1. Methodology of measurements

Three variable stars—DH Peg, DY Peg, and RZ Cep—were selected based on their visibility from our location and their periods. We used CCD imaging at the Clay Telescope to take a total of 872 measurements of these three stars. We exposed the CCD for a specific amount of time (ranging from 20 to 60 seconds), beginning an exposure immediately after the previous had finished. Exposure time and the total number of images taken are presented in Table 2.

Table 2. Exposure time of each star in this study and the total number of observations.

Name	*Exposure Time (seconds)*	*Total Number of Observations*
DH Peg	60	170
DY Peg	20	432
RZ Cep	30	270

Note that during some exposures, clouds moved between the telescope and the star, obscuring the star in question from view. For this reason, approximately 50 images were removed before analysis and were not accounted for in the light curves. Photometric measurements were conducted only on the images without cloud cover.

3.2. Time frame

The time frame of the observations are presented in Table 3. The times are presented in Julian Date (JD) and the durations (ΔT) are presented in minutes.

Table 3. Time frame of the observations.

Name	T_i *(JD)*	T_f *(JD)*	*ΔT (minutes)*
DH Peg	2456861.69705717	2456861.84179564	208.423
DY Peg	2456869.69427083	2456869.81443287	173.033
RZ Cep	2456864.65042824	2456864.85385416	292.933

T_i represents the initial observation time. T_f represents the time of the last observation. ΔT represents the time difference between the first observation and the last.

3.3. Comparison stars

The magnitudes of the stars were measured through comparisons with other nearby standard (non-variable) stars. Each variable star has at least one comparison star with one check star. Aside from DH Peg, each star has two comparison stars and one check star. The comparison stars and check stars assigned to each variable star are shown in Table 4.

Table 4. Variable stars and their comparison stars.

Name	*Comparison Star 1*	*Comparison Star 2*	*Check Star*
DH Peg	TYC 565-1155-1	Not Used	BD+06 4987
DY Peg	BD+16 4876	GSC 01712-00542	GSC 01712-01246
RZ Cep	TYC 4273-435-1	TYC 4273-1351-1	TYC 4273-659-1

Note that there are special exceptions for check stars BD+06 4987 and TYC 4273-659-1. BD+06 4987 was not used during the first six observations of DH Peg because it was not in the image produced by the CCD. TYC 4273-659-1 was not used during the first 118 observations of RZ Cep for the same reason.

Details regarding the properties of the comparison stars, taken from the SIMBAD astronomical database, are shown in Table 5.

4. Results

4.1. Photometric measurements

Our photometric measurements for DH Peg, DY Peg, and RZ Cep are now available in the AAVSO International Database (AAVSO 2014). All uploaded measurements can be found under the observer codes MSAD, PDCA, AIBA, and FSHA.

Table 5. Properties of the comparison stars.

Name	*Type*	*R.A, (J2000)* h m s	*Dec. (J2000)* ° ′ ″	*Apparent Mag. (Visual filter)*
TYC 565-1155-1	DH Peg Comparison Star 1	22 15 35.426	+06 53 28.32	10.08
BD+06 4987	DH Peg Check Star	22 15 00.980	+06 54 29.29	9.90
BD+16 4876	DY Peg Comparison Star 1	23 08 44.272	+17 18 18.86	11.0
GSC 01712-00542	DY Peg Comparison Star 2	23 08 51.53	+17 10 49.1	11.70
GSC 01712-01246	DY Peg Check Star	23 08 40.56	+17 08 14.4	11.10
TYC 4273-435-1	RZ Cep Comparison Star 1	22 39 19.125	+64 52 07.99	12.02
TYC 4273-1351-1	RZ Cep Comparison Star 2	22 39 46.798	+64 50 42.27	12.03
TYC 4273-659-1	RZ Cep Check Star	22 40 05.439	+64 57 18.97	10.84

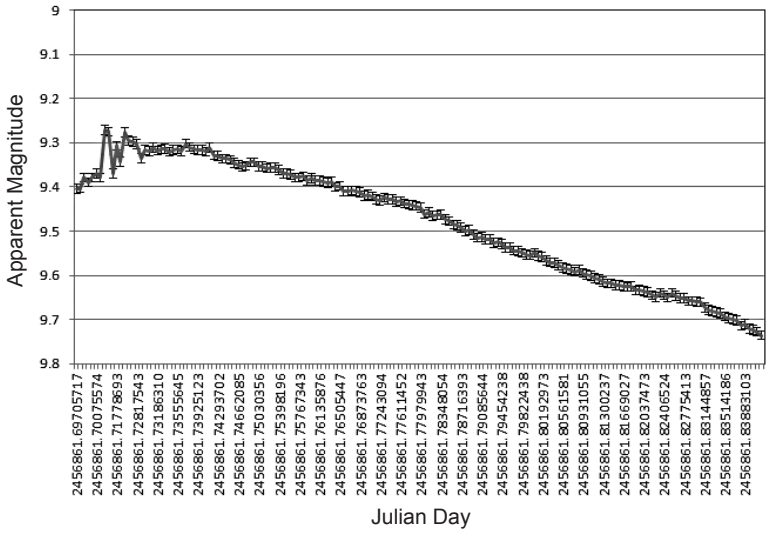

Figure 1. The authors' light curve for the RRC variable DH Peg.

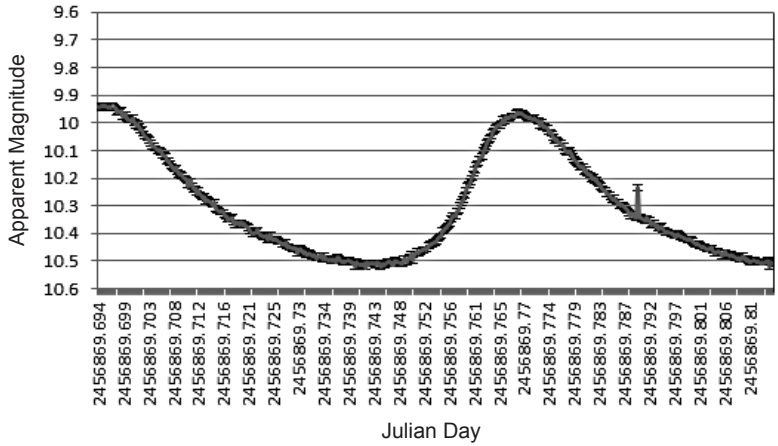

Figure 2.The authors' light curve for the SX Phe variable DY Peg.

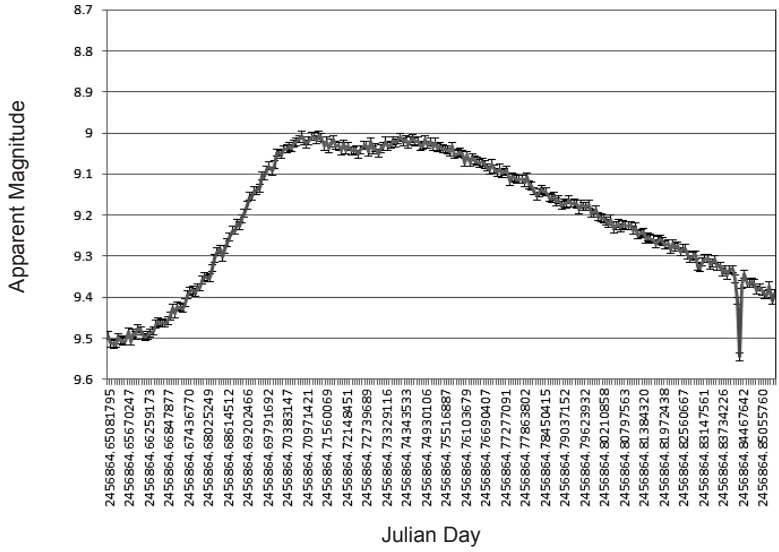

Figure 3. The authors' light curve for the RRC variable RZ Cep.

4.2. Light curves of the stars

The authors' light curves of the stars are shown in Figure 1 (DH Peg), Figure 2 (DY Peg), and Figure 3 (RZ Cep).

Note that in Figure 1, the first part of the light curve has a relatively erratic behavior. This is a result of a lack of valid data caused by cloud coverage at the time. In addition to this, there are also some inconsistencies seen in the other light curves. For example, the light curve for DY Peg has a sudden peak. After some thought, we concluded this to be a result of cosmic ray interference. Additionally, there is a dip towards the end of the light curve for RZ Cep. We are uncertain of the cause of this dip.

Aside from these few inconsistencies, our light curves follow a very nice trend. The light curve of RZ Cep has a clearly pronounced hump as described by Hopp (1981) and Tifft (1964) as characteristic of RR Lyrae variable stars. This hump is also expected with the light curve of DH Peg. Unfortunately, we experienced heavy cloud coverage during this period of time, leading to the erratic behavior described here and seen in the light curve.

4.3. Epoch comparison

Similar to the method Hopp (1981) used for RR Lyrae variable stars, we consider the epoch to be the maximum magnitude after the initial hump for DH Peg and RZ Cep. The epoch of DY Peg is simply the maximum magnitude. The observed epochs for each of the stars are presented in Table 6.

Table 6. Observed epochs.

Name	*Observed Epoch (JD)*
DH Peg	2456861.7200
DY Peg	2456869.7728
RZ Cep	2456864.7434

To validate the accuracy of our observed epochs we tested them against the predicted epoch of the stars. Note that with all the calculations in this section we assume that the periods of the stars stay constant.

We can use the modulo of the difference between our observed epochs and previously published epochs, with the period to calculate the difference between the predicted epoch and the observed ones. Since the function gives the difference, the output (ideally) should be very close to 0. This "modulo" function is described as:

(Previously Published Epoch – Observed Epoch) mod (Published Period) (1)

Values returned by the modulo function are presented in Table 7.

Table 7. Modulo Function values.

Name	*Observed Epoch (JD)*	*Previously Published Epoch (JD)*	*Published Period*	*Modulo Function*
DH Peg	2456861.7200	2444463.571	0.25551040	0.01786673
DY Peg	2456869.7728	2444502.07044	0.072926297	0.014222824
RZ Cep	2456864.7434	2442635.374	0.3086853	0.09683877

Using the output of the modulo function, we found the number of cycles of fluctuation since the last observed epoch. This was found by using the cycle function described as:

$$(\text{Observed Epoch} \pm \text{Modulo Function Result}) - \text{Previously Published Epoch}) / \text{Published Period}) = \text{Cycle} \in \mathrm{N} \quad (2)$$

This function must return a natural value because the number of times the function reaches the same point must be a positive whole number. Any result that does not satisfy this condition is considered erroneous. Therefore, the cycle function should return only one correct result despite the plus-minus operator.

To find the epoch predicted by previously published data, we used the following function:

$$\text{Predicted Epoch} = \text{Previously Published Epoch} + \text{Period} \times \text{Cycle} \quad (3)$$

Values returned by the above function are presented in Table 8.

Table 8: Epoch Comparison. The predicted epoch was found by the Equation (3). The number of cycles was found by Equation (2).

Name	*Previously Publ. Epoch (JD)*	*Cycles Since Publ. Epoch*	*Predicted Epoch (JD)*	*Observed Epoch (JD)*
DH Peg	2444463.571	48523	2456861.7021	2456861.7200
DY Peg	2444502.07044	169592	2456869.7870	2456869.7728
RZ Cep	2442635.374	46097	2456864.8402	2456864.7434

4.4. Functions for epoch prediction

Using the above data, definitions, and functions, we can conclude that the general function for epoch prediction is described as:

$$\text{Predicted Epoch} = \text{Observed Epoch} + \text{Period} \times \text{Cycle} \quad (4)$$

Where Predicted Epoch is returned in Julian Date and Cycle is the output of the cycle function described in section 4.3.

Assuming periods are constant, we present the following functions for DH Peg, DY Peg, and RZ Cep:

$$\text{DH Peg} = 2456861.72000593 + 0.2555104 \times \text{Cycle} \quad (5)$$

$$\text{DY Peg} = 2456869.77277800 + 0.072926297 \times \text{Cycle} \quad (6)$$

$$\text{RZ Cep} = 2456864.74343533 + 0.3086853 \times \text{Cycle} \quad (7)$$

4.5. Apparent magnitude range

From the photometric measurements collected during this research, we can find both the maximum and minimum magnitude of each star. A comparison of the values we found and previously published values is presented in Table 9.

Table 9. Apparent magnitude range.

Name	*Observed Min. Mag.*	*Observed Max. Mag.*	*Published Min. Mag.*	*Published Max. Mag.*
DH Peg	9.736	9.272	9.8	9.15
DY Peg	10.522	9.938	10.56	10.00
RZ Cep	9.545	9.006	9.72	9.15

4.6 Period of DY Peg

We did not determine the period of DH Peg and RZ Cep because we were not able to collect enough data to complete one whole period fluctuation in brightness of these stars. As a result, any period calculation is impossible. However for DY Peg, we collected sufficient data and were able to calculate its period as:

$$\text{period} = \text{Time at Epoch 2} - \text{Time at Epoch 1} \quad (8)$$

$$\text{period}_{\text{DY Peg}} = 2456869.77277800 - 2456869.69509259 = 0.07768541 \quad (9)$$

We calculated the period of DY Peg to be 0.07768541 day. When compared with previously published data from the *General Catalogue of Variable Stars* (GCVS; Samus *et al.* 2007–2012), 0.072926297 day, our value differs by only 0.00475912 day (6.8531328 minutes).

5. Conclusion

We were able to use the data collected from the photometric measurements described above to derive light curves, epochs, and magnitude ranges of DH Peg, DY Peg, and RZ Cep. We were also able to calculate the epoch-

prediction function of all the stars and derive the period of DY Peg. Our observed measurements are in accordance with previously published data from Hopp (1981), Tifft (1964), Oja (2011), and Hardie and Geilker (1958). In order to glean more information, measurements of these stars would need to be conducted over a longer period of time and with minimal weather interference.

6. Acknowledgements

We would each like to thank Rosanne Di Stefano, Joshua Schroeder, Elizabeth Waagen, Allyson Bieryla, Zoe Bergstrom, and Herman Keith for their continuous guidance throughout this process. Without their assistance, it is unlikely that we would have been able to bring this project to fruition.

This research has made use of the SIMBAD database, operated at CDS, Strasbourg, France, and the International Variable Star Index (VSX), operated by the AAVSO.

References

AAVSO. 2014, observations from the AAVSO International Database (http://www.aavso.org/).

Hardie, R. H., and Geilker, C. D. 1958, *Astrophys. J.*, **127**, 606.

Hopp, U. 1981. *Astrophys. Space Sci.*, **79**, 239.

Oja, T. 2011, *J. Astron. Data*, **17**, 1.

Perryman, M. A. C., European Space Agency Space Science Department, and the Hipparcos Science Team. 1997, *The Hipparcos and Tycho Catalogues*, ESA SP-1200 (VizieR On-line Data Catalog: I/239), ESA Publications Division, Noordwijk, The Netherlands.

Samus, N. N., *et al.* 2007–2012, *General Catalogue of Variable Stars*, online catalogue (http://www.sai.msu.su/groups/cluster/gcvs/gcvs/).

Tifft, W. G. 1964, *Astrophys. J.*, **139**, 451.

Watson, C., Henden, A. A., and Price, C. A. 2014, AAVSO International Variable Star Index VSX (Watson+, 2006–2014; http://www.aavso.org/vsx).

Observations of Novae From ROAD

Franz-Josef Hambsch
Oude Bleken 12, B- 2400 Mol, Belgium; M31@telenet.be

Presented at the 103rd Spring Meeting of the AAVSO, Big Bear Lake, CA, June 13, 2014

Received August 11, 2014; revised September 9, 2014; accepted September 10, 2014

Abstract The author discusses observations of galactic novae and some extragalactic supernovae from his remote observatory ROAD (Remote Observatory Atacama Desert) he commenced in August 2011 with Nova Lupi 2011 (PR Lup). The observed novae are mainly chosen according to *AAVSO Alert Notices* and *AAVSO Special Notices* as published on their website. Examples of dense observations of different novae are presented. The focus goes to the different behaviors of their light curves. It also demonstrates the capability of the remote observatory ROAD.

1. Introduction

Galactic novae and extragalactic supernovae seem to be a very intensive field of research in professional astronomy. Just recently (2013) a conference on Stella Novae: Past and Future Decades was held in Cape Town (http://www.ast.uct.ac.za/stellanovae2013/). It was mentioned in one of the presentations, which are available on the internet, that more than 700 refereed papers on the subject of novae were published in the past decade. The author started to observe novae based on requests from the AAVSO and different mailing list (mainly VSNET and CVNET). Due to the very good observing possibilities at the author's remote observatory ROAD (Remote Observatory Atacama Desert) (300+ clear nights per year) intense observations of those stars were possible. Those observations are mainly done as snapshots every clear night and sometimes also as time series if of interest. During the many clear nights at the remote site a lot of data are being gathered on many stars. In the present paper a selection of novae is presented with their respective light curves based on data from the AAVSO including those of the author.

2. Observatory

The remote observatory in Chile houses a 40-cm f/6.8 Optimized Dall-Kirkham (ODK) from Orion Optics, England. The CCD camera is from FLI and contains a Kodak 16803 CCD chip with 4k × 4k pixels of 9 μm size. The filter wheel is also from FLI and contains photometric BVI filters from Astrodon.

Figure. 1. Photo of the remote telescope installation in Chile in operation at night.

In Belgium, where the author lives, a roll-off-roof observatory is used in addition for variable star observations from the Northern hemisphere, if it ever gets clear. Belgium is famous neither for its good weather nor its lack of light pollution, nevertheless there is still some room for interesting observations. The telescope in Belgium is a Celestron C11 working at f/6.3. The telescope is equipped with an SBIG ST8XME CCD camera using BVRI photometric filters. Soon a Staranalyser SA200 grid for low resolution spectroscopic investigations will also be installed.

Figure 1 shows the remote telescope in Chile in operation at night. The telescope is housed in a clamshell dome, making easy movement of the telescope possible without the need to follow with a shutter of a normal dome.

Images of a night's session are acquired with CCDCommander automation software. Further analysis in terms of determination of the brightness of the stars is done using a program developed by de Ponthière (2010). Differential aperture photometry is used to determine the magnitudes of variable and comparison stars. Uncertainties are determined from the signal-to-noise ratio using Poisson and background noise as well as CCD gain. The calculation is performed in accordance to relation (12) of Newberry (1991). The data are then finally submitted to the AAVSO.

3. Novae

The observed novae were mainly chosen according to announcements in *AAVSO Alert Notices* and *AAVSO Special Notices* (AAVSO 2008–2014). The observations at the remote site began on August, 1, 2011. The first nova which was observed was Nova Lupi 2011 (PR Lup). But before we start to discuss the observations we should look at what is known about novae in literature. Since the author is not a specialist in this field, nor a professional astronomer, he has to rely on the internet and e-mail information on relevant literature. The most comprehensive paper is probably the one of Strope *et al.* (2010). It contains a catalogue of 93 nova light curves with a classification of the

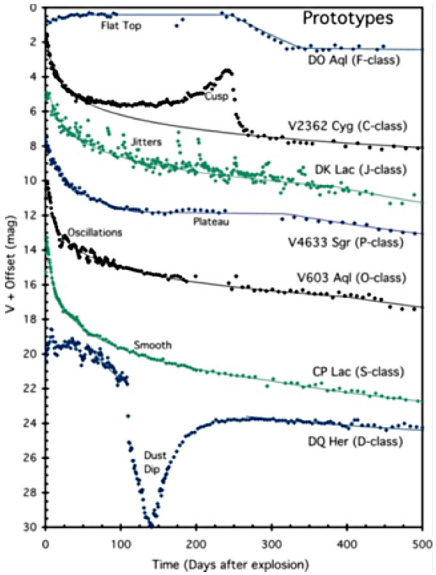

Figure 2. Different prototypes of novae based on the form of their light curve.

light curves (Figure 2) and a list of properties of the novae, like peak magnitudes, decline speeds etc. One of the problems mentioned in this paper is the fact that only very few of the brightest novae were followed more extensively down to quiescence mainly by amateurs and only two of them by professionals. Hence, there is still room for amateur observations if they are done in a more systematic way. The light curves of novae covered in this paper are mainly based on observations from the AAVSO international database. The database contains more than double the number of novae, but only those covered in the article have a decent number of observations. In the paper the light curves could be classified according to seven different types, which are called classes. The prototype light curves of the different classes are given in Figure 2.

In the following a few examples of novae observations from the remote observatory are given. Not all classes could be observed. All images shown are based on the author's observations and additional observations found in the AAVSO International Database (AAVSO 2014). BVI photometric filters were used.

4. Nova Cen 2012-2 (TCP J14250600-5845360)

A new star in Centarus was discovered by J. Seach (Chatsworth Island, NSW Australia) on April 4.765, 2012, using a DSLR with a 50-mm f/1.0 lens. It was the second nova discovered in the constellation Centaurus in 2012.

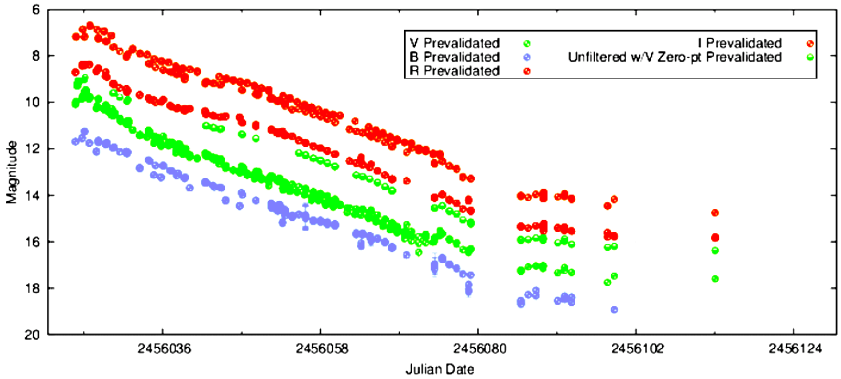

Figure 3. Light curve of Nova Cen 2012-2 (TCP J14250600-5845360) based on observations found in the AAVSO database. Part of the I- and V-band observations were taken remotely at ROAD.

It was assigned the identifier TCP J14250600-5845360 and was published on the Transient Object Confirmation Page of the IAU Central Bureau for Astronomical Telegrams (CBAT TOCP; http://www.cbat.eps.harvard.edu/unconf/tocp.html). Due to the very short focal length of only 50 mm the position of the nova was not very well known. A better astrometric position was determined with the 2-m Faulkes Telescope South by E. Guido, G. Sostero, and N. Howes. A spectroscopic confirmation observation of the novae was performed by T. Bohlsen.

As one can see from the light curve in Figure 3, the nova was discovered before maximum light. Observations at ROAD were started as early as April 5.902, hence just a bit more than one day after the initial discovery. Observations were continued over 46 nights in V and I band filters (Figure 3). A smooth behavior of the light curve was observed (S-type light curve).

5. Nova Mon 2012 (V959 Mon)

Nova Monocerotis 2012 (V959 Mon) was discovered on August, 9.8048 UT, 2012, by S. Fujikawa (Kagawa, Japan) using a 105-mm FL camera lens and a CCD camera at magnitude 9.4 with a clear filter. It was assigned the CBAT TOCP identifier PNV J06393874+0553520. Remote observations at ROAD started on August 12.918 using V and I band filters. The nova was followed both from Chile and from the Astrokolkhoz Observatory, New Mexico. Both snapshot and long time series observations were done (Figure 4). From New Mexico, using two different telescopes and observing the stars over its full observing period during several nights, BVRI time series could be acquired. An analysis of those time series confirmed the 7.1-hour period of this star (Hambsch *et al.* 2013) discovered in UV/X-ray observations of this nova (Osborne *et al.* 2013). As one can see the observations have continued from

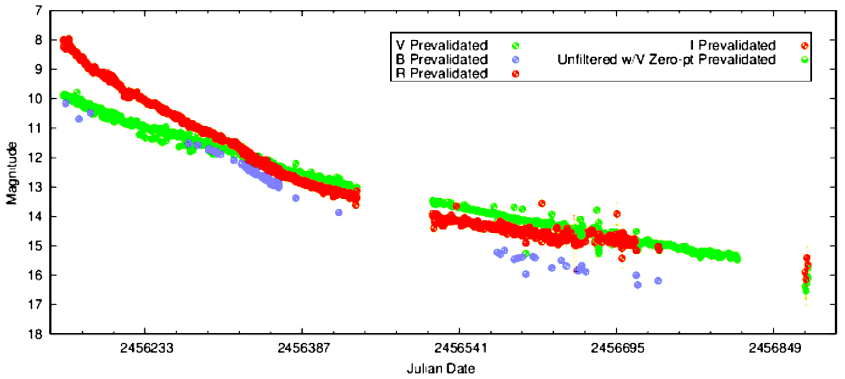

Figure 4. Light curve of Nova Mon 2012 (V959 Mon) based on observations found in the AAVSO database. Most of the observations were taken remotely at ROAD.

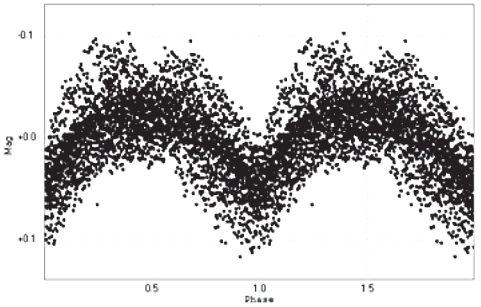

Figure 5. Phase diagram of Nova Mon 2012 (V959 Mon) with P = 0.29575 ± 0.0005 d = 7.098 h.

the discovery until now, only interrupted by the fact that the star's observing season ended. There is a clear behavior visible: that I-band magnitudes do not behave in a way parallel to the V-band magnitudes. Maybe this nova could be regarded as a member of either the smooth or plateau class.

Figure 5 shows the phase diagram of the time series observations from New Mexico. A period of P = 7.098 h was used to generate the image.

6. Nova Oph 2012 (V2676 Oph)

This nova in Ophiuchus was discovered by H. Nishimura (Shizuoka-ken, Japan) on Mar. 25.789, 2012, using a Canon 200mm f/3.2 lens with a Canon EOS 5D digital camera. It was assigned the CBAT TOCP identifier PNV J17260708-2551454. On March 27.74 low-resolution spectra were taken at the 1.3-m Araki telescope at the Koyama Astronomical Observatory (KAO) that confirmed the new object as a classical nova.

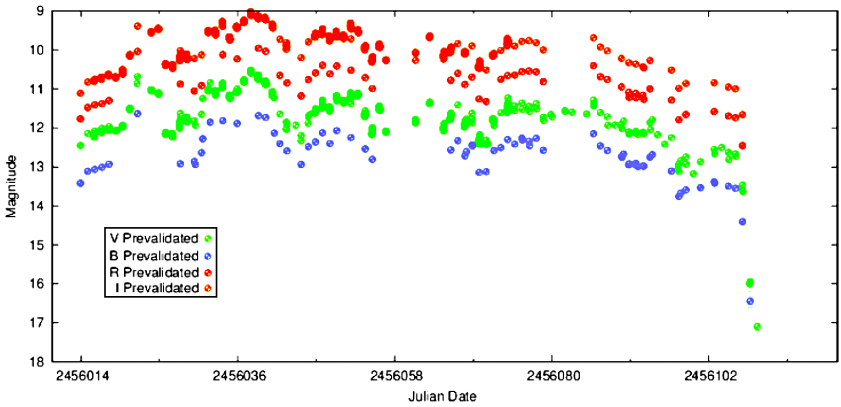

Figure 6. Light curve of Nova Oph 2012 (V2676 Oph) based on observations found in the AAVSO database. Part of the I- and V-band observations are taken remotely at ROAD.

Observations started at ROAD on March 28.865 UT using V- and I-band filters. Observations were conducted as snapshots during 42 nights. Figure 6 shows the light curve based on all observations found in the AAVSO International Database. Clearly the shape of the light curve is very different to the previous ones and shows a kind of jitter or oscillations, yielding a light curve showing minima and maxima until after about 85 days, when an abrupt decline starts. Unfortunately no further observations were performed after this drop.

7. Nova Sgr 2014 (PNV J18250860-2236024)

Another example of a recently newly discovered nova in Sagittarius is Nova Sgr 2014 (PNV J18250860-2236024). It was discovered by S. Furuyama, (Ibaraki-ken, Japan) on January 26.857, 2014, using a 200-mm f/2.8 lens and CCD camera. A low-dispersion spectrum (R about 980 at 650 nm) of the object was obtained using the 2-m Nayuta telescope at the Nishi-Harima Astronomical Observatory, Japan, which confirmed the nature of the object as a nova.

Observations started on January 28.393, using V- and I-band filters. Observations were conducted as snapshots one-and-a-half days after the discovery. Observations are still ongoing as the nova is still bright.

Figure 7 shows the light curve based on all observations sent to the AAVSO. From ROAD the majority of data are taken for this star. From the light curve it is clear that oscillations in the brightness of the nova exist and it belongs to the oscillation class. Based on the most recent observations the light curve has changed and a drop in magnitude in both I- and V-bands is visible. It will be interesting to see the behavior of this star in the months to come.

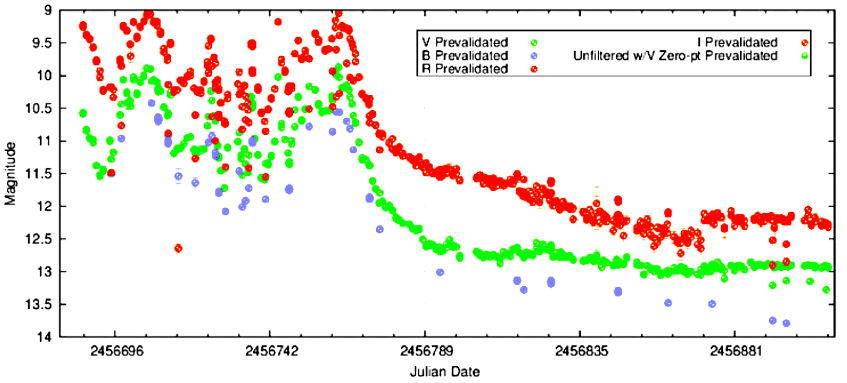

Figure 7. Light curve of Nova Sgr 2014 (PNV J18250860-2236024) based on observations found in the AAVSO database. Most of the I- and V-band observations are taken remotely at ROAD.

8. Supernova SN 2013aa in NGC 5643

SN 2013aa in NGC 5643, a galaxy in the constellation Lupus, was observed after an e-mail alert. It was discovered by S. Parker (Canterbury, New Zealand) on February 13.621, 2013. Its identifier is PSN J14323388-4413278. In Figure 8 observations of the AAVSO database are shown of which observations from ROAD form the majority. Observations started as snapshots on February 15.895 UT in V- and I-band filters. From Figure 8 it is obvious that in the I band the light curve showed a second brightening about 40 days after maximum brightness. Also, the V maximum brightness came after the I-band maximum by about 10 days. Then the supernova was brighter in V for about 20 days compared to the I-band brightness.

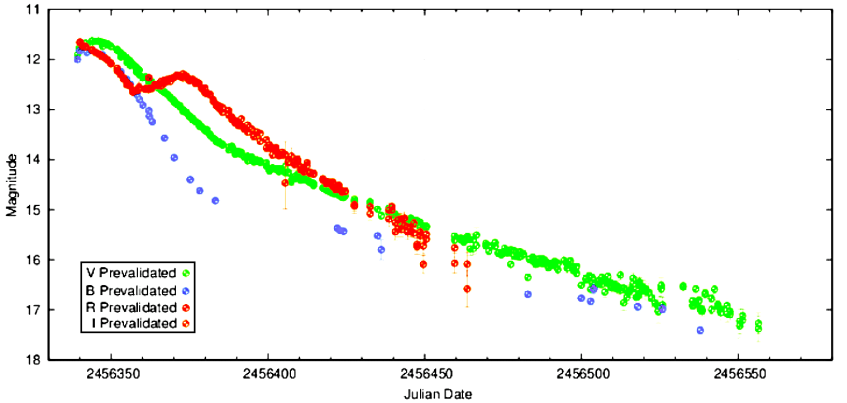

Figure 8. Light curve of Supernova SN 2013aa in NGC 5643 based on observations found in the AAVSO database. Most of the I- and V-band observations are taken remotely at ROAD.

Observations extended over a period of 171 nights with only a few interruptions due to bad weather.

9. Nova Trianguli Australis 2008 (NR TrA)

This nova was observed in collaboration with the Center for Backyard Astrophysics (CBA). The nova was shining at about visual magnitude 8.5 in April 2008. Time series observations were started March 27, 2013, and lasted for 33 nights. The present brightness of this nova is around magnitude 15.5. Figure 9 shows the phase diagram of the observations. This figure was generated using a period of 5.2599 h ± 0.0013.

This period is very close to the one observed at the CTIO 1.3-m telescope in Chile. This CTIO result was presented at the conference mentioned in the introduction in 2013 in Cape Town, South Africa. The presentations given can be found on the website of the conference. It shows that with amateur equipment and many clear nights, results can be achieved which are comparable to professional investigations.

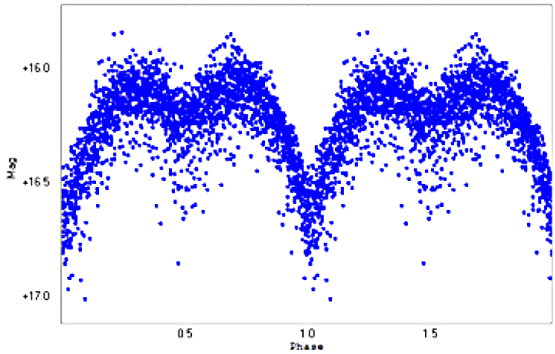

Figure 9. Phase diagram of NR TrA (Nova TrA 2008) with P = 5.2599 h ± 0.0013.

10. Conclusion

The remote observatory under pristine skies in the Atacama Desert opens up many possibilities to observe variable stars. Intensive follow-up observations over many days, weeks, or even months are possible due to the stable weather conditions. The examples given show impressively what is possible. Collaborations are searched for in order to contribute to scientific research of common interest.

11. Acknowledgements

For this research the information given in *AAVSO Alert Notices* and *AAVSO Special Notices* has been used. Also, the information given in the International Variable Star Index (VSX), operated by the AAVSO, was used.

References

AAVSO. 2008–2014, *AAVSO Alert Notices* (http://www.aavso.org/alert-notice-archive) and *AAVSO Special Notices* (http://www.aavso.org/special-notice-archive).

AAVSO. 2014, observations from the AAVSO International Database, private communication.

de Ponthierre, P. 2010, LESVEPHOTOMETRY software (http://www.dppobservatory.net/AstroPrograms/Software4VSObservers.php).

Hambsch, F.-J., Krajci, T., and Banerjee, D. P. K. 2013, *Astron. Telegram*, No. 4803, 1.

Newberry, M. 1991, *Publ. Astron. Soc. Pacific*, **103**, 122.

Osborne, J. P., Beardmore, A., and Page, K. 2013, *Astron. Telegram*, No. 4727, 1.

Strope, R. J., Schaefer, B. E, and Henden, A. A. 2010, *Astron. J.*, **140**, 34.

Watson, C., Henden, A. A, and Price, C. A. 2014, AAVSO International Variable Star Index (http://www.aavso.org/VSX).

BVRI Photometry of SN 2013ej in M74

Michael W. Richmond
School of Physics and Astronomy, Rochester Institute of Technology, 84 Lomb Memorial Drive, Rochester, NY 14623; mwrsps@rit.edu

Received May 19, 2014; revised June 24, 2014; accepted June 25, 2014

Abstract I present BVRI photometry of the type IIP supernova 2013ej in M74 from 1 to 179 days after its discovery. These photometric measurements and spectroscopic data from the literature are combined via the expanding photosphere method to estimate the distance to the event, which is consistent with that derived by other methods. After correcting for extinction and adopting a distance modulus of $(m - M) = 29.80$ mag. to M74, I derive absolute magnitudes $M_B = -17.36$, $M_V = -17.47$, $M_R = -17.64$, and $M_I = -17.71$. The differences between visual measurements and CCD *V*-band measurements of SN 2013ej are similar to those determined for type Ia supernovae and ordinary stars.

1. Introduction

On UT 2013 July 25.45, the Lick Observatory Supernova Search (LOSS) detected a new point source in the nearby galaxy M74 (NGC 628); when the object appeared again and brighter the next night, LOSS alerted other astronomers to the presence of this new object. Within days, spectroscopy revealed it to be a young type II supernova, designated SN 2013ej (Kim *et al.* 2013). Because its host is so nearby (less than 10 Mpc; see section 5) and so well studied, and because the event was caught within a few days of the explosion, SN 2013ej provides a fine opportunity for us to study the properties of a massive star before and after it undergoes core collapse.

I present here photometry of SN 2013ej in the *BVRI* passbands obtained at the RIT Observatory, starting one day after the announcement and continuing for a span of 179 days. Section 2 describes the observational procedures, the reduction of the raw images, and the methods used to extract instrumental magnitudes. In section 3, I explain how the instrumental quantities were transformed to the standard Johnson-Cousins magnitude scale. I illustrate the light curves and color curves of SN 2013ej in section 4 and comment briefly on their properties. In section 5, I discuss extinction along the line of sight to this event. In section 6, I discuss attempts to measure the distance to M74, and use the Expanding Photosphere Method (EPM) to perform my own estimate; I adopt a distance and convert the apparent magnitudes at peak to absolute magnitudes. Visual measurements of this event collected by the American Association of Variable Star Observers (AAVSO 2013) are compared to CCD *V*-band measurements in section 7. I summarize the results of this study in section 8.

2. Observations

This paper contains measurements made at the RIT Observatory, near Rochester, New York. The RIT Observatory is located on the campus of the Rochester Institute of Technology, at longitude 77:39:53 West, latitude +43:04:33 North, and an elevation of 168 meters above sea level. The eastern horizon is bright and dominated by a large pine tree. Measurements during the first two weeks, and particularly on the very first night, were taken at low airmass and not far from the tree's branches. I used a Meade LX200 f/10 30-cm telescope and SBIG ST-8E camera, which features a Kodak KAF1600 CCD chip and astronomical filters made to the Bessell (1990) prescription; with 3 × 3 binning, the plate scale is 1.85" per pixel. To measure SN 2013ej, I took a series of 30-second exposures through each filter, using the autoguider if possible; the only guide star was very faint in the *B*-band, so most of those images were unguided. The number of exposures per filter ranged from ten, at early times, to fifteen or thirty at late times. I typically discarded a few images in each series due to trailing. I acquired dark and flatfield images each night, except for UT Dec 17; the images from that night were reduced using dome flats taken the following evening. In most cases, I chose to use dome flats over twilight sky flatfield images.

I combined ten dark images each night to create a master dark frame, and ten flatfield images in each filter to create a master flatfield frame. After applying the master dark and flatfield images in the usual manner, I examined each cleaned target image by eye. I discarded trailed and blurry images and measured the Full Width at Half Maximum (FWHM) of those remaining. The XVista (Treffers and Richmond 1989) routines STARS and PHOT were used to find stars and to extract their instrumental magnitudes, respectively, using a synthetic aperture with radius of 4 pixels (= 7.4"), slightly larger than the FWHM (which was typically 4" to 5").

As Figure 1 shows, SN 2013ej lies in the outskirts of one of the spiral arms of M74. How much light from other objects in the area falls into the aperture used to measure the supernova? I examined high-resolution HST images of this region, using ACS WFC data in the F435W, F555W, and F814W filters originally taken as part of proposal GO-10402 (PI: Chandar). See Fraser *et al.* (2014) for a detailed analysis of the progenitor's light in these images. Within a circle of radius 7.4" centered on the SN's position are ten or so point sources of roughly equal brightness, with magnitudes of roughly $B \sim 25$, $I \sim 23$. The combined light of these sources is too small to make a significant addition to the light of the SN itself. However, a considerably brighter source lies at R.A. $01^h\ 36^m\ 48.55^s$, Dec. +15º 45' 26.5", a distance of 7.7" to the southeast of SN 2013ej. Comparing it to the progenitor in the HST images, I measure magnitudes of $B = 22.64$, $V = 21.15$, $I = 18.10$. The *I*-band value agrees well with an entry in the *USNO B1.0 Catalog* (Monet *et al.* 2003). Since this star lies at the edge of

the synthetic aperture used to measure the SN, some of its light was attributed to the SN in my measurements. In the *B* and *V* images, SN 2013ej was at least 3.9 magnitudes brighter than this star at all times, and so the contaminating flux was at most a few percent. In the *R* and *I* images, on the other hand, this star's light may have been important at late times. In the last *I*-band measurement, for example, roughly one-sixth of the measured light may have come from this star. Since the exact amount of contamination depends on details of the seeing and shape of the point-spread function on each night, I have made no correction for this effect; but the late-time measurements reported here are slightly brighter than they ought to be, especially in the red passbands.

Between July and early September, 2013, I measured instrumental magnitudes from each exposure and applied inhomogeneous ensemble photometry (Honeycutt 1992) to determine a mean value in each passband. Starting on UT Sep 11, 2013, in order to improve the signal-to-noise ratio, I combined the good images for each passband using a pixel-by-pixel median procedure to yield a single image with lower noise levels. I then extracted instrumental magnitudes from this image in the manner described above. In order to verify that this change in procedure did not cause any systematic shift in the results, I also measured magnitudes from the individual exposures at these late times, reduced them using ensemble photometry, and compared the results to those measured from the median-combined images. As Figure 2 shows, there were no significant systematic differences.

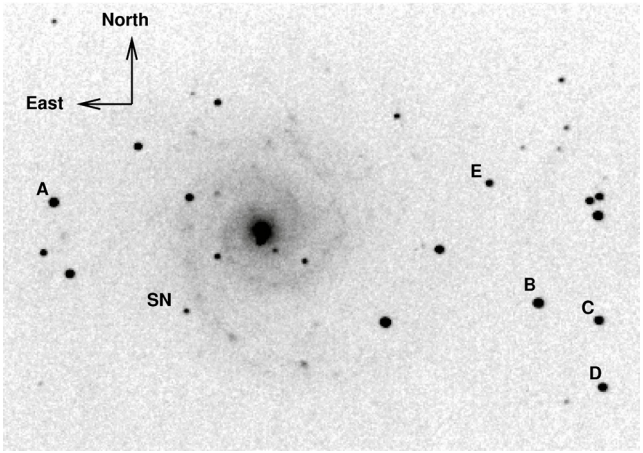

Figure 1. An R-band image of M74 from RIT, 15 × 30 seconds exposure time, showing stars used to calibrate measurements of SN 2013ej. North is up, East to the left. The field of view is roughly 12 by 9 arcminutes.

Table 1. Photometry of comparison stars.

Star	*R.A. (J2000)* *h m s*	*Dec. (J2000)* *° ′ ″*	*B*	*V*	*R*	*I*
A	01 36 58.63	+15 47 46.7	13.012 ± 0.019	12.510 ± 0.019	12.154 ± 0.019	11.834 ± 0.019
B	01 36 19.55	+15 45 22.4	13.848 ± 0.026	13.065 ± 0.022	12.622 ± 0.025	12.152 ± 0.027
C	01 36 14.64	+15 44 58.6	14.338 ± 0.029	13.692 ± 0.024	13.329 ± 0.029	12.964 ± 0.030
D	01 36 14.60	+15 43 39.5	14.832 ± 0.027	13.912 ± 0.023	13.416 ± 0.026	12.939 ± 0.030
E	01 36 23.06	+15 47 45.4	15.192 ± 0.034	14.613 ± 0.027	14.275 ± 0.034	13.915 ± 0.036

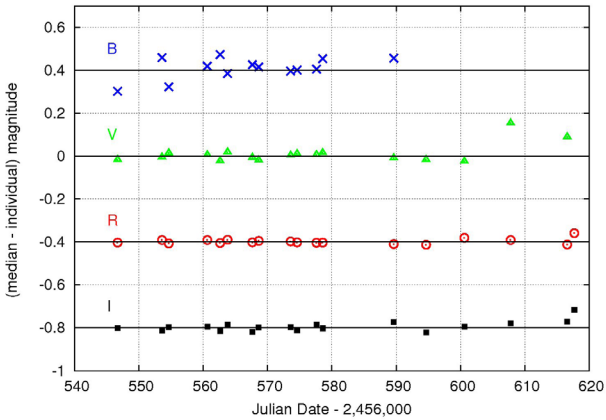

Figure 2. Difference between instrumental magnitudes extracted from median-combined images and from individual images at RIT. The values have been shifted for clarity by 0.4, 0.0, –0.4, –0.8 magnitude in B, V, R, I, respectively.

3. Photometric calibration

In order to transform the instrumental measurements into magnitudes in the standard Johnson-Cousins BVRI system, I used a set of local comparison stars, supplied by the AAVSO in their chart 12459CA. These reference stars are listed in Table 1, and Figure 1 shows their location.

In order to correct for differences between the RIT equipment and the Johnson-Cousins system, I observed the standard fields PG1633+009 and PG2213-006 (Landolt 1992) on several nights and compared the instrumental magnitudes to catalog values. Linear fits to the differences as a function of color yielded the following relationships:

$$B = b + (0.231 \pm 0.012) \times (b - v) + Z_B \quad (1)$$

$$\mathrm{V} = \mathrm{v} - (0.079 \pm 0.017) \times (\mathrm{v} - \mathrm{r}) + Z_V \quad (2)$$

$$R = r - (0.087 \pm 0.021) \times (r - i) + Z_R \quad (3)$$

$$I = i - (0.018 \pm 0.040) \times (r - i) + Z_I \quad (4)$$

In the equations above, lower-case symbols represent instrumental magnitudes, upper-case symbols Johnson-Cousins magnitudes, and Z the zeropoint in each band. Stars A, B, C, D, and E were used to set the zeropoint for each image. Table 2 lists the calibrated measurements of SN 2013ej made at RIT. The first column shows the mean Julian Date of all the exposures taken during each night. In most cases, the span between the first and last exposures was less than 0.04 day, but on a few nights, clouds interrupted the sequence of observations. Contact the author for a dataset providing the Julian Date of each measurement individually.

Table 2. Photometry of SN 2013cj

JD–2456500	*B*	*V*	*R*	*I*	*comments*
0.71	12.945 ± 0.059	12.999 ± 0.025	12.972 ± 0.060	12.967 ± 0.056	high airmass
3.80	12.714 ± 0.035	12.647 ± 0.012	12.566 ± 0.021	12.537 ± 0.025	cirrus
4.73	12.693 ± 0.020	12.615 ± 0.019	12.509 ± 0.027	12.446 ± 0.058	cirrus
6.81	12.624 ± 0.047	12.524 ± 0.021	12.404 ± 0.018	12.373 ± 0.025	
8.75	12.668 ± 0.048	12.522 ± 0.014	12.370 ± 0.030	12.275 ± 0.037	clouds
9.73	12.700 ± 0.056	12.513 ± 0.042	12.350 ± 0.034	12.318 ± 0.041	
10.83	12.715 ± 0.028	12.553 ± 0.032	12.321 ± 0.043	12.291 ± 0.052	clouds
14.69	12.964 ± 0.056	12.527 ± 0.075	12.297 ± 0.051	12.239 ± 0.034	clouds
15.70	12.973 ± 0.036	12.548 ± 0.013	12.303 ± 0.015	12.219 ± 0.030	
19.70	13.239 ± 0.032	12.586 ± 0.026	12.310 ± 0.028	12.176 ± 0.035	
20.68	13.351 ± 0.086	12.601 ± 0.028	12.309 ± 0.043	12.149 ± 0.042	cirrus
21.70	13.421 ± 0.084	12.651 ± 0.032	12.339 ± 0.031	12.177 ± 0.043	
24.69	13.564 ± 0.094	12.748 ± 0.039	12.378 ± 0.028	12.237 ± 0.051	
25.69	13.734 ± 0.137	12.787 ± 0.058	12.429 ± 0.026	12.211 ± 0.034	nearby moon
28.70	13.831 ± 0.056	12.864 ± 0.038	12.470 ± 0.025	12.255 ± 0.036	
29.66	13.939 ± 0.090	12.904 ± 0.027	12.507 ± 0.030	12.290 ± 0.038	
33.68	14.109 ± 0.085	13.026 ± 0.045	12.574 ± 0.023	12.340 ± 0.028	
38.62	14.346 ± 0.140	13.142 ± 0.034	12.677 ± 0.021	12.403 ± 0.062	clouds
39.79	14.406 ± 0.039	13.164 ± 0.026	12.686 ± 0.019	12.446 ± 0.030	
41.75	14.442 ± 0.052	13.228 ± 0.024	12.734 ± 0.020	12.491 ± 0.045	clouds
44.62	14.495 ± 0.096	13.291 ± 0.037	12.765 ± 0.024	12.514 ± 0.035	high airmass
46.68	14.642 ± 0.094	13.302 ± 0.028	12.824 ± 0.027	12.542 ± 0.051	
53.57	14.747 ± 0.084	13.438 ± 0.031	12.902 ± 0.026	12.587 ± 0.029	nearby moon

Table continued on next page

Table 2. Photometry of SN 2013cj

JD–2456500	*B*	*V*	*R*	*I*	*comments*
54.63	14.889 ± 0.048	13.450 ± 0.039	12.909 ± 0.016	12.627 ± 0.021	nearby moon
60.62	14.932 ± 0.055	13.538 ± 0.055	13.007 ± 0.018	12.699 ± 0.026	
62.62	14.993 ± 0.056	13.570 ± 0.041	13.006 ± 0.016	12.691 ± 0.026	clouds
63.77	14.955 ± 0.072	13.618 ± 0.025	13.037 ± 0.020	12.746 ± 0.025	
67.62	15.082 ± 0.070	13.634 ± 0.041	13.080 ± 0.020	12.759 ± 0.022	
68.62	15.119 ± 0.060	13.650 ± 0.046	13.110 ± 0.022	12.780 ± 0.030	hazy
73.59	15.285 ± 0.067	13.733 ± 0.031	13.172 ± 0.037	12.864 ± 0.031	
74.59	15.234 ± 0.068	13.771 ± 0.040	13.191 ± 0.021	12.900 ± 0.024	
77.60	15.321 ± 0.065	13.858 ± 0.038	13.230 ± 0.022	12.947 ± 0.032	clouds
78.56	15.357 ± 0.093	13.868 ± 0.043	13.280 ± 0.021	12.967 ± 0.027	
89.58	15.807 ± 0.077	14.211 ± 0.034	13.599 ± 0.030	13.300 ± 0.037	clouds
94.65	—	14.299 ± 0.043	13.913 ± 0.024	13.602 ± 0.039	
96.62	16.412 ± 0.149	14.907 ± 0.051	14.174 ± 0.035	13.811 ± 0.050	
100.58	17.166 ± 0.161	15.776 ± 0.079	14.954 ± 0.047	14.631 ± 0.066	clouds
107.79	18.193 ± 0.311	16.612 ± 0.137	15.388 ± 0.062	15.044 ± 0.082	
110.64	—	16.309 ± 0.133	15.378 ± 0.082	15.100 ± 0.119	clouds
113.64	—	16.572 ± 0.160	15.584 ± 0.083	15.219 ± 0.110	clouds
116.59	—	16.478 ± 0.123	15.501 ± 0.064	15.180 ± 0.090	
117.71	—	16.444 ± 0.135	15.497 ± 0.078	15.132 ± 0.107	cirrus
130.48	—	16.889 ± 0.247	15.763 ± 0.110	15.674 ± 0.175	cirrus
143.52	—	17.235 ± 0.237	16.001 ± 0.100	15.561 ± 0.149	clouds
155.49	—	17.089 ± 0.217	16.144 ± 0.109	16.132 ± 0.196	

The uncertainties listed in Table 2 incorporate the uncertainties in instrumental magnitudes and in the offset used to shift the instrumental values to the standard scale, added in quadrature. As a check on their size, I chose a region of the light curve, 40 < JD – 2456500 < 80, in which the magnitude appeared to be a linear function of time. I fit a straight line to the measurements in each passband, weighting each point based on its uncertainty; the results are shown in Table 3. The reduced χ^2 values are all less than 1.0, which suggests that the tabulated uncertainties slightly overestimate the random scatter from one measurement to the next.

4. Light curves

The light curves in each passband, uncorrected for any extinction, are shown in Figure 3. SN 2013ej is clearly a type IIP event, defined by a period of roughly 60 days during which the apparent brightness decreases very slowly. The plateau phase ends at Julian Date ~2456590, after which there is a sharp drop lasting a week or so. The light curve then decreases at a moderate pace for another month, to the end of the observations.

Table 3. Linear fit to light curves 40 < JD – 2456500 < 80.

Passband	*Slope (mag./day)*	*Reduced χ^2*
B	0.0238 ± 0.0012	0.6
V	0.0167 ± 0.0004	0.3
R	0.0141 ± 0.0003	0.5
I	0.0131 ± 0.0006	0.8

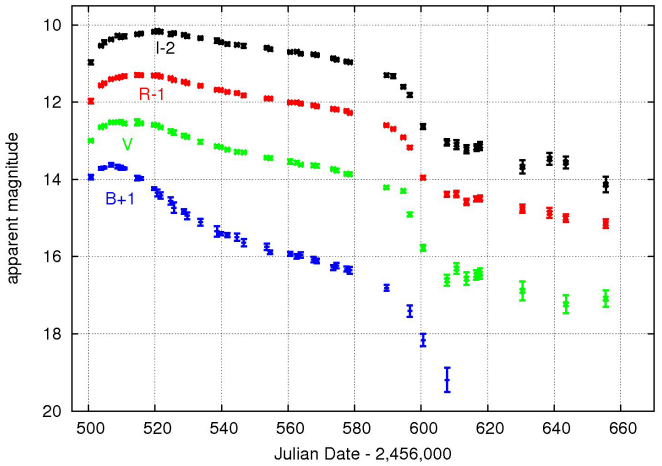

Figure 3. Light curves of SN 2013ej measured at RIT Observatory. The *B*, *R*, and *I* data have been offset vertically for clarity. No correction for extinction has been made.

Table 4. Apparent magnitudes at maximum light.

Passband	*JD–2456500*	*Magnitude*
B	7.3 ± 0.2	12.64 ± 0.01
V	12.1 ± 1.0	12.48 ± 0.02
R	14.9 ± 1.0	12.28 ± 0.01
I	19.0 ± 2.0	12.17 ± 0.02

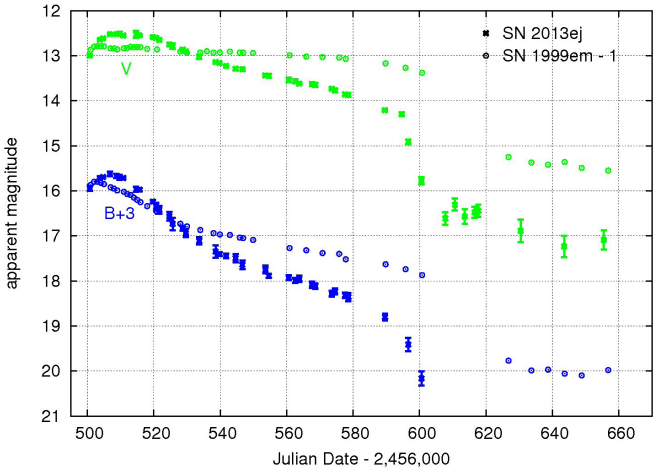

Figure 4. Light curves of SNe 2013ej and 1999em compared in the *B* and *V* passbands. The measurements of SN 1999em have been shifted horizontally (by 5,019 days) and vertically (by –1 mag.) for easier comparison.

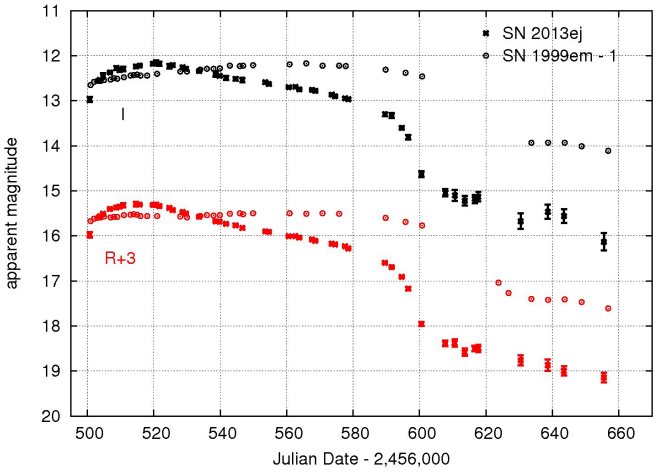

Figure 5. Light curves of SNe 2013ej and 1999em compared in the *R* and *I* passbands. The measurements of SN 1999em have been shifted horizontally (by 5,019 days) and vertically (by –1 mag.) for easier comparison.

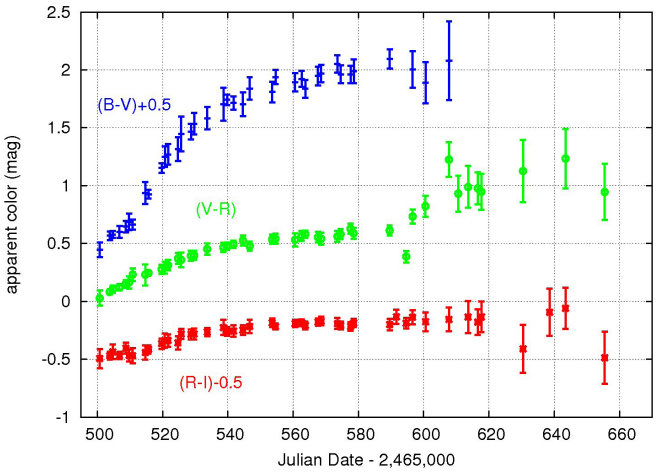

Figure 6. Color curves of SN 2013ej measured at RIT Observatory. The (*B*–*V*) and (R–I) data have been offset vertically for clarity. No correction for extinction has been made.

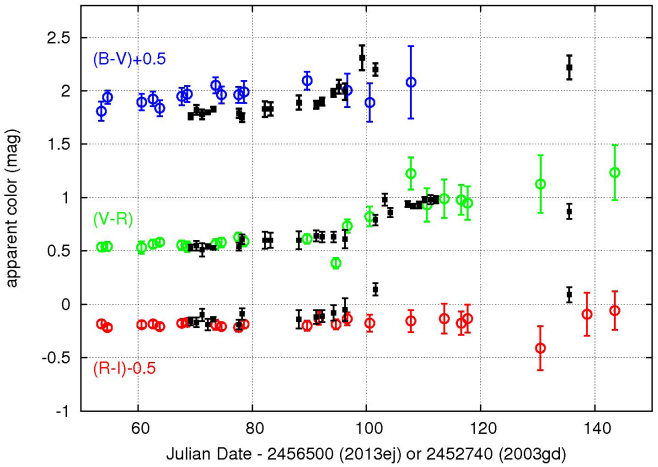

Figure 7. Color curves of SN 2013ej (large circles) compared with those of SN 2003gd (small black squares). The (B–V) and (R–I) data have been offset vertically for clarity. No correction for extinction has been made.

In order to determine the time and magnitude at peak light, I fit second- and third-order polynomials to a subset of measurements around maximum light in each passband. Table 4 lists the results. Maximum light occurs earliest in the *B*-band and successively later at longer wavelengths.

The well-observed type IIP SN 1999em (Leonard *et al.* 2002) provides a good comparison to SN 2013ej. In Figures 4 and 5, one can see that SN 2013ej rises to and falls from an early peak in all four passbands, while SN 1999em has such a peak only in *B*; its light curve is nearly flat in the other passbands. The

plateau phase ends slightly later in SN 1999em, and the drop to the late-time decline is very similar.

The colors of SN 2013ej changed considerably at the blue end of the visible spectrum, but very little at the red end. As Figure 6 indicates, the (*B–V*) color increased monotonically by about 1.5 magnitudes over one hundred days. The most rapid change occurred as the light curve fell after maximum in *B*, but the increase then slowed during the plateau phase. The (*R–I*) color, on the other hand, remained nearly constant, increasing by only 0.3 magnitude from maximum light to the plateau phase. The magnitude measurements after the end of the plateau phase are so noisy that it is hard to see any significant change in color at that time.

One can compare the colors of SN 2013ej to those of SN 2003gd, another type IIP SN in M74; this will inform the discussion of extinction in section 5. However, since SN 2003gd was discovered long after maximum light, this comparison is restricted largely to the plateau phase, and one cannot align the two events in time with any precision. Figure 7 shows the two events were very similar: SN 2003gd had a slightly smaller (*B–V*) color, but only by 0.15 magnitude at most.

5. Extinction

There are several different methods one can use to estimate the extinction along the line of sight to SN 2013ej. One can begin with the effects of dust and gas within our own galaxy: the foreground Milky Way reddening to M74 is estimated by Schlafly and Finkbeiner (2011) to be $E(B–V) = 0.062$. Note that this value is an average based on infrared maps with a beam size of order 6 arcminutes, which subtends roughly 17 kpc at the distance of M74.

In order to determine the extinction due to material within M74 itself, one might use SN 2003gd as a probe. Both it and SN 2013ej exploded within the outer southern arm of M74, the former roughly 40 degrees farther along the arm from the center of the galaxy. The similarity of the colors of these events suggests that they suffered equally from reddening. Hendry *et al.* use the colors of SN 2003gd itself, nearby stars, and nearby HII regions to derive $E(B–V) = 0.14 \pm 0.06$; this implies that the reddening contributions from M74 and the Milky Way are roughly equal.

A more direct approach is to use high-resolution spectra of SN 2013ej itself to measure the absorption lines of neutral sodium (Na I), which are correlated with extinction along the line of sight. Valenti *et al.* (2014) provide in their Figure 3 a detailed graph of the spectrum centered on the NaI D lines. As they state, this spectrum shows clearly the absorption lines due to gas within the Milky Way, but no evidence for any absorption by gas in M74. Using a digitized version of their spectrum, I measure the equivalent widths of the Milky Way components to be EW(NaI D_1) = 0.20Å and EW(NaI D_2) = 0.26Å.

The relationship in Equation 9 of Poznanski *et al.* (2012) then yields $E(B–V) = 0.049 \pm 0.010$. I will adopt this value for all following analysis.

Taking the relationships between reddening and extinction given in Schlegel *et al.* (1998) one can compute the extinction in each passband to be $A_B = 0.20 \pm 0.04$, $A_V = 0.15 \pm 0.03$, $A_R = 0.12 \pm 0.02$, and $A_I = 0.08 \pm 0.02$. If one were to choose the slightly higher reddening given by Schlafly and Finkbeiner (2011) of $E(B–V) = 0.062$, one would derive slightly larger extinctions of $A_B = 0.27 \pm 0.05$, $A_V = 0.21 \pm 0.04$, $A_R = 0.17 \pm 0.03$, and $A_I = 0.12 \pm 0.03$.

Note that the adopted reddening is roughly 0.09 magnitude smaller than that of SN 2003gd, which is consistent with the difference in the $(B–V)$ colors of the two supernovae during the plateau phase of their evolution. Both the colors of the SN 2013ej and the high-resolution spectra of Valenti *et al.* (2014) indicate that there was very little material along the line of sight within M74, and little circumstellar material surrounding the progenitor itself.

6. The distance to M74 and absolute magnitudes of SN 2013ej

In order to calculate the absolute magnitude of SN 2013ej, one must know the distance to its host galaxy. Many attempts have been made to determine this distance, using a variety of methods. The appearance of the brightest individual stars has been used to derive distance moduli of $(m – M) = 29.3$ (Sohn and Davidge 1996), 29.32 (Sharina *et al.* 1996), and 29.44 (Hendry *et al.* 2005). Sandage and Tammann (1974) measured the angular sizes of the three largest HII regions to estimate $(m – M) = 31.46$. Hendry *et al.* (2005) applied the Standardised Candle Method of Hamuy and Pinto (2002) to spectra and photometry of SN 2003gd to derive $(m – M) = 29.9^{+0.6}_{-0.7}$; they also determined a distance by assuming that SNe 2003gd and 1999em were identical, yielding $(m – M) = 30.12 \pm 0.32$. More recently, Herrmann *et al.* (2008) used the Planetary Nebula Luminosity Function (PNLF) to determine a precise value of $(m – M) = 29.67^{+0.06}_{-0.07}$. Jang and Lee (2014) kindly provided results in advance of their publication of a distance based on the Tip of the Red Giant Branch (TRGB); using HST images, they find $(m – M) = 29.91 \pm 0.04$ (rand) ± 0.12 (sys).

6.1. Applying the Expanding Photosphere Method (EPM) to SN 2013ej

The Expanding Photosphere Method (EPM) applies basic physics to determine the distance to a supernova (Kirshner and Kwan 1974; Schmidt *et al.* 1992). Using spectra or photometry, one estimates the temperature of the photosphere at a set of times; assuming that it radiates approximately as a blackbody, one can compute the luminosity per unit area. If the photosphere expands freely, then a combination of radial velocity measurements and the time since explosion permits one to compute the size of the photosphere. One can multiply these quantities to determine the luminosity of the photosphere, then compare to the observed brightness to find the distance to the event.

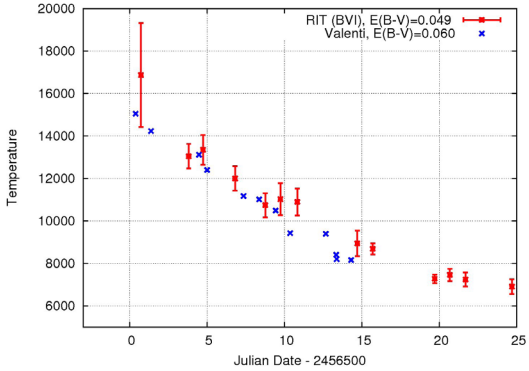

Figure 8. Temperature of SN 2013ej based on blackbody fits to *BVI* photometry from RIT, and based on *UBgVrRiI* photometry from Valenti *et al.*

Following the procedures described by Bose and Kumar (2014), I applied this technique to SN 2013ej. The temperature was calculated based on *BVI* photometry; the *R*-band values were ignored, due to the presence of strong Hα features. To estimate the uncertainties in the temperatures, I used a Monte Carlo approach: I generated thousands of instances of artificial photometric measurements by adding random gaussian noise to the actual magnitudes, then fit blackbody spectra to those artificial measurements. The temperatures derived from RIT photometry (after corrections for extinction) are shown in Figure 8; they are slightly larger than those computed by Valenti *et al.* (2014), which is somewhat surprising, since my adopted reddening is smaller than that of Valenti *et al.* (2014). However, both sets of temperatures, for the most part, do agree within the uncertainties of the RIT values. Since the RIT dataset lacks spectroscopy, I adopted the radial velocities described in Valenti *et al.* (2014), covering epochs $5 < \text{JD} - 2456500 < 22$.

The procedures of Bose and Kumar (2014) yield a semi-independent distance for each passband of photometric measurements; they are not fully independent due to the photometric color corrections, and due to the combination of magnitudes into colors which are used to determine the temperature. Plotting the time of each measurement against the ratio of angular size to photospheric velocity yields a graph in which the slope is the distance to the supernova, and the y-intercept is the time at which the size would be zero; the actual time of explosion will be somewhat later, since the star's initial size will always be larger than zero. Figure 9 shows the results of the analysis for all four passbands of RIT photometry, and Table 5 lists them.

The weighted average of these distances is $D = 9.1 \pm 0.4$ Mpc, corresponding to a distance modulus $(m - M) = 29.79 \pm 0.11$. One might conclude that the time of the explosion is roughly $t_0 \sim 2456493$, if one ignores the initial radius of the progenitor. The rise time, from explosion to maximum light, would then range

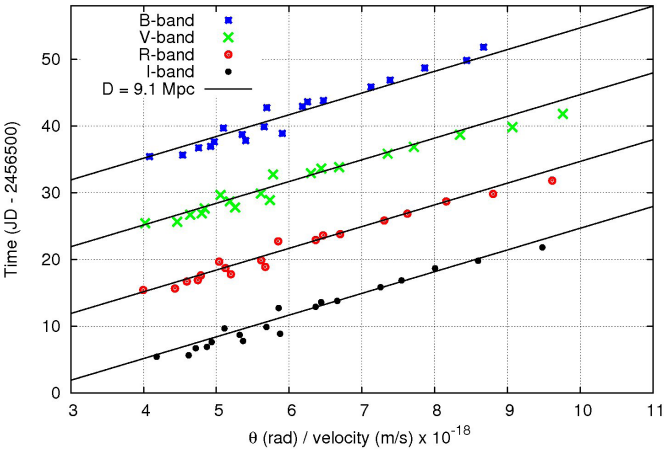

Figure 9. Distance to SN 2013ej based on EPM. The data have been shifted vertically for clarity by 30, 20, 10 days in *B*, *V*, *R*, respectively. A line corresponding to the average distance $D = 9.1$ Mpc has been drawn to guide the eye.

Table 5. Results of EPM applied to SN 2013ej.

Passband	*Distance (Mpc)*	*Time of explosion*[a]
B	10.4 ± 1.1	–9.6
V	8.5 ± 0.8	–6.4
R	8.8 ± 0.7	–6.8
I	9.4 ± 0.9	–8.2

[a]*JD–2456500; does not account for initial radius.*

from 14 days in *B* to 26 days in *I*, increasing monotonically with wavelength. This is considerably shorter than the values estimated for most of the sparsely-sampled type IIP SNe modelled by Sanders *et al.* (2014), but similar to the rise times for the well-observed type IIP SN 2012aw (Bose *et al.* 2013).

6.2. Summary of distance measurements

I give greatest weight to the PNLF (Herrmann *et al.* 2008) and TRGB (Jang and Lee 2014) methods, and so adopt a distance modulus of $(m - M) = 29.8 \pm 0.2$. Using this value, and the extinction in each passband, one can calculate the absolute magnitude of SN 2013ej at maximum light; the results are shown in Table 6.

How does this event compare to other type IIP SNe? Richardson *et al.* (2002) examine the absolute magnitudes of 29 type IIP events, finding a mean value $M_B = -17.00 \pm 1.12$. It appears that SN 2013ej falls close to the middle of this distribution, indicating that it was typical of its class.

Table 6. Absolute magnitudes at maximum light, corrected for extinction.

Passband	*Magnitude*[a]
B	–17.36 ± 0.04 ± 0.20
V	–17.47 ± 0.04 ± 0.20
R	–17.64 ± 0.02 ± 0.20
I	–17.71 ± 0.03 ± 0.20

[a]*Absolute magnitude followed by random uncertainty, then systematic uncertainty.*

7. Visual vs. CCD measurements

Because SN 2013ej was one of the closest supernovae in the past few decades, it was monitored intensively by visual observers. It provides us with a rare opportunity to compare visual measurements of a type IIP supernova to CCD *V*-band measurements.

I collected visual estimates from the AAVSO's website (AAVSO 2014). There were a total of 119 measurements, all with validation flag value "Z," indicating that they had been checked only for typos and data input errors. The visual measurements cover the period $1 < \text{JD} - 2456500 < 105$, which starts shortly before maximum light and continues to the end of the plateau phase. For each of the CCD V-band measurements, I estimated a simultaneous visual magnitude by fitting an unweighted low-order polynomial to the visual measurements within *N* days; due to the decreasing frequency of visual measurements and the less sharply changing light curve at late times, the value *N* was increased from 5 days to 8 days at JD 2456540 and again to 30 days at JD 2456565. The differences between the polynomial and each V-band measurement are shown as a function of CCD (*B*–*V*) color in Figure 10.

An unweighted linear fit to these differences yields the relationship

$$(\text{visual} - \text{V})_{2013\text{ej}} = -0.15 + (0.25 \pm 0.02) \times (B-V). \quad (5)$$

This is very similar to the relationship between visual and CCD *V*-band measurements of the type Ia SN 2011fe found by Richmond and Smith (2012):

$$(\text{visual} - \text{V})_{2011\text{fe}} = -0.09 + (0.19 \pm 0.04) \times (B-V). \quad (6)$$

The fact that two SNe of different type are perceived by human eyes in a similar fashion is consistent with the fact that their light is dominated by the continuum at these relatively early times. In fact, the degree to which eyes judge a supernova to be fainter as it grows redder agrees with the relationship for ordinary stars measured by Stanton (1999), further suggesting that human eyes are responding primarily to the continuum emission of supernovae.

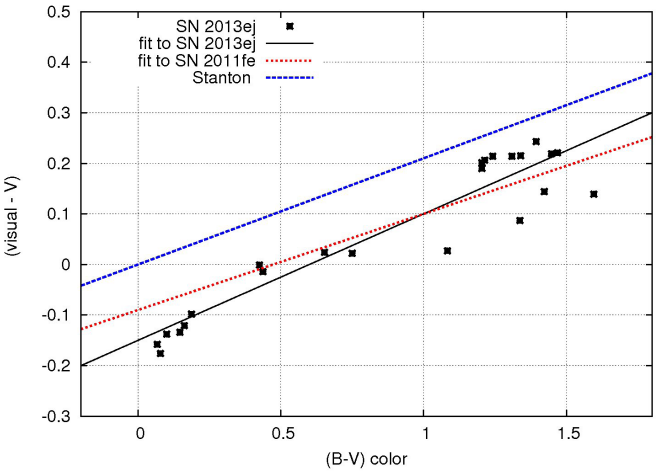

Figure 10. Difference between visual and CCD *V*-band measurements of SN 2013ej, together with relationships for SN 2011fe (Richmond ans Smith 2012) and variable stars (Stanton 1999).

8. Conclusion

Photometric *BVRI* measurements from the RIT Observatory of SN 2013ej for six months after its discovery show that it was a typical type IIP supernova. After correcting for extinction and assuming a distance modulus $(m - M) = 29.8$, I find absolute magnitudes of $M_B = -17.36$, $M_V = -17.47$, $M_R = -17.64$, and $M_I = -17.71$. Applying the expanding photosphere method to this event yields a distance modulus of $(m - M) = 29.79 \pm 0.11$, agreeing well with other recent values. The very low extinction along the line of sight, and the proximity of its host galaxy M74, make this one of the brightest core-collapse supernovae since 1993. As a result, many visual observers were able to monitor SN 2013ej for over three months; the differences between their estimates and CCD *V*–band measurements reveal the same trend with color that one sees in type Ia supernovae and in ordinary stars.

9. Acknowledgements

We thank Arne Henden and the staff at AAVSO for providing a sequence of comparison stars near M74, and the many observers who contribute their time, energy, and measurements to the AAVSO. Stefano Valenti very gently pointed out an error in the early version of this work and kindly provided temperatures based on his own photometry. Insung Jang cheerfully volunteered to choose M74 as the next target in his project to measure distances to nearby galaxies.

The anonymous referee made several suggestions which improved this paper. MWR is grateful for the continued support of the RIT Observatory by RIT and its College of Science.

References

AAVSO. 2013, observations from the AAVSO International Database (http// www.aavso.org).
Bessell, M. S. 1990, *Publ. Astron. Soc. Pacific*, **102**, 1181.
Bose, S., and Kumar, B. 2014, *Astrophys. J.*, **782**, 98.
Bose, S., *et al.* 2013, *Mon. Not. Roy. Astron. Soc.*, **433**, 1871.
Fraser, M., *et al.* 2014, *Mon. Not. Roy. Astron. Soc.*, **439**, 56.
Hamuy, M., and Pinto, P. A. 2002, *Astrophys. J.*, **566**, 63.
Hendry, M. A., *et al.* 2005, *Mon. Not. Roy. Astron. Soc.*, **359**, 906.
Herrmann, K. A., Ciardullo, R., Feldmeier, J. J., and Vinciguerra, M. 2008, *Astrophys. J.*, **683**, 630.
Honeycutt, R. K. 1992, *Publ. Astron. Soc. Pacific*, **104**, 435.
Jang, I. S., and Lee, H. M. 2014, private communication.
Kim, M., *et al.* 2013, *Cent. Bur. Astron. Telegrams,* No. 3606, 1.
Kirshner, R. P., and Kwan, J. 1974, *Astrophys. J.*, **193**, 27.
Landolt, A. U. 1992, *Astron. J.*, **104**, 340.
Leonard, D. C., *et al.* 2002, *Publ. Astron. Soc. Pacific*, **114**, 35.
Monet, D. G., *et al.* 2003, *Astron. J.*, **125**, 984.
Poznanski, D., Prochaska, J. X., and Bloom, J. S. 2012, *Mon. Not. Roy. Astron. Soc.*, **426**, 1465.
Richardson, D., Branch, D., Casebeer, D., Millard, J., Thomas, R. C., and Baron, E. 2002, *Astron. J.*, **123**, 745.
Richmond, M. W., and Smith, H. A. 2012, *J. Amer. Assoc. Var. Star Obs.*, **40**, 872.
Sandage, A., and Tammann, G. A. 1974, *Astrophys. J.*, **194**, 559.
Sanders, N. E., *et al.* 2014, arXiv 1404.2004S.
Schlafly, E. F., and Finkbeiner, D. P. 2011, *Astrophys. J.*, **737**, 103.
Schlegel, D. J., Finkbeiner, D. P., and Davis, M. 1998, *Astrophys. J., Suppl. Ser.*, **500**, 525.
Schmidt, B. P., Kirshner, R. P., and Eastman, R. G. 1992, *Astrophys. J.*, **395**, 366.
Sharina, M. E., Karachentsev, I. D., and Tikhonov, N. A. 1996, *Astron. Astrophys., Suppl. Ser.*, **119**, 499.
Sohn, Y-J., and Davidge, T. J. 1996, *Astron. J.*, **111**, 2280.
Stanton, R. H. 1999, *J. Amer. Assoc. Var. Star Obs.*, **27**, 97.
Treffers, R. R., and Richmond, M. W. 1989, *Publ. Astron. Soc. Pacific*, **101**, 725.
Valenti, S., *et al.* 2014, *Mon. Not. Roy. Astron. Soc.*, **438**, 101.

23 New Variable Stars

Maurice Clark
Texas Tech University, Physics Department, P.O. Box 41051, Lubbock, TX 79409; maurice.clark@ttu.edu

Received May 20, 2014, accepted June 30, 2014

Abstract I report the discovery of 23 new variable stars: ten W UMa eclipsing (USNO-B1.0 1070-0023351, USNO-B1.0 1023-0051547, USNO-B1.0 1024-0049987, USNO-B1.0 1023-0051277, USNO-B1.0 1289-0181948, USNO-B1.0 1287-0180792, USNO-B1.0 1287-0177514, GSC 01965:01128, USNO-B1.0 1395-0370184, USNO-B1.0 1395-0370731); four which may be W UMa eclipsing (USNO-B1.0 0943-0001247, GSC 05581:00450, USNO-B1.0 0820-0342790, USNO-B1.0 1026-0049630); four other eclipsing (GSC 00008:00428, USNO-B1.0 1287-0181263, GSC 00814:00461, GSC 01665:01505); one RR Lyr ((GSC 00540:00848); one that might be an RR Lyr ((GSC 05568:00529); and three others for which the type could not be determined (USNO-B1.0 1287-0181515, USNO-B1.0 1288-0184031, USNO-B1.0 1295-0192642).

1. Introduction

As a long-time observer of asteroid light curves, I have accumulated a considerable amount of data of various areas of the sky. Typically, the observations are around 4–7 hours on a single field. Recently I decided to go back and examine all of these images with the aim of seeing if there was anything else of interest in these fields. While the observations were made continuously for many hours on a single field, that field was almost always covered only for one night. This meant that any new variables found would be short-period—mostly, although not exclusively, WUMa eclipsing binaries. The search has proved more successful than I expected, and a lot of fun. However it has resulted in one problem: how to fit time for follow-up observations in between all the asteroid work. As a result of this, several of the variable stars reported here are in need of follow-up observations to better refine the periods and in two cases, to determine the type of variable.

2. Instrumentation used

The data were obtained with two PlaneWave 20-inch f/6.8 cassegrain telescopes operating at prime focus. One of these telescopes is the personal property of the author while the other is the main instrument at the Preston Gott Observatory run by the Physics Department of Texas Tech University. Both telescopes are located at the Preston Gott Observatory, situated at

coordinates 33° 44' 53" N 101° 57' 30" W, about 25 km north of Lubbock, Texas. Both telescopes are equipped with SBIG STL 1001E CCD cameras. These cameras use a Kodak Enhanced KAF-1001E monochrome sensor equipped with an array of 1024 × 1024, 24 µ pixels, for a resulting sampling of 1.43 arcsec/pixel. Skies at the observatory are relatively dark with zenith limiting magnitudes typically around 6.7. Under these conditions, it is possible to reach 20th magnitude with unfiltered three-minute integrations.

3. Data collection

All images were unfiltered. This is normal for asteroid photometry since the spectrum is basically solar in the visible and near infra-red. The spectral response of the CCD chip means that the photometry approximates Johnson-Cousins R.

Normal exposure times were 180 seconds with an average download time of about three seconds per frame. The CCD control program was CCDSOFT v5 (Software Bisque 2012). The images were calibrated using darks and sky flats.

4. Data analysis

The images were initially examined using the "Variable Star Search" routine in MPO CANOPUS (Warner 2012). This routine scans a set of images and looks for objects that vary in brightness, compared to a number of comparison stars selected by the observer. The results are then displayed as a Magnitude-RMS diagram for the observer to check. As shown in Figure 1, numerous possible variable objects are located by the software. These need to be examined to sort out real variables from the false positives. In the case of the object displayed in

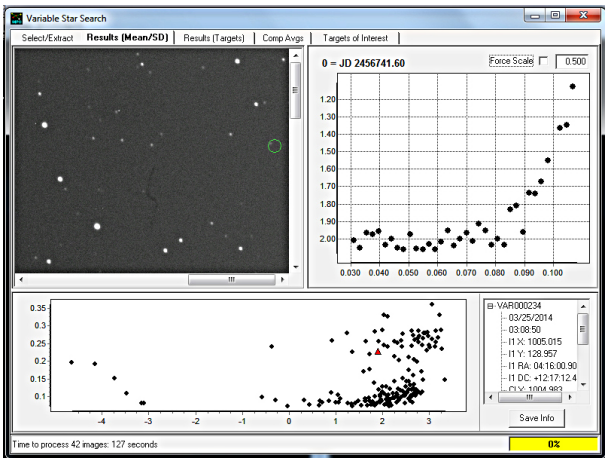

Figure 1. Plot of possible variable objects. X-axis is brightness arbitrary magnitude units. Y-axis is magnitudes RMS.

Figure 1, it was simply a hot pixel. These comprise the majority of the detections.

Most times an actual variable star will show up clearly in the data as shown in Figure 2. Several times more than one variable star would be visible in a set of images. Any variable stars found were then checked against the AAVSO Variable Star Index (http://www.aavso.org/vsx/) to see if they were already

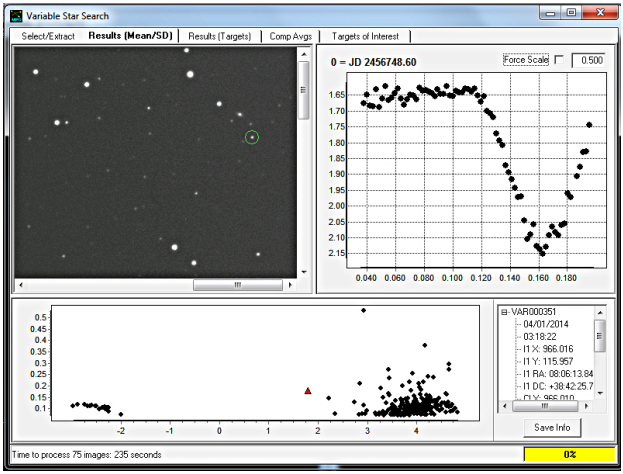

Figure 2. Plot of eclipsing variable star as detected by the "Variable Star Search" utility.

known. For the most part, no variables were listed near the location in question.

Once any likely variable stars were found, they were then analysed using the photometry routines within CANOPUS to yield more precise light curves and, where possible, periods. Comparison stars were chosen from those in the images that had solar-type spectra. Five such comparison stars were used for each variable.

5. Results

To date, I have found 27 new variable stars in my asteroid images, and one that I suspect to be variable. Of those that are confirmed as variable, 23 are reported here. Three of the 27 stars are not discussed as they are the subject of a separate paper to be presented at a conference in June 2014. The details of each of the 23 new variable stars are given in Table 1 in order of increasing Right Ascension. Finder charts, phase plots, and light curves for these 23 stars are shown in Figures 3 through 46.

Acknowledgements

This work has made use of the VizieR catalogue access tool, CDS, Strasbourg, France, and the International Variable Star Index (VSX) operated by the AAVSO.

Table 1. Information about 23 new variable stars.

Star Name and cross-identification	*Position USNO-B1.0 (J2000) R.A.* h m s	*Dec.* ° ′ ″	*Discovery Date (by image)*	*Type*	*Magnitude*	*Period*	*Amplitude*	*Epoch (HJD)*
USNO-B1.0 0943-0001247 2MASS J00095378+0420182	00 09 53.754	04 20 18.18	2012 12 12	WUMa?	16.9 R	8h?	0.4	2456214.596362
GSC 00008:00428 USNO-B1.0 0954-0002869 2MASS J00184579+0527357 UCAC4 478-000501	00 18 45.791	05 27 35.87	2012 10 14	Eclipsing	14.1 R	?	0.4	2456214.646277
USNO-B1.0 1070-0023351 2MASS J02130384+1704255 UCAC4 536-003923 SDSS J021303.84+170425.4	02 13 03.840	17 04 25.71	2012 10 09	W UMa	15.39 R	6.917h	0.92	2456684.566031
USNO-B1.0 1026-0049630 2MASS J04142099+1236292	04 14 20.980	12 36 29.27	2012 12 12	W UMa?	16.3 R	6h+?	0.3?	2456727.619196
USNO-B1.0 1023-0051547 2MASS J04154996+1223131	04 15 49.945	12 23 13.17	2012 12 12	WUMa	18.4 R	6.704h	0.54	2456273.718834
USNO-B1.0 1024-0049987 2MASS J04143495+1229014 UCAC4 063.6455698	04 14 34.932	12 29 01.50	2012 12 12	WUMa	16.23 R	7.145h	0.66	2456273.718834

Table continued on following pages

Table 1. Information about 23 new variable stars, cont.

Star Name and cross-identification	*Position USNO-B1.0 (J2000) R.A.* h m s	*Dec.* ° ′ ″	*Discovery Date (by image)*	*Type*	*Magnitude*	*Period*	*Amplitude*	*Epoch (HJD)*
USNO-B1.0 1023-0051277 2MASS J04143679+1221448 UCAC4 063.6533998	04 14 36.778	12 21 45.03	2012 12 12	W UMa	15.94 R	6.274	0.38	2456273.718834
USNO-B1.0 1295-0192642 2MASS J08005119+3933183 SDSS J080051.19+393318.3	08 00 51.195	39 33 18.79	2012 01 03	?	17.0 R	45.22h	0.7	2455929.660188
USNO-B1.0 1289-0181948 2MASS J08042441+3854362 UCAC4 645-045175 SDSS J080424.40+385436.2	08 04 24.402	38 54 36.50	2011 12 29	WUMa	14.8 R	6.1099h	0.20	2455924.635036
USNO-B1.0 1287-0180792 2MASS J08042435+3845428 SDSS J080424.34+384542.9	08 04 24.345	38 45 43.29	2011 12 29	WUMa	16.7 R	5.3487h	0.19	2455924.637193
USNO-B1.0 1287-0181263 UCAC4 644-044338 2MASS J08061380+3842255 SDSS J080613.81+384225.5	08 06 13.818	38 42 25.83	2011 12 29	Eclipsing	16.0 R	19.537h?	0.55	2455923.626735

Table continued on following pages

Table 1. Information about 23 new variable stars, cont.

Star Name and cross-identification	*Position USNO-B1.0 (J2000) R.A.* h m s	*Dec.* ° ′ ″	*Discovery Date (by image)*	*Type*	*Magnitude*	*Period*	*Amplitude*	*Epoch (HJD)*
USNO-B1.0 1287-0177514 SDSS J080706.96+382856.7	08 07 06.969	38 28 57.49	2011 12 27	WUMa	18.7 R	5.5548h	0.52	2455922.691446
USNO-B1.0 1287-0181515 SDSS J080714.27+384304.2	08 07 14.273	38 43 04.85	2011 12 28	?	15.3 R	12.8h??	0.25	2455923.626735
USNO-B1.0 1288-0184031 UCAC4 645-045277 2MASS J08063051+3848435 SDSS J080630.51+384843.4	08 06 30.521	38 43 43.62	2014 04 08	?	16.2 R	4.31h?	0.09?	2456755.643176
GSC 00814:00461 USNO-B1.0 1023-0198594 UCAC4 512-046328 2MASS J08042435+3845428 SDSS J085346.66+121822.8	08 53 46.669	12 18 23.01	2014 03 25	Eclipsing	15.6 R	5.013h?	0.54	2456741.721395
GSC 01965:01128 USNO-B1.0 1175-0215277 UCAC4 588-046057 2MASS J09301659+2734517 SDSS J093016.58+273451.7	09 30 16.580	27 34 52.26	2011 01 02	W UMa	13.7 R	6.110h	0.09	2455563.719881

Table continued on following pages

Table 1. Information about 23 new variable stars, cont.

Star Name and cross-identification	*Position USNO-B1.0 (J2000) R.A. h m s*	*Dec. ° ' "*	*Discovery Date (by image)*	*Type*	*Magnitude*	*Period*	*Amplitude*	*Epoch (HJD)*
GSC 05568:00529 USNO-B1.0 0791-0263951 UCAC4 396-058141 2MASS J14370018-1048533 SDSS J093016.58+273451.7	14 37 00.198	-10 48 53.35	2011 05 12	RR Lyr?	14.3 R	12.46h?	0.9?	2455693.648030
GSC 05581:00450 USNO-B1.0 0821-0348315 UCAC4 411-060065 2MASS J15162584-0752270	15 16 25.848	-07 52 27.07	2014 03 30	W UMa?	13.8 R	8.4h?	0.4	2456746.817471
USNO-B1.0 0820-0342790 UCAC4 698-084455 2MASS J20471515+4931378	15 16 29.403	--07 54 00.26	2014 03 30	W UMa?	16.3 R	8h+	0.4	2456746.817471
USNO-B1.0 1395-0370184 UCAC4 698-084455 2MASS J20471515+4931378	20 47 15.147	49 31 38.12	2010 10 22	W UMa	14.7 R	4.718h	0.35	2455494.572038

Table continued on next page

Table 1. Information about 23 new variable stars, cont.

Star Name and cross-identification	*Position USNO-B1.0 (J2000) R.A.* *h m s*	*Dec.* *° ′ ″*	*Discovery Date (by image)*	*Type*	*Magnitude*	*Period*	*Amplitude*	*Epoch (HJD)*
USNO-B1.0 1395-0370731 UCAC4 698-084559 2MASS J20474625+4932024	20 47 46.209	49 32 02.88	2010 10 22	W UMa	14.9 R	8.0269h	0.31	2455494.572038
GSC 00540:00848 USNO-B1.0 0962-056701 UCAC4 482-128284 2MASS J21221863+0615034 SDSS J212218.63+061503.3	21 22 18.631	06 15 03.69	2011 07 6	RR Lyr	14.5 R	24.360h	1.2	2455748.702837
GSC 01665:01505 USNO-B1.0 1050-0607272 UCAC4 526-146088 2MASS J21400677+1503109	21 40 06.775	15 03 11.05	2010 10 22	Eclipsing	13.9 R	4.66h??	0.15	2455494.703877

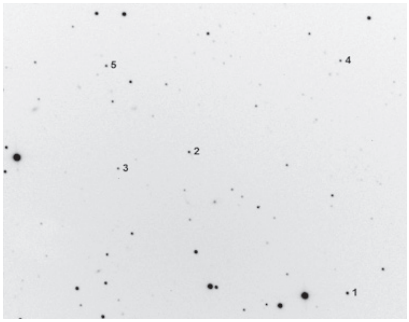

Figure 3. Finder for USNO-B1.0 0943-0001247.

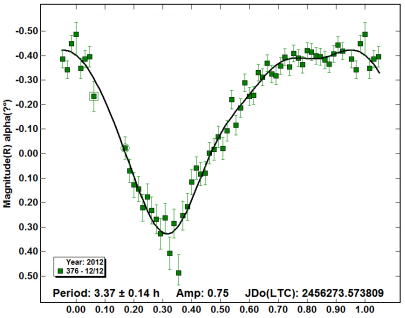

Figure 4. USNO-B1.00943-0001247 phase plot.

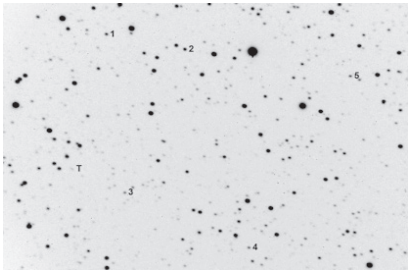

Figure 5. Finder for GSC 00008:00428.

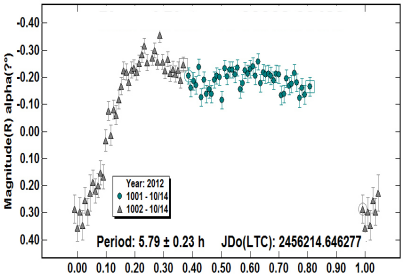

Figure 6. GSC 00008:00428 phase plot.

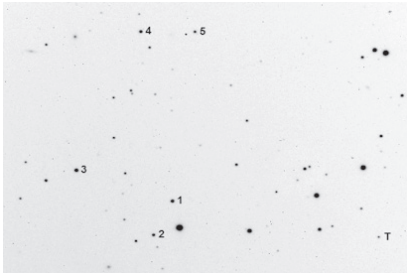

Figure 7. Finder for USNO-B1.0 1070-0023351.

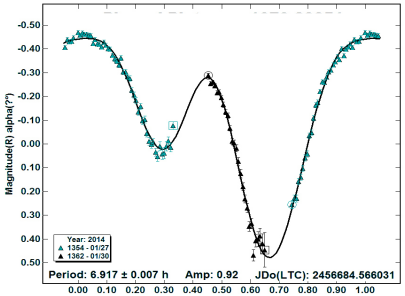

Figure 8. USNO-B1.01070-0023351 phase plot.

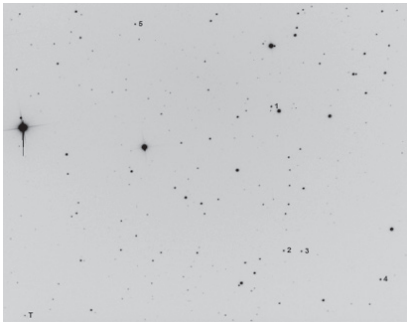

Figure 9. Finder for USNO-B1.0 1026-0049630.

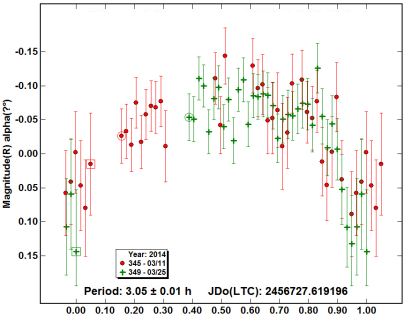

Figure 10. USNO-B1.01026-0049630 phase plot.

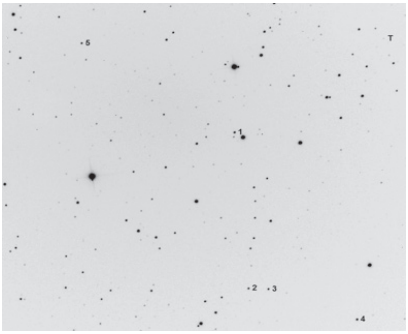

Figure 11. Finder for USNO-B1.0 1023-0051547.

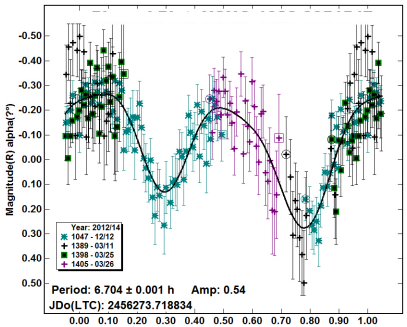

Figure 12. USNO-B1.0 1023-0051547 phase plot.

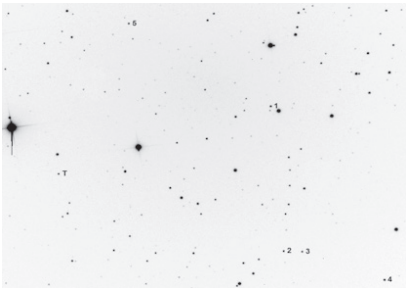

Figure 13. Finder for USNO-B1.0 1024-0049987.

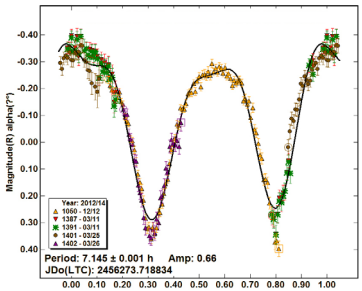

Figure 14. USNO-B1.0 1024-0049987 phase plot.

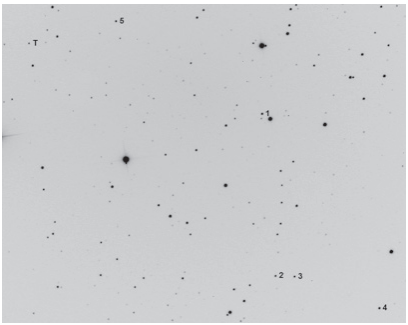

Figure 15. Finder for USNO-B1.0 1023-0051277.

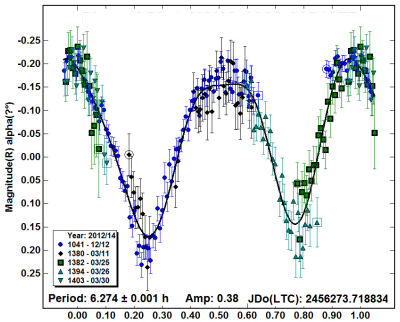

Figure 16. USNO-B1.0 1023-0051277 phase plot.

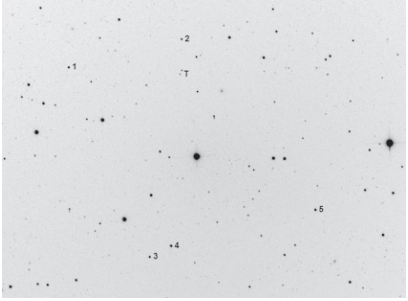

Figure 17. Finder for USNO-B1.0 1295-0192642.

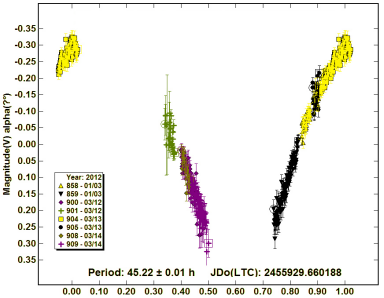

Figure 18. USNO-B1.0 1295-0192642 phase plot.

Figure19.FinderforUSNO-B1.0 1289-0181948.

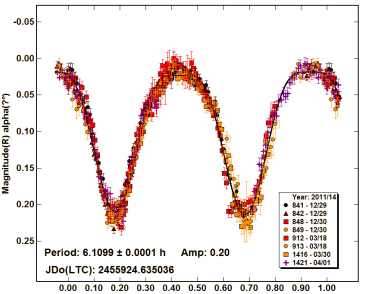

Figure20.USNO-B1.0 1289-0181948phaseplot.

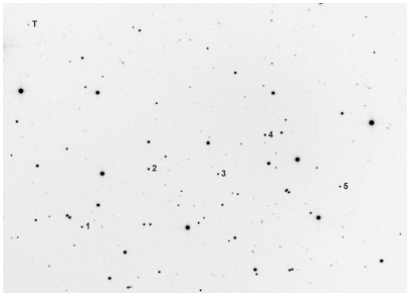

Figure21.FinderforUSNO-B1.01287-0180792.

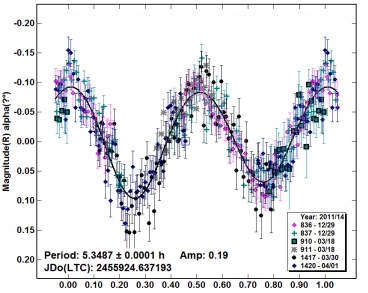

Figure22.USNO-B1.01287-0180792phaseplot.

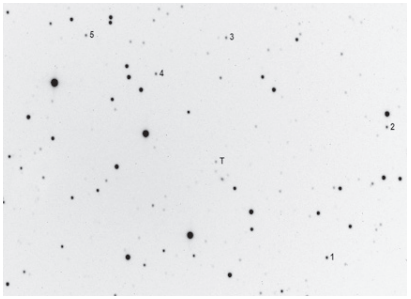

Figure23.FinderforUSNO-B1.01287-0181263.

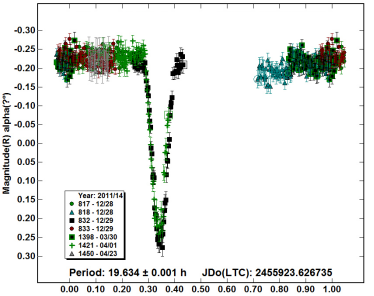

Figure24.USNO-B1.01287-0181263phaseplot.

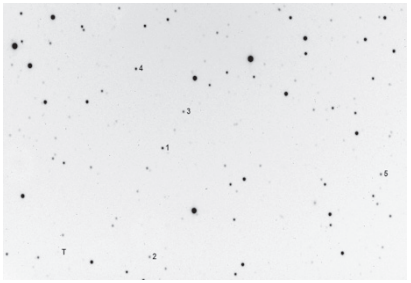

Figure25.FinderforUSNO-B1.01284-0177514.

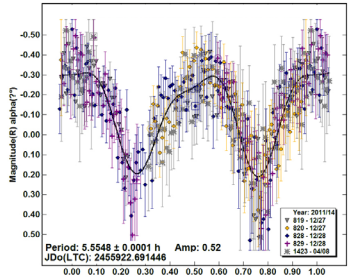

Figure26.USNO-B1.01284-0177514phaseplot.

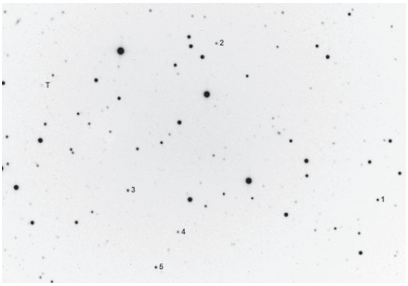

Figure 27. Finder for USNO-B1.0 1287-0181515.

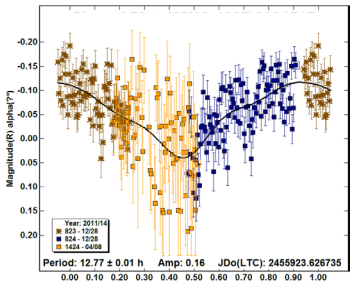

Figure 28. USNO-B1.0 1287-0181515 phase plot.

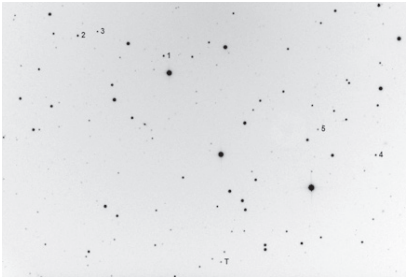

Figure 29. Finder for USNO-B1.0 1288-0184031.

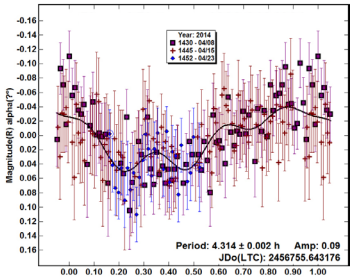

Figure 30. USNO-B1.0 1288-0184031 phase plot.

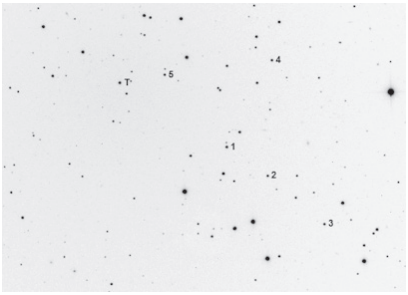

Figure 31. Finder for GSC 00814:00461.

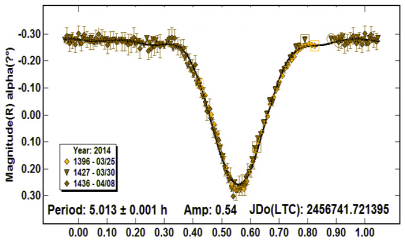

Figure 32. GSC 00814:00461 phase plot.

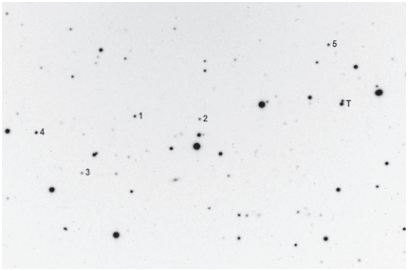

Figure 33. Finder for GSC 01965:01128.

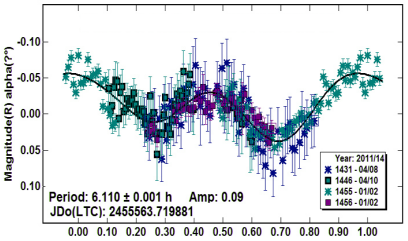

Figure 34. GSC 01965:01128 phase plot.

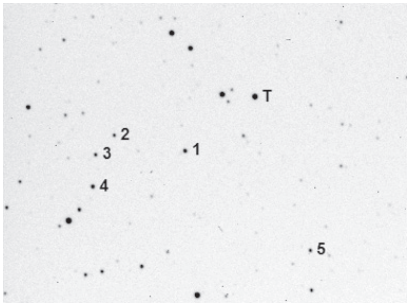

Figure 35. Finder for GSC 05568:00529.

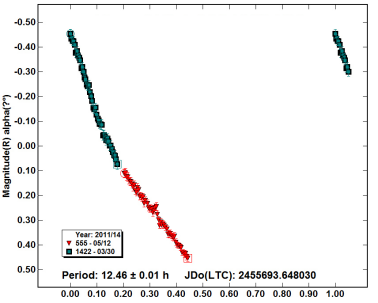

Figure 36. GSC 05568:00529 phase plot.

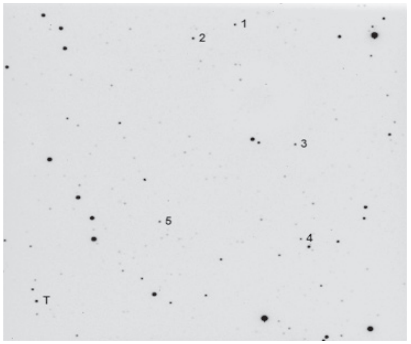

Figure 37. Finder for GSC 05581:00450.

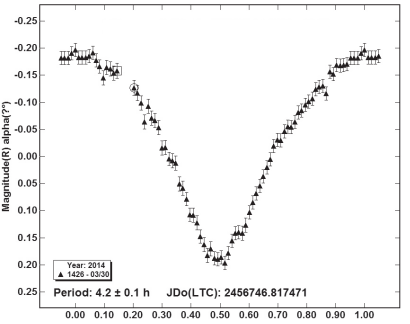

Figure 38. GSC 05581:00450 phase plot.

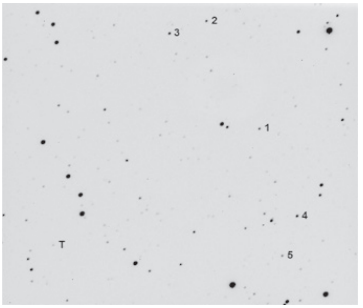

Figure39. Finder for USNO-B1.0 0820-0342790.

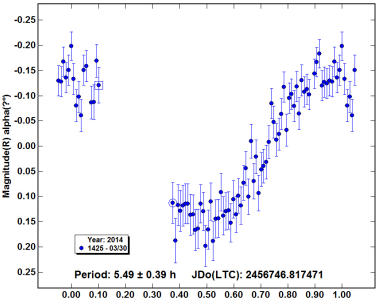

Figure40. USNO-B1.0 0820-0342790 phase plot.

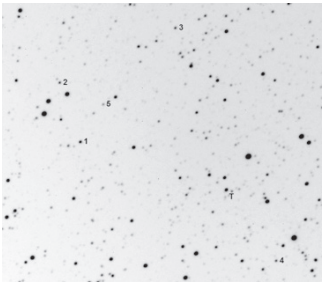

Figure41. Finder for USNO-B1.0 1395-0370184.

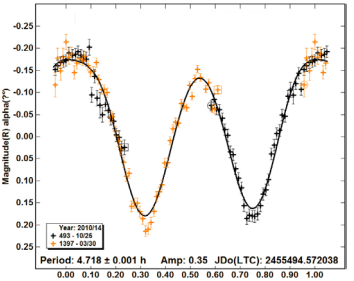

Figure42. USNO-B1.0 1395-0370184 phase plot.

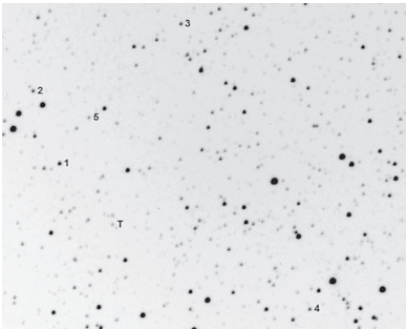

Figure43. FinderforUSNO-B1.0 1395-0370731.

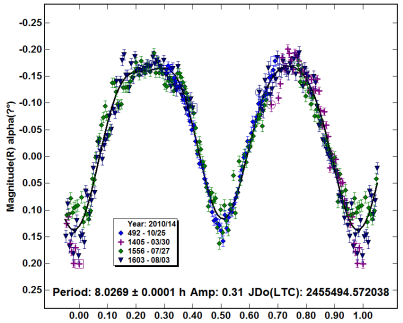

Figure44. USNO-B1.0 1395-0370731 phaseplot.

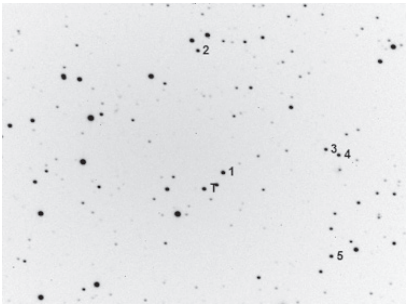

Figure 45. Finder for GSC 00540:00848.

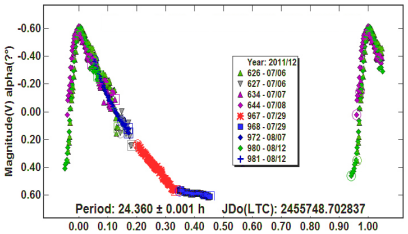

Figure 46. GSC 00540:00848 phase plot.

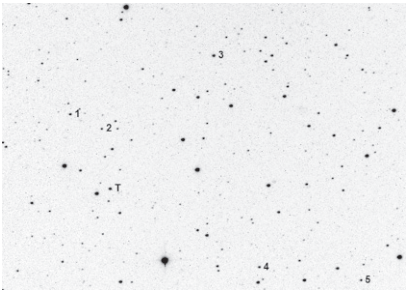

Figure 47. Finder for GSC 01665:01505.

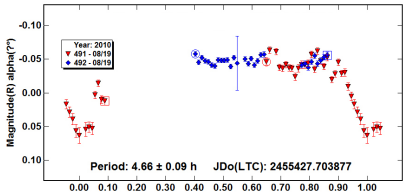

Figure 48. GSC 01665:01505 phase plot.

References

Software Bisque. 2012, CCDSOFT CCD control software (http://www.bisque.com).

Warner, B. D. 2012, MPO CANOPUS, version 10.4.3.17, BDW Publishing, Colorado Springs, CO (http://minorplanetobserver.com).

Twenty-Two New Variable Stars in the Northern Sky and Light Elements Improvement for PT Lyr, [WM2007] 1157, and [WM2007] 1160

Riccardo Furgoni
Keyhole Observatory MPC K48, Via Fossamana 86, S. Giorgio di Mantova (MN), Italy; riccardo.furgoni@gmail.com

and

AAMN Gorgo Astronomical Observatory MPC 434, S. Benedetto Po (MN), Italy

Received April 17,2014; revised April 28, 2014; accepted April 28, 2014

Abstract I report the discovery of twenty-two new variable stars in the Northern Sky: eleven eclipsing, seven pulsating (one of which is suspected), three rotating, and one of unspecified type. Three already known variables (PT Lyr, [WM2007] 1157, and [WM2007] 1160) have been studied more carefully in order to clarify their characterization or provide updated ephemeris.

1. Introduction

A new photometric campaign aimed at the discovery of variable stars was carried out from the Keyhole Observatory (MPC K48) in S. Giorgio di Mantova, Italy. Three separate fields were observed, located in the constellations Cassiopeia, Lacerta, and both Lyra and Cygnus, over a period of forty-one nights, obtaining 4,492 images in the V passband with an overall exposure time of almost 150 hours. Subsequently, the light curves of all stars in the fields have been visually inspected in order to determine the candidate variables, starting with those that have an RMS scatter vs. magnitude higher than normal. When possible, the observations were combined with CTI-I Survey (Wetterer and McGraw 2007), NSVS (Woźniak *et al.* 2004), and SuperWASP (Butters *et al.* 2010) datasets in order to improve the precision in the determination of the period, magnitude range, and the type of variability.

Some known variables in the fields (PT Lyr, [WM2007] 1157, and [WM2007] 1160) have been studied more carefully in order to clarify their characterization or provide updated ephemeris.

2. Instrumentation used

The data were obtained with a Celestron C8 Starbright, a Schmidt-Cassegrain optical configuration with aperture of 203 mm and central obstruction of 34%.

The telescope was positioned at coordinates 45°12'33"N 10°50'20"E (WGS84) at the Keyhole Observatory, a roll-off roof structure managed by

the author. The telescope was equipped with a focal reducer Baader Planetarium Alan Gee II able to bring the focal length from 2030 mm to 1413 mm in the optical train used. The focal ratio is down to f/6.96 from the original f/10.

The pointing was maintained with a Syntha NEQ6 mount guided via a Baader Vario Finder telescope equipped with a Barlow lens capable of bringing the focal length of the system to 636 mm and focal ratio of f/10.5. The guide camera used was a Magzero MZ-5 with a Micron MT9M001 monochrome sensor. The CCD camera used was a SBIG ST8300 m with monochrome sensor Kodak KAF8300. Photometry in the Johnson V passband was performed with an Astrodon Photometrics Johnson-V 50 mm round unmounted filter, equipping a Starlight Xpress USB filterwheel.

The camera is equipped with a 1000X antiblooming: after exhaustive testing it has been verified that the zone of linear response is between 1000 and 20000 ADU, although up to 60000 ADU the loss of linearity is less than 5%. The CCD is equipped with a single-stage Peltier cell $\Delta T = 35 \pm 0.1°$ C which allows the cooling at a stationary temperature.

3. Data collection

The observed fields are centered respectively at coordinates (J2000) R.A. $19^h\,19^m\,00^s$, Dec. +28° 03' 30", R.A. $22^h\,41^m\,00^s$, Dec. +48° 00' 00", and R.A. $02^h\,53^m\,09^s$, Dec. +62° 02' 00". The dimensions for all are 44' × 33' with a position angle of 360°.

These fields were chosen to maximize the possibility of discovering new variable stars. Their determination was made trying to meet the following criteria:

- low galactic latitude to have a greater number of sources;
- equatorial coordinates compatible with low air masses for most of the night in the observing site;
- low or no presence of already known variables, where this element has been determined by analyzing the distribution of the variables in the International Variable Star Index (Watson *et al.* 2007) operated by the AAVSO.

The observations were performed with the CCD at a temperature of –10°C (in summer and fall) and –20°C (in winter) in binning 1 × 1. The exposure time was 120 seconds with a delay of 1 second between the images and an average download time of 11 seconds per frame. Once the images were obtained, the calibration frames were taken for a total of 100 dark of 120 seconds each, 200 darkflat of 2 seconds, and 50 flat of 2 seconds. The darkflats and darks were taken only the first observation session for every field and used for all other sessions. The flats were taken for each session as the position of the CCD camera could be varied slightly, as well as the focus point.

The calibration frames were combined with the method of the median, and the masterframes obtained were then used for the correction of the images taken. All images were then aligned and an astrometric reduction was made to implement the astrometrical coordinate system WCS in the FITS header. These operations were conducted entirely through the use of MAXIMDL version 5.23 (Diffraction Limited 2012).

4. Methods and procedures

This work is a continuation of the wider survey activity conducted from the Keyhole Observatory-MPC K48 for the discovery of new variable stars. In this section, the methods and procedures used are presented in a very schematic way; details can be found in the author's previously published work (see, in particular, Furgoni (2013a and 2013b)). The technique used for the determination of the magnitude was differential photometry, ensemble-type, in almost all cases. As is known, it is necessary to have comparison stars with magnitudes accurately determined in order to obtain reliable measurements, and as close to the standard system as possible. Since the entire observational campaign was conducted with the use of the Johnson V filter, the comparison star magnitudes were obtained:

- as a first choice from the APASS (Henden *et al.* 2013) V-magnitude data provided by the AAVSO;
- as a second choice deriving the V magnitude from the CMC14 (Copenhagen Univ. Obs. 2006) r' magnitude as described in Dymock and Miles (2009).

In both cases the calculated magnitude for the check star was only slightly different from the respective APASS V magnitude and CMC14-derived V magnitude. In fact, in the first case, the average error was normally of the order of 0.01–0.02 magnitude, while in the second case it never exceeded 0.05 magnitude. These errors are stable even when using stars with moderately different color indices.

The search for new variable stars was performed using the same technique described in the author's previously published work; the method involves the distinction between discovery-nights and follow-up nights. The first is needed to determine if the chosen field contains potential candidate variables through the creation of a magnitude-RMS diagram and the accurate visual inspection of all light curves down to sixteenth magnitude. If in the discovery-night the chosen field does not appear interesting, it is discarded without further analysis. The follow-up nights are necessary for the collection of data concerning variable star candidates. In any case, any follow-up night is checked again by a magnitude-RMS scatter diagram. In this case, however, the light curves of the

stars in the field are not inspected visually due to the long time needed for the operation. The combination of these two methods ensures a good compromise between the need to maximize the chance of discovery and the need to obtain the maximum from the data gradually collected.

Before proceeding further with the analysis, the time of the light curves obtained was heliocentrically corrected (HJD) in order to ensure perfect compatibility of the data with other observations carried out, even at a considerable distance in time. When necessary, the determination of the period was calculated using the software PERIOD04 (Lenz and Breger 2005), using a Discrete Fourier Transform (DFT). The average zero-point (average magnitude of the object) was subtracted from the dataset to prevent the appearance of artifacts centered at a frequency 0.0 of the periodogram. The calculation of the uncertainties was carried out with PERIOD04 using the method described in Breger *et al.* (1999).

To improve the period determination, the NSVS and SWASP photometric data were used when available. However, due to high scattering which in some cases affects them, the data with high uncertainties were eliminated. The NSVS and SWASP data were also corrected in their zero-point to make them compatible with the author's V-band data. Having the same zero-point is indeed crucial for correct calculation of the PERIOD04 Discrete Fourier Transform.

5. New variable stars and known variables studied

In this survey twenty-two new variable stars were discovered and three already known variables (PT Lyr, [WM2007] 1157, and [WM2007] 1160) were studied more carefully. The population of the new variables is as follows:

- 11 eclipsing (4 βLyr, 4 β Per, and 3 W UMa)
- 7 pulsating (6 δ Sct (one suspected), 1 Semiregular)
- 3 rotating (3 rotating ellipsoidal)
- 1 unspecified (but with evident signs of periodicity)

The coordinates of all new variable stars discovered in this survey are reported as they appear in the UCAC4 catalogue (Zacharias *et al.* 2012) and differ from the detected positions by never more than 0.5".

5.1. [WM2007] 1157

Position (UCAC4): R.A. (J2000) = $19^h\,18^m\,27.56^s$, Dec. (J2000) = +28° 01" 55.0"

Cross Identification: 2MASS J19182756+2801550; UCAC4 591-078527

Variability Type: δ Sct

Magnitude: Max. 14.30 V, Min. 14.49 V

Main Period: 0.043525536(4) d

Secondary Period: 0.05312469(1) d

Epoch Main Period: 2456505.39440(27) HJD

Epoch Secondary Period: 2456505.54615(54) HJD

Ensemble Comparison Stars: UCAC4 591-078539 (CMC14 derived 13.542 V); UCAC4 591-078567 (CMC14 derived 13.890 V)

Check Star: UCAC4 591-078567

Notes: J–K = 0.078. The star shows a clear, continuous modulation of the light curve.

Fourier spectrum and phase plots are shown in Figures 1, 2, and 3.

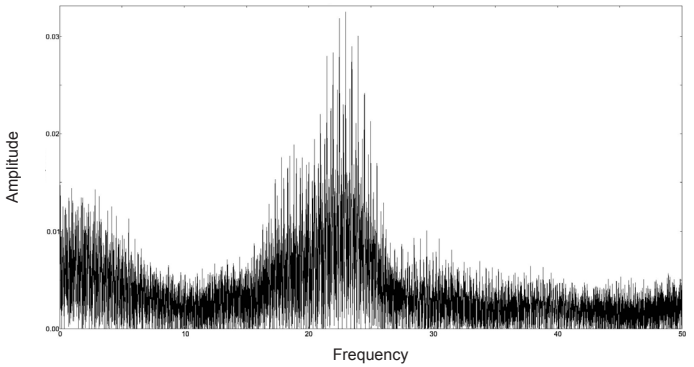

Figure 1. Fourier spectrum of [WM2007] 1157.

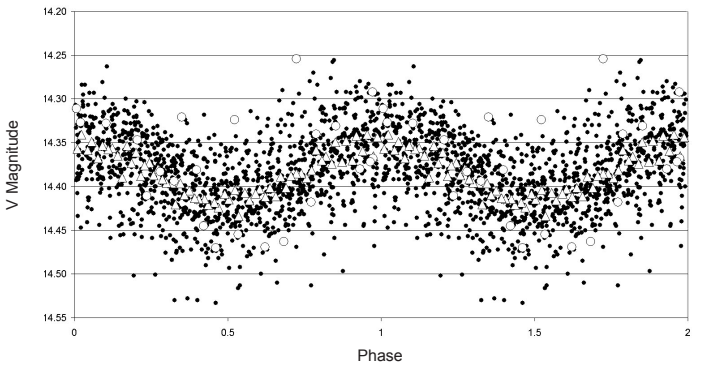

Figure 2. Main Period Phase plot of [WM2007] 1157. Filled circles denote Furgoni data; open triangles denote Furgoni data (binning 20); open circles denote CTI-I survey data.

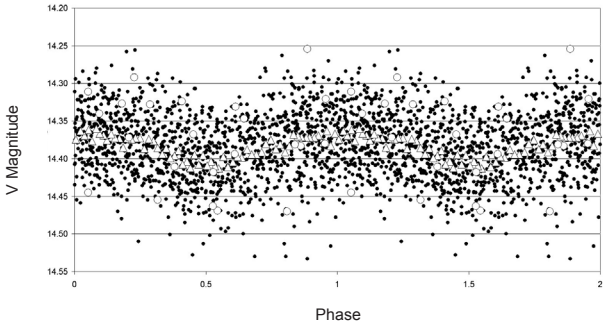

Figure 3. Secondary Period Phase plot of [WM2007] 1157. Filled circles denote Furgoni data; open triangles denote Furgoni data (binning 20); open circles denote CTI-I survey data.

5.2. [WM2007] 1160

Position (UCAC4): R.A. (J2000) = $19^h\ 20^m\ 03.51^s$, Dec. (J2000) = +28° 04' 24.4"

Cross Identification: 2MASS J19200351+2804246; UCAC4 591-079175

Variability Type: W UMa

Magnitude: Max. 15.50 V, Min. 16.08 V

Period: 0.4978081(1) d

Epoch: 2456462.5052(7) HJD

Ensemble Comparison Stars: UCAC4 591-079193 (CMC14 derived 14.326 V); UCAC4 591-079139 (CMC14 derived 13.806 V)

Check Star: UCAC4 591-079214

Notes: J–K = 0.45. Phase Plot is shown in Figure 4.

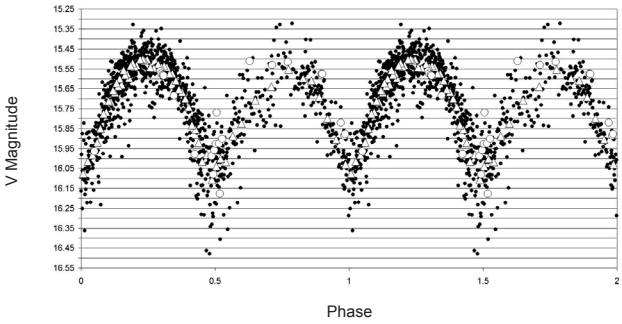

Figure 4. Phase plot of [WM2007] 1160. Filled circles denote Furgoni data; open triangles denote Furgoni data (binning 20); open circles denote CTI-I survey data.

5.3. PT Lyr

Position (UCAC4): R.A. (J2000) = $19^h\,18^m\,29.40^s$, Dec. (J2000) = +27° 55' 41.4"

Cross Identification: VV 108

Variability Type: RR Lyrae (ab type)

Magnitude: Max. 15.41 V, Min, 16.80 V

Period: 0.5159309(15) d

Epoch: 2456462.515(2) HJD

Ensemble Comparison Stars: UCAC4 590-080143 (CMC14 derived 13.298 V); UCAC4 590-080184 (CMC14 derived 14.295 V)

Check Star: UCAC4 590-080067

Notes: Rise duration 13%. Phase plot is shown in Figure 5.

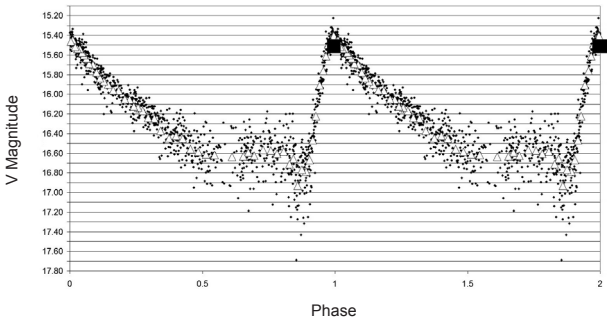

Figure 5. Phase plot of PT Lyr. Filled circles denote Furgoni data; open triangles denote Furgoni data (binning 20); large squares denote VV108 published time of maximum (Miller and Wachmann 1963).

5.4. 2MASS J19181000+2801294

Position (UCAC4): R.A. (J2000) = $19^h\,18^m\,10.00^s$, Dec. (J2000) = 28° 01' 29.6"

Cross Identification: UCAC4 591-078397

Variability Type: β Per

Magnitude: Max. 15.83 V, Min. 16.82 V

Period: 0.89394(12) d

Epoch: 2456508.3230(42) HJD

Ensemble Comparison Stars: UCAC4 591-078539 (CMC14 derived 13.542V); UCAC4 591-078667 (CMC14 derived 13.676 V)

Check Star: UCAC4 591-078567

Notes: J–K = 0.23. Eclipse duration 16%. Phase plot is shown in Figure 6.

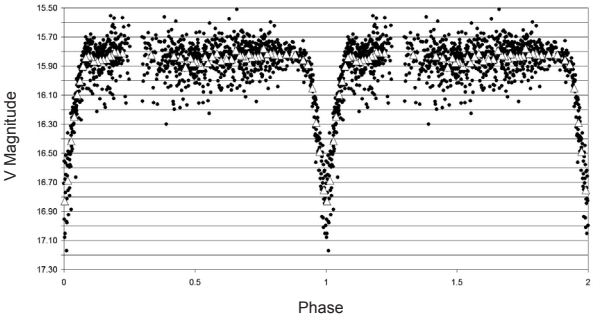

Figure 6. Phase plot of 2MASS J19181000+2801294. Filled circles denote Furgoni data; open triangles denote Furgoni data (binning 20).

5.5. 2MASS J19194398+2758145

Position (UCAC4): R.A. (J2000) = $19^h\,19^m\,43.98^s$, Dec. (J2000) = 27° 58' 14.5"

Cross Identification: NOMAD1 1179-0436600

Variability Type: W UMa

Magnitude: Max. 15.6 V, Min. 16.4 V

Period: 0.311487(7) d

Epoch: 2456462.5530(16) HJD

Ensemble Comparison Stars: UCAC4 590-080783 (CMC14 derived 11.119 V); UCAC4 590-080567 (CMC14 derived 11.781 V)

Check Star: UCAC4 590-080651

Notes: Aperture photometry was performed on the blended source formed by the variable and the close companion 2MASS J19194382+2758185 that lies 4.4" away. Subsequently, the magnitude of the companion (13.45 V) was measured from a stack of 30 frames (in order to improve the SNR and highlight the small separation) and subtracted from the blended source. Phase plot is shown in Figure 7.

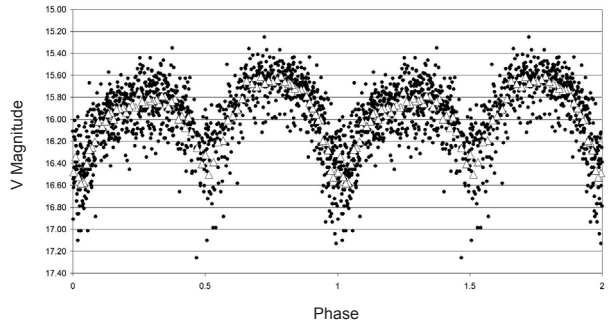

Figure 7. Phase plot of 2MASS J19194398+2758145. Filled circles denote Furgoni data; open triangles denote Furgoni data (binning 15).

5.6. GSC 02132-03510

Position (UCAC4): R.A. (J2000) = $19^h\,17^m\,52.22^s$, Dec. (J2000) = +27° 54' 31.7"

Cross Identification: 2MASS J19175221+2754317; UCAC4 590-079883

Variability Type: δ Sct

Magnitude: Max. 11.62 V, Min. 11.64 V

Period: 0.096578(4) d

Epoch: 2456495.41908(7) HJD

Ensemble Comparison Stars: UCAC4 590-080116 (CMC14 derived 11.275 V); UCAC4 590-080091 (CMC14 derived 12.223 V)

Check Star: UCAC4 590-080046

Notes: J–K = 0.23. Phase plot is shown in Figure 8.

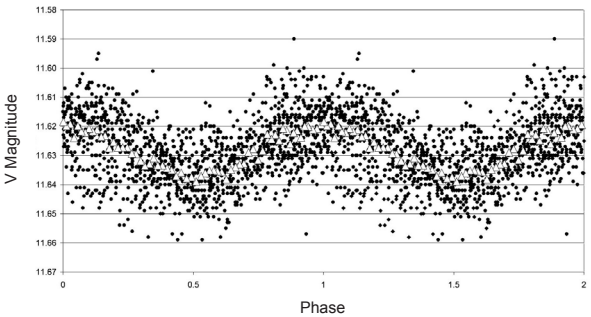

Figure 8. Phase plot of GSC 02132-03510. Filled circles denote Furgoni data; open triangles denote Furgoni data (binning 20).

5.7. GSC 02136-03136

Position (UCAC4): R.A. (J2000) = $19^h\,20^m\,34.93^s$, Dec. (J2000) = +28° 13' 31.6"

Cross Identification: 2MASS J19203492+2813315; UCAC4 592-078257

Variability Type: δ Sct

Magnitude: Max. 12.475 V, Min. 12.495 V

Period: 0.079901(3) d

Epoch: 2456505.5814(7) HJD

Ensemble Comparison Stars: UCAC4 591-078993 (CMC14 derived 10.762 V); UCAC4 591-079007 (CMC14 derived 12.075 V)

Check Star: UCAC4 591-078915

Notes: J–K = 0.23. Phase plot is shown in Figure 9.

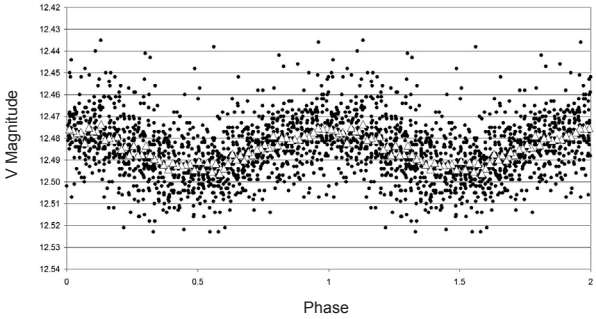

Figure 9. Phase plot of GSC 02136-03136. Filled circles denote Furgoni data; open triangles denote Furgoni data (binning 20).

5.8. GSC 03625-01173

Position (UCAC4): R.A. (J2000) = $22^h\,42^m\,09.90^s$, Dec. (J2000) +47° 45' 26.7"

Cross Identification: 2MASS J22420989+4745267; UCAC4 689-119504; NSVS 6068811

Variability Type: β Lyr

Magnitude: Max 12.57 V, Min. 12.95 V

Period: 0.9921132(3) d

Epoch: 2456560.418(2) HJD

Ensemble Comparison Stars: UCAC4 689-119409 (APASS 12.382 V); UCAC4 689-119403 (APASS 12.443 V)

Check Star: UCAC4 689-119442

Notes: Secondary minimum = 12.80 V. Phase plot is shown in Figure 10.

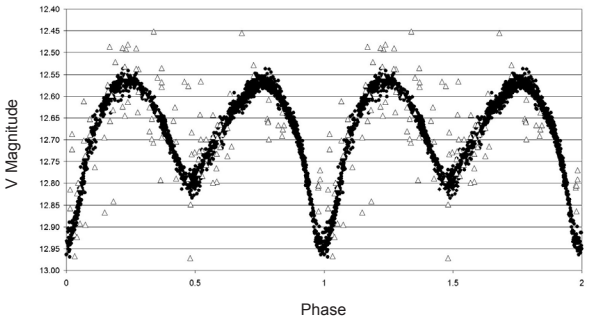

Figure 10. Phase plot of GSC 03625-01173. Filled circles denote Furgoni data; open triangles denote NSVS data (with error less than 0.1 magnitude).

5.9. 2MASS J22405571+4804277

Position (UCAC4): R.A. (J2000) = $22^h\,40^m\,55.72^s$, Dec. (J2000) = +48° 04' 27.9"

Cross Identification: UCAC4 691-117787; NSVS 6067528

Variability Type: β Lyr

Magnitude: Max. 13.57 V, Min. 14.16 V

Period: 0.763656(16) d

Epoch: 2456559.3958(12) HJD

Ensemble Comparison Stars: UCAC4 691-117919 (CMC14 derived 12.358 V); UCAC4 691-117825 (CMC14 derived 12.301 V)

Check Star: UCAC4 691-117831

Notes: Secondary minimum = 13.75 V. Phase plot is shown in Figure 11.

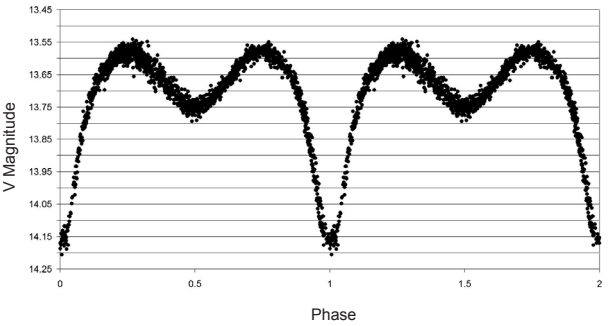

Figure 11. Phase plot of 2MASS J22405571+4804277. Filled circles denote Furgoni data.

5.10. 2MASS J22421092+4807300

Position (UCAC4): R.A. (J2000) = $22^h\,42^m\,10.93^s$, Dec. (J2000) = +48° 07' 30.0"

Cross Identification: UCAC4 691-118072; USNO-B1.0 1381-0557121

Variability Type: W UMa

Magnitude: Max. 15.50 V, Min. 15.67 V

Period: 0.267008(3) d

Epoch: 2456559.404(1) HJD

Ensemble Comparison Stars: UCAC4 691-118056 (CMC14 derived 14.835 V); UCAC4 691-118045 (CMC14 derived 14.969 V)

Check Star: UCAC4 691-118048

Notes: Phase plot is shown in Figure 12.

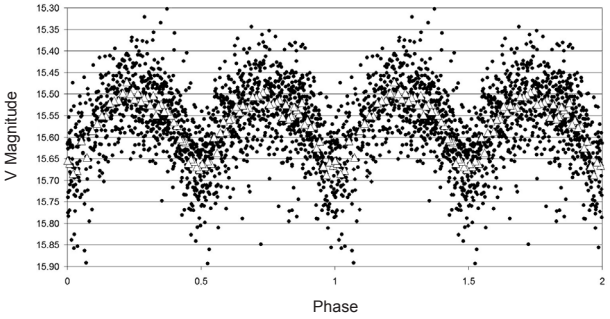

Figure 12. Phase plot of 2MASS J22421092+4807300. Filled circles denote Furgoni data; open triangles denote Furgoni data (binning 20).

5.11. GSC 03624-02592

Position (UCAC4): R.A. (J2000) = $22^h\,40^m\,30.81^s$, Dec. (J2000) +47° 48' 10.5"

Cross Identification: 2MASS J22403080+4748105; UCAC4 690-119955; NSVS 6067049

Variability Type: δ Sct

Magnitude: Max .12.79 V, Min. 12.82 V

Period: 0.072472(2) d

Epoch: 2456549.4393(7) HJD

Ensemble Comparison Stars: UCAC4 690-119902 (CMC14 derived 11.383 V); UCAC4 690-119823 (CMC14 derived 11.625 V)

Check Star: UCAC4 690-120037

Notes: Phase plot is shown in Figure 13.

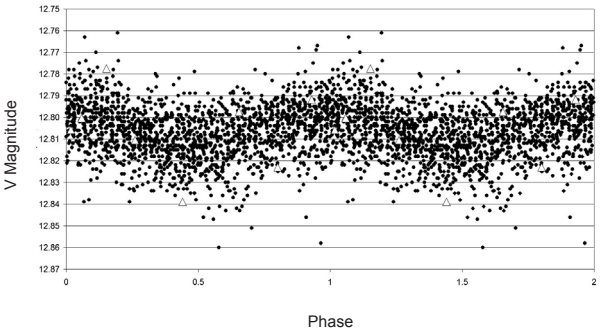

Figure 13. Phase plot of GSC 03624-02592. Filled circles denote Furgoni data; open triangles denote NSVS data (error less than 0.1 magnitude; binning 20).

5.12. GSC 03624-02115

Position (UCAC4): R.A. (J2000) = $22^h\,40^m\,57.49^s$, Dec. (J2000) = 47° 54' 20.9"

Cross Identification: 2MASS J22405748+4754206; UCAC4 690-120057; NSVS 6067581

Variability Type: Semiregular Late-type (SRB)

Magnitude: Max. 12.65 V, Min. 13.02 V

Period: 55.5(1) d

Epoch: 2456531.7(5) HJD

Ensemble Comparison Stars: UCAC4 690-119902 (CMC14 derived 11.383 V); UCAC4 690-119823 (CMC14 derived 11.625 V)

Check Star: UCAC4 690-120037

Notes: J–K = 1.25. NSVS magnitude contaminated by GSC 03624-02481 (V = 12.1; sep. 46") and other nearby stars. NSVS range has been corrected and shifted in the phase plot. Light curve and phase plot are shown in Figures 14 and 15.

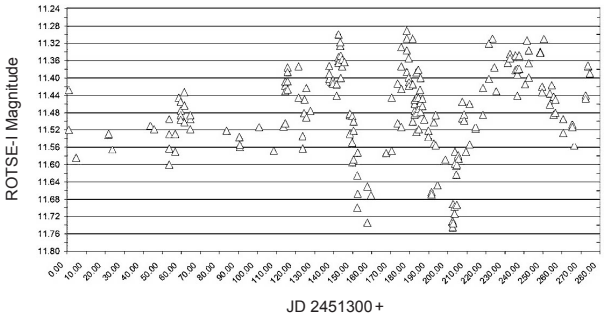

Figure 14. NSVS light curves of GSC 03624-02115 (after subtraction of the blended source GSC 03624-02481; V 12.1; separation 46").

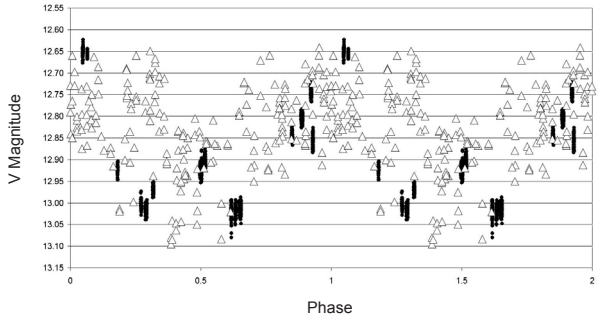

Figure 15. Phase plot of GSC 03624-02115. Filled circles denote Furgoni data; open triangles denote NSVS data (magnitude of the blended source GSC 03624–02481; +1.35 magnitude offset).

5.13. GSC 03625-01798

Position (UCAC4): R.A. (J2000) = $22^h 42^m 59.93^s$, Dec. (J2000) = +47° 57' 43.4"

Cross Identification: 2MASS J22425993+4757434; UCAC4 690-120491

Variability Type: Rotating ellipsoidal

Magnitude: Max. 13.79 V, Min. 13.85 V

Period: 0.55392(2) d

Epoch: 2456623.323(2) HJD

Ensemble Comparison Stars: UCAC4 690-120342 (CMC14 derived 11.762 V); UCAC4 690-120233 (CMC14 derived 11.810 V)

Check Star: UCAC4 690-120294

Notes: J–K = 0.65. Secondary minimum = 13.83 V. Phase plot is shown in Figure 16.

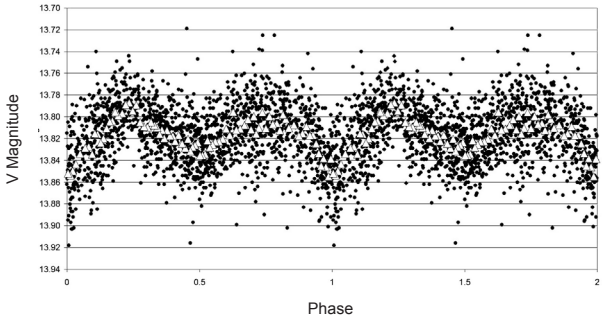

Figure 16. Phase plot of GSC 03625-01798. Filled circles denote Furgoni data; open triangles denote Furgoni data (binning 20).

5.14. GSC 04052-01292

Position (UCAC4): R.A. (J2000) = $02^h 52^m 44.53^s$, Dec. (J2000) = +62° 00' 13.4"

Cross Identification: 2MASS J02524451+6200133; UCAC4 761-021866; NSVS 1888262

Variability Type: β Per

Magnitude: Max. 13.88 V, Min. 14.62 V

Period: 1.00599(8) d

Epoch: 2456712.241(1) HJD

Ensemble Comparison Stars: UCAC4 760-023030 (APASS 11.963 V); UCAC4 760-022993 (APASS 11.608 V)

Check Star: UCAC4 760-022973

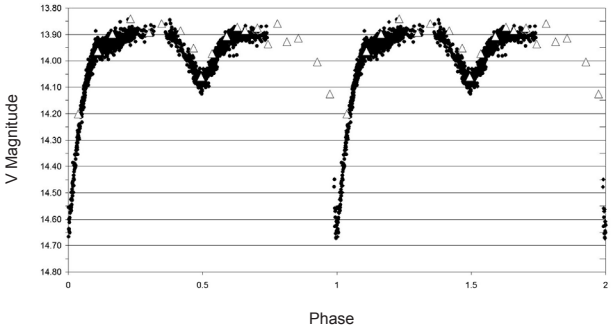

Figure 17. Phase plot of GSC 04052-01292. Filled circles denote Furgoni data; open triangles denote NSVS data (+0.16 magnitude offset; binning 20).

Notes: Eclipse duration 20%. Secondary minimum = 14.07 V. Phase plot is shown in Figure 17.

5.15. GSC 04051-02709

Position (UCAC4): R.A. (J2000) = $02^h\,50^m\,12.66^s$, Dec. (J2000) = 62° 04' 55.0"

Cross Identification: 2MASS J02501265+6204549; UCAC4 761-021561

Variability Type: β Per

Magnitude: Max. 12.88 V, Min. 13.22 V

Period: 1.57580(6) d

Epoch: 2456711.250(4) HJD

Ensemble Comparison Stars: UCAC4 761-021680 (APASS 12.068 V); UCAC4 761-021669 (APASS 12.142 V)

Check Star: UCAC4 761-021632

Notes: Eclipse duration 18%. Secondary minimum = 13.15 V. Phase plot is shown in Figure 18.

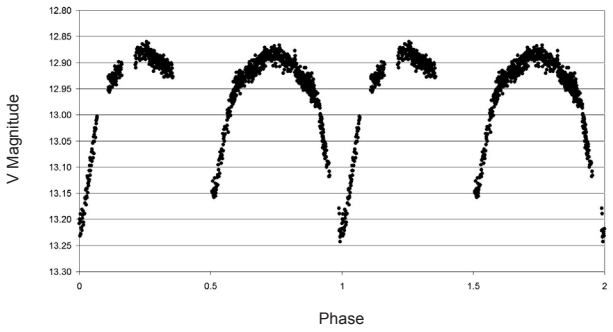

Figure 18. Phase plot of GSC 04051-02709. Filled circles denote Furgoni data..

5.16. GSC 04052-01378

Position (UCAC4): R.A. (J2000) = $02^h\,53^m\,08.34^s$, Dec. (J2000) = +62° 06' 10.5"

Cross Identification: UCAC4 761-021922; NSVS 1888562; 1SWASP J025308.36+620610.7

Variability Type: β Per

Magnitude: Max. 11.76 V, Min. 12.08: V

Spectral type: B2

Period: 18.3024(1) d

Epoch: 2451403.83(1) HJD

Ensemble Comparison Stars: UCAC4 761-021906 (APASS 12.498 V); UCAC4 761-021905 (APASS 12.566 V)

Check Star: UCAC4 761-022036

Notes: Primary eclipse duration 2%:. Secondary minimum = 12.06 V with eclipse duration 6%:. The great difference between eclipse duration in Min. and Min. II is indicative of a very eccentric system. Min. II observations are better phased with slightly shorter period suggesting possible apsidal motion. Elements for Min. II are HJD 2451486.75 + 18.3007 × E. Spectral type taken from Skiff (2009–2013). Phase plots are shown in Figures 19, 20, 21, and 22.

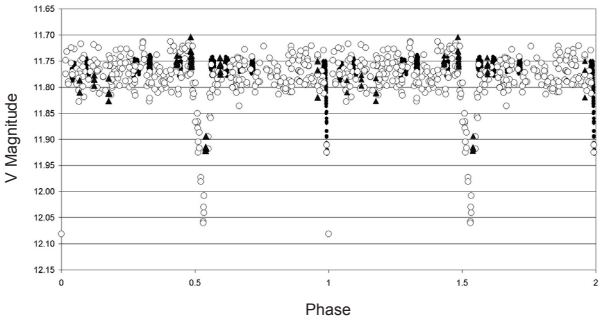

Figure 19. Phase plot of GSC 04052-01378. Filled circles denote Furgoni data; open circles denote NSVS data (+0.15 magnitude offset); filled triangles denote SWASP data (+0.08 magnitude offset).

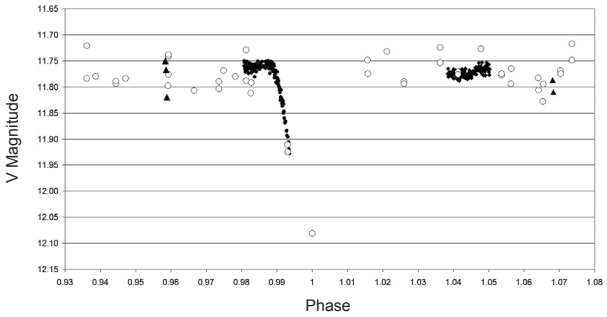

Figure 20. Phase plot of GSC 04052-01378 (Zoom on primary minimum). Filled circles denote Furgoni data; open circles denote NSVS data (+0.15 magnitude offset); filled triangles denote SWASP data (+0.08 magnitude offset).

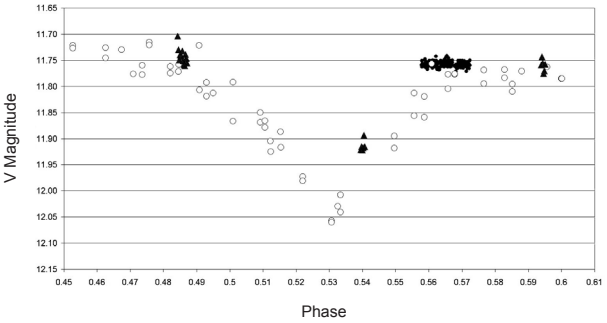

Figure 21. Phase plot of GSC 04052-01378 (Zoom on secondary minimum). Filled circles denote Furgoni data; open circles denote NSVS data (+0.15 magnitude offset); filled triangles denote SWASP data (+0.08 magnitude offset).

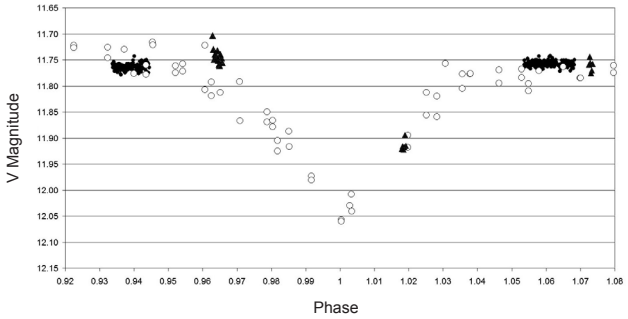

Figure 22. Phase plot of GSC 04052-01378 (Zoom on secondary minimum phased on its own elements; possible apsidal motion). Filled circles denote Furgoni data; open circles denote NSVS data (+0.15 magnitude offset); filled triangles denote SWASP data (+0.08 magnitude offset). Period = 18.3007 d; HJDmin = 2451486.75.

5.17. 2MASS J02530428+6208007

Position (UCAC4): R.A. (J2000) = $02^h\,53^m\,04.31^s$, Dec. (J2000) = +62° 08' 00.8"

Cross Identification: UCAC4 761-021911; USNO-B1.0 1521-0094336

Variability Type: β Lyr

Magnitude: Max. 14.06 V, Min. 14.23 V

Period: 0.81069(2) d

Epoch: 2456631.343(1) HJD

Ensemble Comparison Stars: UCAC4 761-021906 (APASS 12.498 V); UCAC4 761-021905 (APASS 12.566 V)

Check Star: UCAC4 761-022036

Notes: Secondary minimum = 14.17 V and secondary maximum = 14.10 V. Phase plot is shown in Figure 23.

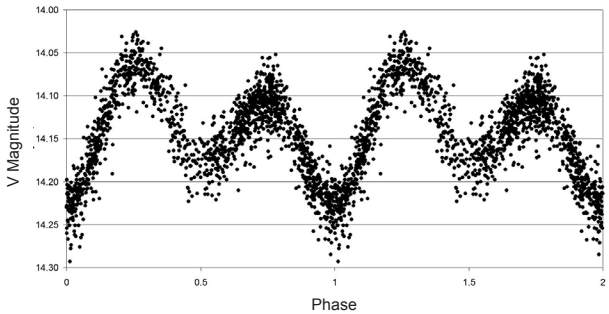

Figure 23. Phase plot of 2MASS J02530428+6208007. Filled circles denote Furgoni data.

5.18. 2MASS J02524261+6157132

Position (UCAC4): R.A. (J2000) = $02^h\,52^m\,42.65^s$, Dec. (J2000) = +61° 57' 13.2"

Cross Identification: UCAC4 760-023072; 1SWASP J025242.72+615713.1

Variability Type: β Lyr

Magnitude: Max. 14.90 V, Min. 15.27 V

Period: 1.56250(9) d

Epoch: 2456713.405(3) HJD

Ensemble Comparison Stars: UCAC4 760-023030 (APASS 11.963 V); UCAC4 760-022993 (APASS 11.608 V)

Check Star: UCAC4 760-022973

Notes: Secondary minimum = 15.05 V. Phase plot is shown in Figure 24.

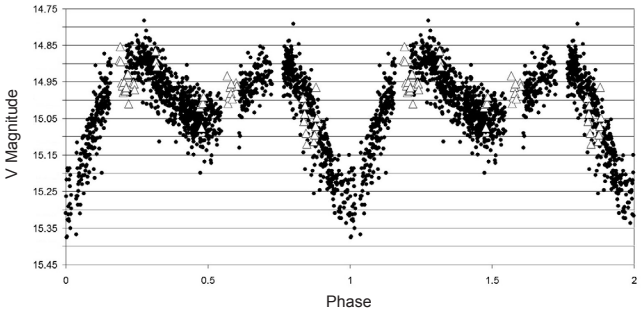

Figure 24. Phase plot of 2MASS J02524261+6157132. Filled circles denote Furgoni data; open triangles denote SWASP data (+1.53 magnitude offset).

5.19. GSC 04048-00893

Position (UCAC4): R.A. (J2000) = $02^h\,51^m\,29.89^s$, Dec. (J2000) = +61° 47' 11.3"

Cross Identification: 2MASS J02512989+6147113; UCAC4 759-022788; 1SWASP J025129.87+614711.4

Variability Type: W UMa

Magnitude: Max. 13.82 V, Min. 14.31 V

Period: 0.433010(2) d

Epoch: 2456711.3693(5) HJD

Ensemble Comparison Stars: UCAC4 760-022986 (APASS 12.842 V); UCAC4 759-022881 (APASS 13.308 V)

Check Star: UCAC4 760-022963

Notes: Possible presence of O'Connell effect with secondary maximum = 13.84 V. Phase plot is shown in Figure 25.

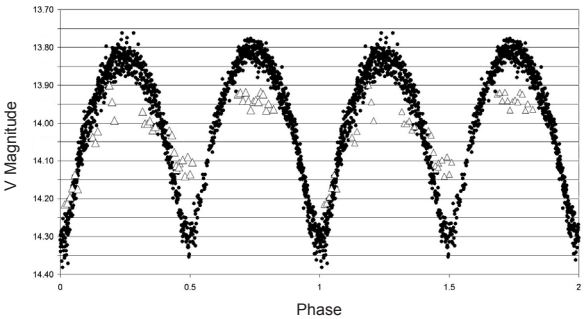

Figure 25. Phase plot of GSC 04048-00893. Filled circles denote Furgoni data; open triangles denote SWASP data (+0.95 magnitude offset).

5.20. GSC 04052-01674

Position (UCAC4): R.A. (J2000) = $02^h\,55^m\,39.74^s$, Dec. (J2000) = +62° 10' 08.5"

Cross Identification: 2MASS J02553971+6210083; UCAC4 761-022258

Variability Type: δ Sct

Magnitude: Max. 12.855 V, Min. 12.875 V

Period: 0.0390453(4) d

Epoch: 2456698.3064(3) HJD

Ensemble Comparison Stars: UCAC4 761-022128 (APASS 12.013 V); UCAC4 761-022146 (APASS 12.741 V)

Check Star: UCAC4 762-023189

Notes: Phase plot is shown in Figure 26.

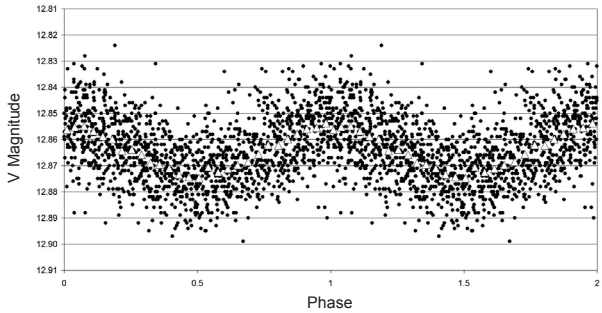

Figure 26. Phase plot of GSC 04052-01674. Filled circles denote Furgoni data; open triangles denote Furgoni data (binning 50).

5.21. GSC 04052-01198

Position (UCAC4): R.A. (J2000) = $02^h\,54^m\,22.56^s$, Dec. (J2000) = +62° 13' 27.2"

Cross Identification: 2MASS J02542256+6213271; UCAC4 762-023119

Variability Type: δ Sct

Magnitude: Max. 12.06 V, Min. 12.07 V

Period: 0.072480(2) d

Epoch: 2456698.3438(7) HJD

Ensemble Comparison Stars: UCAC4 761-022128 (APASS 12.013 V); UCAC4 761-022146 (APASS 12.741 V)

Check Star: UCAC4 762-023189

Notes: Phase plot is shown in Figure 27.

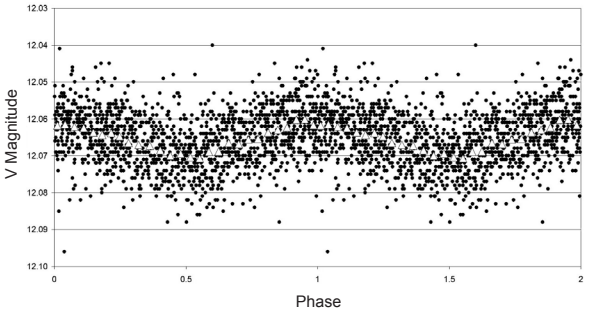

Figure 27. Phase plot of GSC 04052-01198. Filled circles denote Furgoni data; open triangles denote Furgoni data (binning 50).

5.22. GSC 04052-01238

Position (UCAC4): R.A. (J2000) $02^h\,52^m\,26.85^s$, Dec. (J2000) = +61° 57' 00.4"

Cross Identification: 2MASS J02522686+6157004; UCAC4 760-023032

Variability Type: δ Sct (uncertain)

Magnitude: Max. 13.21 V, Min. 13.23 V

Period: 0.124125(6) d

Epoch: 2456630.470(2) HJD

Ensemble Comparison Stars: UCAC4 760-023030 (APASS 11.963 V); UCAC4 760-022993 (APASS 11.608 V)

Check Star: UCAC4 760-022973

Notes: B–V = 0.80; J–K = 0.40. Probably a reddened δ Sct but it might be short period ELL. Phase plot is shown in Figure 28.

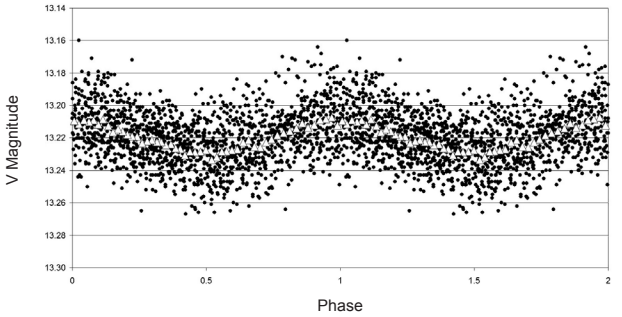

Figure 28. Phase plot of GSC 04052-01238. Filled circles denote Furgoni data; open triangles denote Furgoni data (binning 30).

5.23. 2MASS J02533682+6153083

Position (UCAC4): R.A. (J2000) = $02^h\,53^m\,36.81^s$, Dec. (J2000) = +61° 53' 08.4"

Cross Identification: UCAC4 760-023199; USNO-B1.0 1518-0086484

Variability Type: Rotating ellipsoidal

Magnitude: Max. 14.48 V, Min. 14.55 V

Period: 0.58555(2) d

Epoch: 2456631.421(1) HJD

Ensemble Comparison Stars: UCAC4 760-023181 (APASS 11.403 V); UCAC4 760-023174 (APASS 11.373 V)

Check Star: UCAC4 760-023206

Notes: Phase plot is shown in Figure 29.

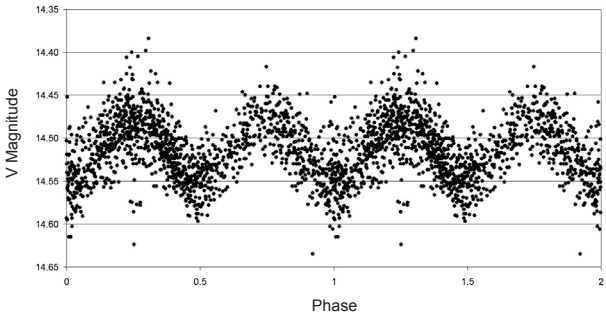

Figure 29. Phase plot of 2MASS J02533682+6153083. Filled circles denote Furgoni data.

5.24. GSC 04052-00946

Position (UCAC4): R.A. (J2000) = $02^h\,54^m\,59.05^s$, Dec. (J2000) = +62° 03' 11.2"

Cross Identification: J02545903+6203112; UCAC4 760-023199

Variability Type: Rotating ellipsoidal

Magnitude: Max. 11.43 V, Min. 11.46 V

Spectral Type: A5V

Period: 1.10349(4) d

Epoch: 2456701.462(4) HJD

Ensemble Comparison Stars: UCAC4 761-022213 (APASS 11.238 V); UCAC4 761-022128 (APASS 12.013 V)

Check Star: UCAC4 761-022184

Notes: Spectral type taken from Skiff (2009–2013). Phase plot is shown in Figure 30.

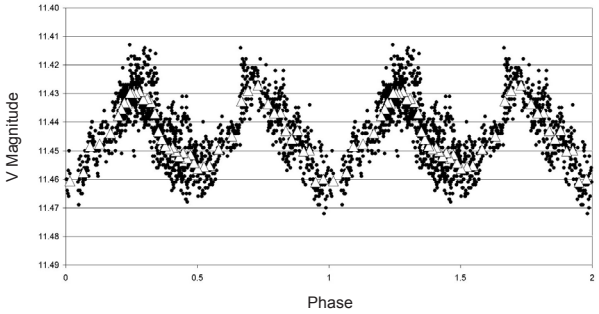

Figure 30. Phase plot of GSC 04052-00946. Filled circles denote Furgoni data; open triangles denote Furgoni data (binning 30).

5.25. GSC 04048-00441

Position (UCAC4): R.A. (J2000) = $02^h\,53^m\,58.73^s$, Dec. (J2000) = +61° 47' 46.3"

Cross Identification: 2MASS J02535873+6147462; UCAC4 759-023133

Variability Type: Var (Unspecified)

Magnitude: Max. 12.4 V, Min. 12.5 V

Period: 0.27534(2) d

Epoch: 2456630.456(1) HJD

Ensemble Comparison Stars: UCAC4 760-023181 (APASS 11.403 V); UCAC4 760-023174 (APASS 11.373 V)

Check Star: UCAC4 760-023206

Notes: B–V = 0.47; J–K = 0.54. Mean magnitude change superposed on the 0.27534 d. (amplitude 0.05 magnitude) variations. Type ELL with P = 0.5507 d. is possible. Check star stable with uniform 0.03-magnitude scattering. Fourier spectrum, light curve, and Phase plot are shown in Figures 31, 32, and 33.

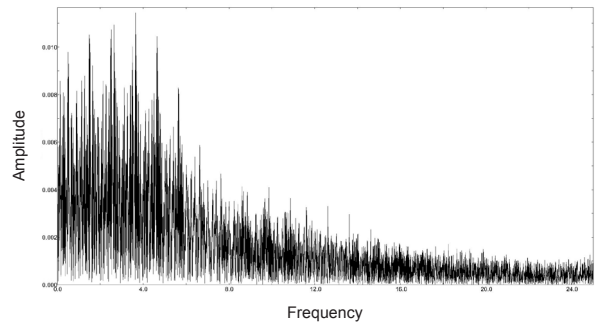

Figure 31. Fourier spectrum of GSC 04048-00441 (after detrending for the progressive fading).

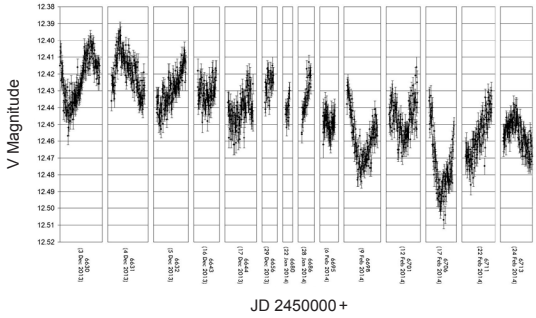

Figure 32. Light curve of GSC 04048-00441.

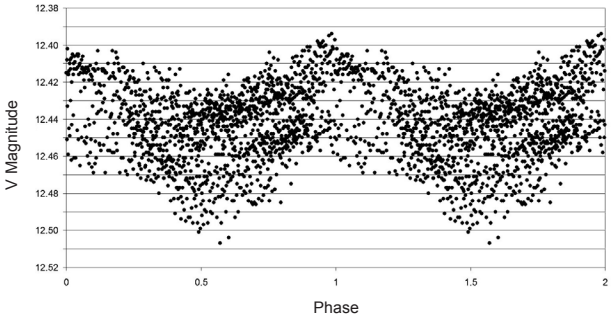

Figure 33. Phase plot of GSC 04048-00441; filled circles denote Furgoni data.

6. Acknowledgements

I wish to thank Sebastian Otero, member of the VSX team and AAVSO external consultant, for his helpful comments on the new variable stars discovered. This work has made use of the VIZIER catalogue access tool, CDS, Strasbourg, France, and the International Variable Star Index (VSX) operated by the AAVSO, Cambridge, Massachusetts. This work has made use of NASA's Astrophysics Data System and data products from the Two Micron All Sky Survey, which is a joint project of the University of Massachusetts and the Infrared Processing and Analysis Center/California Institute of Technology, funded by the National Aeronautics and Space Administration and the National Science Foundation.

This work has made use of the ASAS3 Public Catalog, NSVS data obtained from the Sky Database for Objects in Time-Domain operated by the Los Alamos National Laboratory, and data obtained from the SuperWASP Public Archive operated by the WASP consortium, which consists of representatives from the Queen's University Belfast, the University of Cambridge (Wide Field Astronomy Unit), Instituto de Astrofisica de Canarias, the Isaac Newton Group

of Telescopes (La Palma), the University of Keele, the University of Leicester, the Open University, the University of St Andrews, and the South African Astronomical Observatory.

This work has made use of The Fourth U.S. Naval Observatory CCD Astrograph Catalog (UCAC4).

References

Breger M., *et al.* 1999, *Astron. Astrophys.*, **349**, 225.

Butters, O. W., *et al.* 2010, *Astron. Astrophys.*, **520**, L10.

Copenhagen University Observatory, Institute of Astronomy. 2006, *Carlsberg Meridian Catalog 14* (CMC14), Copenhagen Univ. Obs. Inst. Astron., Cambridge.

Diffraction Limited. 2012, MAXIMDL image processing software (http://www.cyanogen.com).

Dymock, R., and Miles, R. 2009, *J. Br. Astron. Assoc.*, **119**, 149.

Henden, A. A., *et al.* 2013, AAVSO Photometric All-Sky Survey, data release 7 (http://www.aavso.org/apass).

Furgoni, R. 2013a, *J. Amer. Assoc. Var. Star Obs.*, **41**, 41.

Furgoni, R. 2013b, *J. Amer. Assoc. Var. Star Obs.*, **41**, 283.

Lenz, P., and Breger, M. 2005, *Commun. Asteroseismology*, **146**, 53.

Miller, W. J., and Wachmann, A. A. 1963, *Ric. Astron.* (Specola Vaticana), **6**, 401.

Skiff, B. A. 2009–2013, *General Catalogue of Stellar Spectral Classifications*, CDS/ADC Collection of Electronic Catalogues, 1, 2023 (2013), Lowell Observatory, Flagstaff, AZ (http://cdsarc.u-strasbg.fr/viz-bin/Cat?B/mk).

Watson, C. L., *et al.* 2007, *J. Amer. Assoc. Var. Star Obs.*, **35**, 414.

Wetterer, C. J., and McGraw, J. T. 2007, *Astron. J.*, **133**, 2883.

Woźniak, P. R., *et al.* 2004, *Astron. J.*, **127**, 2436.

Zacharias, N., Finch, C., Girard, T., Henden, A., Bartlett, J., Monet, D., and Zacharias, M. 2012, *The Fourth US Naval Observatory CCD Astrograph Catalog* (UCAC4; http://arxiv.org/abs/1212.6182).

Multi-band Differential Photometry of the Eclipsing Variable Star NSVS 5750160

Robert C. Berrington
Ball State University, Dept. of Physics and Astronomy, Muncie, IN 47306; rberring@bsu.edu

Erin M. Tuhey
Ball State University, Dept. of Physics and Astronomy, Muncie, IN 47306; emtuhey@bsu.edu

Received April 15, 2014; revised April 24, 2014; accepted April 25, 2014

Abstract We present new multi-band differential aperture photometry of the eclipsing variable star NSVS 5750160. The light curves are analyzed with the Wilson-Devinney model to determine best-fit stellar models. Our models show that NSVS 5750160 is consistent with a W-type W Ursae Majoris eclipsing variable star, and require the presence of a spot to fit the observed O'Connell effect. Two different spot models are presented but neither model is conclusive.

1. Introduction

The Northern Sky Variability Survey (NSVS; Woźniak *et al.* 2004) catalogue entry star 5750160 was originally classified as a W Ursae Majoris contact binary by Hoffman *et al.* (2009). The NSVS is a search for variability in the stars observed with the Robotic Optical Transient Search Experiment (ROSTE-I). The primary goal of the NSVS is to search for optical transients associated with quick response to Gamma-Ray Burst (GRB) events reported from satellites to measure optical light curves of GRB couterparts. When no GRB events were available ROSTE-I was devoted to a systematic sky patrol of the sky northward of declination –38°. The star NSVS 5750160 can be found at the celestial coordinates R.A. $20^h40^m52^s.4$, Dec. +40° 13' 18.6" (J2000.0). The automated classification system developed by Hoffman *et al.* (2009) reported a photometric period of P = 0.33847 day.

In this paper we present a new extensive photometric study of this system. The paper is organized as follows. Observational data acquisition and reduction methods are presented in section 2. Time analysis of the photometric light curve and Wilson-Devinney models are presented in section 3. Discussion of the results and future directions are presented in section 4.

2. Observational data

We present new three-filter photometry of the eclipsing variable star candidate NSVS 5750160. The data were taken by the Meade 0.4-meter Schmidt

Cassegrain telescope within the Ball State University observatory located atop the Cooper science complex. All exposures were acquired by a Santa Barbara Instruments Group (SBIG) STL-6303e camera through the Johnson-Cousins B, V, and R (R_C) filters on the nights of July 24, 25, and 27, 2013. All images were bias- and dark-current subtracted, and flat-field corrected using the CCDRED reduction package found in the Image Reduction and Analysis Facility (IRAF; National Optical Astronomy Observatories 2014). All photometry presented in this study is differential aperture photometry, and was performed on the target eclipsing candidate and two comparison standards by the AIP4WIN photometry package (Berry and Burnell 2005). Over the three nights, a total of 406 images were images were taken in B and V, and 402 images in R_c. Figure 1 shows a representative exposure with the eclipsing star candidate and the two comparison stars marked. We have chosen the Tycho catalogue star (Hog *et al.* 1998) TYC 3170-822-1 as the primary comparison star (C1). The folded light curves (see section 3.1) for the instrumental differential B, V, and R_C magnitudes are shown in Figure 2. We define the differential magnitude by the variable star magnitude minus C1 (Variable − C1). Also shown in Figure 2 (bottom panel) is the differential V magnitude of C1 minus the second comparison star (C2) or the check star. The comparison light curve was inspected for variability. None was found.

Measured instrumental B and V differential magnitudes were reduced to Johnson B and V magnitudes by comparison with known calibrated magnitudes for C1. The star C1 has measured Johnson B and V magnitudes of 11.44 ± 0.06 and 10.71 ± 0.05, respectively (Hog *et al.* 1998). The calibrated V light curve with the B–V color index versus orbital phase is shown in Figure 3 with error bars removed for clarity. Simultaneous B and V magnitudes are used to determine B–V colors by linear interpolating between measured B magnitudes to a similar time for measured V magnitudes.

3. Analysis

3.1. Period analysis and ephemerides

Heliocentric Julian dates (HJD) for the observed times of minimum were calculated for each of the B, V, and R band light curves shown in Figure 2 for all observed primary and secondary minima. A total of two primary eclipses and four secondary eclipses were observed for each band. The times of minimum were determined by the algorithm described by Kwee and van Woerden (1956). Similar times of minimum from differing band passes were compared and no significant offsets or wavelength-dependent trends were observed. Similar times of minimum from each of the band passes were averaged together and reported in Table 1 along with 1σ error bars.

Light curves were inspected by the PERANSO software (Vanmunster 2011) to determine orbital periodicity by applying the analysis of variance (ANOVA)

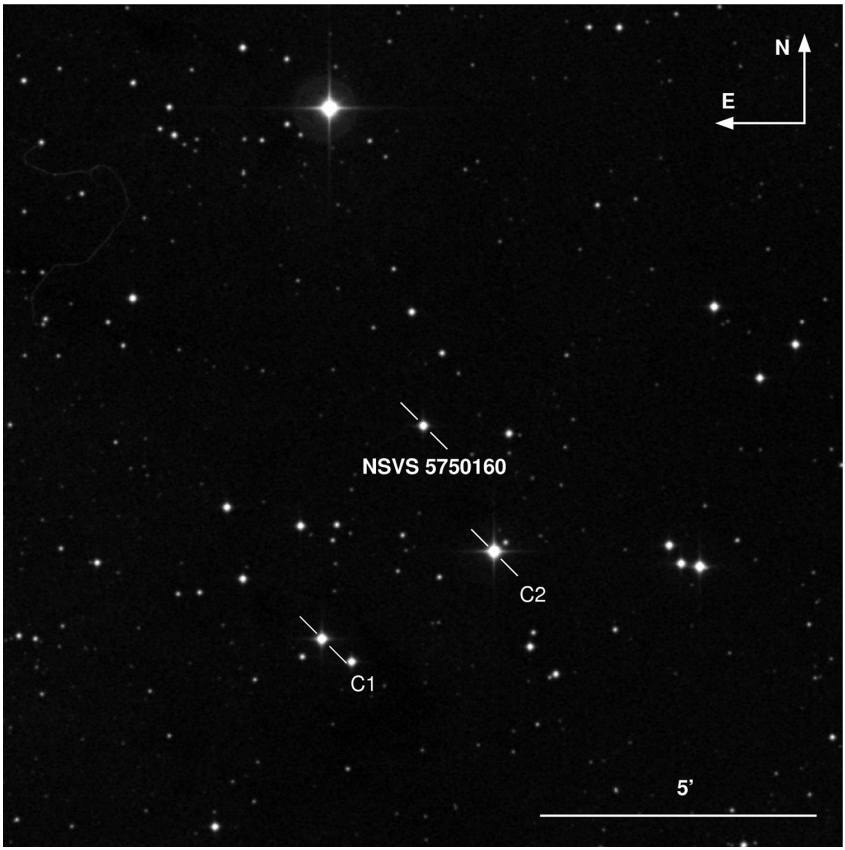

Figure 1. Star field containing the variable star NSVS 5750160. The location of the variable star is shown along with the comparison (C1) star and the check (C2) star used to calculate the differential magnitudes reported in Figure 2.

statistic which uses periodic orthogonal polynomials to fit observed light curves (Schwarzenberg-Czerny 1996). Our best-fit orbital period was found to be 0.33847 ± 0.00060 day and is similar to the orbital period reported by Hoffman *et al.* (2009) which uses the photometric data reported by the NSV Survey (Woźniak *et al.* 2004). The resulting linear ephemeris becomes

$$T_{\min} = 2456492.85265(23) + 0.33847(60)\, E. \quad (1)$$

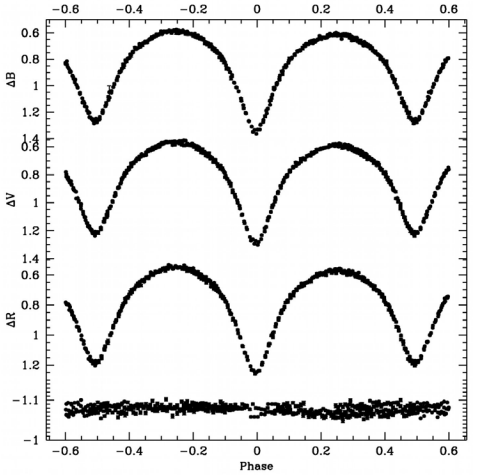

Figure 2. Folded light curves for differential aperture Johnson-Cousins B, V, and R magnitudes. Phase values are defined by Equation 2. Top three panels show the folded light curves for Johnson B (top panel), Johnson V (middle panel), and Cousins R (bottom panel) magnitudes. Bottom panel shows differential Johnson V band magnitudes for the comparison minus the check star. All error bars are 1σ error bars with typical values <0.01 magnitude (smaller than a point size). Repeated points do not show error bars (points outside the phase range of –0.5, 0.5).

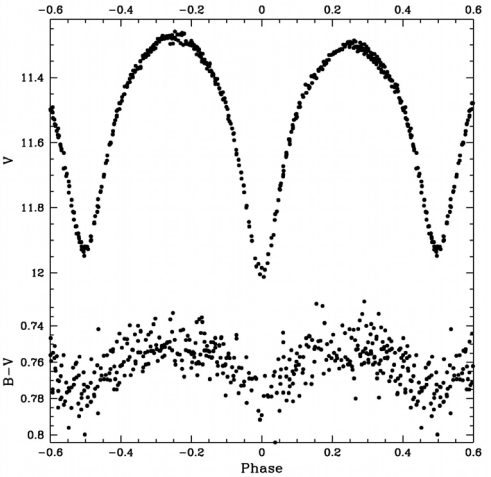

Figure 3. Folded light curve for differential aperture Johnson V magnitudes (top panel) and B–V color (bottom panel) versus orbital phase. Phase values are defined by Equation 2. Error bars are not shown for clarity. All B–V colors are calculated by subtracting linearly-interpolated B magnitudes from measured V magnitudes.

Table 1. Calculated heliocentric Julian dates (HJD) for the observed times of minimum of NSVS 5750160.

T_{min}	*Eclipse*	*E*	*(O–C)*
2456492.68280 ± 0.00022	s	–0.5	–0.000615
2456492.85265 ± 0.00023	p	0	0
2456493.69792 ± 0.00017	s	2.5	–0.000905
2456493.86810 ± 0.00021	p	3	0.00004
2456496.74478 ± 0.00029	s	11.5	–0.000275
2456497.76032 ± 0.00021	s	14.5	–0.000145

Notes: Observed times of minimum (column 1); the type of minimum (column 2).Observed minus Calculated (O–C) residual (column 4) values are given for the linear ephemeris given in Equation 1. Reported times are averaged from the individual B-, V-, and R-band times of minimum determined by the algorithm descried by Kwee and van Woerden (1956). O–C values are given in units of days with primary eclipse values determined from integral epoch numbers, and secondary eclipse values determined from half integral epoch numbers (column 3).

Figure 2 shows the folded differential magnitudes versus orbital phase for NSVS 5750160 for the B, V, and R Johnson-Cousins bands folded over the period determined by the NSVS (see Equation 1). The orbital phase (Φ) is defined as:

$$\Phi = \frac{T - T_0}{P} - \text{Int}\left(\frac{T - T_0}{P}\right), \quad (2)$$

where T_0 is the ephemeris epoch and is the time of minimum of a primary eclipse. Throughout this paper we will use the value of 2456492.68280 for T_0. The variable T is the time of observation, and P is the period of the orbit. The value of Φ ranges from a minimum of 0 to a maximum of 1.0. All light curve Figures plot phase values (–0.6,0.6) where the negative values are given by $\Phi - 1$.

The Observed minus Calculated residual times of minimum (O–C) were determined from Equation 1 and are given in Table 1. The best-fit linear line determined by a linear regression to the O–C residual values is shown in Figure 4, and indicates the times of minima are well described by a period of 0.338511 ± 0.000085 day, and is consistent with our previous determination of the orbital period at $< 1\sigma$.

Figure 5 shows the folded V band light curve measured from this study along with the measured values extracted from the NSV Survey (NSVS; Woźniak *et al.* 2004) with standard rejected flags set. The temporal coverage of the NSVS is sporadic and no individual times of minimum were observed over duration of the survey. Temporal coverage of NSVS spans one calendar year starting April 1, 1999 (JD 2451270) to March 30, 2000 (JD 2451633). All

magnitudes reported by NSVS are unfiltered CCD magnitudes whose range is limited by the sensitivity of the CCDs. Spectral response of CCD resulted in an effective wavelength best matched to the Johnson R band, but were calibrated to the Johnson V-band filter by comparison with Tycho catalogue stars and is the most likely explanation for the offset observed in Figure 5 between our measured V-band magnitudes and the NSVS V-band magnitudes. This indicates that both data sets are consistent with the ephemeris

$$T_{\min} = 2456492.85265(23) + 0.338511(85)\, E, \quad (3)$$

and with the original period of 0.33847 day at $<1\sigma$ deviation. Because of the sporadic coverage of NSVS, it is not possible to determine if the revised period reflects a possible period change or a more accurate period. As previously noted, when using only our photometric data, we derive a period of 0.33847 day, and it will be the assumed period for the remainder of this study unless otherwise noted.

Effective temperature and spectral type are estimated from the B–V color index values measured at orbital quadrature (± 0.25 orbital phase) with a value of B–V = 0.75 ± 0.07. This results in an estimated stellar mass $M_{\star} = 0.98^{+0.05}_{-0.07}\, M_{\odot}$ derived from Equation 4 of Harmanec (1988). Effective temperatures and errors were estimated by Table 3 from Flower (1996) to be $T_{\rm eff} = 5413 \pm 200$ K. Interstellar extinction estimates following Schlafly and Finkbeiner (2011) at the galactic coordinates for the object are unreliable due to the object's proximity to the galactic plane. These interstellar extinction models are based on line-of-sight galactic column densities. Along with the clumpy nature of the dust distribution in the galactic plane, there are a number of points that indicate that the B–V value is near the correct value. The corresponding stellar spectral type for the observed B–V is G8 (Johnson 1966). The light curve shows evidence of a star spot, seen in later-type stars and consistent with the estimated spectral type (see section 3.3). Furthermore, we report consistent distance estimates to the object using two different techniques (see section 4). The observed B–V was used to estimate the effective temperature, and became the starting point for subsequent stellar modeling. To confirm these conclusions, spectroscopic follow-up to confirm the spectral type, interstellar reddening, and radial velocities to measure stellar masses is necessary to gain further insight.

3.2. Light curve analysis

All observations taken during this study were analyzed using the Physics of Eclipsing Binaries (PHOEBE) software package (Prša and Zwitter 2005). The PHOEBE software package is a modeling package that provides a convenient, intuitive graphical user interface (GUI) to the Wilson-Devinney (WD) code (Wilson and Devinney 1971). In the version of PHOEBE used in this study, several advancements have been included in the package that facilitate the fitting

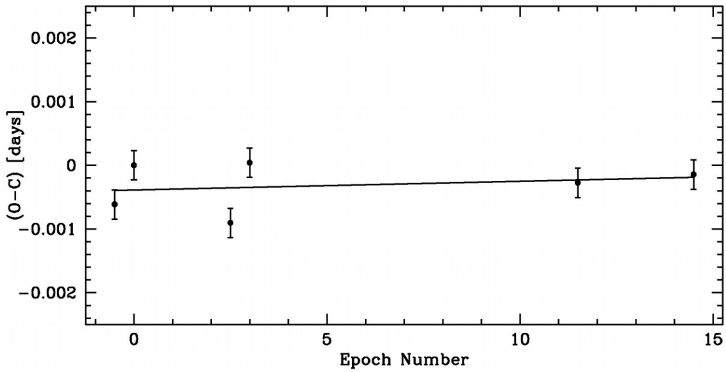

Figure 4. Observed minus calculated residual times of minimum (O–C) versus orbital epoch number. All point values are given in Table 1. Secondary times of minimum are plotted at half integer values, and all error bars are 1σ error bars. Solid curve shows the best-fit linear line determined by a linear regression fit to the O–C residual values.

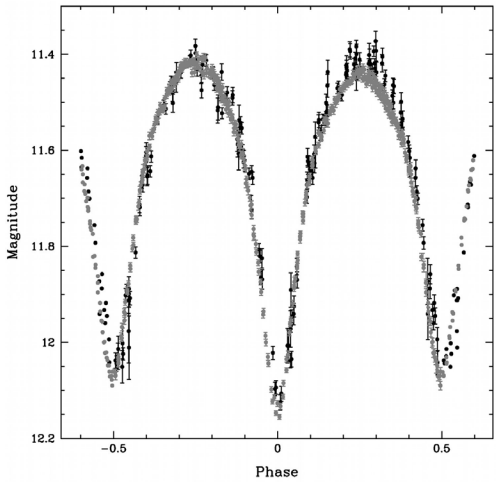

Figure 5. Folded light curve for Johnson V magnitudes. Gray points are measured magnitudes from the Ball State University 0.4m telescope. Measured values from the NSV Survey (Woźniak *et al.* 2004) are shown by the black points. All error bars are 1σ error bars. Repeated points do not show error bars.

process. These include the inclusion of the Nedler and Mead downhill simplex (Nedler and Mead 1965) minimization algorithm into the fitting procedure that greatly increases the chance of a successful model convergence (Prša and Zwitter 2005).

All three Johnson-Cousins B, V, and R_C bands were fit simultaneously by the following procedure. Initial fits were performed assuming a common convective

envelope in direct thermal contact, resulting in a common surface temperature of $T_{\rm eff}$ = 5413 K determined by the procedure discussed in section 3.1. Orbital period was set to the value of 0.33847 ± 0.00060 day. Surface temperatures imply that the outer envelopes are convective, so the gravity brightening coefficients β_1 and β_2, defined by the flux dependency $F \propto g^{\beta}$, were initially set at the common value consistent with a convective envelope of 0.32 (Lucy 1967). The more recent studies of Alencar and Vaz (1997) and Alencar *et al.* (1999) predict values for $\beta \approx 0.4$. These values were also used and had no effect on the resulting best-fit model. We adopted the standard stellar bolometric albedo $A_1 = A_2 = 0.5$ as suggested by Ruciński (1969), with two possible reflections.

The fitting procedure was used to determine the best-fit stellar models and orbital parameters from the observed light curves shown in Figure 2. Initial fits were performed assuming a common convective envelope in thermal contact which assumes similar surface temperatures for both stars. After normalization of the stellar luminosity, the light curve was crudely fit by altering the stellar shape by fitting the Kopal (Ω) parameter. The Kopal parameter describes the equipotential surface that the stars fill. For overcontact binaries, this has the effect of determining the shape of the stars, and has a strong effect on the global morphology of the light curve.

Initial fits were performed assuming the outer convective envelope was in thermal contact, and therefore both the primary and secondary stars have similar effective temperatures ($T_{\rm eff}$). After the fit could no longer be improved, we started to consider the other parameters to fit the light curve. These parameters included the effective temperature of the primary star $T_{\rm eff,1}$, the mass ratio $q = M_2/M_1$, and the orbital inclination i. It became apparent that the models could not represent the observed light curve without decoupling stellar luminosities from $T_{\rm eff}$. We interpreted this as evidence that the stars were not in thermal contact and therefore could have differing surface temperatures. All further model fits were performed assuming the primary and secondary components were not in thermal contact.

All model fits were performed with a limb darkening correction. The limb-darkening correction takes the form

$$\mathcal{L}_{\lambda}(\mu) = 1 - x_{\lambda}(1 + \mu) - y_{\lambda} f_{\lambda}(\mu) \qquad (4)$$

where $\mu = \cos(\varphi)$ and represents the cosine of the angle (φ) with the emergent luminosity normal to the stellar surface. The function $\mathcal{L}_{\lambda}(\mu)$ is the ratio of the emergent luminosity at a given μ with the emergent luminosity normal ($\mu = 1$) to the stellar surface. The coefficients x_{λ} and y_{λ} are determined by stellar properties and are known as the linear and non-linear coefficients, respectively. Finally, the function $f_{\lambda}(\mu)$ is the non-linear functional form of the limb-darkening correction. PHOEBE allows for differing functional forms to be specified by the user for the non-linear component. Studies by Diaz-Cordoves and Gimenez

(1992) and van Hamme (1993) have shown that early type stars ($T_{\rm eff} > 9000$ K) are best fit by a square root law given by the functional form ($f_\lambda(\mu) = (1-\sqrt{\mu})$). Late type stars ($T_{\rm eff} < 9000$ K) are best described by the logarithmic law first suggested by Klinglesmith and Sobieski (1970) and given by the functional form ($f_\lambda(\varphi) = \mu \log(\mu)$). In our study, fits were attempted for both laws. In both cases, the values for the linear (x_λ) and non-linear (y_λ) coefficients were determined at each fitting iteration by the van Hamme (1993) interpolation Tables. In both cases our best-fit models used the logarithmic law, and therefore support the conclusions of Diaz-Cordoves and Gimenez (1992) and van Hamme (1993).

Figures 6–8 show the folded Johnson B-, Johnson V-, and Cousins R-band light curves along with the synthetic light curve calculated by the best-fit model, respectively. The best-fit models were determined by the aforementioned fitting procedure. Note how the synthetic light curve consistently under-predicts the observed light curve for phases in the interval –0.5,0, and over-predicts for phases in the interval 0,0.5. The parameters, along with 1σ error bars describing this best-fit model, are given in column 2 of Table 2. The best-fit model is consistent with an overcontact binary described by a filling factor $\mathcal{F} = 0.0677$. The filling factor is defined by the inner and outer critical equipotential surfaces that pass through the L_1 and L_2 Lagrangian points of the system. For our system the these equipotential surfaces are $\Omega(L_1) = 4.265$ and $\Omega(L_2) = 3.697$.

3.3 Spot model

It is apparent from Figures 6–8 that the previous model is unable to reproduce accurately the observed light curve. To improve the fit, a single spot was necessary. Unfortunately, all we have at our disposal are the observed light curves, and differing spot models may be degenerate to the observed light curve.

Initial models started from the model without spots determined in section 3.2. We were unsuccessful with simultaneous convergence of the remaining parameters. Both the spot radius and spot longitude also eluded successful convergence. All fits were performed by manually changing the spot radius, then converging the spot temperature factor. Once a satisfactory convergence was determined, the spot parameters were then held fixed and the stellar parameters were then allowed to converge to the final model. Figures 9–11 show the final best-fit stellar model.

The best-fit model with a single cool spot on the primary star is given in Table 3. Spot parameters given by the WD model are the longitude θ, colatitude ϕ, radius ρ, and temperature factor ($\tau = T_{\rm spot} / T_{\rm eff}$). The spot longitude is measured counterclockwise (CCW) relative to orbital motion from the L_1 Lagrangian point. Spot colatitude is measured from stellar rotation axis with the equator represented by $\phi = 90°$. Light curves were found to be minimally dependent on the spot's colatitude and therefore difficult to converge when allowed to vary. All spot models restricted spots to be located on the equator ($\phi = 90°$).

Table 2. Model parameters determined by the best-fit WD model as fit in sections 3.2 and 3.3.

Parameter	*Symbol*[1]	*Value*	
		Best fit (spots not allowed)	*Best fit (spots allowed)*
Period	P [days]	0.338511 ± 0.000085	0.338511 ± 0.000085
Epoch	T_0 [HJD]	2456492.85265 ± 0.00023	2456492.85265 ± 0.00023
Inclination	i [°]	79.35 ± 0.05	79.05 ± 0.04
Surface Temperature[2]	$T_{eff,1}$ [K]	5290 ± 200	5253 ± 200
Surface Temperature[2]	$T_{eff,2}$ [K]	5167 ± 200	5133 ± 200
Surface Potential[3]	$\Omega_{1,2}$ [—]	4.227 ± 0.002	4.081 ± 0.002
Limb Darkening	$x_{bol,1,2}$	0.608	0.607
Limb Darkening	$y_{bol,1,2}$	0.167	0.180
Limb Darkening	$x_{B,1,2}$	0.754	0.754
Limb Darkening	$y_{B,1,2}$	–0.144	–0.128
Limb Darkening	$x_{V,1,2}$	0.739	0.740
Limb Darkening	$y_{V,1,2}$	0.099	0.115
Limb Darkening	$x_{R,1,2}$	0.677	0.680
Limb Darkening	$y_{R,1,2}$	0.219	0.232

[1] 1 for primary stellar component, 2 for secondary stellar component. [2] Errors estimated from color values in Figure 3. [3] Surface potential for both stars (contact/overcontact binaries) defined to be equal for both stars. Note: Errors 1σ except where otherwise given.

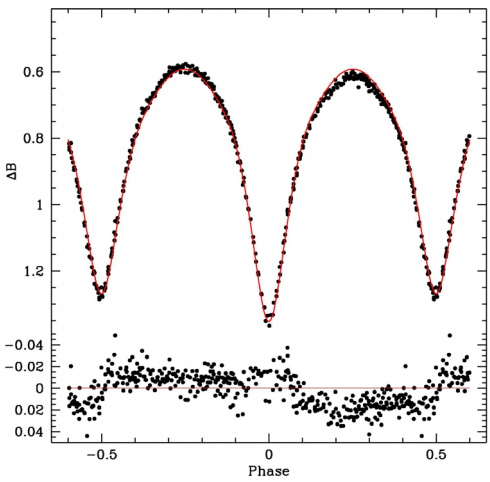

Figure 6. Best-fit WD model fit without spots (solid curve) to the folded light curve for differential aperture Johnson B (top panel). The best-fit orbital parameters used to determine the light curve model are given in Table 2. The bottom curve shows residuals from the best-fit model (solid curve). Error bars are omitted from the points for clarity.

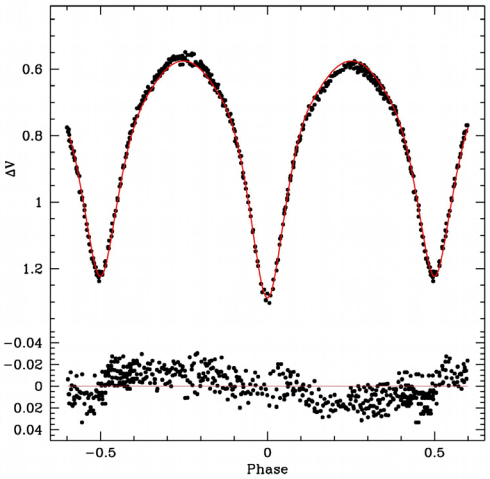

Figure 7. Best-fit WD model fit without spots (solid curve) to the folded light curve for differential aperture Johnson V (top panel). The best-fit orbital parameters used to determine the light curve model are given in Table 2. The bottom curve shows residuals from the best-fit model (solid curve). Error bars are omitted from the points for clarity.

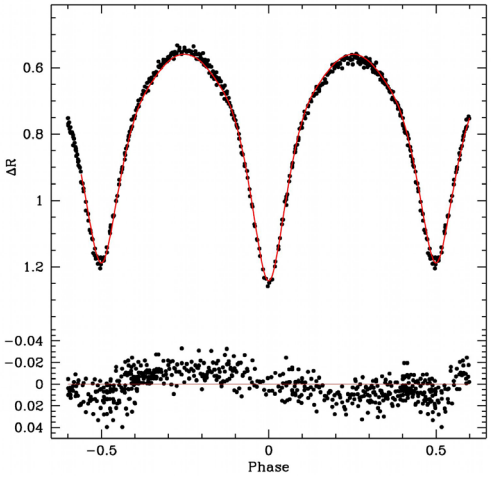

Figure 8. Best-fit WD model fit without spots (solid curve) to the folded light curve for differential aperture Cousins R (top panel). The best-fit orbital parameters used to determine the light curve model are given in Table 2. The bottom curve shows residuals from the best-fit model (solid curve). Error bars are omitted from the points for clarity.

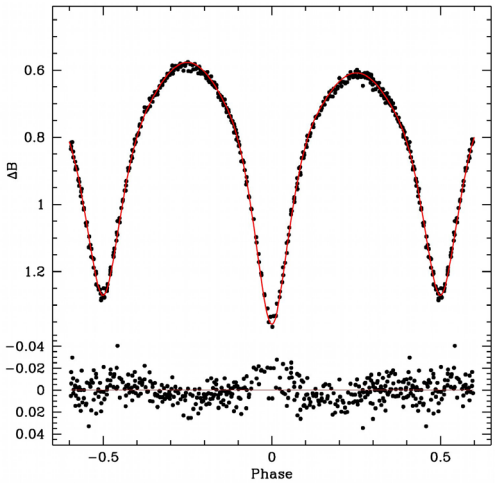

Figure 9. Best-fit WD model fit with spots (solid curve) to the folded light curve for differential aperture Johnson B (top panel). The best-fit orbital parameters used to determine the light curve model are given in Table 2. The bottom panel shows residuals from the best-fit model (solid curve). Error bars are omitted from the points for clarity.

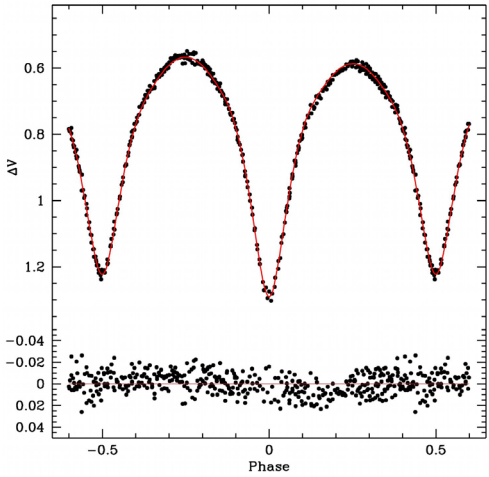

Figure 10. Best-fit WD model fit with spots (solid curve) to the folded light curve for differential aperture Johnson V (top panel). The best-fit orbital parameters used to determine the light curve model are given in Table 2. The bottom panel shows residuals from the best-fit model (solid curve). Error bars are omitted from the points for clarity.

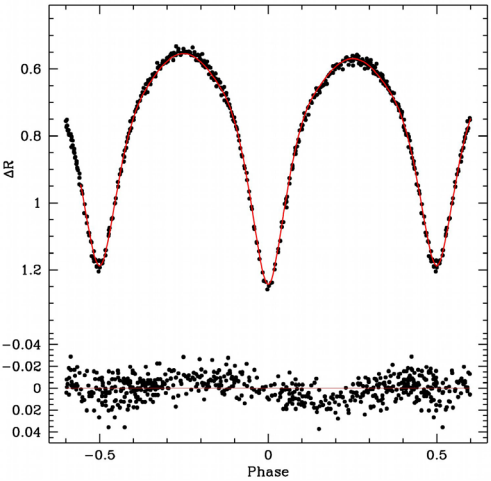

Figure 11. Best-fit WD model fit with spots (solid curve) to the folded light curve for differential aperture Cousins R (top panel). The best-fit orbital parameters used to determine the light curve model are given in Table 2. The bottom panel shows residuals from the best-fit model (solid curve). Error bars are omitted from the points for clarity.

Table 3. Best-fit Spot models. All parameters are for the primary stellar component.

Description	*Parameter*	*Cold Spot Model*	*Hot Spot Model*
Spot colatitude	ϕ_1 [°]	90	90
Spot longitude	λ_1 [°]	270	90
Spot radius	ρ_1 [°]	11	13
Temperature	τ_1	0.77	1.11

Table 4. Absolute parameters used to determine best-fit models.

Parameter	*Value*
M_1 [$M_\odot$]	0.84
M_2 [$M_\odot$]	1.12
a [$R_\odot$]	2.56
R_1 [$R_\odot$]	0.92
R_2 [$R_\odot$]	1.05
log (g_1) [cm s^{-2}]	4.43
log (g_2) [cm s^{-2}]	4.44
$\overline{\rho}_1$ [g cm^{-3}]	1.51
$\overline{\rho}_2$ [g cm^{-3}]	1.40
$M_{bol,1}$	5.34
$M_{bol,2}$	5.16

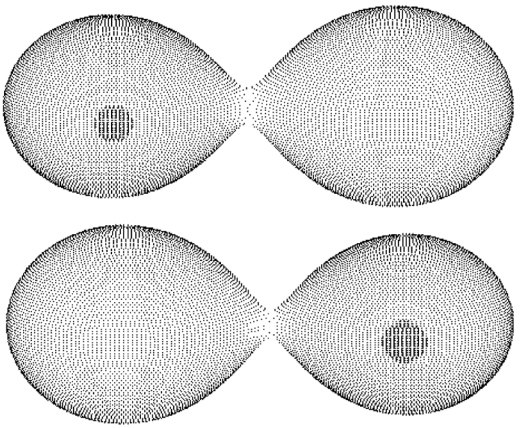

Figure 12. Graphical representation for the best-fit cold spot WD model (top panel) and hot spot WD model (bottom panel). The best-fit orbital parameters used to determine the light curve model are given in Table 2.

In our second attempt we tried a single hot spot on the primary but on the opposite side of the star. Best fits were determined using the algorithm described above. Spot parameters are given in Table 3. Fits were similar to the cool spot model fits with similar residuals to those for the cold spot model. Graphical representations for both the hot spot WD model and the cold spot WD model are shown in Figure 12.

4. Discussion and conclusions

Figure 5 shows a comparison of the NSVS light curve with the light curve measured during this study. It is immediately apparent that the NSVS light curve shows similar heights for max I ($\Phi = 0.25$) and max II ($\Phi = -0.25$). Differing heights between max I and max II is known as the O'Connell (1951) effect. In contrast the light curve measured during this study does shows a positive (max I > max II) O'Connell effect. Numerous models have been presented as a possible explanation, but many deal with impacting (Shaw 1994) or absorbing (O'Connell 1951) gas streams which are unlikely for overcontact binaries. As we showed in section 3.3, a model with a single spot can explain the observed O'Connell effect.

Given the absolute parameters in Table 4, we can estimate the distance to NSVS 5750160. Taken from Flower (1996), the bolometric corrections (BC) used for the primary and secondary star are $BC_1 = -0.195$ and $BC_2 = -0.237$, respectively. From the bolometric magnitudes reported in Table 4 and the BC, the combined visual magnitude is $M_V = 4.28$. Furthermore, Ruciński and Duerbeck (1997) determined that the absolute visual magnitude is given by

$$M_V = -4.44 \log_{10}(P) + 3.02(B - V) + 0.12 \quad (5)$$

to within an accuracy of ± 0.1. Our calculated value differs from the absolute magnitude determined from Equation 5 ($M_V = 4.47$) by 0.19 magnitude. This agreement ($< 2\sigma$) in the absolute visual magnitudes confirms the initial determination of M_V. The distance modulus of the system $(m - M) = 6.97$ for our calculated value, and 6.78 for value obtained from Equation 5. This corresponds to a distance of 247.8 pc and 227.8 pc, respectively. Agreement of these distance estimates also supports our conclusions regarding the interstellar extinction from section 3.1.

Stellar mean densities ($\overline{\rho}$) are given in Table 4, and Mochnacki (1981) showed they are given by

$$\overline{\rho}_1 = \frac{0.0189}{r_1^3(1 + q)P^2}, \overline{\rho}_2 = \frac{0.0189q}{r_2^3(1 + q)P^2}, \quad (6)$$

where the stellar radius r is normalized to the semimajor axis. We determined

the values for the primary and secondary components to be 1.51 g cm^{-3} and 1.40 g cm^{-3}, respectively.

This study has confirmed that NSVS 5750160 is a W UMa contact binary not in thermal contact, and with the hotter, smaller star eclipsed during primary minimum it is a member of the W-type subclass. Our measured light curve shows a positive O'Connell (1951) effect which could not be explained without the presence of stellar spots. We showed that light curve can be well described by the presence of either a cool or a warm star spot on the primary star. However, we cannot exclude possible alternative explanations, and comment that further spectroscopic studies will greatly enhance our knowledge of this system.

References

Alencar, S. H. P., and Vaz, L. P. R. 1997, *Astron. Astrophys.*, **326**, 257.

Alencar, S. H. P., Vaz, L. P. R., and Nordlund, Å. 1999, *Astron. Astrophys.*, **346**, 556.

Berry, R., and Burnell, J. 2005, AIP4WIN (version 2.2.0), provided with *The Handbook of Astronomical Image Processing*, Willmann-Bell, Richmond, VA.

Diaz-Cordoves, J., and Gimenez, A. 1992, *Astron. Astrophys.*, **259**, 227.

Flower, P. J. 1996, *Astrophys. J.*, **469**, 355.

Harmanec, P. 1988, *Bull. Astron. Inst. Czechoslovakia*, **39**, 329.

Hoffman, D. I., Harrison, T. E., and McNamara, B. J. 2009, *Astron. J.*, **138**, 466.

Hog, E., Kuzmin, A., Bastian, U., Fabricius, C., Kuimov, K., Lindegren, L., Makarov, V. V., and Roeser, S. 1998, *Astron. Astrophys.*, **335**, L65.

Johnson, H. L. 1966, *Ann. Rev. Astron. Astrophys.*, **4**, 193.

Klinglesmith, D. A., and Sobieski, S. 1970, *Astron. J.*, **75**, 175.

Kwee, K. K., and van Woerden, H. 1956, *Bull. Astron. Inst. Netherlands*, **12**, 327.

Lucy, L. B. 1967, *Z. Astrophys.*, **65**, 89.

Mochnacki, S. W. 1981, *Astrophys. J.*, **245**, 650.

National Optical Astronomy Observatories. 2014, CCDRED, reduction package in the Image Reduction and Analysis Facility (IRAF; http://iraf.net/), version 2.16.

Nedler, J. A., and Mead, R. 1965, *Comput. J.*, **7**, 308.

O'Connell, D. J. K. 1951, *Publ. Riverview College Obs.*, **2**, 85.

Prša, A., and Zwitter, T. 2005, *Astrophys. J.*, **628**, 426 (PHOEBE software package v0.31a).

Ruciński, S. M. 1969, *Acta Astron.*, **19**, 245.

Ruciński, S. M., and Duerbeck, H. W. 1997, *Publ. Astron. Soc. Pacific*, **109**, 1340.

Schlafly, E. F., and Finkbeiner, D. P. 2011, *Astrophys. J.*, **737**, 103.

Schwarzenberg-Czerny, A. 1996, *Astrophys. J., Lett. Ed.*, **460**, L107.

Shaw, J. S. 1994, *Mem. Soc. Astron. Ital.*, **65**, 95.

van Hamme, W. 1993, *Astron. J.*, **106**, 2096.

Vanmunster, T. 2011, Light Curve and Period Analysis Software, PERANSO v.2.50 (http://www.cbabelgium.com).

Wilson, R. E., and Devinney, E. J. 1971, *Astrophys. J.*, **166**, 605.

Woźniak, P. R., *et al.* 2004, *Astron. J.*, **127**, 2436.

First Photometric Study of the Short Period Solar Type Binary V1073 Herculis and the Possible Detection of a Dwarf Companion

Ronald G. Samec
Faculty Research Associate, Pisgah Astronomical Research Institute, One Pari Drive, Rosman, NC 28772; address email correspondence to ronaldsamec@gmail.com

James Kring
Justin Benkendorf
James Dignan
Astronomy Program, Department of Physics and Engineering, Bob Jones University, 1700 Wade Hampton Boulevard, Greenville, SC 29614

Walter Van Hamme
Florida International University, Department of Physics, University Park, Miami, FL 33199

Danny R. Faulkner
Johnson Observatory, 1414 Bur Oak Court, Hebron, KY 41048

Received September 3, 2014; revised October 8, 2014; accepted October 13, 2014

Abstract V1073 Herculis is a very short period, P=0.294281673(4) day, active solar type eclipsing binary. It was observed in May 2012 with the Lowell Observatory 31-inch NURO reflector. This period study consists of some 54 times of minimum light covering nearly 18,000 orbits. A very low amplitude, 0.002-day sinusoidal variation is detected with a period of 11.25 years, which may indicate the presence of a dwarf third component. The temperature of the binary is ~5200K. A preliminary simultaneous Wilson-Devinney Program solution including a q-search reveals that the system has a mass ratio of 0.4, nearly identical component temperatures, and a cool magnetic spot with a T-factor of 0.86 with a spot radius of 22 degrees. The Roche Lobe fill-out is 0.18. The inclination is 82 degrees which results in a brief total eclipse.

1. Introduction

This paper represents the first precision and multicolor photometric study of the interesting, high amplitude solar type W UMa eclipsing binary, V1073 Her.

2. History and observations

V1073 Her (GSC 2625.1563, ROTSE1 J180835.74+334205.7) was imaged in test fields of the ROTSE all-sky survey (Akerlof *et al.* 2000). The first

unfiltered CCD light curves were taken by Blätter and Diethelm (2000). These curves are shown in Figure 1. It was included in the NSVS survey (Hoffman *et al.* 2009) and is classified as a W UMa variable. Eclipse timings have been given in Diethelm (2003, 2004, 2006), Brát *et al.* (2007), Nelson (2008, 2009), Brát *et al.* (2008, 2011), Hübscher (2007), Diethelm (2012), Hübscher (2009), Hübscher *et al.* (2012), and Hoňková *et al.* (2013). It was included in the "77th Name list of variable stars" (Kazarovets *et al.* 2003), and also appeared in the catalog of field contact binary stars, (Pribulla *et al.* 2003). Updated elements were given by Kreiner (2004). It was listed in "A Catalog of 1022 Bright Contact Binary Stars" by Gettel *et al.* (2006). Its period was listed as 0.294283d along with color indices J–H = 0.352, H–K = 0.100.

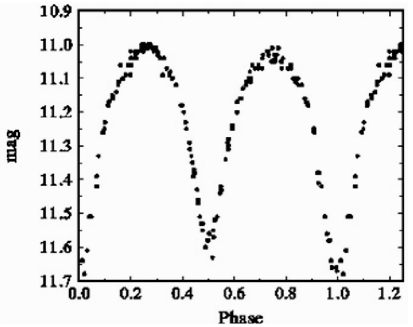

Figure 1. The first unfiltered CCD light curves ov V1073 Her were taken by Blätter and Diethelm (2000).

This system was observed as a part of our student/professional collaborative studies of interacting binaries from data taken from NURO observations (National Undergraduate Research Observatory). The observations were taken by Ron Samec, Justin Benkendorf, and James Dignan. Reduction and analyses were mostly done by Ron Samec and James Kring.

Our 2012 BVRI light curves were taken with the Lowell 0.81-m reflector in Flagstaff on 7, 9, 11, and 12, May 2012, with CRYOTIGER cooled (–100C) 2048 × 2048 NASACAM and standard UBVR$_c$I$_c$ Johnson-Cousins filters. Individual observations included 265 in B, 247 in V, and 254 in both R and I. The probable error of a single observation was 5 mmag in B and 3 mmag in V, R, and I. The stars in this study (Table 1) were chosen in the same field (V−C has $|\Delta(B-V)| < 0.2$) as designated on the finding chart included for the convenience of future observers (Figure 2). Figures 3a and 3b show sample observations and color curves on 9 and 11 May 2012. Our observations are given in Tables 2a, 2b, 2c, and 2d, in delta magnitudes, ΔB, ΔV, ΔR, and ΔI, in the sense of variable minus comparison star.

Table 1. The variable (V), comparison (C), and check (K) stars in this study.

Star	*Name*	*R.A. (2000)* *h m s*	*Dec. (2000)* ° ′ ″	*V*	*B–V*	*Source**
V	V1073 Her	18 08 35.766	+33 42 05.45	11.616	0.936	*Guide 9*
C	TYC 2625 1672	18 08 22.876	+33 38 26.14	11.24	0.763	*Guide 9*
K	TYC 2629 1443	18 08 39.323	+33 48 14.38	10.98	0.757	*Guide 9*

**Guide 9 (Project Pluto 2012).*

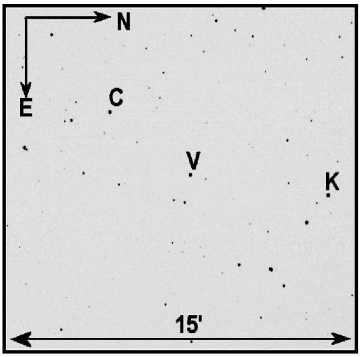

Figure 2. Finding Chart, V1073 Her. Variable (V), Comparison (C), and Check (K).

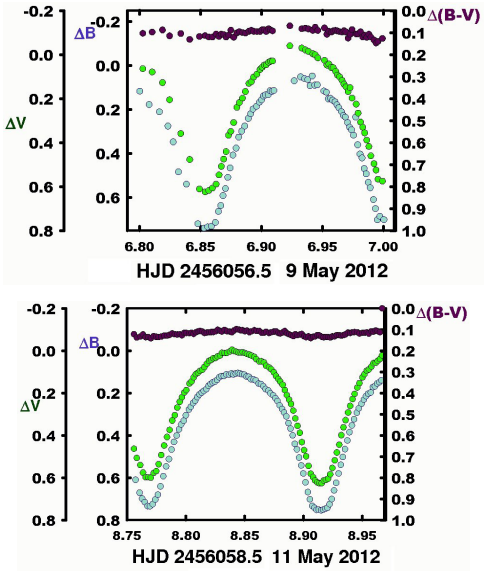

Figure 3. (a, top panel) B,V delta magnitudes from sample observations and color curves on May 9, 2012. (b, bottom panel). B,V delta magnitudes and color curves on May 11, 2012.

Table 2a. V1073 Her observations ΔB, variable minus comparison star.

ΔB	BHJD 2455800+	ΔB	BHJD 2455800+	ΔB	BHJD 2455800+	ΔB	BHJD 2455800+
0.411	4.9655	0.114	6.9070	0.715	8.7651	0.105	8.8443
0.327	4.9726	0.117	6.9086	0.734	8.7674	0.108	8.8461
0.289	4.9766	0.113	6.9102	0.735	8.7695	0.111	8.8479
0.252	4.9805	0.069	6.9269	0.725	8.7719	0.113	8.8498
0.223	4.9845	0.051	6.9321	0.703	8.7741	0.122	8.8516
0.196	4.9884	0.059	6.9353	0.680	8.7763	0.123	8.8536
0.155	4.9932	0.063	6.9380	0.641	8.7785	0.134	8.8553
0.144	5.0017	0.091	6.9398	0.593	8.7809	0.136	8.8577
0.177	6.8079	0.089	6.9437	0.547	8.7833	0.140	8.8595
0.210	6.8163	0.087	6.9458	0.512	8.7856	0.155	8.8620
0.275	6.8233	0.115	6.9512	0.467	8.7879	0.157	8.8638
0.347	6.8276	0.121	6.9533	0.431	8.7900	0.168	8.8660
0.483	6.8319	0.151	6.9549	0.401	8.7922	0.181	8.8678
0.539	6.8385	0.149	6.9567	0.372	8.7942	0.188	8.8702
0.719	6.8478	0.157	6.9583	0.348	8.7961	0.201	8.8720
0.739	6.8530	0.164	6.9603	0.331	8.7982	0.211	8.8744
0.733	6.8560	0.178	6.9619	0.305	8.8000	0.224	8.8762
0.730	6.8590	0.191	6.9635	0.278	8.8026	0.237	8.8780
0.713	6.8622	0.209	6.9656	0.265	8.8043	0.258	8.8798
0.663	6.8647	0.234	6.9688	0.247	8.8062	0.275	8.8819
0.636	6.8666	0.259	6.9706	0.236	8.8080	0.292	8.8836
0.591	6.8685	0.280	6.9723	0.219	8.8098	0.310	8.8855
0.559	6.8705	0.292	6.9739	0.206	8.8116	0.342	8.8873
0.508	6.8724	0.316	6.9755	0.198	8.8135	0.368	8.8891
0.465	6.8743	0.360	6.9789	0.190	8.8153	0.400	8.8909
0.407	6.8766	0.402	6.9808	0.181	8.8175	0.440	8.8927
0.375	6.8792	0.420	6.9825	0.166	8.8193	0.466	8.8945
0.325	6.8813	0.468	6.9842	0.157	8.8211	0.505	8.8964
0.298	6.8838	0.492	6.9859	0.150	8.8229	0.542	8.8982
0.275	6.8863	0.531	6.9876	0.146	8.8248	0.580	8.9000
0.240	6.8892	0.555	6.9892	0.138	8.8266	0.622	8.9018
0.219	6.8911	0.609	6.9918	0.125	8.8285	0.668	8.9038
0.198	6.8930	0.650	6.9935	0.120	8.8303	0.702	8.9056
0.185	6.8959	0.701	6.9951	0.120	8.8324	0.733	8.9076
0.166	6.8984	0.685	6.9971	0.112	8.8345	0.742	8.9094
0.155	6.9001	0.700	7.0004	0.113	8.8369	0.752	8.9112
0.138	6.9017	0.610	8.7573	0.108	8.8388	0.751	8.9130
0.133	6.9033	0.671	8.7607	0.112	8.8405	0.754	8.9150
0.132	6.9055	0.699	8.7629	0.108	8.8425	0.751	8.9168

Table continued on next page

Table 2a. V1073 Her observations ΔB, variable minus comparison star, cont.

ΔB	*BHJD 2455800+*	*ΔB*	*BHJD 2455800+*	*ΔB*	*BHJD 2455800+*	*ΔB*	*BHJD 2455800+*
0.747	8.9186	0.155	8.9627	0.101	9.8837	0.470	9.9264
0.742	8.9204	0.149	8.9646	0.103	9.8855	0.507	9.9284
0.725	8.9223	0.140	8.9664	0.117	9.8874	0.544	9.9302
0.701	8.9241	0.183	9.8411	0.123	9.8892	0.582	9.9320
0.660	8.9261	0.152	9.8464	0.127	9.8911	0.618	9.9339
0.624	8.9279	0.148	9.8484	0.129	9.8929	0.663	9.9357
0.580	8.9300	0.138	9.8502	0.146	9.8947	0.689	9.9376
0.539	8.9318	0.125	9.8526	0.157	9.8965	0.730	9.9416
0.502	8.9336	0.125	9.8544	0.166	9.8984	0.740	9.9487
0.465	8.9354	0.100	9.8578	0.177	9.9002	0.728	9.9505
0.424	8.9374	0.106	9.8596	0.192	9.9021	0.709	9.9523
0.385	8.9392	0.099	9.8616	0.203	9.9039	0.678	9.9541
0.353	8.9413	0.092	9.8634	0.217	9.9057	0.639	9.9559
0.324	8.9431	0.086	9.8654	0.228	9.9075	0.608	9.9577
0.293	8.9454	0.086	9.8672	0.249	9.9095	0.574	9.9596
0.272	8.9472	0.083	9.8690	0.254	9.9113	0.544	9.9614
0.250	8.9496	0.079	9.8708	0.281	9.9133	0.504	9.9633
0.231	8.9514	0.082	9.8726	0.302	9.9151	0.481	9.9651
0.214	8.9533	0.080	9.8744	0.327	9.9169	0.449	9.9670
0.203	8.9551	0.080	9.8762	0.350	9.9188	0.421	9.9688
0.197	8.9573	0.087	9.8780	0.377	9.9208	0.394	9.9706
0.172	8.9591	0.091	9.8798	0.412	9.9226	0.372	9.9724
0.168	8.9609	0.095	9.8816	0.442	9.9246		

Table 2b. V1073 Her observations ΔV, variable minus comparison star.

ΔV	*BHJD 2455800+*	*ΔV*	*BHJD 2455800+*	*ΔV*	*BHJD 2455800+*	*ΔV*	*BHJD 2455800+*
0.404	4.9582	0.058	6.9005	0.566	6.9956	0.034	8.8254
0.282	4.9661	0.048	6.9022	0.538	6.9976	0.027	8.8271
0.183	4.9730	0.046	6.9038	0.575	6.9992	0.023	8.8291
0.149	4.9770	0.035	6.9059	0.573	7.0009	0.010	8.8308
0.123	4.9809	0.030	6.9075	0.555	7.0026	0.010	8.8350
0.098	4.9849	0.029	6.9091	0.595	7.0059	–0.004	8.8393
0.070	4.9889	0.018	6.9106	0.463	8.7559	0.005	8.8431
0.043	4.9936	–0.001	6.9193	0.507	8.7583	0.008	8.8448
0.030	4.9976	–0.030	6.9331	0.540	8.7613	0.009	8.8467
0.020	5.0021	–0.021	6.9361	0.576	8.7636	0.007	8.8484
0.018	6.7960	–0.015	6.9385	0.598	8.7658	0.011	8.8503
0.064	6.8027	–0.004	6.9421	0.598	8.7680	0.015	8.8521
0.079	6.8104	0.001	6.9441	0.600	8.7702	0.019	8.8541
0.127	6.8188	0.015	6.9462	0.578	8.7726	0.023	8.8559
0.205	6.8246	0.026	6.9517	0.569	8.7748	0.029	8.8583
0.245	6.8289	0.047	6.9537	0.536	8.7769	0.040	8.8600
0.359	6.8338	0.043	6.9553	0.493	8.7791	0.051	8.8626
0.477	6.8412	0.059	6.9572	0.448	8.7816	0.050	8.8644
0.611	6.8492	0.059	6.9588	0.408	8.7840	0.055	8.8665
0.624	6.8538	0.076	6.9608	0.374	8.7862	0.071	8.8683
0.618	6.8568	0.093	6.9624	0.330	8.7885	0.079	8.8708
0.607	6.8598	0.101	6.9640	0.305	8.7907	0.087	8.8726
0.589	6.8628	0.117	6.9661	0.269	8.7928	0.102	8.8749
0.547	6.8652	0.134	6.9677	0.241	8.7948	0.119	8.8767
0.508	6.8671	0.146	6.9693	0.220	8.7967	0.133	8.8786
0.475	6.8690	0.168	6.9711	0.198	8.7987	0.146	8.8804
0.441	6.8710	0.150	6.9727	0.186	8.8005	0.161	8.8824
0.367	6.8730	0.197	6.9743	0.155	8.8031	0.186	8.8842
0.349	6.8749	0.243	6.9760	0.145	8.8049	0.210	8.8860
0.309	6.8772	0.225	6.9777	0.126	8.8067	0.231	8.8878
0.240	6.8798	0.266	6.9793	0.111	8.8085	0.252	8.8896
0.218	6.8819	0.307	6.9813	0.104	8.8104	0.283	8.8914
0.198	6.8844	0.330	6.9830	0.095	8.8121	0.320	8.8932
0.168	6.8868	0.356	6.9846	0.090	8.8140	0.355	8.8950
0.131	6.8897	0.389	6.9864	0.077	8.8158	0.388	8.8970
0.123	6.8916	0.418	6.9881	0.061	8.8180	0.432	8.8987
0.102	6.8936	0.460	6.9897	0.048	8.8198	0.470	8.9006
0.089	6.8963	0.496	6.9923	0.043	8.8217	0.499	8.9024
0.067	6.8989	0.525	6.9940	0.036	8.8234	0.544	8.9044

Table continued on next page

Table 2b. V1073 Her observations ΔV, variable minus comparison star, cont.

Δ*V*	*BHJD 2455800+*	Δ*V*	*BHJD 2455800+*	Δ*V*	*BHJD 2455800+*	Δ*V*	*BHJD 2455800+*
0.581	8.9062	0.094	8.9539	–0.024	9.8786	0.322	9.9252
0.597	8.9082	0.088	8.9557	–0.019	9.8804	0.353	9.9270
0.613	8.9100	0.075	8.9578	–0.014	9.8822	0.389	9.9289
0.622	8.9118	0.059	8.9596	–0.012	9.8843	0.413	9.9307
0.626	8.9136	0.057	8.9615	–0.001	9.8860	0.451	9.9326
0.626	8.9156	0.048	8.9632	0.005	9.8879	0.504	9.9344
0.613	8.9173	0.039	8.9652	0.006	9.8897	0.526	9.9363
0.610	8.9192	0.022	8.9670	0.013	9.8916	0.558	9.9381
0.605	8.9210	0.061	9.8422	0.029	9.8934	0.589	9.9422
0.584	8.9228	0.042	9.8470	0.038	9.8953	0.604	9.9473
0.554	8.9246	0.030	9.8490	0.040	9.8971	0.595	9.9492
0.518	8.9267	0.030	9.8508	0.055	9.8990	0.573	9.9510
0.481	8.9285	0.017	9.8531	0.066	9.9008	0.552	9.9529
0.444	8.9305	0.006	9.8549	0.071	9.9027	0.532	9.9547
0.399	8.9323	–0.002	9.8584	0.089	9.9044	0.494	9.9565
0.362	8.9341	–0.008	9.8602	0.102	9.9063	0.466	9.9583
0.328	8.9359	–0.009	9.8622	0.104	9.9081	0.434	9.9602
0.292	8.9380	–0.022	9.8640	0.128	9.9101	0.397	9.9620
0.261	8.9398	–0.025	9.8660	0.147	9.9118	0.370	9.9638
0.228	8.9418	–0.024	9.8678	0.170	9.9138	0.330	9.9656
0.204	8.9436	–0.031	9.8696	0.185	9.9156	0.312	9.9675
0.174	8.9459	–0.029	9.8714	0.211	9.9175	0.283	9.9693
0.153	8.9477	–0.027	9.8732	0.229	9.9193	0.259	9.9712
0.126	8.9502	–0.029	9.8750	0.260	9.9213	0.231	9.9729
0.111	8.9520	–0.022	9.8768	0.290	9.9232		

Table 2c. V1073 Her observations ΔR, variable minus comparison star.

Δ*R*	*BHJD 2455800+*	Δ*R*	*BHJD 2455800+*	Δ*R*	*BHJD 2455800+*	Δ*R*	*BHJD 2455800+*
0.173	4.9664	–0.025	6.9009	0.467	6.9960	0.051	9.9104
0.105	4.9734	–0.033	6.9025	0.470	6.9979	0.067	9.9122
0.066	4.9773	–0.041	6.9042	0.481	6.9996	0.086	9.9142
0.038	4.9813	–0.050	6.9063	0.496	7.0012	0.104	9.9160
0.011	4.9852	–0.051	6.9078	0.506	7.0029	0.134	9.9179
–0.006	4.9892	–0.067	6.9094	–0.025	9.8429	0.148	9.9197
–0.030	4.9940	–0.070	6.9110	–0.047	9.8473	0.173	9.9217
–0.052	4.9979	–0.109	6.9196	–0.056	9.8493	0.201	9.9235
–0.062	5.0025	–0.113	6.9237	–0.058	9.8511	0.240	9.9255
–0.052	5.0064	–0.107	6.9339	–0.072	9.8535	0.266	9.9274
–0.035	6.7967	–0.102	6.9367	–0.078	9.8553	0.312	9.9293
–0.026	6.8043	–0.094	6.9388	–0.082	9.8588	0.335	9.9311
–0.018	6.8120	–0.116	6.9406	–0.098	9.8605	0.379	9.9330
0.062	6.8204	–0.099	6.9425	–0.097	9.8626	0.407	9.9348
0.136	6.8255	–0.078	6.9445	–0.102	9.8642	0.433	9.9367
0.182	6.8298	–0.071	6.9466	–0.105	9.8663	0.465	9.9385
0.271	6.8353	–0.049	6.9520	–0.103	9.8681	0.498	9.9426
0.424	6.8432	–0.019	6.9541	–0.101	9.8699	0.514	9.9477
0.510	6.8503	–0.048	6.9557	–0.108	9.8717	0.495	9.9496
0.515	6.8545	–0.029	6.9575	–0.104	9.8736	0.476	9.9514
0.520	6.8575	–0.019	6.9591	–0.102	9.8753	0.448	9.9532
0.493	6.8604	–0.005	6.9612	–0.108	9.8771	0.422	9.9550
0.468	6.8632	0.008	6.9628	–0.101	9.8789	0.394	9.9569
0.427	6.8656	0.016	6.9644	–0.098	9.8808	0.368	9.9586
0.395	6.8675	0.024	6.9664	–0.091	9.8825	0.334	9.9605
0.365	6.8695	0.050	6.9680	–0.081	9.8846	0.299	9.9623
0.318	6.8714	0.059	6.9696	–0.082	9.8864	0.267	9.9642
0.238	6.8734	0.114	6.9715	–0.081	9.8883	0.240	9.9660
0.248	6.8753	0.130	6.9731	–0.071	9.8901	0.212	9.9679
0.205	6.8776	0.116	6.9747	–0.062	9.8920	0.182	9.9697
0.169	6.8802	0.162	6.9780	–0.055	9.8938	0.169	9.9715
0.135	6.8823	0.183	6.9797	–0.041	9.8956	0.144	9.9733
0.095	6.8848	0.214	6.9817	–0.028	9.8974	0.461	8.7618
0.073	6.8872	0.249	6.9833	–0.021	9.8993	0.467	8.7640
0.042	6.8901	0.259	6.9850	–0.020	9.9011	0.502	8.7662
0.027	6.8920	0.312	6.9868	–0.004	9.9030	0.497	8.7684
0.018	6.8940	0.336	6.9884	0.006	9.9048	0.483	8.7730
0.003	6.8967	0.359	6.9901	0.012	9.9066	0.445	8.7752
–0.018	6.8993	0.441	6.9943	0.031	9.9084	0.423	8.7774

Table continued on next page

Table 2c. V1073 Her observations ΔR, variable minus comparison star, cont.

Δ*R*	*BHJD 2455800+*	Δ*R*	*BHJD 2455800+*	Δ*R*	*BHJD 2455800+*	Δ*R*	*BHJD 2455800+*
0.391	8.7796	–0.063	8.8294	0.053	8.8789	0.455	8.9250
0.348	8.7820	–0.066	8.8312	0.058	8.8807	0.414	8.9271
0.310	8.7843	–0.068	8.8333	0.084	8.8828	0.375	8.9288
0.272	8.7866	–0.075	8.8354	0.101	8.8846	0.333	8.9309
0.241	8.7889	–0.085	8.8378	0.128	8.8864	0.294	8.9327
0.199	8.7911	–0.085	8.8397	0.150	8.8882	0.260	8.9345
0.165	8.7931	–0.074	8.8415	0.178	8.8900	0.230	8.9363
0.141	8.7952	–0.073	8.8434	0.195	8.8918	0.191	8.9383
0.128	8.7971	–0.078	8.8452	0.232	8.8936	0.167	8.9401
0.101	8.7991	–0.074	8.8470	0.266	8.8954	0.129	8.9422
0.085	8.8009	–0.070	8.8488	0.302	8.8973	0.110	8.9440
0.061	8.8035	–0.065	8.8507	0.343	8.8991	0.082	8.9463
0.047	8.8053	–0.068	8.8525	0.387	8.9009	0.060	8.9481
0.037	8.8071	–0.065	8.8545	0.417	8.9027	0.040	8.9505
0.030	8.8089	–0.055	8.8563	0.451	8.9047	0.027	8.9523
0.011	8.8107	–0.049	8.8586	0.485	8.9065	0.008	8.9543
–0.007	8.8125	–0.044	8.8604	0.509	8.9085	–0.003	8.9560
–0.005	8.8144	–0.036	8.8630	0.522	8.9103	–0.011	8.9582
–0.016	8.8162	–0.029	8.8647	0.522	8.9122	–0.022	8.9600
–0.028	8.8184	–0.021	8.8669	0.524	8.9139	–0.030	8.9618
–0.031	8.8202	–0.007	8.8687	0.522	8.9159	–0.040	8.9636
–0.044	8.8220	0.002	8.8712	0.516	8.9177	–0.046	8.9655
–0.044	8.8238	0.014	8.8730	0.512	8.9196	–0.054	8.9673
–0.047	8.8257	0.026	8.8753	0.500	8.9213		
–0.063	8.8275	0.032	8.8771	0.480	8.9232		

Table 2d. V1073 Her observations ΔI, variable minus comparison star, cont.

ΔI	BHJD 2455800+	ΔI	BHJD 2455800+	ΔI	BHJD 2455800+	ΔI	BHJD 2455800+
0.075	4.9667	–0.122	6.9013	0.369	6.9963	–0.041	9.9126
0.009	4.9737	–0.129	6.9029	0.353	6.9983	–0.019	9.9145
–0.032	4.9776	–0.131	6.9045	0.391	6.9999	0.008	9.9164
–0.063	4.9816	–0.160	6.9066	0.349	7.0033	0.030	9.9182
–0.082	4.9855	–0.146	6.9082	–0.123	9.8435	0.056	9.9200
–0.101	4.9895	–0.135	6.9097	–0.151	9.8477	0.080	9.9221
–0.118	4.9943	–0.177	6.9113	–0.149	9.8497	0.108	9.9239
–0.146	4.9982	–0.192	6.9345	–0.159	9.8515	0.135	9.9259
–0.170	5.0027	–0.191	6.9374	–0.168	9.8538	0.170	9.9277
–0.171	5.0067	–0.182	6.9391	–0.171	9.8556	0.202	9.9296
–0.166	6.7974	–0.175	6.9409	–0.187	9.8591	0.231	9.9315
–0.106	6.8057	–0.186	6.9428	–0.188	9.8609	0.262	9.9333
–0.090	6.8133	–0.170	6.9449	–0.195	9.8629	0.303	9.9352
–0.024	6.8217	–0.146	6.9470	–0.190	9.8647	0.330	9.9370
–0.007	6.8263	–0.143	6.9524	–0.198	9.8667	0.346	9.9389
0.035	6.8305	–0.130	6.9544	–0.196	9.8685	0.388	9.9429
0.121	6.8363	–0.123	6.9560	–0.196	9.8703	0.377	9.9480
0.338	6.8451	–0.120	6.9578	–0.203	9.8721	0.364	9.9499
0.396	6.8514	–0.108	6.9595	–0.197	9.8739	0.354	9.9518
0.400	6.8551	–0.094	6.9615	–0.197	9.8757	0.323	9.9536
0.402	6.8581	–0.084	6.9631	–0.202	9.8775	0.295	9.9554
0.387	6.8611	–0.074	6.9647	–0.185	9.8793	0.271	9.9572
0.362	6.8636	–0.063	6.9668	–0.185	9.8811	0.243	9.9590
0.313	6.8660	–0.045	6.9683	–0.185	9.8829	0.200	9.9609
0.275	6.8679	–0.037	6.9700	–0.183	9.8850	0.177	9.9627
0.244	6.8699	–0.030	6.9718	–0.172	9.8868	0.147	9.9645
0.199	6.8718	0.004	6.9734	–0.172	9.8886	0.123	9.9663
0.145	6.8738	0.024	6.9750	–0.165	9.8904	0.092	9.9682
0.139	6.8757	0.050	6.9767	–0.162	9.8923	0.069	9.9700
0.090	6.8780	0.057	6.9784	–0.152	9.8941	0.047	9.9719
0.059	6.8806	0.093	6.9800	–0.139	9.8960	0.313	8.7597
0.021	6.8827	0.128	6.9820	–0.132	9.8978	0.348	8.7622
–0.010	6.8852	0.144	6.9837	–0.118	9.8997	0.362	8.7645
–0.027	6.8876	0.172	6.9853	–0.113	9.9015	0.380	8.7667
–0.059	6.8905	0.198	6.9871	–0.106	9.9034	0.370	8.7689
–0.073	6.8924	0.239	6.9888	–0.090	9.9052	0.374	8.7711
–0.084	6.8944	0.272	6.9904	–0.085	9.9070	0.358	8.7734
–0.096	6.8970	0.315	6.9930	–0.069	9.9088	0.334	8.7756
–0.122	6.8996	0.333	6.9947	–0.052	9.9108	0.296	8.7778

Table continued on next page

Table 2d. V1073 Her observations Δi, variable minus comparison star, cont.

Δ*I*	*BHJD 2455800+*	Δ*I*	*BHJD 2455800+*	Δ*I*	*BHJD 2455800+*	Δ*I*	*BHJD 2455800+*
0.262	8.7800	–0.164	8.8298	–0.052	8.8793	0.322	8.9254
0.226	8.7824	–0.166	8.8316	–0.039	8.8811	0.284	8.9274
0.184	8.7847	–0.175	8.8336	–0.011	8.8831	0.257	8.9292
0.148	8.7870	–0.171	8.8357	0.001	8.8849	0.211	8.9313
0.114	8.7893	–0.186	8.8382	0.020	8.8867	0.178	8.9330
0.086	8.7914	–0.179	8.8400	0.053	8.8885	0.149	8.9349
0.065	8.7935	–0.178	8.8418	0.065	8.8903	0.114	8.9366
0.034	8.7955	–0.180	8.8438	0.103	8.8921	0.075	8.9387
0.011	8.7974	–0.172	8.8455	0.132	8.8939	0.052	8.9405
0.004	8.7995	–0.178	8.8474	0.161	8.8957	0.022	8.9425
–0.033	8.8012	–0.172	8.8491	0.198	8.8977	0.005	8.9443
–0.045	8.8038	–0.167	8.8510	0.229	8.8994	–0.022	8.9466
–0.064	8.8056	–0.168	8.8528	0.264	8.9013	–0.037	8.9484
–0.065	8.8074	–0.160	8.8548	0.301	8.9031	–0.060	8.9509
–0.080	8.8092	–0.155	8.8566	0.333	8.9051	–0.084	8.9527
–0.092	8.8111	–0.139	8.8590	0.361	8.9069	–0.090	8.9546
–0.097	8.8128	–0.143	8.8608	0.378	8.9089	–0.101	8.9564
–0.104	8.8148	–0.134	8.8633	0.392	8.9107	–0.110	8.9585
–0.113	8.8165	–0.126	8.8651	0.399	8.9125	–0.119	8.9603
–0.130	8.8187	–0.113	8.8672	0.398	8.9143	–0.130	8.9622
–0.129	8.8205	–0.102	8.8690	0.398	8.9163	–0.139	8.9639
–0.139	8.8224	–0.097	8.8715	0.395	8.9180	–0.146	8.9659
–0.142	8.8242	–0.086	8.8733	0.390	8.9199	–0.152	8.9677
–0.153	8.8261	–0.074	8.8756	0.376	8.9217		
–0.158	8.8278	–0.063	8.8774	0.345	8.9236		

3. Period study

Four times of minimum light were calculated, 2 primary and 2 secondary eclipses, from our present observations including errors:

HJD I = JD Hel Min I = 2456056.8549±0.0002, 2456058.91485±0.00008 (1)

HJD II = 2456058.7685±0.0002, 2456059.9455±0.0001 (2)

Some 54 timings were used in our period study. A very low amplitude sinusoid was discovered in the calculation of its linear ephemeris. The sinusoidal ephemeris follows the linear one below:

JD Hel Min I = 2451746.5113±0.0004d + 0.29428167±0.00000004×E (3)

JD Hel Min I = 2451746.5108±0.0006d + 0.294281673±0.00000004×E
+0.0025(±0.0003) × *sin*[(0.00045±0.00002) × E+ 2.4±0.2] (4)

The plotted residuals overlaid by the sinusoidal term of Equation 3 is given in Figure 4. The O–C curve is a low amplitude sinusoid, covering some fourteen years and nearly 18,000 orbits. It possibly indicates the presence of a third component. The period of this sinusoid is 11.2 ± 0.5 years. Using the amplitude from the ephemeris, the binary mass of 1.1 solar masses, the mass ratio, and the inclination from our Wilson-Devinney (1971) program solution (the orbital inclination of the close binary), we determined the third body to have ~0.1 $M_{\odot}$, which is slightly above the maximum limit of a brown dwarf (0.075 $M_{\odot}$). Since the orbital inclination of the distant third component does not necessarily have the same inclination as that of the close pair, we calculate the mass for various inclinations. For inclinations 60°, 45°, 30°, and 20°, we obtain masses of 0.11, 0.15, 0.21, 0.33 $M_{\odot}$, respectively. Since no third light was found, we tend to think that the lower masses are near the actual value. Tran *et al.* (2013) have shown that such amplitudes (<0.01d) are expected in spotted contact binaries and can result in quasi-periodic variations of a few hundred days. Although the amplitude variations are on this order, the period found here is much too long to be due to spots. However, a magnetic spot cycle is not out of the question to explain the variation. The times of minimum light and the linear residuals are given in Table 3.

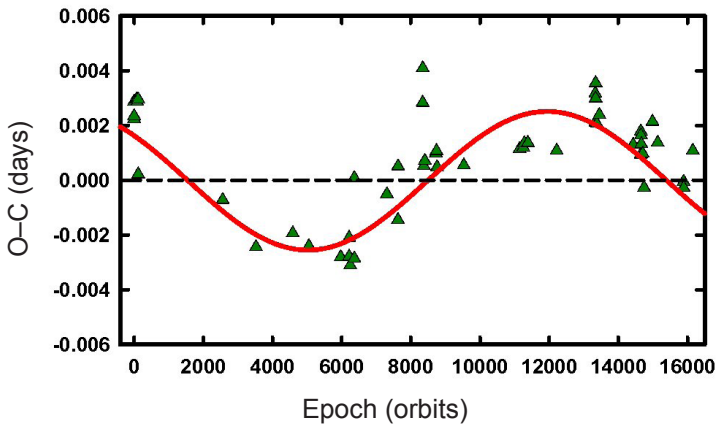

Figure 4. Sinusoidal O–C residuals from the period study.

Table 3. V1073 Her times of minimum light and linear residuals.

No.	*Epochs*	*Cycles*	*Weight*	*O–C*	*References*
1	51258.8894	–1657.0	1.0	0.0029	Blätter and Diethelm 2000
2	51277.8726	–1592.5	1.0	0.0049	Blätter and Diethelm 2000
3	51746.3660	–0.5	1.0	0.0019	BBSAG 2000
4	51746.5125	0.0	1.0	0.0012	BBSAG 2000
5	51768.4372	74.5	0.5	0.0019	BBSAG 2000
6	51773.4399	91.5	0.5	0.0018	BBSAG 2000
7	51781.3856	118.5	1.0	0.0019	BBSAG 2000
8	51781.5300	119.0	1.0	–0.0008	BBSAG 2000
9	51746.5126	0.0	0.0	0.0013	BBSAG 2000
10	52500.1649	2561.0	0.0	–0.0017	Kreiner 2004
11	52783.4093	3523.5	1.0	–0.0035	Diethelm 2003
12	53096.5255	4587.5	1.0	–0.0030	Diethelm 2004
13	53233.5132	5053.0	1.0	–0.0034	Brát *et al.* 2007
14	53504.5462	5974.0	1.0	–0.0038	Brát *et al.* 2007
15	53575.4681	6215.0	0.5	–0.0038	Malkov *et al.* 2006
16	53575.4688	6215.0	0.5	–0.0031	Malkov *et al.* 2006
17	53585.4733	6249.0	0.5	–0.0041	Brát *et al.* 2008
18	53620.3489	6367.5	1.0	–0.0009	Diethelm 2006
19	53620.4931	6368.0	1.0	–0.0039	Diethelm 2006
20	53897.4145	7309.0	1.0	–0.0015	Hübscher 2007
21	53992.3194	7631.5	1.0	–0.0025	Diethelm 2007
22	53992.4685	7632.0	1.0	–0.0005	Diethelm 2007
23	54202.4408	8345.5	1.0	0.0018	Diethelm 2007
24	54202.5892	8346.0	1.0	0.0031	Diethelm 2007
25	54211.8555	8377.5	1.0	–0.0005	Nelson 2008
26	54220.5370	8407.0	1.0	–0.0003	Hübscher 2007
27	54314.4131	8726.0	1.0	0.0000	Brát *et al.* 2007
28	54319.4160	8743.0	1.0	0.0001	Hübscher *et al.* 2009
29	54324.4182	8760.0	1.0	–0.0005	Hübscher *et al.* 2009
30	54551.8980	9533.0	1.0	–0.0005	Nelson 2009
31	55026.4278	11145.5	0.5	0.0001	Brát *et al.* 2011
32	55058.3574	11254.0	0.5	0.0002	Brát *et al.* 2011
33	55067.4803	11285.0	1.0	0.0003	Diethelm 2010
34	55097.3499	11386.5	1.0	0.0004	Hübscher and Monninger 2011
35	55342.4863	12219.5	0.5	0.0001	Brát *et al.* 2011
36	55670.4642	13334.0	1.0	0.0011	Hübscher *et al.* 2012
37	55670.6124	13334.5	1.0	0.0022	Hübscher *et al.* 2012
38	55673.4079	13344.0	1.0	0.0020	Hübscher *et al.* 2012
39	55673.5556	13344.5	1.0	0.0025	Hübscher *et al.* 2012
40	55683.4126	13378.0	0.5	0.0011	Hoňková *et al.* 2013

Table continued on next page

Table 3. V1073 Her times of minimum light and linear residuals, cont.

No.	*Epochs*	*Cycles*	*Weight*	*O–C*	*References*
41	55705.4840	13453.0	1.0	0.0014	Hübscher *et al.* 2012
42	55992.9961	14430.0	1.0	0.0003	Nelson 2013
43	56056.8549	14647.0	1.0	–0.0001	Present observations
44	56058.7686	14653.5	1.0	0.0008	Present observations
45	56058.9149	14654.0	1.0	–0.0001	Present observations
46	56059.9455	14657.5	1.0	0.0006	Present observations
47	56062.4466	14666.0	1.0	0.0003	Hübscher and Lehmann 2013
48	56074.5118	14707.0	1.0	0.0000	Hübscher and Lehmann 2013
49	56085.8404	14745.5	1.0	–0.0013	Diethelm 2012
50	56157.5004	14989.0	1.0	0.0011	Hübscher and Lehmann 2013
51	56201.3476	15138.0	1.0	0.0004	Hübscher and Lehmann 2013
52	56422.3517	15889.0	0.5	–0.0011	Hoňková *et al.* 2013
53	56422.4986	15889.5	0.5	–0.0013	Hoňková *et al.* 2013
54	56500.4846	16154.5	0.5	0.0001	Hoňková *et al.* 2013

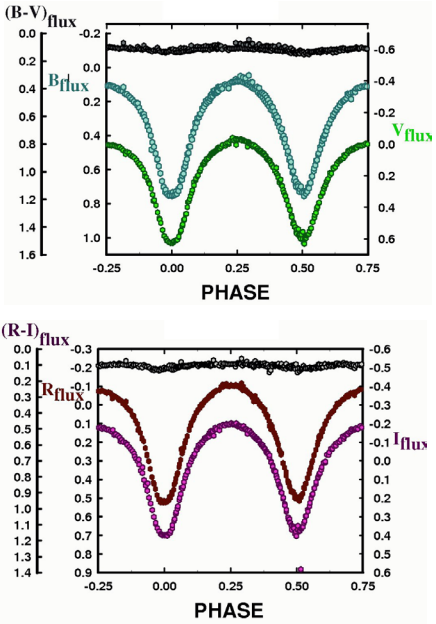

Figure 5. (a, top panel) B,V delta magnitude and color magnitudes vs. phase plots in the sense of V–C. (b, bottom panel) R,I delta magnitude and color magnitudes vs. phase plots in the sense of V–C.

4. Light curves and temperature determination

The light curves were phased using Equation (3). These are given as Figures 5a and 5b. A table of light curve characteristics are given in Table 4. The curves are of high precision with a standard errors of 3–5 mmag. The amplitude of the light curves are 0.6–0.7 magnitude from I to B. The O'Connell effect, which is classically an indication of spot activity, is about 0.03 in all filters, with MAX I (the maximum following MIN I) being the most luminous. Thus, spot activity is expected. The minima are the nearly the same, within 0.02–0.03 magnitude, indicating a high degree of thermal contact. Since the minima are so close it is difficult to say if the binary is W-type or A-type, and season-to-season variations will probably go either way.

2MASS photometry (Skrutskie 2006; TYCHO Hog *et al.* 2000) gives the temperature of the binary as ~5150 ± 300. We used this value for the primary component in our light curve solution.

Table 4. Light curve characteristics.

Filter	*Magnitude*		
	Max. I	*Max. II*	
Phase	0.25	0.75	
B	0.106±0.002	0.077±0.013	
V	0.007±0.005	–0.027±0.003	
R	0.006±0.005	–0.106±0.003	
I	–0.178±0.006	–0.198±0.003	
	Min. II	*Min. I*	
Phase	0.5	0.0	
B	0.749±0.007	0.721±0.017	
V	0.622±0.005	0.586±0.019	
R	0.519±0.003	0.503±0.007	
I	0.398±0.002	0.373±0.016	
	Min. II–Max. II	*Max. I–Max. II*	*Min. II–Min. I*
B	0.672±0.020	0.029±0.015	0.028±0.024
V	0.649±0.008	0.033±0.008	0.035±0.024
R	0.625±0.005	0.029±0.008	0.016±0.010
I	0.596±0.005	0.020±0.009	0.025±0.018

5. Synthetic light curve solution

The B V R and I curves were pre-modeled with BINARY MAKER 3.0 (Bradstreet and Steelman 2004) fits in all filter bands. The parameters were then averaged

Table 5. V1073 Her light curve solution.

Parameters	*Values*
λ_B, λ_V, λ_R, λ_I (nm)	440, 550, 640, 790
$x_{bol1,2}$, $y_{bol1,2}$	0.647 0.647, 0.176 0.176
$x_{1I,2I}$, $y_{1I,2I}$	0.637 0.637, 0.208 0.208
$x_{1R,2R}$, $y_{1R,2R}$	0.724 0.724, 0.200 0.200
$x_{1V,2V}$, $y_{1V,2V}$	0.790 0.790, 0.159 0.159
$x_{1B,2B}$, $y_{1B,2B}$	0.851 0.851, 0.044 0.044
g_1, g_2	0.32, 0.32
A_1, A_2	0.5
Inclination (°)	82.3 ± 0.1
T_1, T_2 (K)	5150, 5176 ± 1
Ω_1, Ω_2	2.640 ± 0.001
$q(m_2/m_1)$	0.404 ± 0.004
$L_1/(L_1+L_2)_I$	0.663 ± 0.001
$L_1/(L_1+L_2)_R$	0.660 ± 0.001
$L_1/(L_1+L_2)_V$	0.658 ± 0.001
$L_1/(L_1+L_2)_B$	0.652 ± 0.001
JD_o (days)	56056.8558 ± 0.00004
Period (days)	0.294264 ± 0.000007
r_1, r_2 (pole)	0.440 ± 0.001, 0.292 ± 0.001
r_1, r_2 (side)	0.472 ± 0.002, 0.306 ± 0.002
r_1, r_2 (back)	0.502 ± 0.002, 0.345 ± 0.004
SPOT Parameters	
Spot I on STAR 1	Cool Spot
Colatitude (°)	93 ± 2
Longitude (°)	244 ± 1
Spot radius (°)	21.8 ± 0.3
Spot T-factor	0.861 ± 0.005

and input into a four-color simultaneous light curve calculation using the Wilson-Devinney Program (W-D, Wilson and Devinney 1971; Wilson 1990, 1994; Van Hamme and Wilson 1998). There is no third light in the solutions. Only small negative and negligible values resulted when it was included in the adjustable parameters, indicating that no third body of appreciable brightness contributes to the overall light of the system. The solution was computed in Mode 3, the contact mode. Convective parameters g = 0.32 A = 0.5 were used. Since the eclipses did not appear to be total (later we found out the eclipses did have a brief time of totality, ~3 minutes in the secondary), a q-search was performed over a mass ratio, q, range of 0.3 to 2.0. The initial and best residual occurred at q = 0.4. The q search mass ratios and residuals are shown in Figure 6.

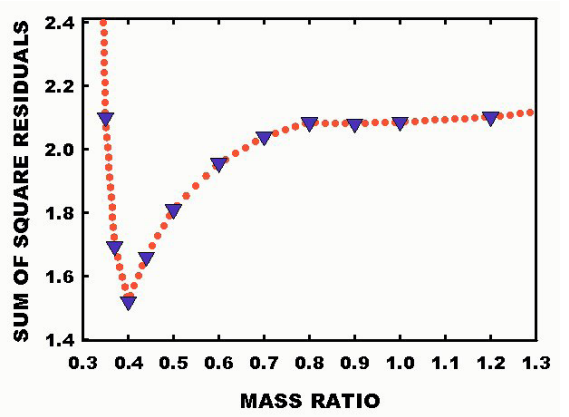

Figure 6. Chart of solution residuals of mass ratios extending from 0.35 to 1.2 minimizes near 0.4.

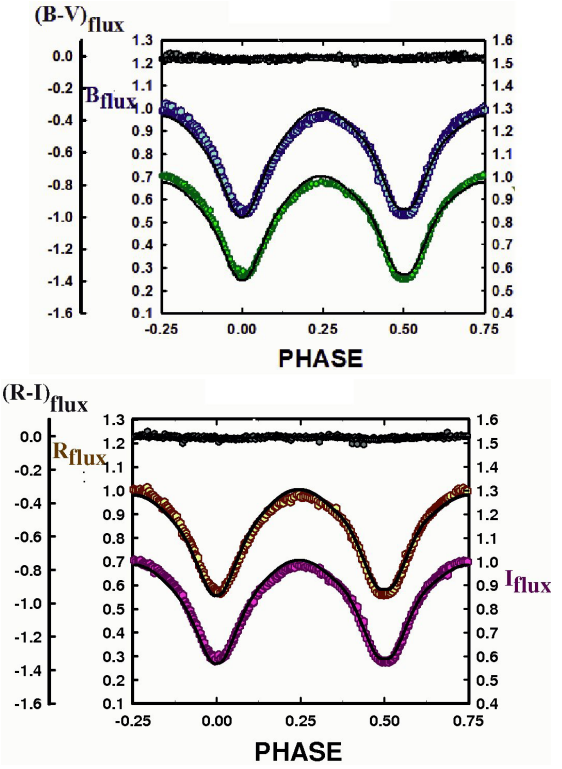

Figure 7. (a, top panel) B,V synthetic light curve solutions overlaying the normalized flux curves. (b, bottom panel) R,I synthetic light curve solutions overlaying the normalized flux curves.

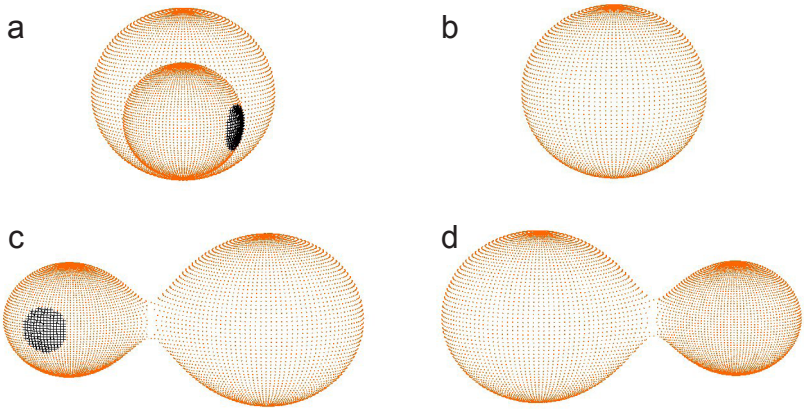

Figure 8. Roche Lobe surfaces from our BVRI solution: (a) phase 0.00 (the primary eclipse); (b) phase 0.25; (c) phase 0.50; (d) phase 0.75.

The mass ratio as well as the other free parameters were allowed to adjust in W-D for the final runs. The synthetic light curve solution is given in Table 5. The normalized curves overlain by our light curve solutions are shown as Figures 7a and 7b. A geometrical representation of the system in Figures 8a–8d is given at quadratures so that the reader may visualize the placement of the spot and the relative size of the stars as compared to the orbit.

6. Conclusion

V1073 Herculis is a very short period (P = 0.294281673(4) day) W UMa totally eclipsing binary. The fourteen-year orbital study (16,000 orbits) reveals a very low amplitude, ~0.0025 day sinusoidal variation with a period of 11.25 years, which may indicate the orbital period of a near-Brown Dwarf third component. This would be one of the first detections of such a body through an O–C study. 2MASS photometry gives a temperature for the primary component of ~5200 K while the Wilson-Devinney Program preliminary solution gives a mass ratio of 0.4, nearly identical component temperatures, and a cool magnetic spot with a T-factor of 0.86 with a spot radius of 22 degrees. The system is magnetically active. The Roche Lobe fill-out is 0.18. The inclination is 82 degrees not quite totally eclipsing. The binary is only slightly of W-type (the less massive component of the binary is slightly hotter). This system is apparently just on the verge of leaving its shallow contact stage and is of intermediate age. Radial velocity curves are needed to confirm or refute our solution and to obtain absolute (not relative) system parameters.

7. Acknowledgements

We wish to thank the National Undergraduate Research Observatory and Lowell Observatory for their allocation of observing time to our program from 2004 to 2012. We also wish to thank Bob Jones University for their support of this and many other projects over the past eighteen years.

References

Akerlof, C., *et al.* 2000, *Astron. J.*, **119**, 1901.
Beob. der Schweizerischen Astron. Ges. (BBSAG). 2000, *BBSAG Bull.*, No. 123, 1.
Blättler, E., and Diethelm, R. 2000, *Inf. Bull. Var. Stars*, No. 4975, 1.
Bradstreet, D. H., and Steelman, D. P. 2004, BINARY MAKER 3.0, Contact Software (http://www.binarymaker.com).
Brát, L., Zejda, M., and Svoboda, P. 2007, *Contrib. Nicholas Copernicus Obs. Planetarium Brno*, **34**, 1.
Brát, L., *et al.* 2008, *Open Eur. J. Var. Stars*, **94**, 1.
Brát, L., *et al.* 2011, *Open Eur. J. Var. Stars*, **137**, 1.
Diethelm, R. 2003, *Inf. Bull. Var. Stars*, No. 5438, 1.
Diethelm, R. 2004, *Inf. Bull. Var. Stars*, No. 5543, 1.
Diethelm, R. 2006, *Inf. Bull. Var. Stars*, No. 5713, 1.
Diethelm, R. 2007, *Inf. Bull. Var. Stars*, No. 5781, 1.
Diethelm, R. 2010, *Inf. Bull. Var. Stars*, No. 5920, 1.
Diethelm, R. 2012, *Inf. Bull. Var. Stars*, No. 6029, 1.
Gettel, S. J., Geske, M. T., and McKay, T. A. 2006, *Astron. J.*, **131**, 621.
Hoffman, D. I., Harrison, T. E., and McNamara, B. J. 2009, *Astron. J.*, **138**, 466.
Høg, E., *et al.* 2000, The Tycho-2 Catalogue of the 2.5 Million Brightest Stars, *Astron. Astrophys.*, **355**, L27.
Hoňková, K., *et al.* 2013, *Contrib. Nicholas Copernicus Obs. Planetarium Brno*, **38**, 1.
Hübscher, J. 2007, *Inf. Bull. Var. Stars*, No. 5802, 1.
Hübscher, J. 2009, *Inf. Bull. Var. Stars*, No. 5874, 1.
Hübscher, J., and Lehmann, P. B. 2013, *Inf. Bull. Var. Stars*, No. 6070, 1.
Hübscher, J., Lehmann, P. B., and Walter, F. 2012, *Inf. Bull. Var. Stars*, No. 6010, 1.
Hübscher, J., and Monninger, G. 2011, *BAV Mitt.*, **214**, 1.
Hübscher, J., Steinbach, H.-M., and Walter, F. 2009, *Inf. Bull. Var. Stars*, No. 5874, 1.
Kazarovets, E. V., Kireeva, N. N., Samus, N. N., and Durlevich, O. V. 2003, *Inf. Bull. Var. Stars*, No. 5422, 1.
Kreiner, J. M. 2004, *Acta Astron.*, **54**, 207.
Malkov, O. Y., Oblak, E., Snegireva, E. A., and Torra, J. 2006, *Astron. Astrophys.*, **446**, 785.

Nelson, R. 2008, *Inf. Bull. Var. Stars*, No. 5820, 1.
Nelson, R. 2009, *Inf. Bull. Var. Stars*, No. 5875, 1.
Nelson, R. 2013, *Inf. Bull. Var. Stars*, No. 6050, 1.
Pribulla, T., Kreiner, J. M., and Tremko, J. 2003, *Contrib. Astron. Obs. Skalnatë Pleso*, **33**, 38.
Project Pluto. 2012, GUIDE, version 9 (http://www.projectpluto.com).
Skrutskie, M. F., *et al.* 2006, "The Two Micron All Sky Survey," *Astron. J.*, **131**, 1163.
Tran, K., Levine, S., Rappaport, S., Borkovits, T., Csizmadia, Sz., and Kalomeni, B. 2013, *Astrophys. J.*, **774**, 81.
Van Hamme, W. V., and Wilson, R. E. 1998, *Bull. Amer. Astron. Soc.*, **30**, 1402.
Wilson, R. E. 1990, *Astrophys. J.*, **356**, 613.
Wilson, R. E. 1994, *Publ. Astron. Soc. Pacific*, **106**, 921.
Wilson, R. E., and Devinney, E. J. 1971, *Astrophys. J.*, **166**, 605.

Recent Minima of 161 Eclipsing Binary Stars

Gerard Samolyk
P.O. Box 20677, Greenfield, WI 53220; gsamolyk@wi.rr.com

Received November 1, 2014; accepted November 1, 2014

Abstract This paper continues the publication of times of minima for 161 eclipsing binary stars from observations reported to the AAVSO EB section. Times of minima from observations received by the author from October 2013 through September 2014 are presented.

1. Recent observations

The accompanying list contains times of minima calculated from recent CCD observations made by participants in the AAVSO's eclipsing binary program. This list will be web-archived and made available through the AAVSO ftp site at ftp://ftp.aavso.org/public/datasets/gsamoj422.txt. This list, along with the eclipsing binary data from earlier AAVSO publications, is also included in the Lichtenknecker database (Kreiner 2011) administrated by the Bundesdeutsche Arbeitsgemeinschaft für Veränderliche Sterne e. V. (BAV) at: http://www.bav-astro.de/LkDB/index.php?lang=en. These observations were reduced by the observers or the writer using the method of Kwee and van Woerden (1956). Column F in Table 1 indicates the filter used. A "C" indicates a clear filter. The standard error is included when available.

The linear elements in the *General Catalogue of Variable Stars* (GCVS; Kholopov *et al.* 1985) were used to compute the O–C values for most stars. For a few exceptions where the GCVS elements are missing or are in significant error, light elements from another source are used: V702 And (Watson *et al.* 2014), V1713 Aql (Paschke 2014), CD Cam (Baldwin and Samolyk 2007), AC CMi (Samolyk 2008), CW Cas (Samolyk 1992a), LQ Dra (Nelson 2014), DF Hya (Samolyk 1992b), DK Hya (Samolyk 1990), V576 Lyr (Nelson 2014), V502 Oph (Paschke 2014), EF Ori (Baldwin and Samolyk 2005), GU Ori (Samolyk 1985). The light elements used for QX And, V728 Her, V582 Lyr, V351 Peg, V1121 Tau, V1223 Tau, V1234 Tau, BS UMa, and MS Vir are from (Kreiner 2004). O–C values listed in this paper can be directly compared with values published in the *AAVSO Observed Minima Timings of Eclipsing Binaries* series.

References

Baldwin, M. E., and Samolyk, G. 2005, *Observed Minima Timings of Eclipsing Binaries No. 10*, AAVSO, Cambridge, MA.

Baldwin, M. E., and Samolyk, G. 2007, *Observed Minima Timings of Eclipsing Binaries No. 12*, AAVSO, Cambridge, MA.

Kreiner, J. M. 2004, *Acta Astron.*, **54**, 207, "Up-to-date linear elements of close binaries," (http://www.as.up.krakow.pl/ephem/).

Kreiner, J. M. 2011, Lichtenknecker-Database of the BAV (http://www.bavdata-astro.de/~tl/cgi-bin/varstars_cgi).

Kholopov, P. N., *et al.* 1985, *General Catalogue of Variable Stars*, 4th ed., Moscow.

Kwee, K. K., and van Woerden, H. 1956, *Bull. Astron. Inst. Netherlands*, **12**, 327.

Nelson, B. 2014, "Bob Nelson's O–C files" (http://www.aavso.org/bob-nelsons-o-c-files).

Paschke, A. 2014, "O–C Gateway" (http://var.astro.cz/ocgate/).

Samolyk, G. 1985, *J. Amer. Assoc. Var. Star Obs.*, **14**, 12.

Samolyk, G. 1990, *J. Amer. Assoc. Var. Star Obs.*, **19**, 5.

Samolyk, G. 1992a, *J. Amer. Assoc. Var. Star Obs.*, **21**, 34.

Samolyk, G. 1992b, *J. Amer. Assoc. Var. Star Obs.*, **21**, 111.

Samolyk, G. 2008, *J. Amer. Assoc. Var. Star Obs.*, **36**, 171.

Watson, C., Henden, A. A., and Price, C. A. 2014, AAVSO International Variable Star Index VSX (Watson+, 2006–2014; http://www.aavso.org/vsx).

Table 1. Recent times of minima of stars in the AAVSO eclipsing binary program.

Star	*HJD 2400000+*	*Cycle*	*O–C (day)*	*F*	*Observer*	*Standard Error (day)*
RT And	56579.5825	24546	–0.0103	V	G. Samolyk	0.0001
RT And	56872.6630	25012	–0.0110	V	G. Samolyk	0.0001
TW And	56929.6908	4344	–0.0499	V	G. Samolyk	0.0001
UU And	56584.7111	10048	0.0689	V	K. Menzies	0.0003
WZ And	56921.8741	23071	0.0676	V	R. Sabo	0.0001
XZ And	56603.6150	24038	0.1749	V	G. Samolyk	0.0001
XZ And	56862.8562	24229	0.1760	V	R. Sabo	0.0001
AB And	56610.5241	61770	–0.0333	V	G. Samolyk	0.0001
AB And	56643.5469	61869.5	–0.0338	V	K. Menzies	0.0001
AB And	56879.6869	62581	–0.0350	V	R. Sabo	0.0001
AB And	56888.8141	62608.5	–0.0349	V	K. Menzies	0.0001
AB And	56900.4300	62643.5	–0.0352	R	L. Corp	0.0001

Table continued on following pages

Table 1. Recent times of minima of stars in the AAVSO eclipsing binary program, cont.

Star	*HJD 2400000+*	*Cycle*	*O–C (day)*	*F*	*Observer*	*Standard Error (day)*
DS And	56594.8035	20239.5	0.0032	V	K. Menzies	0.0003
DS And	56619.5609	20264	0.0029	V	G. Samolyk	0.0001
DS And	56929.7902	20571	0.0029	V	G. Samolyk	0.0002
QX And	56929.8441	10747.5	0.0016	V	G. Samolyk	0.0003
V702 And	56556.3496	9685	0.0141	C	Y. Ogmen	0.0001
CX Aqr	56898.8486	36773	0.0131	V	G. Samolyk	0.0001
XZ Aql	56890.7372	7006	0.1741	V	G. Samolyk	0.0001
OO Aql	56573.6098	35439.5	0.0573	V	G. Samolyk	0.0001
OO Aql	56589.3239	35470.5	0.0609	V	L. Corp	0.0003
OO Aql	56927.6036	36138	0.0593	V	G. Samolyk	0.0002
V1182 Aql	56480.4593	2454	0.0248	C	L. Corp	0.0005
V1713 Aql	56831.7394	8181	–0.0155	V	R. Sabo	0.0003
RX Ari	56610.6607	17688	0.0663	V	G. Samolyk	0.0002
SS Ari	56572.6836	43214	–0.3188	V	R. Poklar	0.0002
SS Ari	56633.5810	43364	–0.3205	V	G. Samolyk	0.0002
SS Ari	56676.6163	43470	–0.3205	V	R. Sabo	0.0004
BQ Ari	56908.8959	19572.5	–0.0275	V	R. Sabo	0.0002
RY Aur	56729.5780	6766	0.0195	V	G. Samolyk	0.0001
SX Aur	56603.7113	13587	0.0161	V	G. Samolyk	0.0001
TT Aur	56671.6781	26584	–0.0055	V	G. Samolyk	0.0001
WW Aur	56723.6470	9417	0.0017	V	G. Samolyk	0.0001
CL Aur	56566.7963	18965	0.1616	V	G. Samolyk	0.0001
EM Aur	56613.8259	14063	–1.1092	V	K. Menzies	0.0005
EP Aur	56567.8221	51198	0.0125	V	G. Samolyk	0.0002
TU Boo	56720.8736	72943.5	–0.1446	V	K. Menzies	0.0001
TU Boo	56795.6194	73174	–0.1469	V	K. Menzies	0.0001
TY Boo	56732.8551	70164	0.0789	V	K. Menzies	0.0001
TZ Boo	56720.7588	57503.5	0.0619	V	K. Menzies	0.0002
VW Boo	56738.8870	74682.5	–0.2282	V	K. Menzies	0.0001
AD Boo	56806.7206	14861	0.0334	V	G. Samolyk	0.0001
GU Boo	54888.5666	–98	0.0001	V	L. Corp	0.0001
GU Boo	56819.2847	3852.5	–0.0096	C	Y. Ogmen	0.0001
CD Cam	56603.8673	5026.5	–0.0034	V	G. Samolyk	0.0006
CD Cam	56924.8240	5446.5	–0.0041	V	G. Samolyk	0.0005
TX Cnc	56765.3567	48981	0.0452	R	L. Corp	0.0004
RT CMa	56633.8395	23195	–0.7490	V	G. Samolyk	0.0001
SX CMa	56610.9066	17556	0.0265	V	G. Samolyk	0.0002
YY CMi	56746.6502	26255	0.0160	V	G. Samolyk	0.0002

Table continued on following pages

Table 1. Recent times of minima of stars in the AAVSO eclipsing binary program, cont.

Star	*HJD 2400000+*	*Cycle*	*O–C (day)*	*F*	*Observer*	*Standard Error (day)*
AC CMi	56753.6495	5506	0.0040	V	G. Samolyk	0.0001
AK CMi	56679.7955	23994	–0.0211	V	R. Sabo	0.0001
AK CMi	56725.6321	24075	–0.0222	V	G. Samolyk	0.0001
AM CMi	56733.6375	30896	0.2138	V	G. Samolyk	0.0004
TV Cas	56681.5628	6664	–0.0277	V	K. Menzies	0.0004
ZZ Cas	56620.5781	18643	0.0092	V	G. Samolyk	0.0001
AB Cas	56924.6078	10396	0.1251	V	G. Samolyk	0.0001
CW Cas	56610.5878	46974.5	–0.0789	V	G. Samolyk	0.0002
CW Cas	56843.8317	47706	–0.0841	V	G. Samolyk	0.0001
CW Cas	56880.8195	47822	–0.0845	V	K. Menzies	0.0001
DZ Cas	56185.7831	35357	–0.1852	V	G. Samolyk	0.0006
IR Cas	56587.6647	20896	0.0086	V	R. Poklar	0.0001
IR Cas	56898.7389	21353	0.0096	V	G. Samolyk	0.0001
IS Cas	56842.8212	15241	0.0677	V	G. Samolyk	0.0003
IT Cas	56619.5649	7149	0.0658	V	G. Samolyk	0.0003
IT Cas	56872.8473	7214	0.0668	V	G. Samolyk	0.0003
IV Cas	56549.3033	15718	–0.1017	C	Y. Ogmen	0.0001
IV Cas	56872.8190	16042	–0.1080	V	G. Samolyk	0.0001
OR Cas	56566.5754	9919	–0.0270	V	G. Samolyk	0.0001
OR Cas	56927.8305	10209	–0.0282	V	G. Samolyk	0.0001
PV Cas	56634.5237	9373	–0.0347	V	G. Samolyk	0.0002
V364 Cas	56886.7561	14616	–0.0238	V	G. Samolyk	0.0002
V523 Cas	55460.3352	60935	0.0900	C	Y. Ogmen	0.0001
U Cep	56615.6221	4843	0.1900	V	G. Samolyk	0.0001
SU Cep	56894.6864	33913	0.0059	V	G. Samolyk	0.0001
WZ Cep	56872.6508	69068	–0.1415	V	G. Samolyk	0.0002
TW Cet	56602.6943	44908.5	–0.0273	V	R. Poklar	0.0002
TW Cet	56927.7833	45934.5	–0.0283	V	G. Samolyk	0.0001
TX Cet	56603.7190	18251	0.0093	V	R. Poklar	0.0002
RW Com	56725.8726	70376	0.0012	V	G. Samolyk	0.0003
RW Com	56738.6891	70430	0.0011	V	K. Menzies	0.0001
RW Com	56741.6539	70442.5	–0.0010	V	K. Menzies	0.0001
RZ Com	56725.7762	64661.5	0.0481	V	G. Samolyk	0.0001
CC Com	56664.0031	77623.5	–0.0214	V	R. Sabo	0.0001
CC Com	56695.8926	77768	–0.0210	V	K. Menzies	0.0001
RW CrB	56753.8457	22029	–0.0012	V	G. Samolyk	0.0001
TW CrB	56735.8844	31989	0.0493	V	K. Menzies	0.0001
W Crv	56746.8200	44060.5	0.0186	V	G. Samolyk	0.0002

Table continued on following pages

Table 1. Recent times of minima of stars in the AAVSO eclipsing binary program, cont.

Star	HJD 2400000+	Cycle	O–C (day)	F	Observer	Standard Error (day)
RV Crv	56723.8314	21003	–0.0885	V	G. Samolyk	0.0003
V Crt	56729.7961	21840	–0.0046	V	G. Samolyk	0.0002
AE Cyg	56831.9048	12635	–0.0042	V	R. Sabo	0.0001
CG Cyg	56842.7937	27597	0.0734	V	G. Samolyk	0.0001
KR Cyg	56924.5997	32915	0.0185	V	G. Samolyk	0.0003
V387 Cyg	56843.7085	45049	0.0203	V	G. Samolyk	0.0001
V388 Cyg	56843.7804	17334	–0.1077	V	G. Samolyk	0.0002
V447 Cyg	56511.3731	12360	0.0958	C	Y. Ogmen	0.0001
V447 Cyg	56532.3344	12369.5	0.1041	C	Y. Ogmen	0.0004
V704 Cyg	56929.6183	33275	0.0337	V	G. Samolyk	0.0002
TT Del	56894.7945	4062	–0.1099	V	G. Samolyk	0.0002
YY Del	56593.5700	17191	0.0100	V	G. Samolyk	0.0001
FZ Del	56923.6029	32685	–0.0299	V	G. Samolyk	0.0001
RZ Dra	56773.8958	22866	0.0600	V	G. Samolyk	0.0003
LQ Dra	56525.3710	209	0.0051	R	Y. Ogmen	0.0001
TZ Eri	56609.8162	5447	0.3155	V	G. Samolyk	0.0001
YY Eri	56589.9254	46682.5	0.1507	V	R. Sabo	0.0001
SX Gem	56610.7643	27493	–0.0551	V	G. Samolyk	0.0005
SX Gem	56610.7644	27493	–0.0550	V	K. Menzies	0.0002
SX Gem	56688.6777	27550	–0.0537	V	K. Menzies	0.0003
WW Gem	56737.7065	24845	0.0352	V	G. Samolyk	0.0003
AL Gem	56620.9214	21775	0.0789	V	G. Samolyk	0.0002
SZ Her	56843.6584	18310	–0.0263	V	G. Samolyk	0.0001
TT Her	56816.4453	18442	0.0417	V	L. Corp	0.0004
TU Her	56801.7769	5620	–0.2279	V	G. Samolyk	0.0001
LT Her	56823.3441	14822	–0.1421	V	Y. Ogmen	0.0001
V728 Her	56766.8327	9053	0.0028	V	G. Samolyk	0.0003
V728 Her	56767.7789	9055	0.0064	V	K. Menzies	0.0001
V1091 Her	56805.3057	11056.5	0.1113	C	Y. Ogmen	0.0001
AV Hya	56773.6097	29412	–0.1095	V	G. Samolyk	0.0002
DF Hya	56725.5929	42158.5	–0.0039	V	G. Samolyk	0.0001
DK Hya	56746.6452	26638	0.0036	V	G. Samolyk	0.0002
SW Lac	56573.6080	35228	–0.0956	V	G. Samolyk	0.0002
SW Lac	56924.6377	36322.5	–0.0949	V	G. Samolyk	0.0003
CO Lac	56567.6736	18826	0.0024	V	G. Samolyk	0.0001
CO Lac	56574.6043	18830.5	–0.0068	V	G. Samolyk	0.0002
XY Leo	56766.6154	41155	0.1169	V	G. Samolyk	0.0001
AP Leo	56725.4405	39941	–0.0144	R	L. Corp	0.0001

Table continued on following pages

Table 1. Recent times of minima of stars in the AAVSO eclipsing binary program, cont.

Star	*HJD 2400000+*	*Cycle*	*O–C (day)*	*F*	*Observer*	*Standard Error (day)*
CE Leo	56778.2805	38661	–0.0206	C	Y. Ogmen	0.0001
RR Lep	56651.7373	28702	–0.0392	V	R. Sabo	0.0002
RY Lyn	56733.6121	9649	–0.0301	V	G. Samolyk	0.0001
UZ Lyr	56754.8230	6908	–0.0303	V	K. Menzies	0.0004
V576 Lyr	56486.3197	735	0.0029	R	Y. Ogmen	0.0001
V582 Lyr	56470.3694	15514	–0.0047	C	Y. Ogmen	0.0001
Beta Lyr	56509.08	581	1.66	R	G. Samolyk	0.03
Beta Lyr	56509.10	581	1.68	B	G. Samolyk	0.02
Beta Lyr	56509.11	581	1.68	V	G. Samolyk	0.03
Beta Lyr	56515.53	581.5	1.64	B	G. Samolyk	0.03
Beta Lyr	56515.56	581.5	1.67	V	G. Samolyk	0.03
Beta Lyr	56515.61	581.5	1.72	R	G. Samolyk	0.04
RW Mon	56753.6389	12105	–0.0785	V	G. Samolyk	0.0001
BB Mon	56737.5960	41021	–0.0043	V	G. Samolyk	0.0001
V502 Oph	56854.4515	18426.5	–0.0030	V	L. Corp	0.0003
V502 Oph	56886.4168	18497	–0.0016	V	L. Corp	0.0003
V508 Oph	56801.8335	33989.5	–0.0216	V	G. Samolyk	0.0003
V1010 Oph	56843.7295	27072	–0.1677	V	G. Samolyk	0.0002
EF Ori	56604.8873	2627	0.0070	V	G. Samolyk	0.0004
EQ Ori	56609.8632	14416	–0.0375	V	G. Samolyk	0.0002
ER Ori	56579.9108	35317.5	0.1122	V	G. Samolyk	0.0001
ER Ori	56634.7423	35447	0.1136	V	G. Samolyk	0.0001
ER Ori	56695.5029	35590.5	0.1165	V	K. Menzies	0.0003
FF Ori	56694.6945	13520	0.0430	C	G. Frey	0.0001
FR Ori	56610.8880	32552	0.0340	V	G. Samolyk	0.0001
FZ Ori	56618.9885	31487.5	–0.0479	V	R. Sabo	0.0002
FZ Ori	56688.5870	31661.5	–0.0470	V	K. Menzies	0.0001
GU Ori	56592.9843	28731	–0.0545	V	R. Sabo	0.0001
GU Ori	56715.5940	28991.5	–0.0572	V	K. Menzies	0.0001
V648 Ori	56654.6683	18849	0.0630	C	G. Frey	0.0001
V648 Ori	56680.6934	18865	0.0646	C	G. Frey	0.0001
U Peg	56634.6557	53693	–0.1523	V	G. Samolyk	0.0001
U Peg	56886.5064	54365	–0.1548	R	L. Corp	0.0001
U Peg	56925.6710	54469.5	–0.1548	V	R. Sabo	0.0001
TY Peg	56620.6228	5229	–0.3796	V	G. Samolyk	0.0001
AT Peg	56906.4119	10197	0.0146	V	L. Corp	0.0004
BB Peg	56580.6570	35453	–0.0104	V	R. Poklar	0.0001
BB Peg	56593.6709	35489	–0.0105	V	G. Samolyk	0.0001

Table continued on following pages

Table 1. Recent times of minima of stars in the AAVSO eclipsing binary program, cont.

Star	HJD 2400000+	Cycle	O–C (day)	F	Observer	Standard Error (day)
BB Peg	56897.6910	36330	–0.0137	V	G. Samolyk	0.0001
BG Peg	56906.8988	5826	–2.1659	V	R. Sabo	0.0002
BX Peg	56619.5935	44306	–0.1076	V	R. Sabo	0.0001
DI Peg	56219.6785	15486	–0.0044	C	G. Frey	0.0001
DI Peg	56229.6439	15500	–0.0045	C	G. Frey	0.0001
DI Peg	56231.7796	15503	–0.0043	C	G. Frey	0.0001
DI Peg	56256.6934	15538	–0.0041	C	G. Frey	0.0001
DI Peg	56557.7946	15961	–0.0013	C	G. Frey	0.0001
DI Peg	56567.7599	15975	–0.0014	C	G. Frey	0.0001
DI Peg	56572.7430	15982	–0.0011	C	G. Frey	0.0001
DI Peg	56577.7255	15989	–0.0013	C	G. Frey	0.0001
DI Peg	56587.6911	16003	–0.0011	C	G. Frey	0.0001
DI Peg	56597.6568	16017	–0.0009	C	G. Frey	0.0001
DI Peg	56602.6394	16024	–0.0010	C	G. Frey	0.0001
V351 Peg	56615.6050	13679	0.0058	C	G. Frey	0.0003
Z Per	56655.5709	3598	–0.2652	V	G. Samolyk	0.0002
RT Per	56610.6411	27354	0.0864	V	N. Simmons	0.0001
RV Per	56573.7908	7361	–0.0019	V	G. Samolyk	0.0002
ST Per	56655.6185	5369	0.3073	V	G. Samolyk	0.0001
IT Per	56609.6175	17752	–0.0285	V	G. Samolyk	0.0004
IU Per	56566.7931	12783	0.0052	V	G. Samolyk	0.0003
IU Per	56681.6349	12917	0.0057	V	K. Menzies	0.0001
V432 Per	56591.6694	64436	0.0240	V	R. Poklar	0.0002
V432 Per	56615.6254	64510.5	0.0270	V	G. Samolyk	0.0002
Y Psc	56574.7805	2905	–0.0136	V	G. Samolyk	0.0001
RV Psc	56663.6112	58272	–0.0586	V	R. Sabo	0.0001
UZ Pup	56725.6319	15238	–0.0090	V	G. Samolyk	0.0001
AV Pup	56737.6404	45942	0.1877	V	G. Samolyk	0.0001
U Sge	56923.6827	11771	0.0012	V	G. Samolyk	0.0001
V1968 Sgr	56887.7883	33852	–0.0163	V	G. Samolyk	0.0003
CC Ser	56800.3306	37437	1.0365	V	Y. Ogmen	0.0001
RW Tau	56634.6893	3955	–0.2595	V	G. Samolyk	0.0001
RZ Tau	56591.9160	45505	0.0718	V	R. Sabo	0.0001
WY Tau	56620.8219	27742	0.0604	V	G. Samolyk	0.0002
AQ Tau	56594.8847	22156	0.5417	V	K. Menzies	0.0002
CT Tau	56613.7159	16810	–0.0604	V	K. Menzies	0.0001
EQ Tau	56590.8546	47979	–0.0291	V	R. Sabo	0.0001
EQ Tau	56619.8684	48064	–0.0299	V	G. Samolyk	0.0001

Table continued on next page

Table 1. Recent times of minima of stars in the AAVSO eclipsing binary program, cont.

Star	*HJD 2400000+*	*Cycle*	*O–C (day)*	*F*	*Observer*	*Standard Error (day)*
V1121 Tau	56685.7383	9931	–0.0105	C	G. Frey	0.0002
V1223 Tau	56649.6955	9811	0.0010	C	G. Frey	0.0002
V1223 Tau	56653.7121	9820	–0.0047	C	G. Frey	0.0002
V1223 Tau	56662.6506	9840	–0.0045	C	G. Frey	0.0002
V1234 Tau	56656.7027	11209	–0.0077	C	G. Frey	0.0002
V1234 Tau	56657.6748	11211.5	–0.0056	C	G. Frey	0.0003
V1234 Tau	56663.6883	11227	–0.0051	C	G. Frey	0.0002
X Tri	56929.9326	14850	–0.0861	V	G. Samolyk	0.0001
RS Tri	56567.7158	9758	–0.0487	V	R. Poklar	0.0001
RS Tri	56634.5274	9793	–0.0495	V	G. Samolyk	0.0002
RV Tri	56593.6441	14012	–0.0386	V	R. Poklar	0.0001
TY UMa	56766.6086	48609	0.3453	V	G. Samolyk	0.0002
UX UMa	56395.2749	96417	–0.0003	C	Y. Ogmen	0.0001
UX UMa	56750.8559	98225	–0.0010	V	K. Menzies	0.0001
UX UMa	56792.3527	98436	–0.0018	C	Y. Ogmen	0.0001
UX UMa	56794.3190	98446	–0.0022	C	Y. Ogmen	0.0001
VV UMa	56766.6178	15932	–0.0569	V	G. Samolyk	0.0001
BS UMa	56409.2698	8944.5	0.0325	C	Y. Ogmen	0.0001
RU UMi	56725.7450	28822	–0.0139	V	G. Samolyk	0.0001
AH Vir	56737.8410	26804	0.2631	V	G. Samolyk	0.0001
AK Vir	56801.6800	11918	–0.0302	V	G. Samolyk	0.0002
AW Vir	56773.7785	33195.5	0.0277	V	G. Samolyk	0.0001
AZ Vir	56753.8036	36541.5	–0.0240	V	G. Samolyk	0.0002
MS Vir	56725.8947	13525.5	–0.0042	V	G. Samolyk	0.0004
BE Vul	56575.5521	10608	0.0883	V	G. Samolyk	0.0003
BS Vul	56613.5046	28031	–0.0297	V	K. Menzies	0.0001
BS Vul	56927.6448	28691	–0.0306	V	G. Samolyk	0.0002
BU Vul	56929.5523	41118	0.0151	V	G. Samolyk	0.0002

The Challenge of Observing the ζ Aurigae Binary Stars

Frank J. Melillo
Holtsville Observatory, 14 Glen-Hollow Dr, E-16, Holtsville, NY 11742; Frankj12@aol.com

Received March 31, 2014; revised May 12, 2014 and June 12, 2014; accepted June 12, 2014

Abstract Observations of the ζ Aurigae binary stars ζ Aur, 31 Cyg, and 32 Cyg were made in V and B during their most recent eclipses. All three stars were measured photometrically mainly in the blue light that traces the hot companion star being eclipsed. The light curves of all three stars show precise timing during the entire recent eclipses. The magnitude and the duration of the eclipses in V and B are described here and predictions are made for the future.

1. Objective

The purpose of monitoring the ζ Aur stars ζ Aur, 31 Cyg, and 32 Cyg was to detect entire eclipses in both (Visual) and (Blue), determining both brightness and amplitude. Each of the three star systems consists of a supergiant class K star and a small hot class B star which revolve around one another, causing the light to be eclipsed as seen from Earth. When the B star was near the limb of the supergiant K star, the atmosphere of the K star was monitored. Information was obtained to measure the intensity of the K star's atmosphere when the B star shone through it (an atmospheric eclipse).

More information was monitored during the partial phases, especially in B light when the B star went behind the K star's limb during totality. How long the B star stayed behind the K star determined the length of the total eclipse. According to Stencel (2013), K supergiants are typically five magnitudes brighter than B stars. Therefore, the magnitudes are mentioned together in the text.

2. Method

Photoelectric photometry was used to monitor the eclipses of ζ Aur, 31 Cyg, and 32 Cyg in V and B. The Johnson filters have a peak spectral response at 4500 Å (blue) and 5400 Å (Visual), respectively.

The readings were taken using an SSP3 OPTEC photometer coupled on a 10-inch f/10 MEADE telescope. For each set of observations on each variable, four readings were taken at 10-second intervals of the variable, sky, and then the comparison stars. This author sometimes monitored three to four sets, depending on the weather conditions and time. To reduce the data, the photometric readings of the variable, sky, and comparison stars were

averaged. Then, the sky was subtracted from the star's readings. That left the ratio brightness between the variable and the comparison stars. Once the ratio was calculated, the variable's brightness could be determined using the known magnitude of the comparison stars. Also, the standard deviation (SD) was calculated to analyze how much error was in the readings. Most of the time, the error ranged from 0.012 magnitude to as much as 0.043 when all the readings were calculated. The altitude was also calculated to determine the air mass during the time of the observations. During the observing run, the higher the stars and the smaller the airmass, the better the chance of getting the accurate readings from the photometer. However, the airmass and extinction corrections were not applied to the reported magnitudes. The measurements are raw photometry, uncorrected for differential extinction between variable and comparison star and not transformed to the Johnson system, which limits their accuracy and application (Table 1).

Many factors that can affect the readings must also be considered: seeing conditions, winds, periodic clock drive error, polar alignment, and the stability of the photometer. During most nights, the seeing conditions were above average with no winds, and the periodic clock drive error was noticeable at times. Being that a portable observatory was used, the polar axis was aligned as close as possible to the celestial north pole. Therefore, in spite of the small drift, the star still stayed inside the reticle circle during the observation. For the SSP-3 OPTEC photometer itself, the unit was turned on at least an hour before the start of the first counts. This warm-up routine continued until the photometer dark count was stable enough for accurate readings; the colder the outside air temperature was, the more time the photometer needed to warm up. The unit was running on a nine-volt battery to avoid a power cord tangle-up during the night's run. In the photoelectric photometry method, the precision can be as little as 0.01 magnitude. The observations were accurate enough to generate the true shape of the light curve.

3. The ζ Aur stars

3.1. ζ Aur

ζ Aur is a supergiant K4II star orbited by a hot B7V star and has a combined magnitude of +3.75 (Hopkins 2013). The prototype of its class, ζ Aur is one of the "Three Kids" stars located near α Aur (Capella). Spectroscopically, it is seen as two stars (supergiant K and small hot B) that eclipse one another.

Every 2.66 years or 972 days, the smaller B star is completely eclipsed by the larger K supergiant. While the stars are of different sizes, only the K star that passes in front of the hot B star can be detected. The B star is approximately magnitude 8, so it dominates the light in the B wavelengths (Stencel 2013). Jeffrey Hopkins (2013) predicted the total eclipse from October 31, 2011, to December 9, 2011, based on his measurements from the 1982, 1985, and

Table 1. Differential photometry of ζ Aur.

		λ Aur +4.71 V comparison star		λ Aur +5.34 B comparison star		
		V filter		B filter		
UT Date	JD 2450000+	Magnitude	Standard Deviation	Magnitude	Standard Deviation	B–V
9/3/2011	5807.77	3.72	0.05050	4.87	0.02760	1.15
9/13/2011	5817.72	3.70	0.03381	4.85	0.05600	1.15
9/19/2011	5823.71	3.72	0.02134	—	—	—
9/30/2011	5834.70	3.75	0.03024	4.88	0.01885	1.13
10/8/2011	5842.76	3.77	0.02204	4.97	0.01165	1.20
10/16/2011	5850.71	3.76	0.01126	4.92	0.01581	1.16
10/22/2011	5856.73	3.77	0.01642	4.94	0.01676	1.17
10/24/2011	5858.71	3.78	0.02375	4.94	0.02387	1.16
10/31/2011	5864.68	3.79	0.02387	5.01	0.01371	1.22
11/2/2011	5867.67	3.94	0.03450	5.39	0.01706	1.45
11/3/2011	5868.71	3.95	0.01246	5.38	0.01389	1.43
11/6/2011	5871.76	3.95	0.01408	5.41	0.01188	1.46
11/13/2011	5878.77	3.91	0.01773	5.44	0.01669	1.53
11/19/2011	5884.71	3.94	0.02605	5.41	0.01414	1.47
11/25/2011	5890.70	3.96	0.02828	5.43	0.01753	1.47
12/2/2011	5897.72	3.94	0.00926	5.42	0.00518	1.48
12/11/2011	5906.73	3.80	0.01963	4.96	0.01587	1.16
12/12/2011	5907.71	3.81	0.01874	4.96	0.01879	1.15
12/25/2011	5920.76	3.80	0.02147	4.96	0.01985	1.16
1/1/2012	5927.73	3.79	0.02014	4.98	0.01978	1.19

2009 eclipses. λ Aur was the comparison star (+4.71 V, +5.34 B). Also, the partial eclipse is known to be very steep. During the partial phases, Contacts I and II and Contacts III and IV may each be a little as one-and-a-half days apart.

The eclipse of ζ Aur was successfully observed during 2011. Twenty nights were monitored in V and nineteen in B (Table 1). Observations started on September 3, 2011 (JD 2455807.77) to establish the light curve baseline. Hopkins calculated the first contact to begin October 29, 2011, and November 19, 2011, time of mid-eclipse. Unfortunately, the author was clouded out for the first contact prediction. Observations on October 31, 2011, at 4:30 UT showed no change in brightness in V. But in B, the brightness may have dipped slightly. On November 2, 2011, at 4:30 UT, it seemed that the eclipse was already in total. Both Contacts I and II were missed due to the weather, but the partial may have lasted less than two days. Totality was predicted to last for thirty-seven days (until December 9, 2011, JD 2455904), but observations showed the eclipse was already over on December 11 at 5:20 UT (JD 2455906.73). Contacts III and IV during egress were also missed because of the cloudy weather. ζ Aur

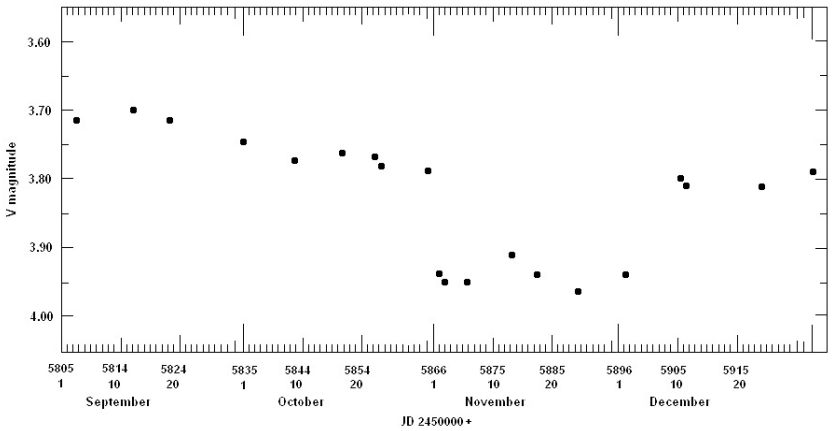

Figure 1. Light curve of ζ Aur, September 1, 2011–December 31, 2011. ζ Aur V magnitude with respect to λ Aur +4.71 magnitude.

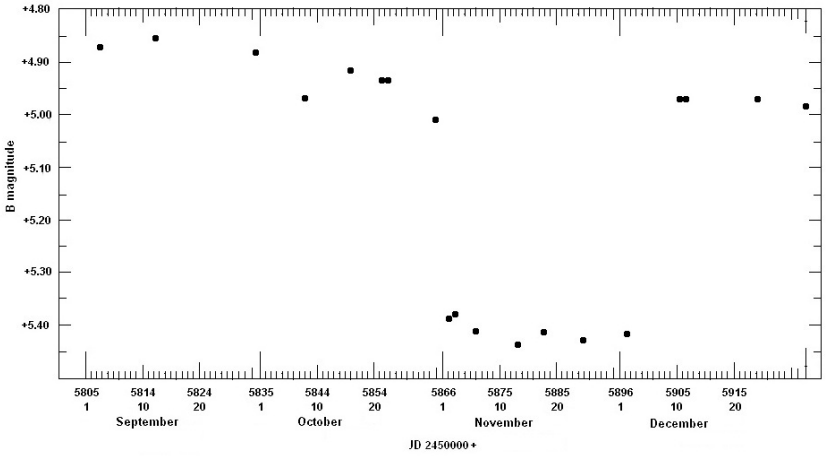

Figure 2. Light curve of ζ Aur, September 1, 2011–December 31, 2011. ζ Aur B magnitude with respect to λ Aur +5.34 magnitude.

was monitored until January 1, 2012 (JD 2455927.73), to make sure the eclipse was truly over. During the eclipse, the brightness dipped about 0.20 magnitude in V and about 0.45 magnitude in B (Figures 1 and 2).

3.2. 32 Cyg

32 Cyg is a supergiant class K3 with a small hot class B3 star and a total magnitude of +4.03 (Hopkins 2013). This binary system was recognized to be one of the ζ Aur group. The eclipse occurs every 1,147.6 days (3.15 years). Every 3.15 years, the smaller B star is partially eclipsed by the larger K star.

The eclipse was predicted to occur between August 26, 2012, and September 11, 2012. The comparison star was 30 Cyg (+4.83 V, +4.92 B). The partial eclipse is known to be very shallow and partial phases may last five to six days.

The eclipse was successfully monitored in V and B on 22 nights (Table 2). The brightness dipped a mere 0.03 magnitude in V and about 0.12 magnitude in B, where the eclipse was clearly evident. Observations were started on August 7, 2012 (JD 2456146.66), to establish a baseline for the light curve. The partial phase began before August 27, 2012 (JD 2456166.54). A total eclipse may have started before September 1, 2012 (JD 2456167.73). The light curve showed that the partial phase between Contacts I and II lasted for six days. Totality may have been over on September 12, 2012 (JD 2456182.67); it is not clear how long totality lasted. Totality may have been very brief during the first half and perhaps was grazing during the second half. Also, Contacts III and IV

Table 2. Differential photometry of 32 Cyg.

		32 Cyg +4.83 V comparison star		*32 Cyg +4.92 B comparison star*		
		V filter		*B filter*		
UT Date	*JD 2450000+*	*Magnitude*	*Standard Deviation*	*Magnitude*	*Standard Deviation*	*B–V*
8/7/2012	6146.66	4.04	0.011	5.33	0.013	1.29
8/13/2012	6152.66	4.01	0.024	5.32	0.017	1.31
8/17/2012	6162.76	4.02	0.011	5.34	0.014	1.32
8/23/2012	6162.73	4.04	0.017	5.33	0.007	1.29
8/24/2012	6163.71	4.04	0.029	5.33	0.010	1.29
8/27/2012	6166.54	4.05	0.019	5.36	0.018	1.31
8/29/2012	6168.67	4.06	0.019	5.41	0.024	1.35
8/30/2012	6169.70	4.05	0.024	5.44	0.025	1.39
8/31/2012	6170.71	4.05	0.033	5.46	0.010	1.41
9/1/2012	6171.73	4.03	0.012	5.40	0.018	1.37
9/3/2012	6173.66	4.05	0.024	5.32	0.019	1.27
9/6/2012	6176.69	4.07	0.016	5.36	0.011	1.29
9/7/2012	6177.73	4.03	0.009	5.34	0.022	1.31
9/8/2012	6178.76	4.03	0.033	5.38	0.030	1.35
9/10/2012	6180.65	4.02	0.028	5.33	0.009	1.31
9/11/2012	6181.71	4.05	0.028	5.35	0.021	1.30
9/12/2012	6182.67	4.05	0.028	5.32	0.013	1.27
9/13/2012	6183.66	4.01	0.015	5.32	0.019	1.31
9/14/2012	6184.70	4.03	0.025	5.32	0.014	1.29
9/17/2012	6187.73	4.03	0.012	5.32	0.015	1.29
9/20/2012	6190.66	4.03	0.011	5.33	0.011	1.30
9/24/2012	6193.69	4.05	0.019	5.34	0.019	1.29

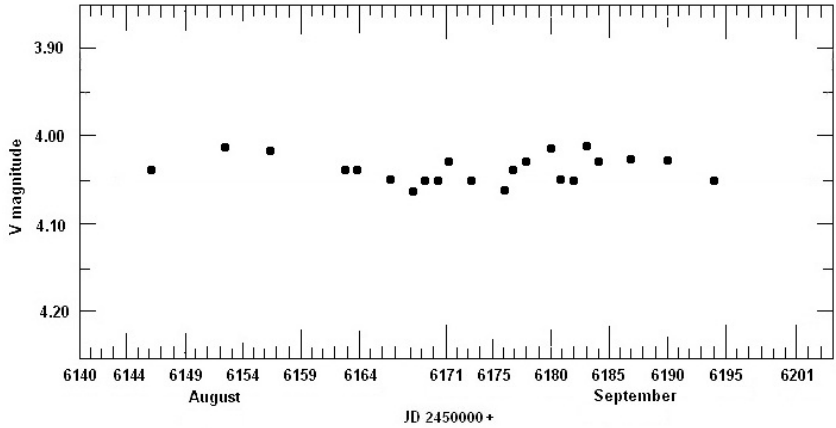

Figure 3. Light curve of 32 Cyg, August 1, 2011–September 18, 2011. 32 Cyg V magnitude with respect to 30 Cyg +4.83 V magnitude.

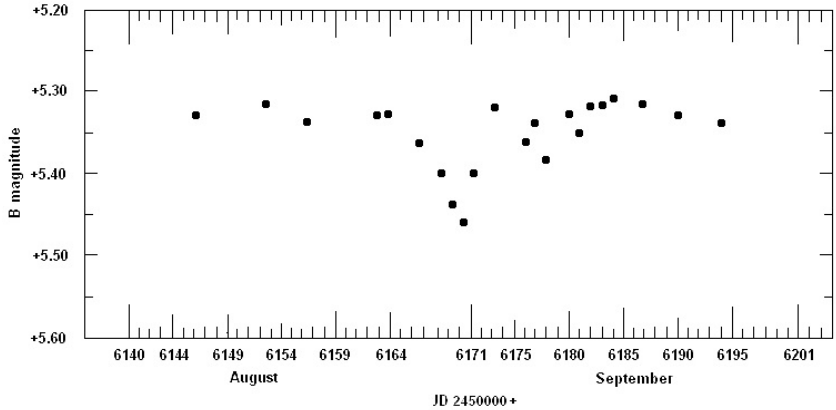

Figure 4. Light curve of 32 Cyg, August 1, 2011–September 18, 2011. 32 Cyg B magnitude with respect to 30 Cyg +4.92 B magnitude.

weren't clear. In addition to a possible grazing eclipse, 32 Cyg may have had an extended atmosphere on one side during the second half of totality. The much larger eclipse amplitude in B (Figures 3 and 4) occurred because the B3 star contributes more of the B light to the system, while the K3 star contributes more of the V light.

3.3. 31 Cyg

31 Cyg is a supergiant class K2 with a small hot class B3 star and has a total magnitude of +3.79. This binary system is also recognized to be one of the ζ Aur star group. The eclipse occurs every 3,784.3 days (10.4 years), making 31 Cyg one of the longest periodic eclipsing binaries. While it is a 10.4 year eclipse,

the author took every opportunity to monitor this star. The eclipse was predicted to begin on October 8, 2013 (JD 2456573), and last nearly 62 days (Stencil 2013) through December 11, 2013 (JD 2456637). The comparison star was 30 Cyg (+4.83 V, +4.92 B). The partial eclipse is known to be very steep and it can be as little as two days between Contacts I and II and Contacts III and IV.

31 Cyg was monitored nineteen nights in V and B (Table 3). The observations started about five weeks before the ingress-predicted date, so the baseline of the light curve could be established. The light curves in both V and B showed normal brightness during the atmospheric eclipse. The last observation before ingress was made on October 3, 2013 (JD 2456568.63). The next observation, on October 14, 2013 (JD 2456579.63), shows the B star already in totality with the supergiant K star. Therefore Contacts I and II were missed due to the cloudy weather. The total eclipse was observed until the predicted date for egress on December 11, 2013 (JD 2456637). Luckily, the egress (Contacts III and IV) was caught. In fact, note that the last six readings, including the time of egress, were made at the same time. Measurements were made right at the start of darkness due to 31 Cyg's low altitude in the NW.

The system was observed for two more weeks to be sure that the eclipse was over.

Stencel *et al.* (1984) carried out a full coverage of the 1982 eclipse. Their photometric study enabled prediction of the 2013 timetable of the eclipse. Throughout the eclipse, the V light curve showed a dip of 0.12 magnitude. The B light curve showed a deeper eclipse of 0.32 magnitude. It was obvious that the B star was being eclipsed and just the supergiant K star was shining alone. The light curves in V and B are a little different from each other during egress, which was caught. It took one day after totality ended for V to return to pre-eclipse brightness, while B took two to three days. The most reasonable explanation for this phenomenon is the fuzziness of the supergiant K star. The K star atmosphere is more opaque at shorter wavelengths, causing the B magnitude to fade and recover more slowly than the V. In V, the supergiant K star's limb is much sharper, with the B star shinning with less contrast (Figures 5 and 6).

4. Discussion

All three ζ Aur binary stars (ζ Aur itself, and 31 and 32 Cyg) were monitored photoelectrically in B and V from Holtsville, Long Island, New York. The eclipses were observed successfully and the results are comparable with eclipses of the past.

More observations are needed for 32 Cyg. It is not clear whether the eclipse was total, grazing, or a combination of both (Griffin 2013). During 2012, the eclipse was seen but totality may have been very brief at the start, followed by sporadic brightness or surges during the second half. Once it reached the pre-

Table 3. Differential photometry of 31 Cyg.

		31 Cyg +4.83 V comparison star		*31 Cyg +4.92 B comparison star*		
		V filter		*B filter*		
UT Date	*JD 2450000+*	*Magnitude*	*Standard Deviation*	*Magnitude*	*Standard Deviation*	*B–V*
09/05/2013	6540.63	3.80	0.010	4.86	0.016	1.06
09/07/2013	6542.62	3.80	0.019	4.89	0.008	1.09
09/09/2013	6544.71	3.80	0.025	4.89	0.011	1.09
09/15/2013	6550.71	3.82	0.008	4.88	0.014	1.06
09/20/2013	6555.72	3.79	0.013	4.89	0.018	1.10
09/26/2013	6561.64	3.80	0.013	4.88	0.008	1.08
09/29/2013	6564.74	3.76	0.021	4.86	0.029	1.10
10/03/2013	6568.63	3.81	0.018	4.88	0.011	1.07
10/14/2013	6579.63	3.91	0.011	5.21	0.005	1.30
10/21/2013	6586.62	3.91	0.006	5.20	0.013	1.29
10/28/2013	6593.70	3.90	0.008	5.22	0.009	1.32
11/09/2013	6605.52	3.91	0.005	5.22	0.013	1.31
11/20/2013	6616.54	3.90	0.013	5.20	0.011	1.30
11/30/2013	6626.50	3.90	0.016	5.21	0.011	1.31
12/11/2013	6637.50	3.93	0.011	5.19	0.009	1.26
12/12/2013	6638.50	3.79	0.018	5.00	0.019	1.21
12/13/2013	6639.50	3.82	0.013	4.92	0.011	1.10
12/17/2013	6643.50	3.82	0.013	4.87	0.018	1.05
12/28/2013	6654.50	3.79	0.008	4.87	0.017	1.08

eclipse brightness after the eclipse ended, its behavior was normal. It seemed to last 11 days. The fluctuation was not seen well in V band but perhaps only in partial. It was much more pronounced in B band where the eclipse was just total and the chromophere of the K star extended farther out. Unfortunately, there were no check stars to further analyze the data to see whether or not the scattering in the light curve was real during the second half of totality. As far as the author can tell, the conditions appeared to be stable.

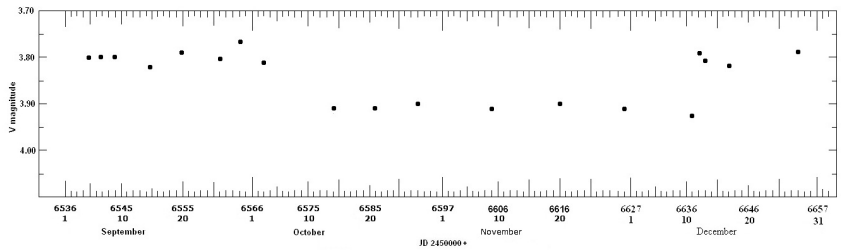

Figure 5. Light curve of 31 Cyg, September 1, 2011–December 31, 2011. 31 Cyg V magnitude with respect to 30 Cyg +4.83 V magnitude.

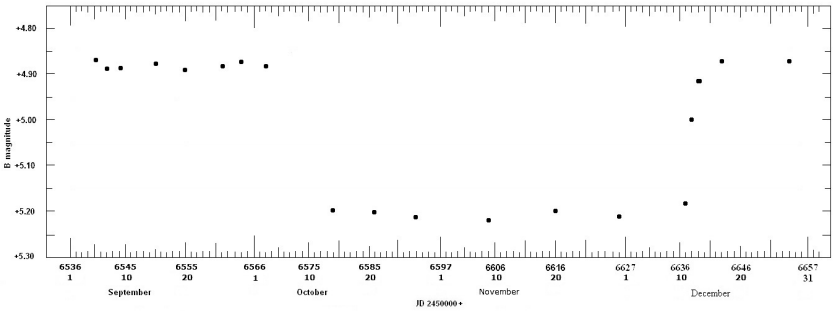

Figure 6. Light curve of 31 Cyg, September 1, 2011–December 31, 2011. 31 Cyg B magnitude with respect to 30 Cyg +4.92 B magnitude.

The next eclipse of 32 Cyg is scheduled for October 18, 2015 (JD 2457314), at mid-eclipse after 1,147 days, or 3.15 years, assuming the predicted date (Hopkins 2013) of September 6, 2012 (JD 2456167) was correct. Anyone who might be interested to observe the next 32 Cygni eclipse should contact the author for a possible observing campaign. Photometric observations are needed. Hopefully, the contact points and the totality/grazing observations eclipse can be solved.

For ζ Aur and 31 Cyg, the light curves may show the eclipse lasting a day or two longer in B than in V. This might be due to the extended atmosphere of the supergiant K star and the result of more absorption involved near the supergiant's limb. But the ingress and egress must be caught to further analyze the contact points.

References

Griffin, E. 2013, private communication.

Hopkins, J. L. 2013, private communication.

Stencel, R. E. 2013, private communication.

Stencel, R. E., Hopkins, J. L., Hagen, W., Fried, R., Schmidtke, P. C., Kondo, Y., and Chapman, R. D. 1984, *Astrophys. J.*, **281**, 751.

Sloan Magnitudes for the Brightest Stars

Anthony Mallama
14012 Lancaster Lane, Bowie, MD 20715; anthony.mallama@gmail.com

Received April 8, 2014; revised June 23, 2014; accepted July 8, 2014

Abstract Sloan magnitudes are reported for 3,969 stars brighter than r' ~ 7. The data are based upon Johnson-Cousins photometry which has been transformed to the Sloan system. Cousins $V–R_C$ and $R_C–I_C$ color indices are also provided as a by-product.

1. Introduction

The Sloan magnitude system is enjoying widespread acceptance in the astronomical community. Besides the Digital Sky Survey which bears its name, the Hubble Space Telescope, Pan-STARRS, and the Large Synoptic Survey Telescope programs are using it. The Sloan survey photometric system has five primary bands, u, g, r, i, and z, which span wavelengths from about 300 nm to one micron. When magnitudes are designated with primes, u', g', r', i', and z', they refer to other telescopes using the Smith *et al.* (2002) u'g'r'i'z' standard-star system, whose pass-bands differ slightly from those of the Sloan survey.

One reason for the popularity of the Sloan system is that these bands are more cleanly separated from one another than in older systems such as UBVRI. Another is that the magnitudes are directly related to absolute fluxes. APASS, the all-sky survey conducted by The American Association of Variable Star Observers (AAVSO 2013), has catalogued the magnitudes of 50 million stars in the range ~7.5 < V < ~17 based on photometry with the Johnson *et al.* (1966) B and V filters and the Sloan g', r', and i' filters. These bands extend from about 400 to 850 nm. An important aspect of the APASS system is that it relates and provides photometry from two heavily used photometric systems. The accuracy is a few hundredths of a magnitude near V = 10 and degrades to ~ 0.1 magnitude at V = 16.5. The magnitudes of stars brighter than V = 10 are systematically too faint because of detector saturation.

The present study provides Sloan magnitudes for the brightest stars. These results are similar in quality to APASS data and they cover a broader range of wavelengths. The magnitudes are derived from Johnson's UBVRI photometry in a two-step process. First, the Johnson magnitudes and color indices were transformed to the Cousins (1976a, 1976b) system. Then, Cousins values were transformed to Sloan magnitudes.

2. Transformation methods

The U, B, and V magnitudes of Johnson *et al.* (1966) and of Cousins (1976a, 1976b) are equivalent, but the R and I bands differ. Taylor (1986) lists four separate equations for transforming the Johnson V–R color index to Cousins $V–R_C$ and four other equations for R–I to $R_C–I_C$. Each equation pertains to specific stellar luminosity classes and a range of color indices. Every coefficient is accompanied by an uncertainty value so that the probable error of the color index can be computed. When more than one equation was applicable to a given star, the color index with the least probable error was adopted. More details of the Johnson-to-Cousins transformation are given in Appendix A.

Two independently derived sets of equations were used to transform between Cousins and Sloan u', g', r', i', and z' magnitudes. Fukugita *et al.* (1996) developed theoretical transformations to the Sloan magnitudes of the 20-inch photometric telescope collocated with the 2.5-m Sloan survey telescope. Smith *et al.* (2002) established a system of 158 standard stars with the 1.0-m telescope at the USNO Flagstaff Station and derived transformations based on actual photometry. More details of the Cousins to Sloan transformations can be found in Appendix B.

3. Sloan magnitude results

The Sloan magnitudes listed in Table 1 are averages based on the transformation equations of Smith *et al.* (2002) and of Fukugita *et al.* (1996). Each value is accompanied by its estimated uncertainty in units of 0.01 magnitude. These estimates are equal to the square roots of the sums of the squares of three components of uncertainties: that of the photometry of Johnson *et al.* (1966), Taylor's (1986) estimates of his transformation errors, and the standard deviation of the mean of each Smith/Fukugita average.

The mean uncertainty for the g', r', i', and z' bands is 0.03 magnitude while that for u' is 0.08 Thus the entries in this catalogue may be used as reference stars for bright objects where moderate accuracy is sufficient. In applications where higher accuracy is required (for example, color transformation) the primary standard stars should be used instead. In these respects, the data are similar to APASS.

The first 1,029 stars are accompanied by magnitudes for all five Sloan bands as well as Cousins $V–R_C$ and $R_C–I_c$ color indices. The remaining 2,940 stars list fewer than five Sloan magnitudes and no Cousins color indices because the Johnson data were incomplete. The absent magnitudes are indicated with the entry "99.99." A portion of Table 1 is included in the paper. The full table is available through the AAVSO ftp site at ftp:ftp.aavso.org/public/datasets/amalaj422.txt; is also available from the author and it will be made available through Vizier.

Table 1. Johnson, Cousins, and Sloan magnitudes for the brightest non-variable stars. This is an abbreviated version of the full table which contains data records for 3,969 stars. The full table is available through the AAVSO ftp site at ftp:ftp.aavso.org/public/datasets/amalaj422.txt.

	Johnson					Cousins		Sloan									
HD	*V*	*U–B*	*B–V*	*V–R*	*R–I*	$V–R_C$	$R_C–I_C$	*u′*		*g′*		*r′*		*i′*		*z′*	
496	3.88	0.84	1.03	0.75	0.52	0.52	0.47	6.62	5	4.35	4	3.55	4	3.30	3	3.18	3
571	5.04	0.26	0.40	0.42	0.29	0.27	0.28	6.65	9	5.17	3	4.96	2	4.91	2	4.90	3
1013	4.80	1.93	1.57	1.34	1.13	0.90	1.05	9.31	14	5.57	5	4.19	5	3.37	3	2.88	3
1280	4.61	0.05	0.06	0.08	0.01	0.03	0.03	5.75	13	4.55	3	4.71	2	4.90	2	5.05	3
1404	4.52	0.07	0.05	0.08	0.00	0.03	0.01	5.68	14	4.45	3	4.62	2	4.83	2	4.99	3
1522	3.55	1.17	1.22	0.85	0.59	0.59	0.52	6.84	7	4.13	4	3.15	5	2.85	3	2.69	3
1581	4.23	0.02	0.58	0.49	0.34	0.32	0.33	5.61	4	4.45	3	4.09	2	3.97	2	3.93	2
2151	2.80	0.11	0.62	0.50	0.34	0.33	0.34	4.33	3	3.05	3	2.64	2	2.53	2	2.49	2
2261	2.40	0.88	1.09	0.81	0.59	0.56	0.52	5.23	4	2.90	4	2.04	4	1.74	3	1.58	3
2262	3.94	0.10	0.17	0.14	0.08	0.07	0.09	5.20	11	3.94	3	3.99	2	4.12	2	4.24	3
2772	4.73	–0.36	–0.10	0.00	–0.12	–0.02	–0.07	5.22	8	4.58	2	4.88	3	5.18	3	5.39	3
3360	3.66	–0.89	–0.19	–0.08	–0.21	–0.08	–0.13	3.38	4	3.46	2	3.86	3	4.21	3	4.46	4
3369	4.36	–0.55	–0.16	–0.04	–0.12	–0.05	–0.07	4.56	6	4.18	2	4.54	3	4.83	3	5.04	4
3546	4.38	0.47	0.87	0.68	0.51	0.47	0.46	6.53	3	4.76	4	4.11	3	3.87	2	3.75	2
3627	3.28	1.48	1.28	0.92	0.66	0.64	0.60	7.02	12	3.89	4	2.84	5	2.47	3	2.26	3
3651	5.86	0.58	0.85	0.65	0.39	0.44	0.37	8.15	4	6.23	4	5.60	3	5.46	2	5.39	2
3817	5.33	0.60	0.89	0.71	0.46	0.49	0.42	7.67	4	5.72	4	5.04	3	4.84	2	4.75	2
3901	4.81	–0.66	–0.10	–0.01	–0.12	–0.03	–0.06	4.90	3	4.66	2	4.97	3	5.25	3	5.46	3
3919	4.59	0.72	0.97	0.75	0.52	0.52	0.47	7.13	4	5.03	4	4.27	3	4.03	2	3.90	2
4128	2.02	0.88	1.01	0.72	0.51	0.50	0.46	4.80	6	2.48	4	1.70	4	1.47	3	1.34	3

4. Summary

A catalogue of Sloan magnitudes for 3,969 stars brighter than r ~7 is presented. The data are based upon Johnson-Cousins UBVRI photometry which has been transformed to the Sloan system. Equations developed by Taylor (1986) were used to transform from the Johnson V–R and R–I color indices to Cousins V–R_C and R_C–I_C and these are reported for 1,029 of the stars. Two independently derived sets of equations (Fukugita *et al.* 1996, and Smith *et al.* 2002) were used to transform from Cousins magnitudes to Sloan u', g', r', i', and z'. The Sloan magnitude results are accurate to a several hundredths of a magnitude and they complement those of the APASS catalogue. Sloan data in the magnitude range 7 to 10 are still needed to fill the gap between the faint limit of this catalogue and the bright limit of APASS.

5. Acknowledgements

Brian Skiff (Lowell Observatory) suggested the transformation method used in this study and provided other helpful information. Comments from two anonymous referees led to improvements in the paper. Thanks are also due to Bruce Krobusek (CVAS) for participating in this project and to Ronald Baker (CVAS) for reviewing an early draft of the manuscript.

References

AAVSO. 2013, APASS: The AAVSO Photometric All-Sky Survey (http://www.aavso.org/apass).

Cousins, A. W. J. 1976a, *Mem. Roy. Astron. Soc.*, **81**, 25.

Cousins, A. W. J. 1976b, *Mon. Notes Astron. Soc. Southern Africa*, **35**,70.

Fukugita, M., Ichikawa, T., Gunn, J. E., Doi, M., Shimasuka, K., and Schneider, D. P. 1996, *Astron. J.*, **111**, 1748.

Johnson, H. L., Mitchell, R. I., Iriarte, B., and Wisniewski, W. Z. 1966, *Commun. Lunar Planet. Lab.*, **4**, 99.

Smith, J. A., *et al.* 2002, *Astron. J.*, **123**, 2121.

Taylor, B. J. 1986, *Astrophys. J., Suppl. Ser.*, **60**, 577.

Appendix A: Johnson to Cousins transformation equations

Taylor (1986) derived four separate equations for transforming the Johnson *et al.* (1996) R–I color index to Cousins (1976a, 1976b) R_C–I_C, and another four equations for V–R to V–R_C. Each equation pertains to specific stellar luminosity classes and a range of color indices as indicated below. The constants C_1 and C_2 apply a zero point offset that depends on right ascension. The transformations for R–I also depend on the factor δ_{BJ}(U–B) which is related to the Balmer-jump

and was defined by Taylor. For some combinations of luminosity class with spectral type this term could not be determined accurately and such stars are not included in this study. Graphs showing the relationship between the Johnson and Cousins color indices follow the equations.

A.1. R–I to R–I_C equations

If 5400 < HR < 7200, C_1 = –0.009; otherwise C_1 = zero.

(1) All luminosity classes:
$R_C–I_C = 0.902\ ((R–I) – C_1) – 0.087\ \delta_{BJ}(U–B) + 0.073$

(2) All luminosity classes in a limited range of color indices:
$R_C–I_C = 0.762\ ((R–I) – C_1) – 0.073\ \delta_{BJ}(U–B) + 0.074$

(3) Giant stars in a limited range of colors:
$R_C–I_C = 0.953\ ((R–I) – C_1) – 0.030$

(4) Dwarf stars in a limited range of color indices:
$R_C–I_C = 0.978\ (R–I) – 0.012$

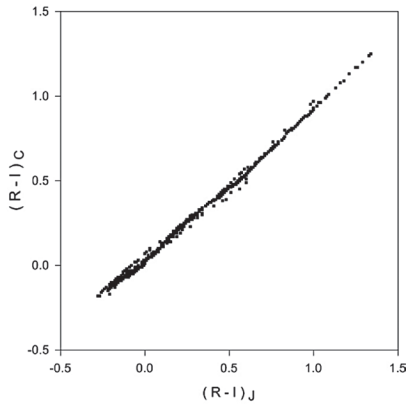

Figure A.1. The transformation from Johnson R–I to Cousins $R_C–I_C$. The function is multi-valued because there are four separate equations which apply to different luminosity classes in addition to the dependence on $\delta_{BJ}(U–B)$.

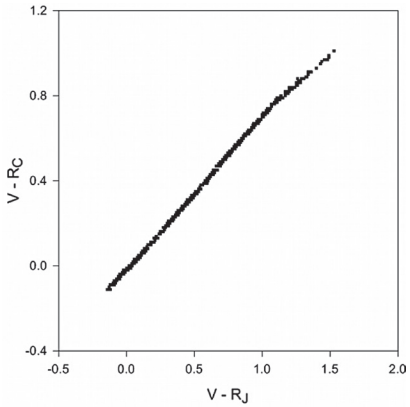

Figure A.2. The transformation from Johnson V–R to Cousins $V–R_C$. Unlike the R–I color index this one is almost single-valued since there is less dependence on luminosity class and no dependence on $\delta_{BJ}(U–B)$.

A.2. V–R to V–R_C equations

If HR > 4700, C_2 = –0.009; otherwise C_2 = zero.

(1) All luminosity classes except red dwarfs; a limited range of color indices:
$V–R_C = 0.717\ ((V–R) – C_2) – 0.021$

(2) All luminosity classes in a limited range of color indices:
$V–R_C = 0.717\ ((V–R) – C_2) – 0.030$

(3) Giants in a limited range of color indices:
$V–R_C = 0.55\ ((V–R) – C_2) + 0.16$

(4) Red dwarfs:
$V–R_C = 0.63\ ((V–R) – C_2) + 0.07$

Appendix B: Cousins to Sloan transformation equations

The equations listed below were used for transformations from Cousins (1976a, 1976b) to Sloan. When two equations are available for the same magnitude the results were averaged. In some cases only one of the two equations could be used because fewer than five Cousins magnitudes or colors were available. Color–color graphs follow the equations.

B.1. Fukugita *et al.* (1996) equations

$g' = V + 0.56\ (B–V) – 0.12$

$r' = V – 0.49\ (B–V) + 0.11$

$r' = V – 0.84\ (V–R_C) + 0.13$

$u'–g' = 1.38\ (U–B) + 1.14$

$g'–r' = 1.05\ (B–V) – 0.23$

$r'–i'$ (for $R_C–I_C < + 1.15$) $= 0.98\ (R_C–I_C) – 0.23$

$r'–i'$ (for $R_C–I_C \geq + 1.15$) $= 1.40\ (R_C–I_C) – 0.72$

$r'–z'$ (for $R_C–I_C < + 1.65$) $= 1.59\ (R_C–I_C) – 0.40$

$r'–z'$ (for $R_C–I_C \geq + 1.65$) $= 2.64\ (R_C–I_C) – 2.16$

B.2. Smith *et al.* (2002) equations

$g' = V + 0.54\ (B–V) – 0.07$

$r' = V – 0.44\ (B–V) + 0.12$

r' (for $V–R_C < 1.00$) $= V – 0.81\ (V–R_C) + 0.13$

r' (for $V–R_C >=1.00$) = … no stars in this range

$u'–g' = 1.33\ (U–B) + 1.12$

$r'–i'$ (for $R_C–I_C < 1.15$) $= 1.00\ (R_C–I_C) – 0.21$

r'–i' (for $R_C–I_C \geq 1.15$) = 1.42 ($R_C–I_C$) – 0.69

r'–z' (for $R_C–I_C < 1.65$) = 1.65 ($R_C–I_C$) – 0.38

r'–z' (for $R_C–I_C \geq 1.65$) … no stars in this range

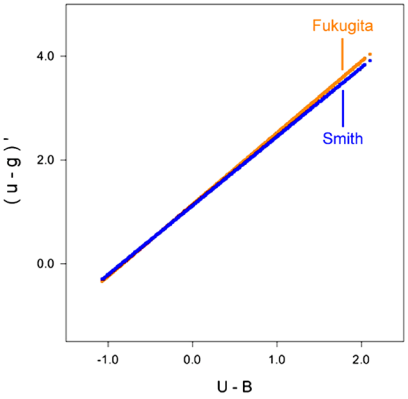

Figure B.1. The (u–g)' color index as a function of U–B.

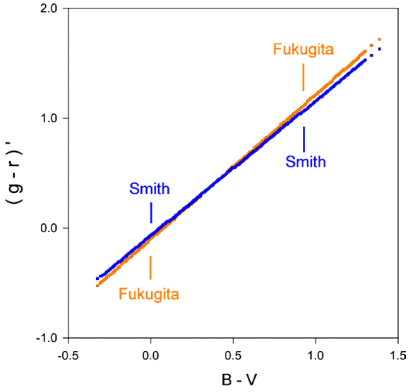

Figure B.2. The (g–r)' color index as a function of B–V.

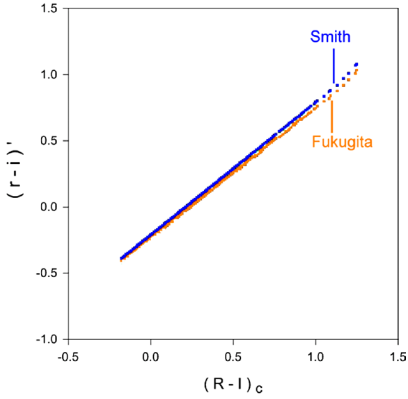

Figure B.3. The (r– i)' color indices as a function of $(R–I)_C$.

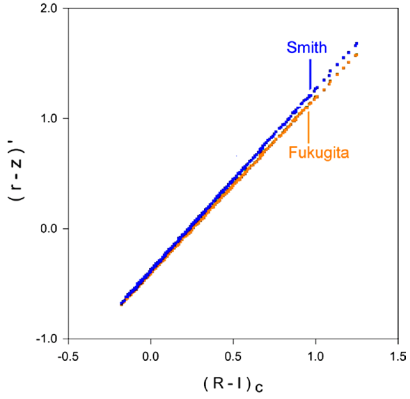

Figure B.4. The (r–z)' color indices as a function of $(R–I)_C$.

Appendix C: Data sources

The following data base files were used as input.

1) Johnson five-color photometry:
http://obswww.unige.ch/gcpd/cgi-bin/getStars.cgi?Ref=15&Photo=08

2) Johnson three-color photometry:
http://cdsarc.u-strasbg.fr/viz-bin/ftp-index?II/5A

3) Skiff luminosity classes and spectral types
http://vizier.u-strasbg.fr/viz-bin/VizieR?-source=skiff%20mk%20type

4) *General Catalogue of Variable Stars*
http://vizier.u-strasbg.fr/viz-bin/VizieR-3?-source=B/gcvs

Methods for O–C (Observed Minus Computed) Diagrams and for the Determination of Light Elements of Variable Stars with Linear and Second Order Polynomial Ephemerides

Roy Andrew Axelsen
P. O. Box 706, Kenmore, Queensland 4069, Australia; reaxelsen@gmail.com

Received July 24, 2014; accepted July 28, 2014

Abstract Methods are described for the construction and analysis of O–C (observed minus computed) diagrams and for the determination of light elements (ephemerides) of variable stars and the standard errors of the elements. The methods described are those that apply: (1) when the period of the star is constant, and (2) when the period of the star is changing continuously, and the light elements can be represented by a second order polynomial function.

1. Introduction

During the past few years, the author performed photometric studies on the monoperiodic high amplitude δ Scuti stars RS Gruis and BS Aquarii (Axelsen 2014a, 2014b). Both of these stars have been studied by several observers over of period of decades, and both exhibit evidence of changes in period (Rodríguez *et al.* 1995; García 2012; Axelsen 2014a; Yang *et al.* 1993; Fu *et al.* 1997; Axelsen 2014b). For RS Gru, historical data and data in recent years revealed period changes that are best expressed as quadratic (second order polynomial) functions, indicating that there have been period changes, but the rates of period change are constant (Rodríguez *et al.* 1995; Axelsen 2014b). The recent behavior of BS Aqr, on the other hand, is best expressed by a linear function, indicating no continuous change in period over recent decades, although period change had occurred previously (Axelsen 2014a).

The author found no entirely satisfactory references in the literature which provided detailed, step by step methods for these types of analysis. Online lecture notes by Bradstreet (1997) on the ephemerides of variable stars did, however, provide some assistance. The steps involved are: tabulation of times of maximum light (TsOM, the times of peak brightness in the light curve) of the variable star in heliocentric Julian days (HJD); calculation of the O–C values; drawing and analysis of the O–C diagram; determination of the light elements for the variable star, and the associated standard errors; and (if the period of a star changes continuously over time) calculation of the rate of change of the period, using appropriate units in which to express the rate of change.

This paper therefore presents the author's personal approach to the analysis of longitudinal data comprising the times of maximum of variable stars with regular periods. The data used as examples are available in the astronomical

literature. Calculations performed on those data are described in this paper, and the results compared with those previously published. The calculations can be replicated by using the methods described herein.

In principle, the calculations can also be applied to times of minimum of eclipsing binary systems. For simplicity of description, however, only times of maximum, such as can be determined for many pulsating variable stars, will be referred to.

2. Data

In the case of BS Aqr, data from the astronomical literature including recent personal observations are used, with all sources referenced in Axelsen (2014a). In the case of RS Gru, data from the astronomical literature are used, with all sources referenced in Rodríguez *et al.* 1995.

3. Analysis, O–C diagrams, and light elements

3.1. Linear ephemeris

The data and the results of calculations of O–C values are listed in Table 1 for BS Aqr, which represent data already published as maxima 35 to 61 of Table 2 in Axelsen (2014a).

The requirements for the calculation of O–C values are the availability of several or many TsOM of a variable star, which may comprise historical data previously reported in the astronomical literature, and/or recent observations. TsOM are in heliocentric Julian days.

The parameters used in the calculation are:

T_0 The initial TOM in heliocentric Julian days (HJD), obtained either recently or at some time in the past. This is the TOM on which the calculations are based.

P_{est} The estimated period in days, obtained either recently or at some time in the past. This is the period on which the calculations are based.

T_n Other TsOM in HJD, from historical data and/or recent observations.

E_n The number of cycles or epochs of the variable star that have elapsed between T_0 and each value of T_n.

It should be explained what each O–C value represents. The "O" (the observed values) represent the observed TsOM, either from the literature or personal observation. If there are sufficient observations of the magnitude of the star on either side of each peak in the light curve, an excellent way to determine each TOM is to fit a 6th-order polynomial expression to the ascending limb, the peak, and the descending limb of the curve. The software program PERANSO (Vanmunster 2013) has a routine for this determination, and provides also the

Table 1. Times of maximum (TsOM) in heliocentric Julian days (HJD) of BS Aqr from 1973 to 2013, representing maxima 35 to 61 from Table 2 of Axelsen (2014a).

Max	*TOM (HJD) T_n*	*Epoch E (Rounded)*	*Epoch E_n*	*(O–C)*	*Primary Source**
35	2441946.67140	–73785	–73785.06973	–0.01379	1
36	2441946.86930	–73784	–73784.06934	–0.01372	1
37	2441947.66200	–73780	–73780.06221	–0.01231	1
38	2441947.86030	–73779	–73779.05980	–0.01183	1
39	2441948.65000	–73775	–73775.06784	–0.01342	1
40	2441948.84890	–73774	–73774.06239	–0.01234	1
41	2441949.64000	–73770	–73770.06335	–0.01253	1
42	2441950.63000	–73765	–73765.05887	–0.01165	1
43	2441950.82950	–73764	–73764.05039	–0.00997	1
44	2445612.72400	–55253	–55253.04974	–0.00984	2
45	2445620.63800	–55213	–55213.04420	–0.00874	2
46	2445625.58300	–55188	–55188.04706	–0.00931	2
47	2445637.64700	–55127	–55127.06313	–0.01249	2
48	2445644.57200	–55092	–55092.05702	–0.01128	2
49	2445997.09200	–53310	–53310.05649	–0.01117	3
50	2448912.80460	–38571	–38571.03060	–0.00605	5
51	2449606.76440	–35063	–35063.04032	–0.00798	5
52	2449606.96210	–35062	–35062.04094	–0.00810	5
53	2449607.95130	–35057	–35057.04050	–0.00801	5
54	2449956.51500	–33295	–33295.03919	–0.00775	5
55	2449957.50480	–33290	–33290.03572	–0.00707	5
56	2450072.04410	–32711	–32711.03568	–0.00706	4
57	2456543.02662	0	0.00000	0.00000	6
58	2456545.00339	10	9.99264	–0.00146	6
59	2456561.02607	91	90.98783	–0.00241	6
60	2456570.12942	137	137.00557	0.00110	6
61	2456592.08450	248	247.98924	–0.00213	6

Primary sources: 1. Elst (1976); 2. Meylan et al. *(1986); 3. Yang* et al. *(1993); 4. Fu* et al. *(1997); 5. Rodríguez* et al. *(1998); 6. Axelsen (2014a).*

Notes: The epochs (number of cycles) are listed with the exact calculated results in the fourth column, and the rounded numbers (from which the O–C values are calculated) in the third column. The last two columns list the O–C (observed minus computed) values and the published sources of the TsOM, respectively. The calculations represent the results of formulae (1) and (2) in the present paper, with P_{est} being the period of Fu et al. *(1997) of 0.197822612 d, and T_0 being the first TOM determined by us in 2013 (maximum 57 in the table), 2456543.026620 HJD.*

standard error of the calculated result. The "C" (the computed values) represent the TsOM of the light curve that would have occurred if P_{est}, the initial estimated period, remained unchanged during the span of time between T_0 and T_n (the

span of time during which the star has been studied). If the period is, in fact, unchanged, then the O–C value will be zero. On the other hand, if the period has changed, O–C will be a non-zero value.

The first calculation which must be made determines the number of cyles or epochs (E_n) of the star which have elapsed between T_0 and T_n, and is represented by the formula:

$$E_n = (T_n - T_0) / P_{est} \quad (1)$$

The resulting numbers, E_n, will be numerals with decimal fractions, as seen in the fourth column of Table 1, and may be positive or negative (or both), depending on which TOM is designated as T_0. These numbers must be reduced to integers, which can be achieved by rounding, shown as the Epoch E in the third column of Table 1.

After the epochs (number of cycles) E in integer format are tabulated, the O–C values can be calculated from the formula:

$$O–C = T_n - (T_0 + E \times P_{est}) \quad (2)$$

All of the above calculations can be made readily using a spreadsheet, and from that spreadsheet the O–C diagram can be charted, with E (epochs) on the x-axis and the O–C values on the y axis.

Figure 1 is an O–C diagram drawn from the data in Table 1. The line represents a least squares linear fit, calculated using Data Analysis, Regression in MICROSOFT EXCEL, and is represented by the equation (with standard errors in brackets):

$$O–C = 0.00000015\ (1)\ E - 0.0016\ (5) \quad (3)$$

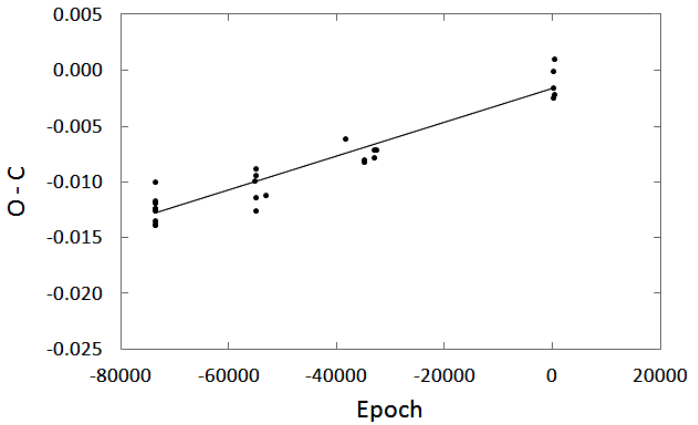

Figure 1. O–C diagram of BS Aqr, drawn from the data of Table 1. The line represents a least squares linear function fitted to the data.

Since the O–C diagram in this example is described by a linear function, the light elements of the star are represented by an equation that describes a linear function. This function can be derived by plotting each TOM on the y-axis against each epoch E on the x-axis (using the data from Table 1), and finding the least squares linear regression of this plot. This type of plot is not usually presented in the literature, but its equation represents the light elements of the star:

$$\text{TOM (HJD)} = 0.19782276\ (5)\ E + 2456543.0250\ (5) \quad (4)$$

The slope of the function is the period, seen above as 0.19782276 d. The last term of the equation (2456543.0250) is the TOM at zero epoch. Standard errors are shown in parentheses. The TOM at any user-nominated epoch can be calculated directly from the above equation by inserting the required value of E.

Since the function fitted to the O–C data is linear, the period of the star has not been changing continuously during the period of the analysis. Since the fitted function has a positive slope, the calculated period of the star is longer than the estimated period P_{est} used to make the calculations of O–C and the number of epochs. A negative slope would indicate that the calculated period is less than the estimated period P_{est}, and a horizontal line would indicate that the calculated period is the same as the estimated period P_{est}.

3.2. Ephemeris described by a second-order polynomial function

The data and the results of calculations of O–C values are listed in Table 2 for RS Gru. The table uses the TsOM and epochs published by Rodríguez *et al.* (1995), and also lists the O–C values calculated by the present author from the initial period and epoch used by Rodríguez *et al.* (1995), namely, 0.14701131 d and HJD 2447464.7095. The O–C diagram from this data is shown in Figure 2, together with the least squares fit from a second-order polynomial function, represented by the generic equation:

$$y = ax^2 + bx + c \quad (5)$$

and specifically by the equation:

$$O–C = –3.14 \times 10^{–12}\ E^2 – 4.46 \times 10^{–7}\ E + 5.92 \times 10^{–4} \quad (6)$$

where O–C represents the values on the y-axis, and E represents the epochs, plotted on the x-axis.

It should be noted that, in the paper by Rodríguez *et al.* (1995), the values listed in the columns under the headings for O–C in their Table 2 are not actually the O–C values themselves, but the residuals from the linear and quadratic regression analysis performed by those authors. Likewise, their O–C diagram does not plot the values themselves, but the residuals of the O–C values from the second-order polynomial (quadratic) least squares fit.

Table 2. Times of maximum (TsOM) of RS Gru from 1952 to 1988, epochs (number of cycles, with only the rounded values shown), and O–C values.

Max	*TOM (HJD) T_n*	*Epoch E (Rounded)*	*(O–C)*	*Primary Source**
1	2434325.2940	–89377	–0.026108	1
2	2434573.4510	–87689	–0.023447	1
3	2436756.5710	–72839	–0.014777	2
4	2436760.5380	–72812	–0.017070	2
5	2436801.5540	–72533	–0.017101	3
6	2436853.3030	–72181	–0.015926	3
7	2441538.4027	–40312	–0.005450	4
8	2441538.5490	–40311	–0.006161	4
9	2441610.4379	–39822	–0.005574	4
10	2441611.3200	–39816	–0.005539	4
11	2441611.4677	–39815	–0.004850	4
12	2441612.3493	–39809	–0.005315	4
13	2441915.4856	–37747	–0.005417	4
14	2442687.5892	–32495	–0.002874	5
15	2443355.4610	–27952	–0.001429	6
16	2443355.6092	–27951	–0.000240	6
17	2443360.4584	–27918	–0.002399	6
18	2443360.6050	–27917	–0.002810	6
19	2447464.7095	0	–0.000600	7
20	2447468.5324	26	0.000018	7
21	2447468.6793	27	–0.000093	7
22	2447472.6489	54	0.000213	7

**1. Hoffmeister (1956); 2. Oosterhoff and Walraven (1966); 3. Kinman (1961); 4. Dean* et al. *(1977); 5. McNamara and Feltz (1976); 6. Balona and Martin (1978); 7. Rodríguez* et al. *(1995).*

Notes: The times of maximum are those published by Rodríguez et al. *(1995). The calculations, employing formulae (1) and (2) of the present paper, use the initial TOM and period published by the same authors, namely, 2447464.7101 HJD, and 0.147010864 d, respectively.*

The importance of the O–C diagram both in Rodríguez *et al.* (1995) and the present paper is that it shows a second-order polynomial function fitted to the data, with the plot of that function being a curve with its concavity facing down. This implies that the period of RS Gru had been continuously decreasing during the span of time covered by the data, from 1952 to 1988. If the plot were a curve with the concavity facing up, the period would have been continuously increasing.

Therefore, the light elements of the star should similarly be described by a second-order polynomial expression, obtained from a graph of the TsOM plotted on the y-axis against epochs E on the x-axis, with the values taken from

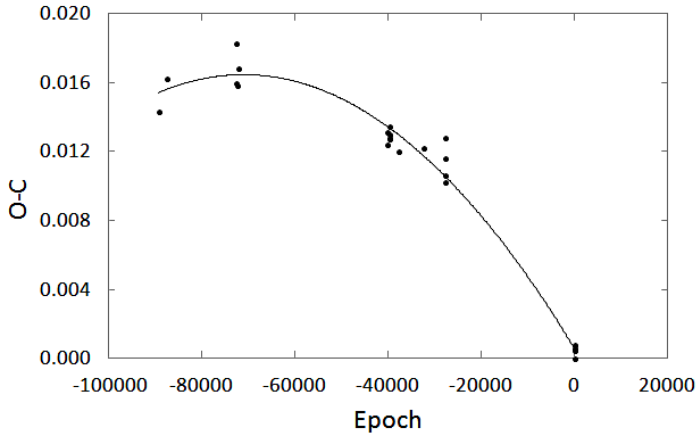

Figure 2. O–C diagram of RS Gru, drawn from the TsOM and epochs published by Rodríguez *et al.* (1995), and listed in Table 2 of the present paper. The curved line represents the second-order polynomial expression fitted to the data.

Table 2. When the data are plotted in this manner, the relationship appears to be linear and is accurately described by a linear function, but we know from the O–C diagram that it should be described by a second-order polynomial expression in order to obtain accurate light elements.

The second-order polynomial expression calculated by the present author for these data using Data Analysis, Regression in MICROSOFT EXCEL is:

$$\text{TOM} = -3.14 \times 10^{-12} (\pm 0.24 \times 10^{-12})\, E^2 + 0.147010864\ (22)\ E + 2447464.7101\ (4) \qquad (7)$$

This expression involves a term that is the square of the epoch. In order to use MICROSOFT EXCEL to perform a least squares second-order polynomial regression, both the epoch and the square of the epoch must first be tabulated so that they can be selected as input for the procedure in EXCEL. Table 3 lists these data, from which Data Analysis, Regression calculated the coefficients shown in Equation 7 above. These coefficients are identical to those published by Rodríguez *et al.* (1995) in their analysis of the same data. This expression represents the light elements of RS Gru, as explained below.

Equation 7 has the generic form $y = ax^2 + bx + c$, already mentioned above as Equation 5. When this generic equation represents the light elements of a variable star, it is best understood when written as:

$$\text{TOM} = AE^2 + PE + T_1 \qquad (8)$$

Here, TOM is the calculated time of maximum in HJD for any input epoch E. P is the period of the star in days at zero epoch, and T_1 is the TOM at zero epoch. If both the period and the TOM are required for any epoch, they can be calculated

Table 3. RS Gru data, with epochs and times of maximum in the second and third columns (values taken from Table 2 above), and the values of the epoch squared in the first column.

Epoch Squared	*Epoch*	*TOM (HJD)*
7988248129	–89377	2434325.2940
7689360721	–87689	2434573.4510
5305519921	–72839	2436756.5710
5301587344	–72812	2436760.5380
5261036089	–72533	2436801.5540
5210096761	–72181	2436853.3030
1625057344	–40312	2441538.4027
1624976721	–40311	2441538.5490
1585791684	–39822	2441610.4379
1585313856	–39816	2441611.3200
1585234225	–39815	2441611.4677
1584756481	–39809	2441612.3493
1424836009	–37747	2441915.4856
1055925025	–32495	2442687.5892
781314304	–27952	2443355.4610
781258401	–27951	2443355.6092
779414724	–27918	2443360.4584
779358889	–27917	2443360.6050
0	0	2447464.7095
676	26	2447468.5324
729	27	2447468.6793
2916	54	2447472.6489

Notes: This table represents the inputs for regression analysis of a second-order polynomial expression. Using "Data Analysis, Regression" in MICROSOFT EXCEL*, the input y range is the third column, the TsOM. The first two columns, selected together, represent the input x range.*

by rescaling the x-axis values so that the epoch of interest is assigned the value zero. Importantly, the coefficient A is related to the rate of change of the period of the star, with the actual rate of change represented by the first differential of this coefficient, which is 2A. This value is not changed if the x-axis values are rescaled to change the zero epoch. It should be noted that the coefficient of the E^2 term in the equation for the ephemeris is the same as the coefficient of the E^2 term in the equation for the O–C diagram (Equation 6 above).

Finally, the results for the rate of change of the period of the star need to be expressed in the appropriate units, as usually reported in the literature. The coefficient -3.14×10^{-12} in Equation 7 above has the units d/cycle (days per cycle), since the TsOM on the y-axis are expressed in HJD, and the number of cycles (or epochs) are on the x-axis. Table 4 lists the sequence of arithmetical steps to show, first, how the coefficient is multiplied by 2 to yield the actual

Table 4. Calculations made by the present author which yield the appropriate units in which to express the rate of change of the period of RS Gru for the years 1952–1988.

Term	*Coefficient*	*SE*	*Units*
A	-3.138×10^{-12}	2.428×10^{-13}	d/cycle
2A	-6.275×10^{-12}	4.857×10^{-13}	d/cycle
Divide by period	-4.269×10^{-11}	3.304×10^{-12}	d/d
Multiply by 365.25	-1.56×10^{-8}	0.12×10^{-8}	d/yr or d yr^{-1}
Divide by period	-10.6×10^{-8}	0.8×10^{-8}	cycle/yr or yr^{-1}

Notes: A = the term in equation (8) TOM = $AE^2 + PE + T_1$ which relates to the rate of change of the period of the star; SE = standard error; d = day; yr = year. The results in the fourth and fifth lines of the table represent the units usually reported in the literature, designated as dP/dT and dP/PdT, respectively. The values above were calculated by the author. The results in the fourth and fifth lines of the table are identical to those published by Rodríguez et al. *(1995).*

rate of change of the period, and then how that value (in units of d/cycle) is progressively converted into dP/dT days per year (d/yr, or d yr^{-1}) and finally dP/PdT cycles per year (cycles/yr or simply y^{-1}). The final values in the last two lines of Table 4, calculated by the present author, are identical to those reported by Rodíguez *et al.* (1995).

4. Conclusions

The aim of this paper is to provide a step by step guide to the analysis of data comprising the times of maximum of variable stars over a substantial period of time, usually years, and which can be examined by the construction of O–C diagrams. A linear O–C plot indicates that the period of the star is not changing during the span of time covered by the analysis. A linear function with a positive slope indicates that the newly determined period of the star is longer than the original estimate, and a linear function with a negative slope indicates that the newly determined period is shorter than that originally estimated. Functions that represent the light elements (the ephemeris) of the star are shown as plots of TsOM on the y axis against epoch (cycle number) on the x-axis, although the actual plot is usually not shown in publications. The slope of the linear function represents the period of the star in days. Where the period of a star is changing continuously, and the O–C diagram can be represented accurately by a second-order polynomial expression, the light elements are also best described by such a polynomial function, which allows an accurate determination of the period at any epoch, the TOM at any epoch, and the rate of change in the period.

5. Acknowledgements

The valuable assistance of Timothy Napier-Munn of the Astronomical Association of Queensland with regression analysis employing MICROSOFT EXCEL is gratefully acknowledged.

References

Axelsen, R. A. 2014a, *J. Amer. Assoc. Var. Star Obs.*, **42**, 37.
Axelsen, R. A. 2014b, *J. Amer. Assoc. Var. Star Obs.*, **42**, 44.
Balona, L. A., and Martin, W. L. 1978, *Mon. Not. Roy. Astron. Soc.*, **184**, 1.
Bradstreet, D. H. 1997, Variable Star Lecture Notes on Ephemerides of Variable Stars, The Bradstreet Observatory at Eastern College (http://templetonhonorscollege.com/publications/ephemerides-variable-stars).
Dean, J. F., Cousins, A. W. J., Bywater, R. A., and Warren, P. R. 1977, *Mem. Roy. Astron. Soc.*, **83**, 69.
Elst, E. W. 1976, *Astron. Astrophys., Suppl. Ser.*, **23**, 419.
Fu, J.-N., Jiang, S.-Y., Gu, S.-H., and Qiu, Y.-L. 1997, *Inf. Bull. Var. Stars*, No. 4518, 1.
García, J. R. 2012, *J. Amer. Assoc. Var. Star Obs.*, **40**, 272.
Hoffmeister, C. 1956, *Veröff. Sternw. Sonneberg*, **3**, 1.
Kinman, T. D. 1961, *Bull. Roy. Greenwich Obs.*, **37**, 151.
McNamara, D. H., and Feltz, K. A., Jr. 1976, *Publ. Astron. Soc. Pacific*, **88**, 510.
Meylan, G., Burki, G., Rufener, F., Mayor, M., Burnet, M. and Ischi, E. 1986, *Astron. Astrophys., Suppl. Ser.*, **64**, 25.
Oosterhoff, P. Th., and Walraven, Th. 1966, *Bull. Astron. Inst. Netherlands*, **18**, 387.
Rodríguez, E., Rolland, A., Costa, V., and Martin, S. 1995, *Mon. Not. Roy. Astron. Soc.*, **277**, 965.
Rodríguez, E., González-Bedolla, S. F., and López-González, M. J. 1998, *Astron. Astrophys.*, **336**, 911.
Vanmunster, T. 2013, Light Curve and Period Analysis Software, PERANSO v.2.50 (http//www.peranso.com/).
Yang, D.-W., Tang, Q.-Q., Jiang, S.-Y., and Wang, H.-S. 1993, *Inf. Bull. Var. Stars*, No. 3831, 1.

Analysis of Great World Wide Star Count Data: 2007–2013

Jennifer J. Birriel
Jessica N. Farrell
Department of Mathematics, Computer Science, and Physics, Morehead State University, Morehead, KY 40351; address email correspondence to j.birriel@morehead-st.edu

Dennis Ward
Education and Public Engagement, National Ecological Observatory Network, 1685 38th Street, Boulder, CO 80301

Received August 6, 2014; revised September 29, 2014; accepted September 30, 2014

Abstract The Great World Wide Star Count (GWWSC) website provides free public access to seven years of naked-eye limiting magnitudes (NELM) reported by citizen scientists from 2007 to 2013. We summarize the data and perform a simple statistical analysis. GWWSC data are compared with the Globe at Night (GaN) data over the same time period. The global average NELM values are generally comparable across the two data sets. Global NELM data seem to reflect shifts in urban versus suburban participation over time, while regional and local NELM data are more likely to reflect changes in night sky brightness.

1. Visual estimates of night sky brightness

The proliferation of man-made lighting for use at night produces a pervasive type of environmental problem known as light pollution (e.g. Dick 1999; Isobe and Hamamura 2000; Rich and Longcore 2005). Artificial light at night that scatters upward increases the brightness of the background sky (e.g. Garstang 1986, 1991; Cinzano and Falchi 2012). This increased brightness reduces the contrast between the background sky and faint stars: as the brightness of the sky increases, fainter stars become invisible to the naked eye (e.g. Moore 2001). This decrease in contrast can also render diffuse objects such as nebulae, galaxies, and the band of the Milky Way invisible.

Night sky brightness as seen from the ground can be estimated using the unaided human eye (e.g. Upgren 1991), photometers (Nawar *et al.* 1998), wide-field CCD cameras (Cinzano and Falchi 2003; Duriscoe *et al.* 2007), DSLR cameras (Zotti 2007), or commercially available Sky Quality Meters (e.g. Smith *et al.* 2008; Birriel *et al.* 2010). Naked-eye or visual estimates are semi-quantitative and subject to errors associated with observer age, visual acuity, and experience. However, visual estimates have several inherent advantages: they are essentially cost-free and can be done with relative ease and little time.

Thus, naked-eye estimates of night sky brightness are extremely useful for acquiring data over large geographic regions and long periods of time.

Night sky brightness can be estimated by examining a bright constellation for the faintest star observable with the naked eye, the so-called Naked-eye limiting visual magnitude (NELM). This is usually done using star charts (e.g. McBeath 1991). NELMs can be decreased by atmospheric turbulence, pollutants, and humidity. NELMs provide a "localized" measurement for the region of sky under examination; a full-scale picture of the sky could be obtained by multiple measurements of NELMs in different regions of the sky (e.g. Moore 2001). The NELM method is a seven-grade scale and requires only the ability to compare a set of charts to a given constellation in the sky. As a result of its ease of use and applicability to the full range of lighting conditions, NELMs are the method of choice for both the Globe at Night (GaN) and the Great World Wide Star Count projects.

2. The Great World Wide Star Count

The Great World Wide Star Count (GWWSC; http://starcount.org) is a citizen science event sponsored by the Windows to the Universe website (W2U; http://windows2universe.org) from the National Earth Science Teachers Association (http://nestanet.org). This W2U program began in 2007 at the University Corporation for Atmospheric Research (UCAR), where it resided until 2010.

The GWWSC observing campaign occurs each year during a two-week period, approximately mid-October to mid-November, when the lunar phase is between waning gibbous and first quarter. The campaign dates are further adjusted to include two full weekends to maximize observing opportunities for younger participants. The GWWSC protocol is similar to that of GaN—participants observe one of two constellations (Cygnus in the Northern Hemisphere and Sagittarius in the Southern Hemisphere), comparing their view with simple star maps of progressively fainter stars to determine the NELM value. The GWWSC was designed as a "complementary" program to GaN with compatible protocols and datasets. The principle differences between the two programs' NELM protocols are that GWWSC (1) takes place in October of each year and (2) utilizes two constellations located higher in the sky for northern and southern observers, while GaN originally took place during March and focused on Orion as being visible from both hemispheres.

Participation in the GWWSC is simple. The downloadable Activity Guide (available in fifteen languages) guides participants through the steps required for safe and successful participation. The actual measurement takes fifteen minutes, primarily waiting for the participant's eyes to dark-adapt. The reporting form closely resembles the online reporting page in order to provide a familiar user experience. Although measurements from commercial Sky Quality Meters

are not directly supported, GWWSC participants are encouraged to enter SQM measurements in the comments field as desired. Once entered into the database via the online reporting form, each observation is instantly displayed on an interactive map, providing the participant with immediate confirmation that his or her observation was successfully submitted. After each annual campaign, the resultant datasets are published online in a variety of formats, including comma-separated values, tab-delimited text, and esri shapefiles (ESRI 1998). Global and regional light pollution maps are created by project staff and published online as well.

3. General summary and statistical analysis

It is of general interest to first note which countries are participating in the GWWSC. Sorting by country and counting the number of contributions from each country is easily done using built in functions in Microsoft EXCEL. The major contributions to GWWSC by country are listed in Table 1. The number of different countries with observations has generally decreased over the years, dropping from 66 countries in the inaugural year 2007 to only 31 countries in 2012 and 2013. It is immediately obvious that the United States, Poland, and Canada are generally major contributors to the GWWSC. Enhanced participation in Canada and Poland was primarily due to the interest and advocacy of their respective national astronomy clubs. In 2010 and 2011, India contributed a large number of data points from New Delhi; this is due to the public awareness campaign, the Great India Star Count (2014) which was conducted in partnership with the GWWSC.

Using the Histogram function in EXCEL, we can generate annual frequency histograms of the global NELMs from 2007 through 2013 (Figure 1). The general shape of the NELM histograms is roughly Gaussian with a peak NELM of about magnitude 4. As with GaN data (Birriel *et al.* 2014), the general shape and centroid of each histogram varies slightly from year to year. In any given year, approximately sixty percent of measured NELMs are between magnitudes 3 and 5.

Descriptive statistics are easily obtained using standard spreadsheet functions. In Table 2, we summarize the descriptive statistics of the GWWSC and GaN data for each year: counts (that is, the number of observations), mean, standard deviation, standard error, five sigma confidence level, and skewness. The means for GWWSC data are fairly comparable to the GaN means until the year 2012. The time evolution of aggregate NELMs from 2006 to 2013 is shown in Figures 2a and 2b. The correlation coefficient, $R^2 = 0.007$, is essentially zero.

The GWWSC data, Figure 2a, do not show the same general "brightening trend" from 2007 to 2012 as the GaN data as noted by Birriel *et al.* (2014). When we include the global mean for the 2013 GaN data, Figure 2b, the slope is still slightly negative and the correlation coefficient, $R^2 = 0.73$, indicates

Table 1. GWWSC contributions by country.

Year	*Number of Countries*	*Top Four Star Count Contributors by %*
2007	66	United States (83.0%), Canada (6.0%), United Kingdom (1.3%), Equatorial Guinea (1.3%)
2008	56	United States (76.3%), Poland (4.3%), Canada (3.5%), Brazil (1.7%)
2009	48	United States (73.5%), Colombia (5.3%), Poland (4.6%), France & United Kingdom (1.3% each)
2010	49	United States (59.4%), India (26.4%), Poland (6.6%), Canada & Chile (0.9%)
2011	52	United States (28.9%), India (46.4%), Poland (12.5%), Canada (7.0%)
2012	31	United States (40.8%), Canada (26.8%), Poland (20.5%), South Africa (2.2%)
2013	31	United States (36.3%), Poland (42.3%), Canada (13.6%), Argentina & Switzerland (1.7% each)

Table 2. Descriptive statistics. Great World Wide Star Count (GWWSC) compared to the Globe at Night (GaN).

Year	*Counts*		*Mean*		*Standard Deviation*		*Standard Error*		*5 Sigma Confidence*		*Skewness*	
	GWWSC	*GaN*	*GWWSC*	*GaN*	*GWWSC*	*GaN*	*GWWSC*	*GaN*	*GWWSC*	*GaN*	*GWWSC*	*GaN*
2007	5458	7261	3.91	3.80	1.50	1.38	0.02	0.02	0.04	0.07	–0.02	0.08
2008	2801	5295	4.07	3.82	1.47	1.34	0.03	0.02	0.05	0.08	–0.11	0.05
2009	1633	14063	3.84	3.69	1.39	1.26	0.03	0.01	0.07	0.05	–0.13	0.20
2010	4024	14394	3.77	3.73	1.53	1.42	0.02	0.01	0.05	0.05	–0.05	0.08
2011	5010	12461	3.24	3.38	1.52	1.27	0.02	0.01	0.04	0.05	0.21	0.12
2012	1921	14896	4.31	3.33	1.46	1.39	0.03	0.01	0.07	0.05	–0.22	0.21
2013	2194	15536	3.83	3.12	1.49	1.50	0.03	0.01	0.03	0.03	–0.02	0.33

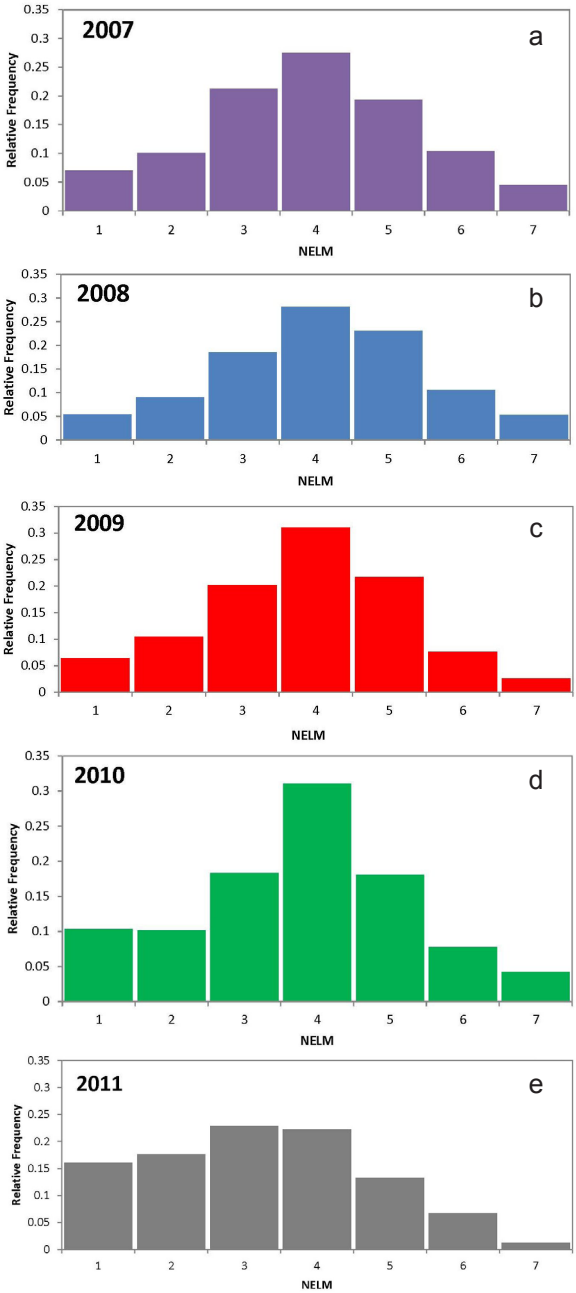

Figure 1a–e. Frequency histograms of naked eye limiting magnitudes (NELMs) for Great World Wide Star Count data from 2007–2013. Some variations occur from year to year but the distributions are roughly Gaussian with a peak around 4 (*Figure continued on next page*).

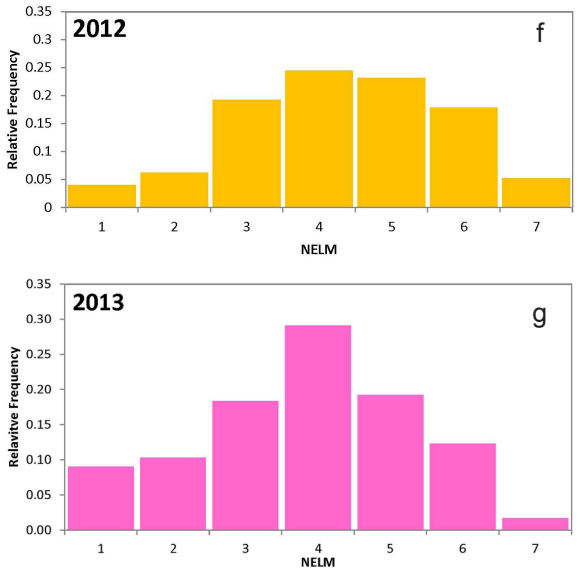

Figure 1f–g. Frequency histograms of naked eye limiting magnitudes (NELMs) for Great World Wide Star Count data from 2007–2013, cont.

Table 3. NELMs by groups for GWWSC data.

	NELM Grouping		
Year	*1+2*	*3+4*	*5+6+7*
2007	0.17	0.49	0.34
2008	0.14	0.47	0.39
2009	0.17	0.51	0.32
2010	0.21	0.49	0.30
2011	0.34	0.45	0.21
2012	0.10	0.44	0.46
2013	0.20	0.47	0.33

Note: NELMs 3+4 Corresponds to medium- to larger-sized cities.

that there is slightly less than a 5% chance that the aggregate NELMs are not correlated with time (Taylor 1997). We perform a one-tailed hypothesis test, with the null hypothesis that the slope is in fact zero for the GaN data. Using EXCEL to perform a linear regression analysis we find a p-value of 0.007, which makes the brightening trend significant at the 1% level. The GaN data appear to indicate a slight brightening of the global or aggregate NELM over the last eight years.

The aggregate NELM for each year of GWWSC data appears to fluctuate

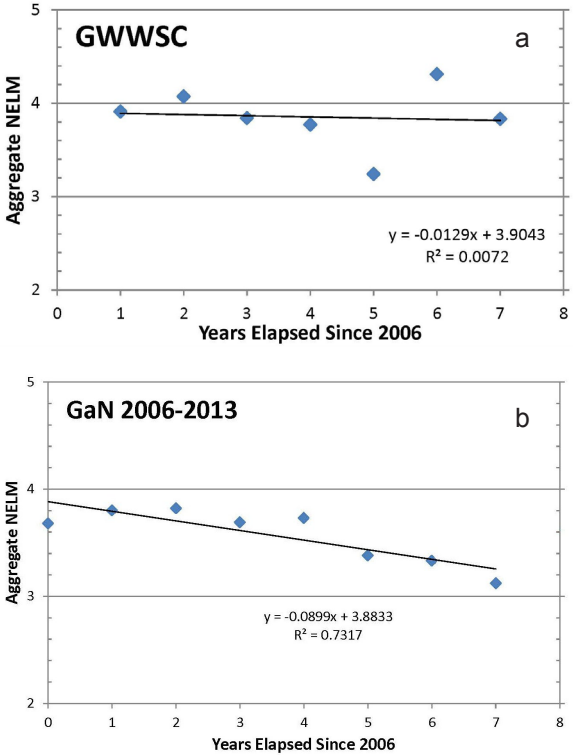

Figure 2a–b. Plots of the time evolution of aggregate or "global" NELM from 2006–2013 for (a) GWWSC and (b) GaN data. The zero year is 2006, which marks the first year of the GaN program. The GWWSC program began in 2007. While the GaN data appear to decrease slightly over time, the GWWSC data do not show this general trend. In both cases, the NELM appears relatively constant until 2010. The changes in NELM can be explained by the proportion of observers reporting from suburban-urban areas versus rural and pristine areas (Tables 2 and 3).

Table 4. NELMs by groups for GaN data.

	NELM Grouping		
Year	*1+2*	*3+4*	*5+6+7*
2007	0.14	0.58	0.28
2008	0.14	0.58	0.28
2009	0.13	0.65	0.22
2010	0.17	0.56	0.27
2011	0.21	0.61	0.18
2012	0.28	0.52	0.20
2013	0.31	0.48	0.21

Note: NELMs 3+4 Corresponds to medium- to larger-sized cities

substantially from 2010 to 2013. On the other hand, from 2007 to 2010 the global mean appears to be relatively constant. A NELM of magnitude 3–4 corresponds to an observing location of a medium- to larger-sized city, while a NELM of magnitude 5–7 corresponds to smaller cities and rural areas. A NELM of magnitude 1–2 means that the observer was located in a highly light-polluted inner city region. In Table 3 we present the annual frequency of each of these three categories for the GWWSC data. From 2007 to 2010, the aggregate contribution in each category remains relatively constant. Note, however, from 2010 to 2013, the aggregate NELM first drops by about 0.5 magnitude from 2010 to 2011, then increases by about 1 magnitude from 2011 to 2012, and then decreases again by about 0.5 magnitude from 2012 to 2013. An examination of Table 3 indicates that these changes reflect changes in the fraction of observers reporting from rural/suburban areas versus large and inner city regions. For example, between 2010 and 2011 the fraction of observers reporting NELMs from magnitudes 1 to 2 increases by thirteen percent while the fraction of observers reporting NELMs from magnitudes 5 to 7 decreases by nine percent. From 2011 to 2012 the aggregate NELM increases by just over 1 magnitude and Table 3 indicates that the fraction of observers reporting from very light-polluted areas drops by 24% and the fraction of observers reporting from less light-polluted areas increases by 25%. In the case of GWWSC data, changes in the aggregate NELM over the 2007–2013 period do not simply reflect changes in light levels, they also show the strong influence of the fraction of observers reporting from rural/suburban versus large/inner city locations.

The same trend appears in the GaN data, at least to some extent. An examination of Table 2 and Figure 2b show that the aggregate NELM of GaN data are all relatively close and the data all exhibit a very small, but similar, skew. The mean NELM has remained relatively constant over the duration of the GaN project: for the first five years the mean remained essentially constant at about magnitude 3.74, but in the last three years the average dropped slightly to magnitude 3.36. Between 2010 and 2011, the aggregate NELM in the GaN data decreases by 0.35 magnitude and the decrease continues for subsequent years. In Table 4, we see that there has been a shift in the fraction of observers reporting from heavily light-polluted areas versus more less light-polluted areas. Between 2010 and 2011, the fraction of observers reporting from suburban and rural areas decreased by 9% while there was a corresponding increase of 4% of observers reporting from the most light-polluted areas. Each subsequent year shows a relatively constant fraction of reporters from suburban/rural areas; however, the fraction of reports from medium-sized cities decreases while the fraction of reports from large/inner city regions increases.

One particularly interesting difference between the GWWSC and GaN data sets is the skewness of the data (see Table 1). In every year but 2011, the skewness of GWWSC data is slightly negative while the GaN data always have a slightly positive skewness. Why might this be the case? The GWWSC

constellations for determining NELM are Cygnus and Sagittarius, which were chosen partially to minimize airmass and light dome effects from nearby cities and towns. However, both of these constellations lie in the band of the Milky Way. The GaN constellation used for NELM determination through 2010 was Orion. Since 2011, the GaN has evolved to include more campaigns and use more constellations. We posit that the GWWSC observers tend to over-estimate night sky brightness compared to GaN observers due to the reduced contrast of stars in Cygnus and Sagittarius relative to the brighter than average natural background from the diffuse light of the Milky Way. The year 2011 might be skewed to the positive due to prevailing weather patterns that year; we suggest that GWWSC and GaN data could be used to study the impact of weather on NELMs.

4. Discussion and future directions

The aggregate annual NELMs for GWWSC and GaN data are generally in good agreement, with a difference of less than 0.2 magnitude, until 2012. This agreement is fairly remarkable given the differences in sample size. However, this can be explained by the fact that from 2007 through 2010, both programs had participants that were dominated by U.S. contributions (see Tables 1 and 5). From 2011 to 2013, U.S. contributions to each campaign were less then 50%. Over the last two years, the three largest contributors to the GWWSC campaigns have been the U.S., Canada, and Poland, whereas the top contributors to the GaN campaigns have been the U.S., India, Poland, and South Korea (almost exclusively from the heavily populated cities of Seoul and Busan). These last two years show the largest difference in aggregate mean. We conclude that this difference is the result of the regional differences in light practices in Asia versus Eastern Europe and Canada.

So, beyond educating the public about light pollution, what is the value of the GWWSC data? GWWSC data is collected in a manner identical to GaN data, using citizen scientists who obtained naked-eye limiting magnitudes by comparing their sky to seven charts of a constellation. Kyba *et al.* (2013) have demonstrated that aggregate GaN data are an accurate tracer of artificial light at night. Kyba *et al.* point out that the great value of GaN data is that aggregate values can ultimately be used to measure increases in sky-glow as measured from the ground up, particularly as the time span increases. In addition, GaN data should be useful for tracking regional changes. We suggest that the GWWSC can be used in conjunction with GaN data to track the rate of change of sky glow both regionally and globally.

5. Acknowledgements

The authors would like to thank the anonymous referee for the useful comments and corrections that helped improve the flow and structure of the

Table 5: GaN contributions by country.

Year	*Number of Countries*	*Top 4 Contributors by %*
2007	62	United States (65.9%), Poland (5.0%), Hungary (3.1%), Canada (3.1%),
2008	61	United States (76.3%), Hungary (5.6%), Romania (2.8%), Czech Republic (2.8%)
2009	81	United States (73.6%), Chile (6.1%), Hungary (1.7%), United Kingdom (1.4%)
2010	85	United States (61.4%), Poland (4.7%), Romania (3.7%), Chile (3.5%)
2011	113	United States (48.0%), Poland (8.5%), India (5.0%), South Korea (3.2%)
2012	92	United States (36.0%), India (14.7%), Poland (7.1%), Argentina (5.2%)
2013	89	United States (39.2%), India (12.4%), South Korea (5.8%), Poland (5.4%)

paper. In addition, the authors thank Dr. Constance Walker for providing a useful summary of the changes in GaN program protocol and campaign windows.

References

Birriel, J. J., Walker, C. E., and Thornsberry, C. R. 2014, *J. Amer. Assoc. Var. Star Obs.*, **42**, 219.

Birriel, J. J., Wheatley, J., and McMichael, C. 2010, *J. Amer. Assoc. Var. Star Obs.*, **38**, 132.

Cinzano, P., and Falchi, F. 2003, *Mem. Soc. Astron. Ital.*, **74**, 458.

Cinzano, P., and Falchi, F. 2012, *Mon. Not. Roy. Astron. Soc.*, **427**, 3337.

Dick, R. 1999, *J. Roy. Astron. Soc. Canada*, **93**, 44.

Duriscoe, D. M., Luginbuhl, C. B., and Moore, C. A. 2007, *Publ. Astron. Soc. Pacific*, **119**, 192.

ESRI. 1998, "ESRI Shapefile Technical Description: An ESRI White Paper—July 1998" (http://www.esri.com/library/whitepapers/pdfs/shapefile.pdf), accessed 9/25/2014.

Garstang, R. H. 1986, *Publ. Astron. Soc. Pacific*, **98**, 364.

Garstang, R. H. 1991, *Publ. Astron. Soc. Pacific*, **103**, 1109.

Great India Star Count. 2014 (http://www.indiaprwire.com/pressrelease/education/20111012100395.htm), accessed 7/11/2014.

Isobe, H. I., and Hamamura, S. 2000, *Astrophys. Space Sci.*, **273**, 289.

Kyba, C. C., *et al.* 2013, *Sci. Rep.*, **3**, 1835 (doi 10.1038/srep01835).

McBeath, A. 1991, *J. Br. Astron. Assoc.*, **101**, 213.

Moore, C. A. 2001, *George Wright Forum*, **18**, 46.

Nawar, S., Morcos, A. B., Metwally, Z., and Osman, A. I. I. 1998, in *Preserving The Astronomical Windows. Proceedings of Joint Discussion number 5 of the 23rd General Assembly of the International Astronomical Union held in Kyoto, Japan 22-23 August 1997*, eds. S. Isobe and T. Hirayama, ASP Conf. Ser. 139, Astronomical Society of the Pacific, San Francisco, 151.

Rich, C., and Longcore, T. (eds.). 2005, *Ecological Consequences of Artificial Light at Night*, Island Press, Washington.

Smith, M. G., Warner, M., Orellana, D., Munizaga, D., Sanhueza, P., Bogglio, H., and Cartier, R. 2008, in *Preparing for the 2009 International Year of Astronomy*, eds. M. G. Gibbs, J. Barnes, J. G. Manning, and B. Partridge, ASP Conf. Ser., 400, Astron. Soc. Pacific, San Francisco, 152.

Taylor, J. R. 1997, *An Introduction to Error Analysis: The Study of Uncertainties in Physical Measurements*, Univ. Science Books, Sausalito, CA, 290.

Upgren, A. R. 1991, *Publ. Astron. Soc. Pacific*, **103**, 1292.

Zotti, G. 2007, in *DarkSky: 7th European Symposium for the Protection of the Night Sky, held Oct. 5–6, Bled, Slovenia* (http://www.darksky2007.si/2.html).

Abstracts of Papers Presented at the Joint Meeting of the Society for Astronomical Sciences and the American Association of Variable Star Observers (AAVSO 103rd Spring Meeting), Held in Ontario, California, June 12–14, 2014

Recovering from the Classical-Nova Disaster

Joseph Patterson
Center for Backyard Astrophysics, 25 Claremont Avenue, Apt. 7C, New York, NY 10027; jop@astro.columbia.edu

Abstract Classical novae rise from obscurity to shine among the brightest stars in the Galaxy. The story of how they return to quiescence is still only dimly known. Vast amounts of energy are loosed upon the white dwarf and its companion, and the light curves of post-novae suggest that they take not a few years, but a few thousand years, to return to quiescence. In the meantime, the secondary may experience a lot of heating from the white dwarf's rediation—enough to overwhelm its intrinsic nuclear luminosity. I'll discuss the stellar physics behind this suggestion, and propose how it might be tested by time-series photometry in the months and years (and if possible, centuries) after outburst.

How Many R Coronae Borealis Stars Are There Really?

Geoffrey C. Clayton
Louisiana State University, Department of Physics and Astronomy, Baton Rouge, LA 70803; gclayton@fenway.phys.lsu.edu

Abstract The R Coronae Borealis (RCB) stars are rare hydrogen-deficient, carbon-rich supergiants. Two evolutionary scenarios have been suggested, a double degenerate merger of two white dwrfs (WDs), or a final helium shell flash in a planetary nebula central star. Only about 100 of the predicted 3,000 RCB stars in the Galaxy have been discovered. But the pace of discovery of new RCB stars in the Milky Way has been accelerating. We recently discovered over twenty new RCB stars by examining ASAS-e light curves. Using the recent release of the WISE All-Sky Catalog, a series of IR color-color cuts have produced a sample of candidates that may yield over 200 new RCB stars. We are trying to obtain spectra of these stars to confirm their identifications. The evidence pointing toward a WD merger or a final-flash origin for RCB stars is contradictory. Increasing the sample of known RCB stars, so that we can better study their spatial distribution in the Galaxy, can give us clues to their origins. Their number and distribution may be consistent with WD mergers. If so, this

would be an exciting result since RCB stars may be low-mass analogs of Type Ia supernovae.

Surveying for Historical Supernovae Light Echoes in the Milky Way Field

Doug L. Welch
Department of Physics and Astronomy, McMaster University, Hamilton, ON L8S 4M1, Canada; welch@physics.mcmaster.ca

Abstract Very luminous, transient events can produce detectable "light echoes"—light scattered by interstellar dust which can arrive much later than the direct light from an outburst. In the last 1,000 years, there have been half a dozen supernovae in the Milky Way which are capable of producing detectable light echoes. Light echo systems have already been found for Tycho (SN 1572) and Cas A. The three-dimensional distribution of light echoes provides one of the few menas for an astronomical source to be inspected from more than one viewpoint. Indications of the degree of asymmetry of supernovae are extremely valuable for understanding the details of the event itself. Amateurs are well-equipped to find the brighter light echoes and in this work I will provide practical guidance on how such surveys may be accomplished and the various science opportunities they provide.

A Crowd-Sourced Light Curve for SN 2014G

John C. Martin
University of Illinois at Springfield, One University Plaza, MS HSB 314, Springfield, IL 62704; jmart5@uis.edu

Abstract SN 2014G was initially classified as a Type IIn (*CBET 3787*) and was later revealed to be a Type II-L (*ATEL 5935*). In addition to having an interesting classification, it was also relatively bright, nearby (peak V ~14.3), and easy to observe with a small- to moderate-sized telescope. We mounted a cooperative effort open to both professional and non-professional observers with the goal of producing a light curve that could accurately measure variations in brightness of 0.1 magnitude with a cadence of one every two days or better. Simply collecting measured magnitudes often results in a light curve with systematic offsets between independent contributors. To minimize that effect without burdening the volunteer observers with too many additional requirements, we collected calibrated images and processed them uniformly to produce the light curve.

The Asynchronous Polar V1432 Aquilae and Its Path Back to Synchronism

David Boyd
CBA (Oxford), 5 Silver Lane, West Challow, Wantage, OX12 9TX, England; davidboyd@orion.me.uk

Joseph Patterson
Department of Astronomy, Columbia University, 550 West 120th Street, New York, NY 10027; jop@astro.columbia.edu

William Allen
CBA (Blenheim), Vintage Lane Observatory, 83 Vintage Lane, RD3, Blenheim 7273, New Zealand

Greg Bolt
CBA (Perth), 295 Camberwarra Drive, Craigie, Western Australia 6025, Australia

Michel Bonnardeau
Le Pavillon, 38930 Lalley, France

Tut Campbell
Jeannie Campbell
CBA (Arkansas), Whispering Pine Observatories, 7021 Whispering Pine Road, Harrison, AR 72601

David Cejudo
CBA (Madrid), Observatorio El Gallinero, El Berrueco, Madrid, Spain

Michael Cook
CBA (Ontario), Newcastle Observatory, 9 Laking Drive, Newcastle, ON L1B 1M5, Canada

Enrique de Miguel
CBA (Huelva), Observatoria Astronomico del CIECM, Parque Dunar Matalascañas, 21760 Almonte, Huelva, Spain

Claire Ding
Department of Astronomy, Columbia University, 550 West 120th Street, New York, NY 10027

Shawn Dvorak
CBA (Orlando), 1643 Nightfall Drive, Clermont, FL 34711

Jerrold L. Foote
CBA (Utah), 4175 E. Red Cliffs Drive, Kanab, UT 84741

Robert Fried
Deceased 2003, formerly at Braeside Observatory, Flagstaff, AZ 86002

Franz-Josef Hambsch
CBA (Mol), Oude Bleken 12, B-2400, Mol, Belgium

Jonathan Kemp
Department of Physics, Middlebury College, Middlebury, VT 05753

Thomas Krajci
CBA (New Mexico), P.O. Box 1351, Cloudcroft, NM 88317

Berto Monard
CBA (Pretoria), P.O. Box 281, Calitzdorp 6661, Western Cape, South Africa

Yemal Ogmen
CBA (Cyprus), Green Island Observatory, Gecitkale, North Cyprus

Robert Rea
CBA (Nelson), Regent Lane Observatory, 8 Regent Lane, Richmond, Nelson 7020, New Zealand

George Roberts
CBA (Tennessee), 2007 Cedarmont Drive, Franklin, TN 37067

David Skillman
CBA (Mountain Meadows), 6-G Ridge Road, Greenbelt, MD 20770

Donn Starkey
CBA (Indiana), 2507 CR 60, Auburn, IN 46706

Joseph Ulowetz
CBA (Illinois), 855 Fair Lane, Northbrook, IL 60062

Helena Uthas
Department of Astronomy, Columbia University, 550 W 120th Street, New York, NY 10027

Stan Walker
CBA (Waiharara), Wharemaru Observatory, P.O. Box 173, Awanui, 0451, New Zealand

Abstract V1432 Aquilae is the only known eclipsing asynchronous polar. In this respect it is unique and therefore merits our attention. We report the results of a 15-year campaign by the globally distributed Center for Backyard Astrophysics to observe V1432 Aql and investigate its return to synchronism. Originally knocked out of synchrony by a nova explosion before observing

records began, the magnetic white dwarf in V1432 Aql is currently rotating slower than the orbital period but is gradually catching up. The fortuitously high inclination of the binary orbit affords us the bonus of eclipses, providing a regular clock against which these temporal changes can be assessed. At the present rate, synchronism should be achieved around 2100. The continually changing trajectory of the accretion stream as it follows the magnetic field lines of the rotating white dwarf produces a complex pattern of light emission which we have measured and documented, providing comprehensive observational evidence against which physical models of the system can be tested.

The Z CamPaign: Year Five

Mike Simonsen
AAVSO Headquarters, 49 Bay State Road, Cambridge, MA 02138; mikesimonsen@aavso.org

Abstract Entering into the fifth year of the Z CamPaign, the author has developed a website summarizing our findings which will also act as a living catalogue of bona fide Z Cam stars, suspected Z Cams, and Z Cam impostors. In this paper we summarize the findings of the first four years of research, introduce the website and its contents to the public, and discuss the way forward into year five and beyond.

Modern V Photometry of the Eclipsing Triple System b Persei

Donald F. Collins
Warren Wilson College, 138 College View Drive, Swannanoa, NC 28778; dcollins@warren-wilson.edu

Jason Sanborn
Lowell Observatory, Northern Arizona University, 1400 West Mars Hill Road, Flagstaff, AZ 86001; jaisen1@lowell.edu

Robert T. Zavala
U.S. Naval Observatory Flagstaff Station, 10391 West Naval Observatory Road, Flagstaff, AZ; bzavala@nofs.navy.mil

Abstract A Complete CCD light curve in V of the bright (V ~ 4.6) ellipsoidal variable star b Persei (not β Persei) has been obtained between November 2013 and February 2014. We recover the small-amplitude 0.065-mag. variation of the ellipsoidal light curve. The period of the ellipsoidal light curve from the 2013–2014 observing season is found to be 1.5273 ± 0.0015 days, consistent with older observations. b Persei is known to be a

triple star system in which several AAVSO contributors recorded the first ever observed eclipse near February 5–6, 2013, of the inner AB stars by the third star C, which has a 702-day edge-on orbit. This eclipse was predicted based on an astrometric orbit from observations with the Navy Precision Optical Interferometer (NPOI). The NPOI provides stellar positions to milliarcsecond precision. We will present results of the orbital analysis of the triple system. The next primary eclipse of b Per is expected near January 12, 2015, and will last about two days. High time-resolution multi-color photometry will be extremely useful as we try to understand the evolutionary states of the close binary in b Per. The close binary may be a non-eclipsing Algol-like system or perhaps evolving towards a mass-transferring Algol-like stage. Time series observations from widely-distributed observers should be able to resolve the eclipse of the individual A and B components of b Persei, thus gaining hidden information about this rarely-observed system. The high brightness of this system enables precision photometry with small telescopes or finder scopes and entry-level filtered monochrome CCD cameras, which are widely available to amateurs worldwide.

A Search for Extreme Horizontal Branch Stars in the General Field Population

Douglas Walker
Department of Physics and Astronomy, University of Canterbury, Christchurch, New Zealand; douglas.walker@pg.canterbury.ac.nz

Michael Albrow
Department of Physics and Astronomy, University of Canterbury, Christchurch, New Zealand; michael.albrow@pg.canterbury.ac.nz

Abstract The study of pulsating Extreme Horizontal Branch (EHB) stars in globular clusters is a new field of stellar research. The initial discovery of three rapidly pulsating EHB stars in ω Centauri was announced at the Fourth Meeting on Hot Subdwarfs and Related Objects held in Shanghai in July 2009. A fourth sdB pulsator was discovered in the remaining photometry data soon afterwards; all were discovered in data obtained by the New Techology Telescope. In March 2013, the Space Telescope Imaging Spectrograph (STIS) was utilized on five consecutive orbits to obtain far-UV imagery of NGC 2808's core, revealing six sdB pulsators with periods 85 to 149 seconds and UV amplitudes from 2.0 to 6.8%. To date (April 2014), these ten EHB pulsators in ω Centauri and NGC 2808 form a unique class of EHB variable closely clustered around $T_{eff} \sim 50{,}000$ K.

This talk describes an initial candidate search for EHB rapidly pulsating sdB stars in the general galactic field population. The search was conducted with the 1-m McLellan telescope at the Mt. John University Observatory (MJUO) at

Lake Tekapo, New Zealand. Observations were conducted utilizing a special high speed f/8 frame-transfer camera called the Puoko-nui. The candidate set of stars was taken from the Edinburgh-Cape Blue Object Survey based on the selection criteria of a (B–V) value of –0.32 to –0.36, corresponding to the desired temperature range T_{eff} ranging from 40,000 to 64,000 K. The objective of this search was to determine whether smaller size telescopes could identify promising sets of candidate sdB pulsators which could be followed up with larger professional systems.

Undergraduate Observations of Separation and Position Angle of Double Stars WDS J05460+2119AB (ARY 6AD and ARY 6 AE) at Manzanita Observatory

Michael J. Hoffert
Concordia University, Irvine, CA; mike.hoffert@cui.edu

Eric Weise
San Diego State University, San Diego, CA; ericdweise@gmail.com

Jenna Clow
Concordia University, Irvine, CA; jenna.clow@eagles.cui.edu

Jacquelyn Hirzel
Concordia University, Irvine, CA; jacquelyn.hirzel@eagles.cui.edu

Brett Leeder
Concordia University, Irvine, CA; brett.leeder@eagles.cui.edu

Scott Molyneux
Concordia University, Irvine, CA; scott.molyneux@eagles.cui.edu

Nicholas Scutti
Concordia University, Irvine, CA; nicholas.scutti@eagles.cui.edu

Sarah Spartalis
Concordia University, Irvine, CA; sarah.spartalis@eagles.cui.edu

Corey Takuhara
Concordia University, Irvine, CA; corey.takuhara@eagles.cui.edu

Abstract Six beginning astronomy students, part of an undergraduate stellar astronomy course, one advanced undergraduate student assistant, and a professor measured the position angles and separations of Washington Double Stars (WDS) J05460+2119 (= WDS J05460+2119AB; also known as ARY 6 AD and ARY 6 AE). The measurements were made at the Manzanita

Observatory (116° 20' 42" W, 32° 44' 5" N) of the Tierra Astronomical Institute on 10 Blackwood Road in Boulevard, California (www.youtube.com/watch?v=BHVdeMGBGDU), at an elevation of 4,500 ft. A Celestron 11-inch HD Edge telescope was used to measure the position angles and separations of ARY 6 AD and ARY 6 AE. The averages of our measurements are as follows: separation AD: trial 1 124.1 arcseconds and trial 2 124.5 arcseconds; separation AE: trial 1 73.3 arcseconds and trial 2 73.8 arcseconds. The averages of positon angle for AD: trial 1 159.9 degrees and trial 2 161.3 degrees, for AE: trial 1 232.6 degrees and trial 2 233.7 degrees.

Kitt Peak Speckle Interferometry of Close Visual Binary Stars

Russell Genet
California Polytechnic State University, Cuesta College, and the University of North Dakota, 4995 Santa Margarita Lake Road, Santa Margarita, CA 93453; russmgenet@aol.com

David Rowe
PlaneWave Instruments; drowesmi@aol.com

Thomas C. Smith
Darkridge Observatory; tcsmith@darkridgeobservatory.org

Alex Teiche
California Polytechnic State University; alexteiche@gmail.com

Richard Harshaw
Brilliant Sky Observatory; rharshaw2@cox.net

Daniel Wallace
University of North Dakota; dwallace006@yahoo.com

Eric Weise
University of California; ericdweise@gmail.com

Edward Wiley
Yankee Tank Creek Observatory; edwiley@sunflower.com

Grady Boyce
Boyce Research Initiatives and Educational Foundation; grady@boyce-astro.org

Patrick Boyce
Boyce Research Initiatives and Educational Foundation; pat@boyce-astro.org

Detrick Branston
National Solar Observatory; dbranston@noao.edu

Kayla Chaney
Concordia University; kayla.chaney@eagles.cui.edu

R. Kent Clark
South Alabama University; rclark@jaguarl.usouthal.edu

Chris Estrada
California State University; prlest0112@hotmail.com

Reed Estrada
Northrop Aviation; reed.estrada@roadrunner.com

Thomas Frey
California Polytechnic State University; t.frey@sbcglobal.net

Wayne L. Green
Boulder Astronomy and Space Society; dxwayne@gmail.com

Nathalie Haurberg
Knox College; nhaurber@knox.edu

Greg Jones
Eclipse Technologies; gregj@eclipse-t.com

John Kenney
Concordia University; john.kenney@cui.edu

Sheri Loftin
Kitt Peak National Observatory; loftin@noao.edu

Izak McGieson
Knox College; izak@halcyon.nu

Rikita Patel
Concordia University; rikitaben.patel@eagles.cui.edu

Josh Plummer
University of South Alabama

John Ridgely
California Polytechnic State University; jridgely@caloly.edu

Mark Trueblood
Winer Observatory; winer.obs@gmail.com

Don Westergren
Morris Ranch Observatory; westergren@nethere.com

Paul Wren
University of North Dakota; paul.wren@gmal.com

Abstract Speckle interferometry can be used to overcome normal seeing limitations by taking many very short exposures at high magnification and analyzing the resulting speckles to obtain the position angles and separations of close binary stars. A typical speckle observation of a close binary consists of 1,000 images, each 20 milliseconds in duration. The images are stored as a multi-plane FITS cube. A portable speckle interferometry system that features an electron-multiplying CCD camera was used by the authors during two week-long observing runs on the 2.1-meter telescope at Kitt Peak National Observatory to obtain some 1,000 data cubes of close binaries selected from a dozen different research programs. Many hundreds of single reference stars were also observed and used in deconvolution to remove undesirable atmospheric and telescope optical effects. The database of well over one million images was reduced with the Speckle Interferometry Tool of PLATESOLVE3. A few sample results are provided. During the second Kitt Peak run, the McMath-Pierce 1.6- and 0.8-meter solar telescopes were evaluated for nighttime speckle interferometry, while the 0.8-meter Coude feed was used to obtain differential radial velocities of short arc binaries.

Orion Project: A Photometry and Spectroscopy Project for Small Observatories

Jeffrey L. Hopkins
Hopkins Phoenix Observatory; 7812 West Clayton Drive, Phoenix, AZ 85033; phxjeff@hposoft.com

Abstract Orion, the hunter, is one of the most famous constellations. Its declination is such that it is visible from most of the civilized world. In addition, most of the stars of Orion are very bright and interesting. Originally this project was called the Betelgeuse Campaign, but four more stars were added so the name was changed to the Orion Project. The project now includes Betelgeuse, Rigel, and the three stars of Orion's belt, Mintaka, Alnilam, and Alnitak. Both photometry and spectroscopy provide data for the project. The project has several goals, the first of which is to help beginners with photometry and spectroscopy. The second goal is to obtain the actual observations and data. Because these stars are very bright, they are seldom observed in detail. Their brightness also poses a problem for most professional observatories. It is hoped that by having observations over a long time, interesting changes can be seen that will warrant closer investigation. As a third goal it is hoped that the procedures refined in the project for spectroscopic data may help promote a similar system for the AAVSO, which has an excellent archive of photometric data, but is still lacking a means of handling spectroscopic data.

Simplified Color Photometry Using APASS Data

Nicholas Dunckel
12971 Cortez Lane, Los Altos Hills, CA 94022; ndunckel@earthlink.net

Abstract APASS, the AAVSO Photometric All-Sky Survey, now contains 47 million stars and covers 97% of the Northern and Southern hemisphere sky. Its extraordinary coverage means that there are multiple APASS-calibrated stars available for color photometry in the field of view of virtually every amateur image. This paper presents a simplified spreadsheet-based procedure that combines raw photometric data with APASS data to calibrate target objects in the same field of view. The complete photometric equations are reviewed and a simplified form is obtained for use within a limited field of view. Raw photometric data and APASS data for that image from AAVSO are combined on a spreadsheet to produce calibrated photometric measurements of target objects within the field of view. The consistency of the fit to the data is shown graphically. Error terms are tracked through the equations to provide the standard deviation of each measurement.

Impact of Observing Parameters on 17 Nights with Nova Del 2013

Wayne L. Green
7131 Oriole Lane, Longmont, CO 80503; dxwayne@gmail.com

Abstract Nova Del 2013 (V339 Del) was reported in *Astronomer's Telegram No. 5279* (PNV 20233073+2046041) on 2013 August 14. On the following day, the University of Colorado, Boulder, granted our observing request for use of the R3000-5000 spectrograph attached to their 60-cm telescope. The planning, operational approach, analysis techniques, results, issues, and operational conclusions for data taken from 15 August through 2 September are reported here.

Pushing the Envelope: CCD Flat Fielding

James Vail
2050 Belmont Avenue, Idaho Falls, ID 83404; vailja@hotmail.com

Abstract In this paper the author discusses the design aspects and considerations of flat field systems. Illumination calculations and construction techniques and materials are investigated. Several actual systems along with testing methods to determine quality are presented.

Toward Millimagnitude Photometric Calibration

Eric Dose
4021 SW 10th Avenue, #412, Topeka, KS 66604; eric@bois-darc.org

Abstract Asteroid roation, exoplanet transits, and similar measurements will increasingly call for photometric precisions better than about 10 millimagnitudes, often between nights and ideally between distant observers. The present work applies detailed spectral simulations to test popular photometric calibration practices, and to test new extensions of these practices. Using 107 synthetic spectra of stars of diverse colors, detailed atmospheric transmission spectra computed by solar-energy software, realistic spectra of popular astronomy gear, and the option of three sources of noise added at realistic millimagnitude levels, we find that certain adjustments to current calibration practices can help remove small systematic errors, especially for imperfect filters, high airmasses, and possibly passing thin cirrus clouds.

Measuring Double Stars with a Dobsonian Telescope by the Video Drift Method

Rick Wasson
24445 Epson Court, Murrieta, CA 92562; ricksshobs@verizon.net

Abstract Equipment, observing procedures, data reduction techniques, and software the author uses to measure double stars with a Dobsonian telescope by the Video Drift Method are described in detail. Challenges encountered with an Alt-Az telescope and data reduction, such as calibration, a continuously rotating field, and digital video pitfalls, along with ways to overcome them are discussed. Early measures from 2011 are presented and compared with measures of well-established sources, validating the use of a Dobsonian telescope to measure double stars by the Video Drift Method.

An Experiment in Photometric Data Reduction of Rapid Cadence Flare Search Data

Gary A. Vander Haagen
825 Stonegate Road, Ann Arbor, MI 48103; garyvh2@gmail.com

Larry E. Owings
23220 Barnes Lane, Colfax, CA 95713; lowings@foothill.net

Abstract A process was developed to utilize a singe star both for tracking and as a differential reference for high time resolution flare surveys. A data pipeline was also developed to process and merge, time stamped, high data rate target and slow data rate comparison star data for million-line files. This process reduced the data reduction time and aided in identification and analysis of photometric flare events during nightly surveys. The optical system employed a pellicle beam splitter for dual beam data collection, one path for a CCD camera for alignment, tracking, and reference and a second path for the silicon photomultiplier collection of the target data. Typical target photometric sampling rates were 100 samples/second. Comparison star flux and sky background was available over a continuous cycle ranging from every 1 to 10 seconds, depending upon the guide star's magnitude and the atmospheric stability. The data pipeline yielded target flux data with corrections for sky background, detector dark count, and differential compensation. The data pipeline was successfully tested using flare search data from YY Gem, where, 81.6 ksec (22.7 hours) of data were collected and one flare detected, resulting in a flare rate of 0.044 flare/hour, consistent with cited research.

Spectro-Polarimetry: Another New Frontier

John Menke
22500 Old Hundred Road, Barnesville, MD 20838; john@menkescientific.com

Abstract The challenge of spectroscopic research on Class B emission stars is to figure out what the emission star is doing that causes changes in the spectrum as often as every day. In many cases, it appears that stellar magnetic fields interacting with gas material from the rotating star are implicated. One effect of that should be increased polarization of the light associated with the spectral features. I have constructed a polarimeter fitted to the home-built spectrometer and 18-inch telescope to allow possible measurement of these effects. Construction, operation, and initial measurements with the spectro-polarimeter (S-P) will be described.

A Strategy for Urban Astronomical Observatory Site Preservation: The Southern Arizona Example

Eric R. Craine
STEM Laboratory, Inc., Tucson, AZ; ercraine@wrc-inc.com

Brian L. Craine
Western Research Company, Inc., Tucson, AZ; blcraine@wrc-inc.com

Patrick R. Craine
STEM Laboratory, Inc., Tucson, AZ; prcraine@gmail.com

Erin M. Craine
STEM Laboratory, Inc., Tucson, AZ; ecraine@dakotacom.net

Scott Fouts
QED Wind Power, Tucson, AZ; scott.fouts@yahoo.com

Abstract Urbanized observatories are under financial pressures for numerous and complex reasons, including concerns that increasing sky brightness will continue to erode their scientific viability. The history of urbanized observatories is one of steady decline and divestiture. We argue that light at night (LAN) impacts of urban growth are inadequately understood, that current measurement techniques are incomplete in scope, and that both limit the effectiveness of mitigation programs. We give examples of these factors for Pima County, Arizona, and propose techniques and a program that could provide focus and power to mitigation efforts, and could extend the longevity of southern Arizona observatories.

SkyGlowNet Sky Brightness Meter (iSBM) Nodes: Cerritos Observatory Station, Tucson, Arizona, and Colorado State University, Fort Collins, Colorado

Roger B. Culver
Department of Physics, Colorado State University, Fort Collins, CO 80523

Erin M. Craine
STEM Laboratory, Inc., Tucson, AZ 85745; ecraine@dakotacom.net

Heather Michalak
Department of Physics, Colorado State Universtiy, Fort Collins, CO 80523; heather.q.lsop@gmail.com

Abstract We present a summary of nearly continuous night-time sky brightness photometry from a ground static survey (GSS) conducted by STEM Laboratory, Inc., at the Global Network of Astronomical Telescopes (GNAT) Cerritos Observatory site in the Tucson Mountain foothills to the west of Tucson, Arizona. We show numerous examples of different sky conditions and their impacts on high-frequency sky brighteness measures. During that time period, a similar installation was established at Colorado State University. We also address problems and solutions related to institutional barriers to that installation.

Ground-based Efforts to Support a Space-based Experiment: the Latest LADEE Results

Brian Cudnik
Mahmudur Rahman
Department of Chemistry and Physics, Prarie View A&M University, P. O. Box 519, M.S. 2230, Prairie View, TX 77446

Abstract The much anticipated launch of NASA's Lunar Atmosphere and Dust Environment Explorer happened flawlessly last October and the satellite has been doing science (and sending a few images) since late Novermber. [The LADEE mission ended with the crash-landing of the spacecraft on the lunar far side on April 17, 2014, capping a successful 140-day mission.] We also have launched our campaign to document lunar meteroid impact flashes from the ground to supply ground truth to inform of any changes in dust concentration encountered by the spacecraft in orbit around the moon. To date I have received six reports of impact flashes or flash candidates from the group I am coordinating; other groups around the world may have more to add when all is said and done. In addition, plans are underway to prepare a program at Prairie View A&M University to involve our physics majors in lunar meteoroid, asteroid occultation, and other astronomical work through our Center for Astronomical Sciences and Technology. This facility will be a control center to not only involve physics majors, but also to include pre-service teachers and members of the outside community to promote pro-am collaborations.

Got Scope? The Benefits of Visual Telescopic Observing in the College Classroom

Kristine Larsen
Central Connecticut State University, 1615 Stanley Street, New Britain, CT 06050; Larsen@ccsu.edu

Abstract The author discusses pedagogical successes achieved in a course based on visual telescopic observation for college students in all majors.

Erratum 1. New Variable Stars Discovered by the APACHE Survey. I. Results After the First Observing Season

Mario Damasso
INAF-Astrophysical Observatory of Torino, Via Osservatorio 20, I-10025 Pino Torinese, Italy; Astronomical Observatory of the Autonomous Region of the Aosta Valley, fraz. Lignan 39, 11020 Nus (Aosta), Italy; Dept. of Physics and Astronomy, University of Padova, Vicolo dell'Osservatorio 3, I-35122 Padova, Italy; mario.damasso@studenti.unipd.it and m.damasso@gmail.com

Andrea Bernagozzi
Enzo Bertolini
Paolo Calcidese
Albino Carbognani
Davide Cenadelli
Astronomical Observatory of the Autonomous Region of the Aosta Valley, fraz. Lignan 39, 11020 Nus (Aosta), Italy

Jean Marc Christille
Dept. of Physics, University of Perugia, Via A. Pascoli, 06123 Perugia, Italy; Astronomical Observatory of the Autonomous Region of the Aosta Valley, fraz. Lignan 39, 11020 Nus (Aosta), Italy

Paolo Giacobbe
INAF-Astrophysical Observatory of Torino, Via Osservatorio 20, I-10025 Pino Torinese, Italy; Dept. of Physics, University of Trieste, Via Tiepolo 11, I-34143 Trieste, Italy

Luciano Lanteri
Mario G. Lattanzi
Richard Smart
Allesandro Sozzetti
INAF-Astrophysical Observatory of Torino, Via Osservatorio 20, I-10025 Pino Torinese, Italy

In the article "New Variable Stars Discovered by the APACHE Survey. I. Results After the First Observing Season" (*JAAVSO*, 2014, **42**, 99–123), Table 1, which appears on pages 103–108, should be replaced with the table given here on the following pages. Columns 6 (Period) and 7 (Amplitude) were originally miswritten due to a production error.

Table 1. Variable stars discovered by APACHE during the first observing season. For stars with two periods indicated, that in parentheses is the one determined from the APACHE data, while the other is estimated from SuperWASP archive data. The amplitudes of the light curves are measured from APACHE data. Time T_0 corresponds to phase = 0 in the folded light curves.

No.	*Name*	*R.A. (2000)*	*Dec. (2000)*	*Mag V*	*Period (days)*	*Amplitude (mag)*	*T_0 (HJD–2455000)*	*Var. Type*	*Note*
1	UCAC4 744-001518	002.6931077	+58.6863575	14.86	7.55 (7.518)	~0.25	1146.3523197	ROT?	(1)
2	UCAC4 743-001636	002.7103159	+58.5618373	10.21	0.10625 (0.09603)	~0.02	1146.3523197	DSCT	(2)
3	UCAC4 758-009639	015.1541895	+61.5753528	14.27	1.20557	~0.6	1146.4105864	E	(3)
4	UCAC4 752-014548	018.8161518	+60.3735250	13.14	1.087	~0.3	1146.3866004	EB	
5	UCAC4 870-000885	018.9877518	+83.9571120	16.77	0.40861	~0.3	1273.2157609	EW	
—	UCAC4 872-000839	021.2561924	+84.2626639	16.17	?	—	RR?		(4)
6	UCAC4 728-026837	044.2308518	+55.5203950	16.38 (GSC2.3)	?	~0.4	1146.4709166	L	
7	UCAC4 618-013561	062.4040074	+33.4937250	12.83	?	~0.25	1162.5960791	L	
8	UCAC4 713-031969	063.5650233	+52.5300092	14.4	6.22	~0.4	1208.3673785	E	(5)
9	UCAC4 709-034533	074.7646086	+51.7157109	10.77	?	~0.05	1328.2561929	L	
10	UCAC4 610-021265	082.4603353	+31.9110003	13.59	0.80089 (0.80086)	~0.3	1210.5113093	EW	(6)
11	UCAC4 619-030850	092.0415889	+33.6711831	13.01	2.008 (2.009)	~0.27	1205.5239017	EB	(7)
12	UCAC4 521-023140	094.9127039	+14.0543662	12.47	~77?	~0.16	1270.3904921	L	(8)
13	UCAC4 624-036803	105.7816774	+34.7009262	15.90	0.21635 (WASP)	~0.25	1246.5895718	EW	(9)
14	UCAC4 715-044844	105.9254200	+52.8823920	13.22	0.3281 (0.32811)	~0.33	1205.4926955	EW	(10)
15	UCAC4 664-056989	179.4896992	+42.6626264	14.19	0.33651	~0.5	1353.4968403	RRab	(11)
16	UCAC4 609-049172	208.1377689	+31.6871487	13.47	0.35471 (0.35470)	~0.16	1301.7535576	EW	(12)
17	UCAC4 666-060394	232.1916465	+43.0916548	12.79	1.9756 (1.9788)	~0.1	1127.3672611	ROT	(13)
18	UCAC4 633-053996	250.3480433	+36.5047900	12.26	?	~0.1	1367.4885131	L	
19	UCAC4 633-054311	250.4026556	+36.4431934	15.06	?	~0.3	1367.4885131	L	(14)

Table continued on following pages

Table 1. Variable stars discovered by APACHE during the first observing season. For stars with two periods indicated, that in parentheses is the one determined from the APACHE data, while the other is estimated from SuperWASP archive data. The amplitudes of the light curves are measured from APACHE data. Time T_0 corresponds to phase = 0 in the folded light curves, cont.

No.	*Name*	*R.A. (2000)*	*Dec. (2000)*	*Mag V*	*Period (days)*	*Amplitude (mag)*	*T_0 (HJD–2455000)*	*Var. Type*	*Note*
20	UCAC4 633-054908	250.4621462	+36.4817620	11.82	?	~0.2	1367.4885131	L	(15)
21	UCAC4 652-057450	253.3608262	+40.3033556	14.83	1.47	~0.45	1420.4785809	EB	
22	UCAC4 592-063874	275.7670439	+28.3080614	14.01 (GSC2.3)	~60?	~0.2	1127.3682196	L	
23	UCAC4 533-077928	279.6991892	+16.4103631	15.12	?	~0.5	1166.3294430	L	
24	UCAC4 533-078069	279.8361324	+16.5350567	14.97 (GSC2.3)	?	~0.2	1166.3294430	L	
25	UCAC4 532-076755	279.8824256	+16.3173617	15.15	0.3199	~0.25	1166.3294430	EW	
26	UCAC4 533-078283	280.0367009	+16.5274503	14.58	?	~0.11	1166.3294430	L	
27	UCAC4 723-061541	283.8471103	+54.4308875	14.33	0.38399 (0.38399)	~0.7	1385.4985908	EW	(16)
28	UCAC4 723-061622	284.1744556	+54.5157323	13.34 (GSC2.3)	?	~0.35	1385.4876350	L	
29	UCAC4 479-089263	284.6627689	+05.7352287	11.68	0.744	~0.1	1473.4154161	RRc	(17)
30	UCAC4 491-099556	284.8352648	+08.1355764	N.A.	?	~0.15	1432.4879724	L	(18)
31	2MASS 18592325+0810247	284.846896	+08.173555	N.A.	?	~0.25	1432.4879724	L	(19)
32	UCAC4 491-099593	284.8855603	+08.0666542	16.48 (GSC2.3)	1.251	~0.35	1432.4879724	EW	
33	2MASS 19000738+0805125	285.030765	+08.086826	19.00 (GSC2.3)	?	~0.25	1432.4879724	L	
34	UCAC4 490-094834	285.0720153	+07.9374948	16.58 (GSC2.3)	?	~0.12	1432.4879724	L	
35	UCAC4 729-060138	290.8229630	+55.6600275	12.76	0.6902 (0.688)	~0.08	1434.3738137	ROT	(20)
36	UCAC4 728-061629	290.9937003	+55.5546067	14.81	0.36689 (0.3669)	~0.2	1434.3728183	EW	(21)
37	UCAC4 728-061766	291.4820559	+55.5007378	15.27 (GSC2.3)	0.189029 (0.1890)	~0.1	1434.3738137	DSCT	(22)

Table continued on following pages

Table 1. Variable stars discovered by APACHE during the first observing season. For stars with two periods indicated, that in parentheses is the one determined from the APACHE data, while the other is estimated from SuperWASP archive data. The amplitudes of the light curves are measured from APACHE data. Time T_0 corresponds to phase = 0 in the folded light curves, cont.

No.	*Name*	*R.A. (2000)*	*Dec. (2000)*	*Mag V*	*Period (days)*	*Amplitude (mag)*	*T_0 (HJD–2455000)*	*Var. Type*	*Note*
38	UCAC4 811-027074	294.4105074	+72.0363334	13.63	?	~0.2	1424.3380554	L	
39	UCAC4 610-092144	297.3880989	+31.8705942	14.72 (NOMAD)	?	~0.1	1127.5857519	L	
40	UCAC4 609-091131	297.4135403	+31.6445878	14.79 (NOMAD)	?	~0.15	1127.5857519	L	
41	UCAC4 609-091297	297.4814474	+31.7204662	17.27 (NOMAD)	?	~0.9	1127.5857519	L	
42	2MASS 19500382+3149132	297.515956	+31.820337	N.A.	?	~0.15	1127.5857519	L	
43	2MASS 19500885+3135499	297.536909	+31.597216	N.A.	?	~0.4	1127.5857519	L	
44	UCAC4 610-092592	297.5731206	+31.9941723	15.53 (NOMAD)	?	~0.2	1127.5857519	L	
45	2MASS 19502059+3152091	297.585806	+31.869217	17.38 (NOMAD)	?	~0.2	1127.5857519	L	
46	2MASS 19502935+3158417	297.622323	+31.978273	N.A.	?	~0.17	1127.5857519	L	
47	UCAC4 610-092815	297.6690953	+31.9639217	15.41 (NOMAD)	0.427	~0.5	1127.5857519	EW	
48	UCAC4 609-091797	297.7097806	+31.6965225	12.70	~40?	~0.13	1127.5857519	L	
49	UCAC4 608-095594	297.7998224	+31.5728037	15.22 (NOMAD)	?	~0.45	1127.5857519	L	
50	2MASS 19511471+3143128	297.811294	+31.720238	17.47	?	~0.14	1127.5857519	L	
51	UCAC4 623-096266	302.9632515	+34.4131084	15.28 (NOMAD)	9.8	~0.45	1416.5074270	PULS	(23)
52	UCAC4 623-096337	303.0224745	+34.4758434	15.87 (NOMAD)	~61?	~0.16	1416.5074270	L	

Table continued on following pages

Table 1. Variable stars discovered by APACHE during the first observing season. For stars with two periods indicated, that in parentheses is the one determined from the APACHE data, while the other is estimated from SuperWASP archive data. The amplitudes of the light curves are measured from APACHE data. Time T_0 corresponds to phase = 0 in the folded light curves, cont.

No.	*Name*	*R.A. (2000)*	*Dec. (2000)*	*Mag V*	*Period (days)*	*Amplitude (mag)*	*T_0 (HJD–2455000)*	*Var. Type*	*Note*
53	UCAC4 621-098928	303.0456662	+34.0879998	13.90	0.1365	~0.07	1416.5076083	DSCT?	
54	UCAC4 622-095023	303.0508565	+34.2564675	14.06 (NOMAD)	?	~0.22	1416.5074270	L	(24)
55	UCAC4 622-095081	303.0868139	+34.3034262	17.07 (NOMAD)	~44?	~0.15	1416.5074270	L	
56	UCAC4 622-095314	303.2126174	+34.2968739	16.19 (NOMAD)	?	~0.12	1416.5074270	L	
57	UCAC4 623-096673	303.2543371	+34.4226409	14.72 (NOMAD)	?	~0.25	1416.5074270	L	
58	UCAC4 622-095521	303.3453327	+34.3789689	13.58	?	~0.3	1416.5074270	L	
59	UCAC4 622-095554	303.3731539	+34.3134381	14.99 (NOMAD)	?	~0.05	1416.5074270	L	
60	UCAC4 516-127264	303.6096042	+13.1699259	12.40	0.575	~0.2	1445.5441597	EW	
—	UCAC4 744-062741	306.3905642	+58.6538473	14.09	1.51?	~0.2	1127.3642954	ROT?	(25)
61	UCAC4 744-062753	306.4085277	+58.7603659	14.17 (GSC2.3)	0.4406 (0.4405)	~0.25	1127.3642954	EW	(26)
62	UCAC4 744-062788	306.5188756	+58.7358845	15.2 (GSC2.3)	0.3495	~0.45	1127.3642954	EW	
63	2MASS 20305052+5547074	307.710540	+55.785416	18.64 (GSC2.3)	?	~2.0	1417.5662968	L	
64	UCAC4 729-067019	307.8310009	+55.7983139	15.56 (GSC2.3)	?	~0.6	1417.5664087	L	
65	UCAC4 731-068791	308.1278424	+56.1299364	14.44	?	~0.4	1417.5664087	L	
66	UCAC4 621-112859	314.4579859	+34.1641767	13.84 (NOMAD)	?	~0.15	1432.5597351	L	(27)
67	UCAC4 617-116284	315.4994471	+33.3210739	14.90 (NOMAD)	?	~0.5	1127.3687558	L	
68	UCAC4 598-126361	317.6277274	+29.4905828	12.48	?	~0.2	1443.4864670	L	
69	UCAC4 621-122572	321.8936342	+34.0494003	12.09	0.43635 (0.438)	~0.1	1445.5736404	EW	(28)
70	UCAC4 590-130214	326.9765700	+27.9013675	12.71	~36	~0.2	1135.4185368	L	(29)

Table continued on following pages

Table 1. Variable stars discovered by APACHE during the first observing season. For stars with two periods indicated, that in parentheses is the one determined from the APACHE data, while the other is estimated from SuperWASP archive data. The amplitudes of the light curves are measured from APACHE data. Time T_0 corresponds to phase = 0 in the folded light curves, cont.

No.	*Name*	*R.A. (2000)*	*Dec. (2000)*	*Mag V*	*Period (days)*	*Amplitude (mag)*	*T_0 (HJD–2455000)*	*Var. Type*	*Note*
71	UCAC4 590-130270	327.0770353	+27.8228681	12.49	1.02500 (1.025)	~0.25	1127.3844791	EW	(30)
72	UCAC4 652-105561	327.4152459	+40.3802687	14.33	?	~0.35	1443.4839005	L	
73	UCAC4 588-128603	330.1270789	+27.4577517	12.72	4.21221 (1.29)	~0.08	1459.5047071	ROT?	(31)
74	UCAC4 789-036290	330.5805324	+67.6531512	16.00 (GSC2.3)	0.17 (0.34)	~0.15	1127.3607291	DSCT (EW)	(32)
75	UCAC4 788-037466	330.9508409	+67.4961639	14.29 (GSC2.3)	0.47	~0.4	1127.3602622	EA	
76	UCAC4 788-037537	331.1173995	+67.4969889	13.66 (GSC2.3)	?	~0.16	1127.3602622	L	
77	UCAC4 788-037577	331.2463553	+67.5745589	15.62 (GSC2.3)	0.36	~0.25	1127.3607291	EW	
78	UCAC4 726-083454	333.0765986	+55.1851717	14.67	?	~0.18	1127.3607291	L	
79	UCAC4 725-086173	333.2373680	+54.9382473	13.34	0.192835	~0.2	1127.3607291	DSCT?	
80	UCAC4 725-086241	333.2829348	+54.8638348	14.33	0.17234	~0.5	1443.4626241	DSCT?	
81	UCAC4 781-040386	333.4526621	+66.1133137	15.43	1.13	~0.2	1127.3604366	EB	
82	UCAC4 726-084171	333.5242624	+55.0744792	12.13	~50	~0.15	1127.3604366	L	
83	UCAC4 859-013147	343.6693409	+81.7063873	12.72	37	~0.17	1385.653719	L	
84	UCAC4 749-082493	352.8942900	+59.7192198	10.64	0.861	~0.2	1146.4200537	EW	

Table continued on next page

Table 1. Variable stars discovered by APACHE during the first observing season, cont.

Notes: (1) Star 1SWASPJ001046.35+584111.0, 1837 points analyzed. APACHE data are less scattered than those of SWASP. (2) Star 1SWASPJ001050.47+583342.6, SWASP data with high scatter, 1969 of 2015 data analyzed (applying a 1-sigma clipping to the original data). (3) Eclipsing binary already known in VSX (Mis V1368) but the orbital period was not reported. (4) The light curve is discussed separately in Figure 2. No SWASP data available for this star. (5) Only the primary minimum detected. (6) Star 1SWASPJ052950.48+315439.8, 7033 of 7110 data points from SWASP analyzed (applying a 3-sigma clipping to the original data). The secondary minimum appears deeper in the light curve from the APACHE survey. Refer to Figure 3 for a comparison between SWASP and APACHE light curves. (7) Star 1SWASPJ060809.97+334016.5, 6223 of 6282 data points from SWASP analyzed (applying a 3-sigma clipping to the original data). The existence of a secondary minimum can be guessed from the APACHE light curve, while is not visible in SWASP data (not shown here). (8) Tentative period, but the phase coverage does not make possible a reliable estimation. (9) Star 1SWASPJ070307.60+344203.60, 4066 of 4305 data points analyzed (applying a 2-sigma clipping to the original data). Even with few data points, this faint star appears to be an eclipsing binary system in the APACHE photometry. From data in the SWASP public archive we derive the best period P=0.21635 day, that in this case we adopted for folding our data because is a far better estimate than that from APACHE data. This star is discussed separately in section 4. (10) Star 1SWASPJ070342.10+525256.8, noisy light curve, 1094 of 1258 data points from SWASP analyzed (applying a 1-sigma clipping to the original data). (11) Star 1SWASPJ115757.51+423945.5, 5509 data points analyzed. From APACHE photometry alone, because the data are few, we could only guess that the star has a short period (<1 day), but a reliable determination was not possible. SWASP photometry helped us in classifying the star's variability and estimating a reliable period. We show part of the APACHE light curve and the SWASP data in Figure 5. (12) Star 1SWASPJ135233.09+314113.8, 7348 of 7425 data points analyzed (applying a 3-sigma clipping to the original data). (13) Star 1SWASPJ152845.99+430530.1, 5387 of 5428 data points analyzed (applying a 3-sigma clipping to the original data). Spotted star. Color indexes B–V = 0.98, V–J = 1.78, V–K = 2.39. Tentantive spectral classification: dK3/dK4. (14) Appears in Kopacki et al. (2003). V from Sandquist et al. (2010). (15) Appears in Kopacki et al. (2003). (16) Star 1SWASPJ185523.32+542551.4, 11972 of 12016 data points analyzed (applying a 3-sigma clipping to the original data). (17) Observations in V band. Color indexes: B–V = 0.95, V–J = 1.7, V–K = 2.33. (18) In on-line archive images it appears as a blended object. Faint, no V available. (19) Faint object in on-line archive images. (20) Star 1SWASP192317.5+553936.2, 12861 of 12919 data points analyzed (applying a 3-sigma clipping to the original data). Results for this star are discussed separately in section 4. (21) Star 1SWASPJ192358.37+553316.9, 12469 of 12596 data points analyzed (applying a 3-sigma clipping to the original data). (22) Star 1SWASPJ192555.70+5530002.9, 12934 photometric points used in the analysis. (23) Undefined type of pulsating star. Modulation possibly due to rotation. We provide a more conservative uncertainty than that calculated as 1/timespan. (24) Star listed in the International Variable Star Index (NSVS J2012124+341522) and classified as L. The reported periodicity of 88 days is not found in our data that clearly show that the possible period should be longer. (25) Star 1SWASPJ202533.73+583913.9, 10637 of 10721 data points analyzed (applying a 3-sigma clipping to the original data). Because of its uncertain classification, this star is discussed separately in section 4. (26) Star 1SWASPJ202538.05+584537.4, 10485 of 10550 data points analyzed (applying a 3-sigma clipping to the original data). The primary minimum is not well sampled in the APACHE light curve. (27) Star listed in the International Variable Star Index (NSV 25408) and classified as an eclipsing binary, but without an estimate of the orbital period. No evidence for eclipses is present in the APACHE data. Rather, the star appears as an irregular variable. Thus we propose a change of variability status for this star. (28) Star 1SWASPJ212734.47+340257.9, 14781 of 14872 data points analyzed (applying a 3-sigma clipping to the original data). (29) Long periodicity, assumed tentatively nearly equal to 36 days by looking at the light curve. (30) Star 1SWASPJ214818.48+274922.0, 14086 of 14151 data points analyzed (applying a 3-sigma clipping to the original data). (31) Star 1SWASPJ220030.52+272728.8, 21352 of 21499 data points analyzed (applying a 3-sigma clipping to the original data). This star is discussed in detail in section 4. Even if the classification remains uncertain, based on SWASP data we suggest this could be a rotating star. (32) Difficult classification, faint star/noisy light curve. We propose two possibilities, with corresponding periodicities.

Erratum 2

JAAVSO Vol. 42, No. 1. Due to a production error, the running headings on pages 53–65 and on page 244 were mislabeled. "*JAAVSO Volume 41, 2013*" should read "*JAAVSO Volume 42, 2014*".

Erratum 3. The AAVSO Widow—or Should We Say Spouse?

Thomas R. Williams
9505 Northpointe Boulevard, Apt 9304B, Spring, TX 77379; trw@rice.edu

In the article "The AAVSO Widow—or Should We Say Spouse?" (*JAAVSO*, 2012, **40**, 77–91), the birth year of Margaret Stewart Lyon Yalden was incorrectly given on page 83. In section 4.2, first paragraph, "Born in 1865" should read "Born in 1858"; and, in the same paragraph, "Five years older than Ernest" should read "Twelve years older than Ernest."

Index to Volume 42

Author

Subject

CATACLYSMIC VARIABLES [See also VARIABLE STARS (GENERAL)]

CATALOGUES, DATABASES, SURVEYS

PHOTOMETRY, CCD

VARIABLE STAR OBSERVING ORGANIZATIONS

VARIABLE STAR OBSERVING [See also INSTRUMENTATION]

VARIABLE STARS (GENERAL)

VARIABLE STARS (INDIVIDUAL); OBSERVING TARGETS

The AAVSO CENTENNIAL HISTORY

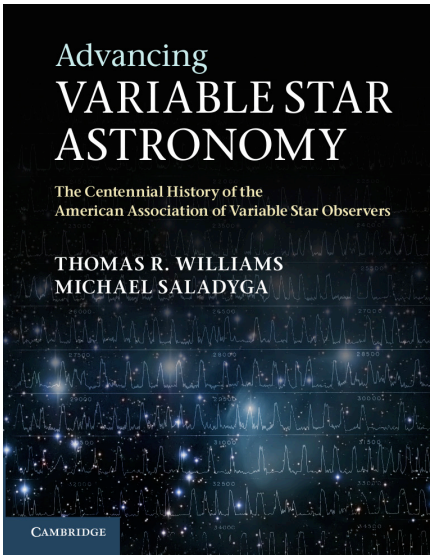

Advancing Variable Star Astronomy: The Centennial History of The American Association of Variable Star Observers

by Thomas R. Williams and Michael Saladyga,
published by Cambridge University Press

To order, visit the AAVSO online store:

http://www.aavso.org/aavso-online-store

or contact the AAVSO,
49 Bay State Road, Cambridge, MA 02138, USA
phone: 617-354-0484 email: aavso@aavso.org

Now also available as a Kindle e-book through Amazon.com